Investigation and prediction of pollution in coastal and estuarine waters, using experimental and numerical methods

Jonathan Auryn King

School of Engineering

Cardiff University, Wales, UK

Supervised by:
Dr Reza Ahmadian and Professor Roger Falconer

This thesis is submitted in partial fulfilment of the requirements for the degree of

Doctor of Philosophy (Ph.D.)

2019

DECLARATION

This work has not been submitted in substance for any other degree or award at this or any other university or place of learning, nor is being submitted concurrently in candidature for any degree or other award.

Signed ..... (candidate) Date .....

STATEMENT 1

This thesis is being submitted in partial fulfilment of the requirements for the degree of PhD.

Signed ..... (candidate) Date .....

STATEMENT 2

This thesis is the result of my own independent work/investigation, except where otherwise stated, and the thesis has not been edited by a third party beyond what is permitted by Cardiff Universitys Policy on the Use of Third Party Editors by Research Degree Students. Other sources are acknowledged by explicit references. The views expressed are my own.

Signed ..... (candidate) Date .....

STATEMENT 3

I hereby give consent for my thesis, if accepted, to be available online in the Universitys Open Access repository and for inter-library loan, and for the title and summary to be made available to outside organisations.

Signed ..... (candidate) Date .....

Acknowledgements

I would like begin by thanking Dr Reza Ahmadian and Professor Roger Falconer for their supervision, support, and guidance throughout my studies. Despite many dead ends, hiccups, and uncertainty as to the direction of my work, it is our numerous meetings, their suggestions and rigorous review that culminated in this thesis.

I addition, I would like to thank Dr Michaela Bray, who first made me aware of, and encouraged me to apply for a studentship. Dr Bray supervised a number of my projects as an undergraduate at Cardiff University and I am grateful that on the back of these she considered me a suitable candidate.

This work was supported by the British Council Newton Fund and WISE CDT EPSRC grant EP/L016214/1, and would not have been possible without the use of the HPC Wales and ARCCA supercomputing facilities. So to everyone involved in the WISE scheme, and the staff at HPC Wales (Ade), and ARCCA (Tom and Andrew), who provided invaluable support in setting up my models on their systems, I give my thanks.

During my time at Tsinghua University Professor Binliang Lin provided me with constant support and I would like to express my gratitude to him and the students in his department, who welcomed me with warm hospitality and showed such kindness and patience.

As much as a PhD is an individual piece of work and can feel incredibly isolating at times, I have also seen it as a collaborative effort. To the rest of WISE cohort 1, who I studied with for a year at Exeter University, thank you, and I wish you all the best for the future. To the PhD students and post-docs at Cardiff who took me under their

wing and offered continued support throughout my time at Cardiff (Bruño, Luis, Pablo and Thanasis), you taught me so much (in many cases more than I had from any lecture), and I can only express my gratitude for the time you gave me.

To my friends in and out of the department (Joe, John, Nejc, the lunch club, Little Goode and Si, Stu, Rob, Zoe and Lou), I am always grateful, you've been there in both the ups and downs and made each day that much more enjoyable. And lastly, to my family (Mum, Rebecca, John, Nana and Grandad), your unconditional love, support and belief in me, even when I haven't believed in myself, has shaped me for the better, inspired me and gave me determination in difficult times.

Cardiff, 2019 Jonathan King

Abstract

In recent years, society has become more aware and concerned with the environmental and human health impacts of population growth and development. In response, a number of legislative measures have been introduced within Europe (and globally), which have sparked much cross-disciplinary research aimed at predicting and quantifying these impacts, and suggesting mitigation measures.

This thesis is focussed on improving current understanding of, and simulating pollutant transport, in the aquatic environment. In particular, bacterial pollution. A number of 2D and 3D hydro-environmental models were developed to predict faecal bacterial levels for a pilot study in Swansea Bay, UK, in order to further current understanding of bacterial processes and evaluate beach management practices.

Of these, a 2D model with an improved method of representing beach sources, and a 3D model with a depth-varying decay rate, were found to improve bacterial concentration predictions in the nearshore zone. These are therefore proposed as the preferred approaches when studying a shallow gradient beach located in in a macro-tidal region (such as Swansea Bay).

Furthermore, it has been shown that the designation of a single monitoring point for Swansea Bay bathing water may not be best practice, as the current sampling point is not representative of the whole bathing water.

In addition, an experimental study was conducted to monitor turbulent diffusion in a uniform channel under low Reynolds number steady flow conditions by tracking the position of floating particles. It was shown that the aspect ratio of a flow and the bed roughness play

an important role in governing the scale of turbulent diffusion and, in the experiential set-up, were more indicative than the measurable turbulent flow properties. Results from this experiment were cross-validated with 2D numerical model simulations and the findings may assist in the prediction of pollutant transport in surface waters.

Contents

The publications derived from the work undertaken in this thesis are one conference paper and one conference poster. In addition, oral and poster presentations have been given to both academics and industry representatives at number of events.

Conference paper

1. **Jonathan King**, Reza Ahmadian, Amyrhul Abu Bakar, Roger A. Falconer. Modelling the impact of microbial sources on water quality: A study on the designated sampling point in Swansea Bay, UK. *36th IAHR World Congress.* Kuala Lumpur, Malaysia. 2017

Conference poster

1. **Jonathan King**, Reza Ahmadian, Amyrhul Abu Bakar, Roger A. Falconer. Modelling the transport and decay of Faecal Indicator Organisms in Estuarine and Coastal Waters. *13th UK Young Coastal Scientists and Engineers Conference (YCSEC).* University of Bath, UK. 2017

Nomenclature

Abbreviations

1D	One-dimensional
2D	Two-dimensional
3D	Three-dimensional
E.coli	*Escherichia coli*
Enterococci	*Intestinal enterococci*
ADCP	Acoustic Doppler Current Profiler
ADE	Advection-Diffusion Equation
ADV	Acoustic Doppler Velocimeter
ANN	Artificial Neural Network
BODC	British Oceanographic Data Centre
BW	Bathing water
C2C	Cloud to Coast
CD	Chart Datum
CFD	Computational Fluid Dynamics
CFL	Courant-Friedrichs-Lewy
cfu	colony forming units
Concn.	Concentration
CPU	Central Processing Unit
CSO	Combined Sewer Overflow
DA	Depth-averaged
DSP	Designated Sampling Point
FC	Faecal Coliforms
FD	Finite difference

FIO	Faecal Indicator Organism
FN	False negative
FOV	Field of view
FP	False positive
FS	Faecal Streptococci
GI	Gastro-intestinal
GPS	Global Positioning System
GPU	Graphics Processing Unit
H	High tide sampling location
HAT	Highest Astronomical Tide
HPC	High-performance computing
L	Low tide sampling location
LAT	Lowest Astronomical Tide
LiDAR	Light Detection and Ranging
M	Mid-tide sampling location
MPI	Message Passing Interface
MSL	Mean Sea Level
MST	Microbial Source Tracking
NRW	Natural Resources Wales
NSE	Nash Sutcliffe Efficiency
NTU	Nepthalotropic Turbidity Units
OD	Ordnance Datum
OpenMP	Open Multi-processing
ppt	parts per thousand
PTV	Particle tracking velocimetry
PVC	Polyvinyl chloride
qPCR	Quantitative polymerase chain reaction
rBWD	revised Bathing Waters Directive [European Parliament, 2006]
RMSE	Root mean square error
TN	True negative
TP	True positive
UV	ultraviolet (light)
VBNC	Viable But Non-Culturable

WWTP	Waste Water Treatment Plant	
Dimensionless parameters		
C_D	Coefficient of discharge	
C_S	Smagorinsky constant	
D	Distribution coefficient for suspension	
D_w	Distribution coefficient for distilled water	
$D_{FC,oral}$	Oral dosage of FIO ingestion	
Fr	Froude number	
fUV	Fraction of UV radiation in visible light	
N	Number of particles	
n	Manning's number (bed roughness)	
P	Probability of contracting GI symptoms	
Re	Reynolds number	
S	Skewness in particle distribution	
S_f	Friction slope	
S_o	Bed slope	
TI	Turbulence intensity	
Greek Symbols		
α	Proportionality constant / coefficient of irradiation	$-$
α_I	Bacterial dependent coefficient of irradiation	$-$
ϵ	Non-dimensional coefficient of turbulent diffusion	$-$
κ	Von-Karman coefficient	$-$
λ	Aspect ratio	$-$
ν	Velocity diffusivity	m^2/s
ν_T	Tracer diffusivity	m^2/s
ρ	Density	kg/m^3
ρ	Fluid pressure	N/m^2
σ	Standard deviation in particle cloud position	m
σ^2	Variance in particle cloud position	m^2
τ	Shear stress	N/m^2
θ	Empirical coefficient for effect of temperature on decay	$-$
Roman Symbols		
b	Flow width	m

C	Depth averaged concentration	$cfu/100ml$
c	Concentration	$cfu/100ml$
C_{sal}	Salinity	ppt
DL	Day length	d
g	Acceleration due to gravity	m/s^2
h	Total depth of water	m
h_c	Water head above weir crest	m
h_w	Weir height	m
I	Light intensity / irradiance	W/m^2
I_0	Surface light intensity	W/m^2
K	Coefficient of turbulent diffusion for floating particles	m^2/s
k	First order decay rate	$1/d$
k_b	Base / dark mortality coefficient	$1/m$
k_d	Lumped bacterial mortality coefficient	$1/m$
k_e	Light extinction coefficient	$1/m$
k_r	Radiation related mortality constant	$m^2/W/d$
k_{cl}	Chloride related mortality constant	$m^3/g/d$
P_s	Percentage of seawater	
Q	Flow rate / discharge	m^3/s
R	Hydraulic radius	m
SD	Secchi depth	m
ss	Suspended sediment concentration	mg/l
t	Time	s
T_{90}	Time taken for the concentration to reduce by 90%	h
TKE	Turbulent kinetic energy	m^2/s^2
U	Depth-averaged flow speed in the x-direction	m/s
u	Flow speed in the x-direction	m/s
$U*$	Shear velocity	m/s
V	Depth-averaged flow speed in the y-direction	m/s
v	Flow speed in the y-direction	m/s
W	Depth-averaged flow speed in the z-direction	m/s
w	Flow speed in the z-direction	m/s
x	Longitudinal flow direction (horizontal space component)	m

y	Transverse flow direction (horizontal space component)	m
z	Vertical flow direction (vertical space component)	m
Z_S	Free surface elevation	m

Superscripts

$(\cdot)'$	Temporally fluctuating variable
$(\cdot)''$	Spatially fluctuating variable
$\overline{(\cdot)}$	Temporally averaged variable
$\overline{\overline{(\cdot)}}$	Spatially averaged variable

Subscripts

$()_0$	Variable at time zero / variable at the bed (i.e. z = 0, whereas z = h at the surface)
$(\cdot)_b$	Base variable (in dark conditions)
$(\cdot)_d$	Combined death rate
$(\cdot)_i$	Light / irradiance dependent variable
$(\cdot)_o$	Reference value
$(\cdot)_s$	Equivalent sediment dependent variable
$(\cdot)_T$	Temperature dependent variable
$(\cdot)_t$	Variable at time t
$(\cdot)_x$	Variable aligned with the x-direction
$(\cdot)_y$	Variable aligned with the y-direction
$(\cdot)_z$	Variable aligned with the z-direction
$(\cdot)_{20}$	Variable at 20 °C
$(\cdot)_\alpha$	Variable averaged over one day
$(\cdot)_{atm}$	Atmospheric variable
$(\cdot)_{exp}$	Experimentally observed variable
$(\cdot)_{pH}$	pH dependent variable
$(\cdot)_{sal}$	Salinity dependent variable

List of Figures

List of Tables

Chapter 1

Introduction

1.1 Overview

The health of near shore coastal waters is a topic of great concern globally. As a result of population growth and industrialisation, the number of polluted discharges into water bodies has increased over the 20th and 21st centuries, at much detriment to the aquatic environment. Of primary concern in this thesis are those containing faecal matter, such as overland run-off and sewage discharges, into rivers, lakes and seas. Such contamination has far reaching consequences, which include; human health impacts through recreational activity [Surfers Against Sewage, 2018] and the consumption of polluted food shellfish [The Guardian, 2001], reduced tourism, and economic losses.

It is therefore important to address this issue by determining the primary sources of pollution at any one location, developing an understanding of the mechanisms which lead to adverse water quality, beach closure, and implementing mitigation strategies; problems which which this thesis aims to address.

One of the most widely recognised indicators of beach quality is the Blue Flag award. This is a globally used standard which rewards well managed beaches, with good water quality and public services [UK Beach Guide, 2018].

One of the key factors used to determine the designation of Blue Flag status is bathing water quality. The existing legislation applicable in the EU is the

revised Bathing Waters Directive [European Parliament, 2006] (see Section 1.1.1), which ensures the monitoring of water quality and defines acceptable standards, based on human health risk. This information is made publicly available through channels such as the Marine Conservation Society [2018] Good Beach Guide and it is therefore in the interest of authorities to invest in measures aimed at reducing aquatic pollution.

The recognition provided by a Blue Flag award can significantly increase the number of visitors to a region [BBC, 2006; Scottish Government, 2018], providing a considerable economic boost, and it is therefore in the interest of governing authorities to seek and retain this. For example, domestic and international visitors to the seaside contributed £6 billion to the UK economy in 2017 [BBC, 2017; Visit Britain, 2017]. Along the 12,000 km of coastline in the UK, there are 606 designated bathing waters, of which, 124 were awarded Blue Flag status in 2018 Blue Flag [2018].

However, designation is awarded annually, and if any issues are identified but no remedial action is taken, causing a loss of Blue Flag status, the consequences can be damaging. For example, reduced tourism and income [Bussi et al., 2017]. To highlight this issue, of the 68 English beaches awarded blue flag status in 2017, 3 lost this designation in 2018 Country Living [2018]. In a recent study, the Scottish Government [2018] predicted a loss of £3 million per year should bathing water quality not be maintained at an acceptable level at popular beaches.

Another financial incentive is the healthcare savings associated with reduced exposure of beach goers to contaminated water [Given et al., 2006]. For example, DeFlorio-Barker et al. [2018] estimated that recreational waterborne illnesses cost the US economy $2.2 to $3.7 billion every year; no data was found to estimate equivalent losses in the UK.

Therefore, in order to facilitate efforts to reduce coastal pollution and improve the quality of bathing waters (in the UK and globally), much research has been carried out in recent years. This has been aimed at improving our understanding of fundamental processes, developing predictive tools, and assessing beach monitoring and management practices. This thesis is intended to support the existing body of published literature within these fields, the outcomes of which will assist engineers in setting up more accurate water quality models and provide advice

on the assessment of bathing waters.

1.1.1 Bathing water assessment: current practice and legislation

The revised Bathing Waters Directive (rBWD, [European Parliament, 2006]), was introduced by the European Parliament in 2007 following guidelines released by the World Health Organisation on safe standards for recreational waters [World Health Organization, 2003a]. It was enforced at the close of the 2015 bathing season and requires member states to ensure that all bathing waters are of 'sufficient' quality. Water quality may be classified as; 'excellent', 'good', 'sufficient' or 'poor', based on the monitored concentration of two Faecal Indicator Organisms (FIOs); *Escherichia coli* and *Intestinal enterococci* (herein referred to as *E.coli* and *Enterococci*, respectively), in colony forming units per 100ml (cfu/100ml). These limits are presented in Table 1.1.

Table 1.1: FIO limits for coastal waters and transitional waters [European Parliament, 2006]

	Quality		
Parameter	**Excellent**	**Good**	**Sufficient**
Intestinal enterococci (cfu / 100ml)	100 (*)	200 (*)	185 (**)
Escherichia coli (cfu/100 ml)	250 (*)	500 (*)	500 (**)

(*) based on a 95-percentile evaluation, (**) based on a 90-percentile evaluation

While they do not directly cause adverse health effects in humans, they may be used as an index to indicate the presence of disease causing pathogens found in faecal matter; for example *Salmonella*, which is linked to gastroenteritis [World Health Organization, 2003a,b].

The directive requires the concentration of these organisms to be monitored over consecutive bathing seasons (May to September), in accordance with a sampling calendar. This is carried out at a single Designated Sampling Point (DSP). However, it should be noted that recent research has raised questions regarding

the rBWD monitoring criteria, suggesting that it should be more specific in defining the location and time of sampling due to temporal and spatial variability in FIO levels [Aragones et al., 2016; Clements et al., 2015].

Samples showing abnormally elevated concentrations, caused as a result of short-term pollution incidents (contamination attributable to a cause, expected to last less than 72 hours), may be disregarded and retaken [European Environment Agency, 2005]; for example after heavy rainfall. However, in order for these events to be identified the event must be predictable and therefore attributable to a cause.

Efforts must also made to reduce the risk of bather exposure to contaminants in addition to providing regular information on bathing water quality, as detailed in the bathing water management plan. In addition, the directive requires the public be made aware of short term pollution incidences, thereby making public health a key driver for prediction.

Due to the time lag between the collection and assessment of individual samples, monitoring in this manner is not a practical way of providing rapid public feedback to prevent exposure [Feng et al., 2015]. To enable accurate and fast dissemination of information it is therefore in the interest of the governing authority to develop predictive tools to provide water quality forecasts and warning systems [Bedri et al., 2014b, 2016; Chen and Liu, 2017; DHI, 2017a,b].

Not only would this comply with the rBWD but it could enable the identification, reduction and removal of major pollution sources, increasing the likelihood of a bathing water being assigned Blue Flag status [Bedri et al., 2015; Lea and Section, 1996].

1.1.2 Tools for water quality assessment and prediction

Sources of pollution may be characterised as diffuse or point source [de Brauwere et al., 2011; Feng et al., 2015; Servais et al., 2007] and include; catchment runoff containing livestock faeces [Campos et al., 2013], intertidal sand [Yamahara et al., 2009], sea birds (gulls) [Alm et al., 2018; Araújo et al., 2014] and Waste Water Treatment Plant (WWTP) discharges [Servais et al., 2007]. Identifying the most prevalent type of pollution is crucial to improving water quality. Methods exist

which enable the identification of specific microbial sources (for example, dairy cattle or gull faeces), referred to as microbial source tracking (MST) methods [Gómez-Doñate et al., 2016; Raith et al., 2013]. However, such information cannot be used to make quantitative predictions of bacterial levels and only facilitates beach improvement.

Other measures are often required to isolate specific sources with a direct impact on a bathing water; for example, computational mathematical models, which in addition, can be used to predict water quality. Statistical models, such as that employed in Swansea Bay [Aberystwyth University and University College Dublin, 2018], are based on environmental data and are capable of accurately predicting bacterial FIO concentrations in real-time [Thoe et al., 2014]. However, these employ 'black-box' approaches [Crowther et al., 2011; Thoe et al., 2014] and cannot be used for primary source identification, nor can they properly capture key input parameters.

Alternatively, deterministic models may be used, which are based on the governing equations of; flow, solute transport, and bacterial decay. Compared to statistical models they allow users to more easily determine and quantify the impact of individual sources (for example; point sources such as sewage outfalls), proving a useful tool for bathing water management [Buer et al., 2018]), and allow the inclusion of new system dynamics or future developments in regions of interest [Evans and Langley, 2017]. It is for these reasons that this study is focussed on the use of deterministic models.

A wide variety of options are presented to the modeller when choosing a piece of software. In many cases, universities will use in-house code or open source software, which is freely available. While in-house code may have distinct advantages over commercial packages, it is often unavailable to other institutions. Therefore, free open-source software is preferable, as any developments can be easily shared within the community. For these reasons, the open-source software package TELEMAC was used [Hervouet, 2007], which is widely used for hydro-environmental modelling applications and has a large developer community.

Similarly, many companies will use commercial software which they have experience in using or have developed themselves. Depending on the scenario being modelled, it may be adequate to use in-built model functions or necessary to de-

velop the code further. Often it is not clear what is the best method, which in the case of engineering consultancies, frequently results in the adoption of simplified methods, regardless of whether they are sufficient. It is therefore in the interest of the research community to conduct more detailed studies and assessments in order to advise on and affect best practice, for wider reaching impact.

1.1.3 High performance computing

In an age where high performance computing (HPC) is becoming commonplace, the ability of models to run in parallel (i.e. on multiple central processing units (CPUs)), is desirable. Many codes have been written using Open Multi-Processing (OpenMP), or Message Passing Interface (MPI), standards which can significantly reduce the run-time of a simulation. In doing so, the application of such techniques facilitates the use of multi-scale and high resolution models (for example, 3D hydro-environmental models), and is is for this reason that the supercomputing facilities run by HPC Wales and ARCCA were used to for the work presented herein (see ARCCA [2018] and Supercomputing Wales [2018] for more information).

It is of interest to the reader to note that in order to increase computational efficiency and reduce model run-time further, the next step in parallelism is the use of graphics processing units (GPUs) instead of CPUs. However, at the time the work herein was carried out, no available software packages made use of this.

1.1.4 Pollution and turbulent diffusion

Population increase, in the UK and internationally, has placed a greater demand on the aquatic environment through increased industrial activity, waste production, and recreation, which in turn has further increased human exposure to pollution. In order to tackle this issue it is necessary to improve our understanding of the mechanisms governing the fate and transport of pollutants in such environments. Increases in computational power and the introduction of new experimental techniques have made it possible to study the motion of floating pollutants at high temporal resolution in low Reynolds flows. This allows for the

extension of previous studies to cover a wider variety of flow conditions which reflect those found in the natural environment, while retaining consistency between experiments in order for direct comparison.

1.2 Research aims and objectives

The prediction of water quality within bathing waters is currently not possible to a sufficient level of accuracy using hydrodynamic (i.e. deterministic) models in order for practical application in the prediction of short term pollution incidents (classified as such under the rBWD), or to provide sub-daily water quality information to the public.

The work contained within this thesis aims to address these shortcomings and contribute to the existing literature by meeting the following objectives:

- To develop new 2D and 3D models for the dynamic prediction of bacterial decay at a high temporal and spatial scales;
- To provide recommendations on the most suitable bacterial models when studying a shallow gradient beach or a macro-tidal environment;
- To investigate the specificity of the rBWD in a case study of Swansea Bay, and determine suitable monitoring strategies for assessing compliance and notifying the public of health risks;

The outcomes of this work provide advice on best practice and allow the engineering modelling community to make more informed choices in future studies. Furthermore, the work was carried out using the open source software TELEMAC, contributing to the range of existing case studies which validate the model performance.

To support the above aims an experiential study was carried out to investigate turbulent diffusion in steady flow conditions. This was focussed on addresses inconsistencies in previous experimental studies and determining the impact of the following parameters on the non-dimensional turbulent diffusion coefficient:

- Bed/boundary roughness

- Aspect ratio of the flow field
- Turbulent properties of the flow field

In doing so it contributes to the parametrisation of turbulence models in order to better predict the motion of pollutants. The findings are applicable to a wide range of hydro-environmental studies, from pollution in small streams to drogue transport in oceans.

1.3 Outline of thesis

The research presented herein is divided into seven chapters, described as follows:

Chapter 2 provides an overview of the published literature, including published reports, related to the research presented in Chapters 4, 5 and 6. This is divided into a number of subsections covering; hydrodynamic / environmental modelling, bacterial decay kinetics, pollution and turbulent diffusion, and describes the progress which has been made to date while highlighting the knowledge gaps which this thesis aims to fill.

Chapter 3 describes the governing equations and theory which form a technical basis for the research presented in Chapters 4, 5 and 6.

Chapter 4 describes an experimental study into the non-dimensional turbulent diffusion coefficient (a parameter used in numerical models), for non-uniform steady flow conditions. It was carried out at the Department of Hydraulic Engineering, Tsinghua University, China. Expanding on previous work on turbulent diffusion theory, a controlled laboratory study was conducted to track the movement of floating PVC particles in a shallow depth flume. This was cross-validated with a numerical study which replicated the experiment using TELEMAC-2D. This provides a context for the following chapters though introduction of turbulence and dispersion and how these are parametrised in numerical models.

Chapters 5 and 6 investigate the use of spatially and temporally variable decay rates in FIO models, using both two-dimensional (2D) and three-dimensional (3D) approaches, with application in a multi-scale hydro-environmental model of Swansea Bay, UK. Chapter 5 describes the model developments (which compliment and expand on the literature), identifies those which are most suitable, and informs on best practice when modelling the transport and decay of FIOs in nearshore coastal waters. Chapter 6 applies these refinements to investigate the compliance of Swansea Bay bathing water with the rBWD.

Chapter 7 contains a summary of the research presented in this thesis, draws together the main conclusions and provides recommendations for bathing water management, operation, and future work.

Chapter 2

Literature review

2.1 Predictive tools for bathing water assessment

Predictive tools for bathing water assessment generally include two major categories; deterministic hydro-environmental models and data driven models. Data-driven models, otherwise known as 'black-box' models, are useful tools for the real-time prediction of water quality. These include linear or multi-variable linear regression models, classification trees and artificial neural networks (ANNs). Predictions are based on key environmental parameters such as; rainfall, river levels, light intensity, time of day, tidal phase and turbidity [Chu et al., 2011; de Souza et al., 2018a; Gronewold et al., 2009; Thoe et al., 2014].

Examples include the models used to provide water quality foreacsts in Cardiff Bay and Swansea Bay, which are used to inform the public how the (predicted) water quality compares with the rBWD guidelines throughout the day [Cardiff Harbour Authority, 2018; Wyer et al., 2015]. Driving parameters include; solar radiation, tidal phase, river discharge and wind speed. de Souza et al. [2018a,b] developed a regression model to predict the FIO concentration in water and mussles in Santa Catarina Bay, Brazil. The model was based on; the human population in nearby catchments, rainfall, solar radiation and temperature. When

all parameters were considered, FIO concentrations were well predicted for the training period, however no significant correlation was found using individual parameters. Thoe et al. [2014] compared five types of models to predict FIO concentrations at Santa Monica Beach, California. The models were based on; antecedent FIO concentrations, rainfall, tide and wave measurements, temperature and storm drain conditions. Of the models tested the classification tree and ANN preformed the best. Zhang et al. [2012] developed an ANN based on 15 environmental variables to predict *Enterococci* concentrations at Holly Beach, Louisiana, USA. The model was capable of predicting concentrations with acceptable accuracy and preformed better than predictions made using a linear regression model.

From this limited review of the available literature it can be seen that statistical models are not only widely used but useful tools for water quality prediction. However, statistical models first undergo 'training' in which they are fed a representative data sample and calibrated. They are then tested on new data and assessed using various performance measures (see Bennett et al. [2013]). Herein lie two problems. Models may be over-trained or over-parametrised such that they perform well in training and poorly when tested on unseen data [García-Alba et al., 2018; Gardner and Dorling, 2000; Karul et al., 2000]. For example, a model trained using a dataset contianing only low (i.e. 'good') bacterial concentrations will perform poorly when used to predict high becerial concentrations that will result in beach failure (with respect to the rBWD). While the extent of this can be mitigated, unless a linear model is used, when it is tested using anomalous or extreme data outside of the calibrated parameter range, it will produce erroneous results. Furthermore, if the underlying system dynamics change then the model must be re-trained. As such, statistical models cannot be used to predict the impact of proposed developments; for example, the Swansea Bay Tidal Lagoon (see Evans and Langley [2017]).

Sensitivity analysis may be used to relate model predictions to specific parameters or predictor variables [Norton, 2015], and multi-variate or uncertainty analysis may be used to track the propagation of parameter uncertainty and interdependence between variables McIntyre [2004]. However, while these offer a means to improve model accuracy, they do not further our understanding of

the governing system dynamics as the cause-effect relationships remain unknown. Therefore, at the time of writing, they have limited application in identifying and reducing, or eliminating, key sources of pollution. This highlights the benefits of deterministic hydro-environmental models.

2.1.1 Hydro-environmental modelling

Over the past few decades, many computational hydro-environmental models have been developed to solve the governing equations of flow and solute transport. These can be resolved in 3D or simplified through depth or area integration; in the case of flow, to yield the 2D shallow water equations or 1D St Venant equations, respectively [Liang et al., 2007]. Examples include; CCHE3D [Chao et al., 2008], the Delft3D suite [Deltares, 2014b], DIVAST [Falconer, 1986], TRIVAST [Lin and Falconer, 1996], EFDC [Hamrick, 1992], FVCOM [Chen, 2010], MIKE11 [DHI, 2013a], MIKE3 FM [DHI, 2013b], SLIM [de Brauwere et al., 2014a; de Brye et al., 2010], TELEMAC-MASCARET [Hervouet, 2007] and TIDE3D [Walters, 1987].

1D models are capable of simulating flow within a longitudinal direction, for example in rivers and streams, however are insufficient when flow is not constrained to a primary direction in the horizontal plane. In such cases, a 2D or 3D approach is required. For example, when studying coastal and estuarine environments [de Brye et al., 2010] where flow is dependent on complex bathymetries or coastline geometry [Olbert et al., 2012; Wu et al., 2005] . Where vertical flow occurs and the effects or presence of a thermocline, halocline or stratification are significant then 3D models are used [Bedri et al., 2014b; Chao et al., 2008; Olbert et al., 2011], otherwise the problem is simplified to a 2D case, such as in a well-mixed estuary [Liang et al., 2010].

2D and 3D models solve discretized numerical approximations of the governing equations across a computational domain, representing the area of interest. Numerical formulation of the equations may use different levels of accuracy. However, first and second order schemes are mainly used in practical cases [Anastasiou and Chan, 1997; Brufau et al., 2002; Liang et al., 2010]. These may be explicit [Gascón and Corberán, 2001; Liang et al., 2010], implicit [Liang et al., 2006], or semi-implicit [Rogers et al., 2003], and use upwind or central difference numerical

approximations [Anastasiou and Chan, 1997; Brufau et al., 2002]. Some examples are; MUSCL [Sanders, 2002], ULTIMATE QUICKEST [Liang et al., 2010], total variation diminishing (TVD) schemes [Gascón and Corberán, 2001; Liang et al., 2006; Rogers et al., 2003] and alternating direction implicit (ADI) schemes [Ahmadian et al., 2015; Deltares, 2014b; Liang et al., 2006].

The grid over which the solution is calculated may be either structured, and solved using finite difference methods or finite volume methods, or unstructured, and solved using finite volume or finite element methods [Anastasiou and Chan, 1997; Avdis et al., 2018; Brufau et al., 2002; de Brye et al., 2010; Simões, 2011]. While finite difference methods are simple to implement and solve, regular structured grids are incapable of accurately capturing domain or shoreline complexities. The use of curvilinear grids provides an improved method of capturing domain geometry while retaining grid structure [Morianou et al., 2016; Ye and McCorquodale, 1997], and nested or quadtree grids may be used to increase grid resolution in areas of interest [Borthwick et al., 2001; FALCONER, 1990; Liang et al., 2008; Park and Borthwick, 2001; Zhang and Wu, 2011]. However, unstructured grids are often the preferred choice where complicated boundaries exist [de Brye et al., 2010; Masters et al., 2015]. These are generally made up of triangular elements [Bomminayuni, 2015; Chen and Liu, 2017; Samaras et al., 2016], and allow for multi-scale models with a smooth transition from regions of low to high mesh resolution through the use of nesting techniques [Plaza et al., 1996; Yu et al., 1998]. One example of a recent departure from this practice has been made in Delft 3DFM, which allows the combination of unstructured and structured grids using pentagons [Deltares, 2016].

Of the available models, this study used TELEMAC-2D and 3D; modules of the TELEMAC suite, developed by Électricité de France [Galland et al., 1991; Hervouet, 2007]. These are freely available, open-source, unstructured, finite element models, with good performance in tidal estuaries and widely used water quality components [Bedri et al., 2014a,b; Jones and Davies, 2006; Malcherek, 2000; Matta et al., 2017; Samaras et al., 2016; Smolders et al., 2015], which make use of MPI for highly parallel computing [Moulinec et al., 2011], and are well suited for application in Swansea Bay; with a complex shoreline geometry and dynamic tidal reigime. The TELEMAC suite of solvers has been widely used in

the field of hydro-environmental engineering and to date has seen application in a variety of studies. This is in part due to the accessibility of the code and the presence of an on-line community to discuss and share model developments. For example, using TELEMAC-2D; Bourban et al. [2014] and Hashemi et al. [2015] studied the potential for tidal energy generation in the UK; Jones and Davies [2005, 2006] studied wind induced circulation in the Irish Sea; Villaret et al. [2013] and Nguyen and Yun [2016] investigated morphodynamic and sediment transport processes in rivers, channels and beaches. Studies using TELEMAC-3D include; an investigation into delta dynamics in Northern Italy [Corti and Pennati, 2000], a model of salinity dynamics in the Scheldt Estuary [Smolders et al., 2015]; a case study into the effect of wind and temperature induced flows in the Itaparica Reservoir, Brazil [Matta et al., 2017]; and a study into water quality processes in lakes [Kopmann and Markofsky, 2000].

2.1.1.1 Previous studies

This section provides a brief overview of modelling studies which have been carried out to date to predict FIO concentrations in estuarine and coastal waters, which are often macro-tidal or highly turbid environmetns [Salomon and Pommepuy, 1990]. Due to the extensive literature on the subject, this discussion is not limited to studies using TELEMAC, however, reference has been made to these where possible. In addition, much of the published research within the field of hydro-bacterial modelling has been undertaken by a small number of academics and institutions, and the following paragraphs therefore attempt to link similar and connected studies together. Further details on the factors which govern bacterial decay and how this is calculated, including references, are given in Section 2.2.

Bedri et al. [2011, 2013, 2014a] carried out a series of studies using TELEMAC-2D and 3D, to investigate the effects of the mixed discharge from a Waste Water Treatment Plant (WWTP), and power plant, on water quality in Dublin Bay, Ireland. Salinity, temperature, *E.coli* concentration and wind effects were coupled within the hydrodynamic models. In the first study, Bedri et al. [2011] compared the 2D and 3D model predictions, having assigned a fixed rate for *E.coli* decay (i.e. a T_{90} value, constant throughout the simulation and not a function of any

other parameters). It was found that the 2D model was unable to account for stratification in the water column and under-predicted wind effects. Moulinec et al. [2011] also reported TELEMAC-2D to be incapable of predicting complex flows, resulting in the under-prediction of *E.coli* transport rates, therefore requiring higher calibrated decay rates compared to the 3D model.

In order to predict bacterial concentrations at higher temporal resolutions, much work has been carried out on the application of variable decay rate models in hydro-environmental studies. Bedri et al. [2013] used that proposed by Mancini [1978] and found a slight improvement in *E.coli* predictions over the use of a constant T_{90} value. The model was then applied by Bedri et al. [2015] to another site in Ireland to investigate the impact of a new WWTP management strategy under wet and dry weather scenarios, in relation to rBWD limits. Similarly, Boye et al. [2014] found that the inclusion of a variable decay rate (as a function of temporally varying parameters), provided better predictions of *E.coli* concentrations in a linked 1D-2D model.

With the benefits of variable decay rate models having been etablished, Gao et al. [2015] conducted a similar study to Boye et al. [2014] and found that tidal cycles have a strong influence on the *E.coli* distribution within estuaries. Huang et al. [2015a,b, 2017] extended this work further by developing a linked catchment-coastal model and found that bacterial-sediment interactions and fluxes are key FIO transport mechanisms, and that their inclusion in models is necessary for the accurate prediction of FIO concentrations.

The Bristol Channel and Severn Estuary, UK is a highly turbid [Stapleton et al., 2007b], macro-tidal envrionment [Bakar et al., 2016], that has been the focus of much research. This includes the work of Schnauder et al. [2007] who used a 2D model to predict the *E.coli* distribution in Carmarthen Bay as a result of 14 land-use management strategies. Bacterial decay was modelled using a simplified approach with single T_{90} value. Gao et al. [2011b, 2013] used an integrated 2D hydrodynamic-sediment transport model to predict the *Enterococci* distribution in the estuary, applying a variable decay rate linked to sediment dynamics, as proposed by Stapleton et al. [2007a]. It was found that in wet weather conditions, river flows were the dominant source of bacteria and more important than sediment flux processes. The most recent study found by the author was carried

out by Bakar et al. [2016, 2017], who studied the inter-tidal environment of the Loghour Estuary and modelled diffuse bacterial loading caused by animal grazing in the salt-marshes, using a spatially varying day/night decay rate.

The Scheldt river and estuary are another river-sea continuum which have seen much interest (see Ouattara et al. [2011]; Smolders et al. [2015]). As a highly turbid environment [de Brauwere et al., 2011], much of this has been related to the simulation of sediment transport processes [Gourgue et al., 2013; van Kessel et al., 2011]. One particular example is the work of de Brauwere et al. [2011, 2014a] and de Brye et al. [2010] who developed a coupled 1D-2D model, linked to a catchment model, to predict *E.coli* concentrations throughout the estuary as a result of different wastewater management strategies. The model was capable of producing long term *E.coli* predictions to within acceptable accuracy but was unable predict variations in *E.coli* concentration at a fine spatial or temporal scale.

2.1.2 Integrated catchment modelling and assessment

Some of the work discussed previously, such as that by de Brauwere et al. [2014a]; Huang et al. [2017] and [Schnauder et al., 2007], has touched on the integration of catchment and hydro-environmental models to determine the impact of land use or wastewater management strategies on pollution levels in receiving waters. Such studies assist in the implementation of River Basin Management Plans, as instructed in the Water Framework Directive (WFD) [European Parliament, 2000], to tackle pollution at the catchment scale [European Environment Agency, 2016].

With regard to bathing waters, this is important in order to establish the impact of activities [Kay et al., 2008] such as agriculture [Cuttle et al., 2016], domestic, and industrial wastewater discharges [Huang et al., 2018]. This is crucial in identifying the pollution sources which are most detrimental to water quality, or are the main reasons for non-compliance with the rBWD, and in order to implement the most effective mitigation strategies.

For example, Bougeard et al. [2011] coupled the Soil and Water Assessment Tool (SWAT) catchment model with the 2D hydrodynamic model MARS to in-

vestigate the impact of *E.coli* fluxes on water and shellfish quality in the Daoulas Estuary, France. The dominant processes were identified and the detrimental effect of rainfall events due to the flushing of pollutants and livestock manure from the catchment, including the time required for the estuary to recover, was studied [Crowther et al., 2011].

In a more recent and comprehensive study, Bedri et al. [2014b, 2016] coupled the Danish Hydraulic Institute (DHI) models; NAM (a rainfall-runoff model), MIKE11 (1D river model) and MIKE3 FM (3D finite volume model), to predict the impact of rainfall events on coastal water quality in Bray, Ireland, in real-time. The model was driven by 5 days of real-time rainfall forecasts, and included FIO loads from agriculture (i.e. animal faeces) and WWTP discharges. Bacterial levels were found to rise rapidly after rainfall events, after which they reduced at a slower rate. Comparison between predicted and recorded FIO levels showed the model using real-time rainfall data to be more reliable in predicting exceedance of the rBWD 'excellent' limit, confirming that rainfall is indicative of coastal water quality.

2.2 Bacterial modelling and decay kinetics

Bacterial decay is known to be a function of; salinity, temperature, sunlight, turbidity and pH [Auer and Niehaus, 1993; Bedri et al., 2015; Hipsey et al., 2008; Kashefipour et al., 2006; Kay et al., 2005; Solic and Krstuloviic, 1992]. There have been many experimental studies to date, both *in-situ* and laboratory based, to determine the influence of one or number of these parameters, and there exist a wide variety of models to calculate decay [Crane and Moore, 1986; de Brauwere et al., 2014b]. However, although the choice of decay mechanism can significantly impact model uncertainty [Gronewold et al., 2009], it is not always clear which is the most appropriate for any given scenario, and selecting a method to represent those which are observed, or expected to prevail at the site of interest, often proves a difficult choice. The following section summarises the available literature and compares the methods used. Note that the treatment used for *E.coli* and *Enterococci* is applicable for other FIOs and as such this work is also included.

The decay of FIOs is generally considered to be a first-order process which can be represented by Chicks Law [Chick, 1908]:

$$\frac{c_t}{c_0} = e^{-kt} \tag{2.1}$$

where c_0 is the concentration at time zero (cfu/100 ml), c_t is the concentration at time t (d) and k is the first-order decay rate (1/d).

There is some evidence that bacteria undergo biphasic decay, with an initially stagnant inactivation period followed by decay (see Section 2.2.2.3), or an initial period of faster decay followed by another period of slower decay [Bakar et al., 2018; Blaustein et al., 2013]. However, the use of such decay models is limited and is not discussed herein.

In the majority of studies, Equation 2.1 is more commonly represented by the differential first-order decay equation [Chapra, 1997; Thomann and Mueller, 1987]:

$$\frac{\partial c}{\partial t} = -kc \tag{2.2}$$

where the first-order decay rate k, is the gradient of the log-linear plot of log concentration versus time. This can be simplified as shown in Equation 2.3 using a natural logarithmic scale respectively [Kashefipour et al., 2002a,b; Kay et al., 2005; Stapleton et al., 2007a]:

$$T_{90} = \frac{2.303}{k} \tag{2.3}$$

The decay rate is now represented more meaningfully by the T_{90} value (d); the time required, in days, for the concentration to reduce by 90% [Guillaud et al., 1997].

Stapleton et al. [2007a] carried out a study on water samples taken from the Severn Estuary and as a result of laboratory experiments, the T_{90} decay rate for

Enterococci under light and dark conditions was found to follow Equations 2.4 and 2.5 respectively:

$$LogT_{90} = 0.0047 * Turbidity + 0.677 \pm 0.2070 \tag{2.4}$$

$$LogT_{90} = 0.0047 * Turbidity + 1.237 \pm 0.199 \tag{2.5}$$

where T_{90} is in hours (h) and turbidity is in nepthalotropic turbidity units (NTU), defined as:

$$Turbidity = 139.479 * Log(ss) - 244.736 \pm 32.678 \tag{2.6}$$

where ss is the suspended sediment concentration (mg/l).

To relate the T_{90} decay rate to both turbidity and variable light intensity Equations 2.7 to 2.10 were used, obtained from regression analysis of experimental data:

$$T_{90} = T_{902} + (T_{901} - T_{90*1}) \tag{2.7}$$

$$T_{901} = \frac{ln10}{K_B * 60 * I} \tag{2.8}$$

$$T_{90*1} = \frac{ln10}{K_B * 60 * I^{exp}} \tag{2.9}$$

$$LogT_{902} = (0.0047 * Turbidity) + 0.677 \tag{2.10}$$

where I is the sunlight intensity (W/m^2), I^{exp} is the fixed irradiance for the experiments (260±14 W/m^2), T_{901} is the sunlight dependent *Enterococci* mortality rate, T_{90*1} is the *Enterococci* mortality rate obtained from laboratory experiments, T_{902} is the turbidity related *Enterococci* mortality rate and $K_B = 1.1 \times 10^{-5}$.

Alternatively, some studies link the T_{90} value to light intensity only. Bellair et al. [1977] carried out *in-situ* experiments on the decay of faecal coliform in seawater, Sydney, Australia, and found that the T_{90} decay rate was related to solar radiation by Equation 2.11:

$$T_{90} = 3.4I^{-0.42} \tag{2.11}$$

where irradiance I has the units of MJ/m^2.

Guillaud et al. [1997] carried out *in-situ* experiments on the decay of *E.coli* along the French coast and found the T_{90} value to follow Equation 2.12, related to light intensity:

$$T_{90} = 53683\overline{I}^{-0.666} \tag{2.12}$$

where $\overline{I}$ is the mean light intensity in the water column. Note that the units specified for light intensity are as they appear in the referenced publication, hence the difference with Equations 2.11 and 2.7 to 2.10.

Similarly, Pommepuy et al. [1992], cited in Stapleton et al. [2007a], found the following relationship between T_{90} and light intensity for Faecal Coliforms (FC):

$$T_{90} = 1.2 \times 10^4 I_n^{-0.56} \tag{2.13}$$

where I_n is the light intensity received by bacteria ($\mu E/m^2/h$).

2.2.1 First order decay processes

In order to separate the effects of the influential parameters on bacterial die-off, it is convenient to decompose the decay rate into multiple variables. These can be treated separately and then combined into a single value. Chapra [1997] defined the combined decay rate (k) as:

$$k = k_T + k_i + k_s \tag{2.14}$$

where k_T, k_i and k_s are the temperature, light and equivalent sediment dependent decay rates respectively (see Sections 2.2.1.1, 2.2.1.3 and 2.2.2.1). This assumes that the effect of each is independent.

Similarly, though excluding sedimentation effects, Deltares [2014a] define the combined decay rate as:

$$k = k_T + k_i \tag{2.15}$$

Kashefipour et al. [2006] chose to exclude temperature effects and defined the first-order decay rate as a function of a basic dark decay rate (k_b) and light intensity (see Equation 2.16). The value of the dark decay rate not only varies between species of bacteria but will also depend on the choice of die-off model [Gronewold et al., 2011].

$$k = k_b + k_i \tag{2.16}$$

Alternatively, irradiation effects may be considered a function of temperature [Chapra, 1997; Huang et al., 2015b] and the equation for combined effects,

excluding sedimentation losses, can be written as:

$$k = (k_b + k_{sal} + k_i)\,\theta^{(T-20)} \tag{2.17}$$

where k_{sal} is the salinity dependent decay rate (see Section 2.2.1.2), $k_b = 0.8$ (the base decay rate in fresh water at 20°C under dark conditions) and $\theta = 1.07$ for freshwater [Mancini, 1978].

A similar approach was used by McCorquodale et al. [2004] who defined the combined mortality as:

$$k = (k_{sal} + k_i + k_s)\,\theta^{(T-20)} \tag{2.18}$$

de Brauwere et al. [2011] ignored the effects of irradiance and defined the combined mortality based on temperature and sedimentation effects:

$$k = k_T + k_s \tag{2.19}$$

In addition, predation losses (see Section 2.2.2.2) may be included and treated as a temperature dependent parameter (Droste [1997], cited in Yang et al. [2008]):

$$k = (k_b + k_i + k_s + k_p)\,\theta^{(T-20)} \tag{2.20}$$

where k_p is the predation dependent decay rate.

In all these approaches the similarity with Equation 2.22 should be noted, whereby the terms in parentheses before θ can be considered equivalent to the first-order decay rate at 20°C (k_{20}).

Alternatively, rather than defining the decay rate for each factor, an empirically defined decay rate combining the effect of all factors may be used. Steets and Holden [2003] used a single death coefficient for all physiochemical factors

(k_d) and an additional sedimentation term (k_s):

$$k = k_d + k_s \tag{2.21}$$

The calibration of models such as this, with fewer decay parameters, may require an effectively larger value as the influence of multiple parameters is lumped together.

2.2.1.1 Temperature dependence

Temperature is known to positively correlate with decay, up to 30°C [de Brauwere et al., 2014b; Solic and Krstuloviic, 1992]. Its effect on the first-order decay rate is given by the following equation [Mancini, 1978]:

$$k_T = k_{20}\theta^{(T-20)} \tag{2.22}$$

where k_{20} is the first-order decay rate at 20°C, k_T is the decay rate at temperature T (°C) and θ is an empirical coefficient determined from experimental data. Typical values of k_{20} are 0.8 for freshwater and 1.40 for saltwater, $\theta = 1.07$.

This is based on the Arrhenius equation, which describes the effect of temperature on first-order reaction rates [Auer and Niehaus, 1993; Blaustein et al., 2013]:

$$k = Ae^{(E_a/RT)} \tag{2.23}$$

where A is the pre-exponential factor, E_a is the activation energy, R is the gas constant and T is the temperature (°K).

In some studies a sigmoidal relationship has been observed between decay rate

and temperature [de Brauwere et al., 2011, 2014b]:

$$k_T = k_{20} \frac{e^{-\frac{(T-25)^2}{400}}}{e^{-\frac{25^2}{400}}} \tag{2.24}$$

where $k_{20} = 1.25 \times 10^{-5}$ (1/s). However, this equation is comparable with Equation 2.22 in the range of 5°C to 25 °C.

At low temperatures the decay rate is independent of temperature, therefore in modelling applications a threshold temperature is often specified below which k_T is considered zero [Deltares, 2014a].

2.2.1.2 Salinity dependence

Bacterial decay is known to increase with salinity [Palazón et al., 2017; Solic and Krstuloviic, 1992]. Mancini [1978] found a linear empirical equation to represent the relationship between decay rate and salinity in saline and fresh water, independent of sunlight effects:

$$k_{sal} = 0.8 + 0.006 P_s \tag{2.25}$$

where P_s is the percentage sea water.

Assuming the salinity of seawater is within the range 30 to 35 ppt this can be written as follows [Chapra, 1997]:

$$k_{sal} = 0.8 + 0.002 C_{sal} \tag{2.26}$$

where C_{sal} is salinity (ppt or g/L).

However, the effect of salinity is considered a function of temperature and thus is incorporated within Equation 2.22 to yield Equation 2.27, describing the

combined effects of temperature and salinity:

$$k_T = k_{sal} 1.07^{(T-20)} \tag{2.27}$$

To the same effect, Equation 2.28 may be used in place of Equation 2.27. This is the approach used by Deltares [2014a] in the water quality module of the open source model Delft3D:

$$k_T = (k_b + k_{sal})\, k_t^{(T-20)} \tag{2.28}$$

where k_b is the base decay rate, k_t is a temperature related decay coefficient equivalent to k_{20} and k_{sal} is defined as:

$$k_{sal} = k_{cl} C_{sal} \tag{2.29}$$

where k_{cl} is the chloride related mortality constant ($m^3/g/d$). This is a modelled substance within the Delft3D suite.

Similarly, Boye et al. [2014] expressed the effects of salinity as:

$$k_{sal} = \theta_s C_{sal} \tag{2.30}$$

where θ_s is an empirical coefficient and C_{sal} is salinity (ppt).

Alternative relationships that have been proposed are shown in Equation 2.31 [McCorquodale et al., 2004] and Equation 2.32 [Canteras et al., 1995], however their use in other studies is limited.

$$k_{sal} = 0.0014 {C_{sal}}^2 + 0.002 C_{sal} + 0.0253 \tag{2.31}$$

$$k_{sal} = 1.012^{C_{sal}} \tag{2.32}$$

2.2.1.3 Sunlight dependence

Sunlight is known to have a detrimental effect on bacterial survival, with many studies linking faster decay to increased light intensity. Palazón et al. [2017] studied the *E.coli* concentration at 299 beaches along the Spanish coast and found a positive correlation between increased ultraviolet (UV) light intensity and *E.coli* decay. Aragones et al. [2016] carried out a similar study and found elevated *E.coli* and *Enterococci* concentrations in areas subject to fewer hours of sunshine. Other research has emphasised the importance of diurnal variations in solar radiation, resulting in greater die-off rates at midday, alongside peak light intensity (see Bellair et al. [1977]; Feng et al. [2015]). This has been incorporated in studies through the use of differential day and night decay rates [Kashefipour et al., 2002b]. Boye et al. [2014] developed this concept further and found that better predictions of FC concentration were obtained when calculating decay as a function of light intensity, which was considered to vary throughout the day, following a sinusoidal function.

Mancini [1978] expressed the effect of irradiation on the decay rate as shown in Equation 2.33:

$$k_i = \overline{I} = \frac{I_a}{k_e h}\left[1 - e^{k_e h}\right] \tag{2.33}$$

where k_i is the irradiance related mortality constant, k_e is the light extinction coefficient (1/m) and I_a is the average daily light intensity (ln/h). $\overline{I}$ is the depth averaged light intensity, calculated from depth integration of the Beer-Lambert law, which describes an exponential decrease in decay rate with depth within a

layer of well mixed water [Auer and Niehaus, 1993; Chapra, 1997]:

$$I(z) = I_0 e^{-k_e z} \tag{2.34}$$

where I_0 is the surface light intensity and $I(z)$ is the light intensity at depth z (where z = 0 at the surface and z = h at the bed).

Chapra [1997] modified Equation 2.33 to include a proportionality constant α, however this value is close to unity and can be ignored:

$$k_i = \alpha \overline{I} \tag{2.35}$$

Boye et al. [2014] instead specified this value as the coefficient of irradiation α_I which must be explicitly defined based on the type of bacteria being modelled.

The light extinction coefficient is a function of water turbidity and can be calculated based on the Secchi-depth or suspended solids concentration using Equation 2.36 [Chapra, 1997; Gin and Goh, 2013], 2.37 [Chapra, 1997; Gin and Goh, 2013] or 2.38 [Yang and Liu, 2017]:

$$k_e = \frac{1.8}{SD} \tag{2.36}$$

$$k_e = 0.55 ss \tag{2.37}$$

$$k_e = 0.69 ss + 24.09 \tag{2.38}$$

where SD is the Secchi-depth (m) and ss is the suspended solids concentration (mg/l).

This attenuation of light with depth and the effect on bacterial decay has since been verified in a number of studies. Solic and Krstuloviic [1992] investigated the die-off of FC in seawater and found an inverse relationship between the T_{90} value and depth due to the reduction in solar radiation. Similarly, Mattioli et al. [2017] studied the decay of *E.coli* and *Enterococci* samples in marine water at three different water depths and observed faster decay at shallower depths.

Note that while many of the studies discussed herein account for the attenuation of light with depth, at the time of writing the author was unable to find a published study which calculated a depth variable decay rate in a 3D model. Studies such as that by Bedri et al. [2013] use a constant value throughout the depth, as do studies using 2D models.

To account for the significance of UV radiation on bacterial decay compared to other frequencies present in sunlight [Cho et al., 2016; Whitman et al., 2015], Equation 2.39 calculates decay based on the fraction of UV radiation within visible light (f_{UV}) [Deltares, 2014a]:

$$k_i = k_r DL f_{UV} \frac{I_a}{k_e h} \left[1 - e^{k_e h}\right] \tag{2.39}$$

where k_r is a radiation related mortality constant ($m^2/W/d$), h is the depth of water (m) and DL is the day length (i.e. fraction of a day).

Kashefipour et al. [2006] studied the near-shore waters off the Scottish Coast, UK, and found the following relationship through calibration of a numerical model, which is derived from Equation 2.16:

$$k = k_b + 0.236 I^{0.629} \tag{2.40}$$

where $k_b = 2.63$ and I is the surface radiance (direct solar radiation plus diffuse sky radiation) in W/m^2.

It should be noted that this equation should only be used for similar studies due to the significant spatial variation of parameters such as water temperature, salinity and turbidity, making it study site specific.

Similarly, Alkan et al. [1995] carried out a series of laboratory experiments on the decay of *E.coli* and *Enterococci* in seawater and found that their die-off rates could be represented by Equations 2.41 and 2.42, respectively:

$$k_{EC} = A_{EC} + 1.3 \times 10^{-5} I_0 \tag{2.41}$$

$$k_{ENT} = A_{ENT} + 1.1 \times 10^{-5} I_0 \tag{2.42}$$

where k_{EC} and k_{ENT} are the decay dates for *E.coli* and *Enterococci* respectively, A_{EC} and A_{ENT} are combined factors related to experimental conditions and sample properties; turbidity, sewage content and sample mixing; and I_0 is the surface light intensity (W/m^2).

2.2.1.4 pH dependence

Optimum conditions for bacterial survival are cited as being between pH 5.5 and pH 7.5, with bactericidal effects only significant at extreme ends of the scale [Kay et al., 2005; Solic and Krstuloviic, 1992]. As such, in natural waters where the pH is generally neutral the effect is negligible.

Wilkinson et al. [1995] expressed the influence of pH on the decay rate as follows:

$$k_{pH} = k_{min} cosh \left\{ \alpha \left(pH_{k_{min}} - pH \right) \right\} \tag{2.43}$$

where $pH_{k_{min}}$ is the pH at which the decay rate is minimum (k_{min}) and α is a constant.

2.2.2 Additional effects

2.2.2.1 Sediment interactions

The presence of sediment in the water column is known to affect the bacterial population in a number of ways. As previously discussed, increased turbidity reduces the light penetration in the water column [Boye et al., 2014; Pommepuy et al., 1992], which in turn reduces the effect of irradiation on decay [Gutiérrez-Cacciabue et al., 2016]. Kay et al. [2005] carried out a series of *Enterococci* die-off experiments using samples taken from the Severn Estuary, UK, and found that at high turbidites (i.e. $>$ 200 Nephelometric Turbidity Units, NTU), bacterial decay was similar under irradiated and dark conditions. Guillaud et al. [1997] carried out similar experiments using samples taken along the French coast and found the following relationship between *E.coli* decay and the suspended sediment concentration:

$$k = 0.1899 ss^{0.799} \tag{2.44}$$

where ss is the suspended sediment concentration (mg/l).

Miller and Zepp [1979] proposed a modification to the light attenuation function (see Equation 2.33), to account for increased diffuseness in sediment laden water:

$$k_i = \alpha_I \frac{I_0(t)}{k_e h} \left[1 - e^{k_e h}\right] \frac{D}{D_w} \tag{2.45}$$

where D and D_w are the average distribution coefficients for suspension and distilled water respectively, and their ratio is the light intensity attenuation modification.

This is as a result of light scattering caused by sediment particles in suspension, which causes a relative increase in the calculated light intensity, compared to the attenuation models discussed thus far. However, it should be noted that this study only considered processes in the surface photic zone (up to 10 cm

deep), and that scattering is dependent on the sediment type, limiting the extent to which the findings may be applied elsewhere. Indeed, the author was able to find only one subsequent study which used this model (see Huang et al. [2015b]).

In comparison, recent years have seen a large number of studies focussed on the interaction between bacteria and sediment in the water column. Bacteria may exist as free-living, or adsorbed to the surface of sediment particles [Gao et al., 2013; Wilkinson et al., 1995; Wyness et al., 2018]. In the latter case the transport of bacteria is governed by sediment transport processes, which can lead to the removal of bacteria from the water column through sedimentation [Chen and Liu, 2017; Hassard et al., 2016]. Conversely, the addition of bacteria is possible though the resuspension of bed sediments [de Brauwere et al., 2014a; Ouattara et al., 2011]. In some cases, under specific environmental conditions, bacteria may also desorb from the surface of particles [Brookes et al., 2004; de Brauwere et al., 2014b; Hassard et al., 2016].

The mechanisms by which bacteria adsorb and desorb from sediments are not completely understood [Huang et al., 2015b], and are currently the focus of research (see Wyness et al. [2018]). While these are of little interest to engineers it is important that deterministic models reflect reality. It is known that bacteria adsorb more readily to finer particles such as clay or silts [Campos et al., 2013; Wilkinson et al., 1995]. It is therefore important to not only determine the types of sediment present in the water column [Palazón et al., 2017], but to distinguish between sediment fractions [Yang and Liu, 2017], such as cohesive and non-cohesive sediments [Yang et al., 2008]. For each type the ratio of free-living and attached bacteria must be determined [Chapra, 1997; de Brauwere et al., 2014b]. This is often referred to as the partition coefficient [Gao et al., 2011a], which alongside the particle settling velocity, has a significant impact on the quantity of bacteria removed from the water column [Chen and Liu, 2017].

When attached to particles, either in the water column or the bed sediment, the decay rate of bacteria is known to be reduced through shielding from sunlight and predation [Kay et al., 2005; Wilkinson et al., 1995; Zhang et al., 2015] (see Section 2.2.2.2). Brown and Boehm [2015] calculated the decay rate of *Enterococci* in beach sand and found it to be up to 10 times slower than in seawater. Furthermore, some studies have observed bacterial growth in sand when exposed

to wetting and drying cycles [Yamahara et al., 2009], such as that in intertidal environments [Feng et al., 2015], or the swash-zone of a beach [Solo-Gabriele et al., 2015]. In any case, it is clear that beach sands may be considered a significant non-point source [Aragones et al., 2016; Huang et al., 2017; Pachepsky and Shelton, 2011] and sink of bacteria.

Various models exist to account for these processes; for example, the introduction of an equivalent first order decay / loss term by Auer and Niehaus [1993] to account the removal of bacteria from the water column through adsorption and sedimentation. Gao et al. [2011a]; Huang et al. [2015a]; Yang and Liu [2017] and Yang et al. [2008] included mass flux terms in the advective transport equation, thereby enabling explicit integration of bacteria and sediment transport models. However, no models exist which fully resolve all the processes described, as those which lead to adsorption and desorption are not yet well understood.

2.2.2.2 Predation losses

In addition to sedimentation induced loses, bacteria is a food source for protozoa and may be removed from the water column through predation [de Brauwere et al., 2014b]. Connolly et al. [1999] and Yang et al. [2008] accounted for these effects by the inclusion of an equivalent first order loss coefficient due to predation.

However, it is argued that as predation rates are linked to temperature, an additional predation decay term is unnecessary, as these effects are indirectly included within the temperature related decay term [de Brauwere et al., 2014b].

2.2.2.3 Viable But Non-Culturable bacteria

It has been shown that is some cases, when exposed to conditions that trigger die-off, bacteria such as *E.coli* can enter what is known as a Viable But Non-Culturable (VBNC) state, in which they are not detectable by traditional culture based techniques, but persist in the environment [Gin and Goh, 2013]. Quantitative polymerase chain reaction (qPCR), staining, or taxon-specific fluorescent *in-situ* hybridization techniques must be used to detect bacteria in this state [Hassard et al., 2016]. Removal of the applied stress allows cells to return to normal activity, which may then be detected [Arana and Barcina, 2008]. Not

only does this have implications regarding the method of assessment used when measuring the FIO concentration at a bathing water, but it also raises questions in relation to the decay rate of bacteria in this state. For example, Gin and Goh [2013] studied the die-off of *Enterococci* and found that bacteria in a VBNC state decay at a slower rate. However, to the knowledge of the author, differentiating between culturable and VBNC cells has not been included in any models to date.

2.3 Risk of gastroenteritis

It is widely known that there is an increased risk of recreational users of bathing waters, such as surfers, contracting an illness or infection after wet weather events; for example, gastroenteritis [Arnold et al., 2017; Soller et al.]. Though *E.coli* concentration has been linked as an indicator in the past [Jang et al., 2017], *Enterococci* is now more widely accepted as a predictor for infection [Kay et al., 2005]. Three models have been found to provide quantifiable risk estimates based on the *Enterococci* concentration in bathing waters.

Cabelli et al. [1982] studied the rate of illness as a result of swimming in polluted water and found a linear relationship between *Enterococci* concentration and highly credible gastro-intestinal (GI) symptoms:

$$P = 0.2 + 12.2log(C) \tag{2.46}$$

where P is the probability, based on symptoms per 1000 persons, and C is the bacterial concentration (cfu/100 ml). The study was carried out in New York, US.

Kay et al. [1994] conducted similar trials in the UK using Faecal Streptococci (FS), synonymous with *Enterococci* [Byappanahalli et al., 2012], as an indicator. It was found that for bathers exposed to concentrations greater than 32 cfu/100 ml, the following equation could be used to predict the probability of contracting

GI symptoms:

$$ln(P) = 0.20102\sqrt{(C-32)} - 2.3561 \tag{2.47}$$

At concentrations below 33 cfu/100 ml there was no significant correlation. This model was used by Falconer et al. [1998] to predict the risk of infection based on 3D numerical model simulations of two bathing waters in the UK.

Haas et al. [1999] proposed another model, which was used by Huang et al. [2015a] to predict the GI health risks at different tidal phases in the Ribble Estuary, UK:

$$P = 1 - \left(1 + \left(\frac{D_{FC,oral}}{N_{50}}\right) * \left(2^{\frac{1}{\alpha}}\right)\right)^{-\alpha} \tag{2.48}$$

where $D_{FC,oral}$ is the number of FIO ingested (see Huang et al. [2015a] for details on calculation of this value), $N_{50} = 5.96\text{x}10^5$ and $\alpha = 0.49$.

2.4 Turbulent diffusion

2.4.1 Previous studies

In chronological order, this section describes studies which have been carried out to date on the tracking of surface particles or drogues in laboratory and field environments. Also included are those which investigate the lateral turbulent diffusion of a tracer, as the lateral dispersion of floating particles and a dissolved tracer is approximately equal [Sayre and Chang, 1968] (see Section 3.2.3).

If the reader is unfamiliar with turbulent diffusion theory, please see Chapter 3, Sections 3.2.3 and 3.4.1 for further information on the non-dimensional turbulent diffusion coefficient, the difference between diffusion and dispersion and the transport of a dissolved tracer versus floating particles.

In the earliest study the author was able to find, Orlob [1959] tracked the motion of floating polyethylene discs in a 4 ft by 38 ft and 8 inch deep experimental flume, with a rough bed, to study the transverse diffusion coefficient in a 2D broad open channel flow, conditions at the centre of which broadly satisfy the assumption of homogeneous turbulence. Particles of diameter 1/8 inch were released one at a time and the transverse position tracked at fixed distances from the source. Similar experiments were also made with dye tracer. Limitations in the available techniques required a graphical approach to data analysis, whereby the standard deviation was calculated using the probability of the arrival of a particle at a point, based on observation data. Dye studies revealed diffusion increased with distance downstream of a point source, with the diffusion coefficient reaching a maximum value governed by the limiting eddy scale. It was found that Equations 3.41 and 3.42 are applicable to homogeneous turbulent flow. However, it was not possible to study the Richardson-Okubo power by means of floating particle experiments, due to the limiting eddy size being less than the particle diameter. The non-dimensional transverse turbulent diffusion coefficient at the surface was calculated to be 0.17.

Sayre and Chamberlain [1964] conducted another laboratory study into transverse turbulent diffusion, in a 8 ft by 2 ft by 150 ft experimental flume with an 8 inch deep sand bed. A single set of steady uniform flow conditions were studied where; flow rate (q) = 0.21 m^3/s, flow depth (h) = 18 cm, bed slope (S_o) = friction slope (S_f) = 7.1e-4. The method of particle release and measurements of dispersion were carried out in a similar manner to Orlob [1959]. As found by Orlob [1959], transverse turbulent diffusion increased with distance from the source, up to a limiting value. The non-dimensional transverese turbulent diffusion coefficient at the surface was calculated to be 0.24 [Sayre and Chang, 1968].

Sayre and Chang [1968] compared the longitudinal dispersion and transverese diffusion of dye, floating polyethylene particles, and suspended sediment in a 7.83 ft by 2 ft by 150 ft experimental flume with increased roughness. This was the same flume used by Sayre and Chamberlain [1964] with a reduced width. Three different hydraulic conditions were considered for which steady uniform

flow was established prior to particle release. Particles were released sequentially in a similar manner to previous studies. The time taken for particles to reach a number of locations downstream of the source point was recorded to measure longitudinal diffusion. Transverse diffusion was measured in the same manner as in previous studies. The non-dimensional coefficient of longitudinal dispersion of the dye was calculated as 5.3, similar to that proposed by Elder [1959]. For the floating particles, the non-dimensional coefficient of longitudinal turbulent diffusion was calculated as 0.25. Assuming homogeneous turbulence, the non-dimensional coefficient of transverse diffusion for dye (0.23), was predicted for floating particles.

Engelund [1969] carried out a particle tracking study in a 7 ft wide flume and found that the non-dimensional longitudinal and transverse turbulent diffusion coefficients for a particle at the surface were 0.045 and 0.22 respectively. While the transverse diffusion coefficient showed good agreement with previous studies, there was significant discrepancy in the longitudinal direction. However, as for the studies of Sayre and Chang [1968], this difference highlighted anisotropy, and that the assumption of homogeneous turbulence does not hold true when the flow is predominantly aligned to one axis. A single floating particle, 9mm in diameter, was released along the centreline of the flume. After a specified time interval (up to 20 s) an image of the water surface was taken by a camera situated above the flume, from which the particle position was recorded. The experiment was repeated to obtain multiple images of the particle at fixed intervals of time after release. This process was repeated for two flow depths (5.45 cm and 17.3 cm), and two bed roughness values. The combined record of particle positions was used to calculate the diffusion parameters.

In his doctoral thesis titled 'Characteristics of Transverse Mixing in Open-Channel Flows', Okoye [1970] studied the relationship between the non-dimensional coefficient of transverse turbulent diffusion (ϵ_y), of a dissolved tracer, and the as-

pect ratio; defined as:

$$\lambda = \frac{b}{h} \tag{2.49}$$

where λ is the aspect ratio (dimensionless), b is the flow width (m) and h is the flow depth (m).

Two experimental flumes were used; (i) 0.85 m by 18.3 m and (ii) 1.1 m by 40 m, and the water depth was varied between 1.5 cm and 22 cm. The smaller flume had steel sides and a steel bed, while the larger flume had glass sides and a steel bed. ϵ_y was found to decrease from 0.24 to 0.093 as the aspect ratio decreased from 67 to 5. In experiments where other factors, such as the depth and bed roughness, were changed but the aspect ratio of the flow unaltered, there was little difference in the measured non-dimensional turbulent diffusion coefficient. This was explained by considering a fixed depth of water; a reduction in the lateral turbulence scale occurred as the width decreased (i.e. λ decreases), which was accompanied by a reduction in the tracer diffusion. Despite the observed relationship between ϵ_y and λ, a comparison with the measured values for natural channels confirmed the values of ϵ_y to be higher than expected. This was thought to be due to the presence of secondary currents and increased lateral velocity gradients generated at channel bends and in non-uniform channels. Additional experiments were carried out in the larger flume with the bed covered by 3/4 inch rock to increase the bottom friction. However, no significant relationship was established between ϵ_y and shear velocity (otherwise known as friction velocity).

Cederwall [1971] studied transverse diffusion in a 1.1 m by 40 m flume with a stainless steel bed. Floats of near neutral buoyancy were released into the flow and the transverse position measured at fixed locations downstream. The floats projected 6 cm below the surface of the water, with a Plexiglass wing attached to the base. Three wing sizes were used; 4 cm, 8 cm and 16 cm. The experiments were repeated for two flow conditions: q = 0.067 m^3/s, h = 16.5 cm and q = 0.054 m^3/s, h = 9.8 cm. The transverse diffusion coefficient was found to decrease with increasing float size, the explanation being that particles were not influenced by

turbulent fluctuations of a smaller size than themselves.

While laboratory studies are valuable for generating a controlled environment in which studies are repeatable, the flow conditions are significantly different to those found in natural environments. It is therefore necessary to conduct field studies in order to obtain useful data for environmental and model applications. The following publications are field studies focussed on river environments.

Suara et al. [2015] developed a high resolution, GPS tracked floating drifter for calculation of particle dispersion, to be used for shallow water studies. These were used by Suara et al. [2017], in combination with low resolution drifters, to study the diffusivity in a tidal estuary. Particle dispersion was observed to increase over time. For drifter separation distances less than 0.5 m the Richardson-Okobo power law (see Equation 3.42) was found to be applicable, while the relative diffusivity decreased with increased separation.

Han et al. [2016] used an array of floating drifters to study the effect of meanders on the spread of floating pollutants. The experimental flume used was 5 m in width and over 100 m in length, with natural material on the bed and banks; hence close to the conditions in a natural river environment. Diffusion was found to increase with sinuosity; dimensionless longitudinal and transverse diffusion coefficients were found to be in the ranges 5.94 to 14.55 and 0.37 to 2.61, respectively.

2.4.2 Knowledge gaps

A wide range of studies have been carried out to date on the dispersion of floating pollutants. However, direct comparisons are difficult due to inconsistencies in the experimental conditions and techniques. It is reasonable to expect, and is the case, that there are variations between the theoretical and observed non-dimensional turbulent diffusion coefficients. However, understanding the cause of these differences remains of interest.

Although previous studies have been carried out using a variety of bed conditions, the effect of boundary roughness on the non-dimensionless turbulent diffusion coefficient remains unknown, as is the relationship between the turbulent properties of the flow field and the non-dimensional turbulent diffusion coefficient.

Furthermore, at the time of study the author was not aware of any relevant publications which cross-validate experimental and numerical models of floating particle dispersion.

Chapter 3

Governing equations and model details

3.1 Introduction

This chapter describes the governing equations of fluid flow and solute transport used by hydrodynamic models. However, as there already exists a large body of literature which covers the derivation and numerical solution of these equations, a detailed explanation of each has been omitted to avoid repetition. Instead, only the information deemed essential for this research has been included, with direction to additional sources given where required.

In addition, further details are given on the TELEMAC model suite and the equations of bacterial decay used in this study. For a detailed description of their implementation within the TELEMAC framework, see Chapter 5, Section 5.4.

3.2 Hydrodynamic processes

3.2.1 Conservation of mass and momentum

In multi-scale hydrodynamic numerical models, the most commonly used governing equations of fluid motion are the 3D Reynolds Averaged Navier Stokes equations of flow. Assuming the hydrostatic pressure hypothesis, these are herein expressed in their reduced form, as applied in TELEMAC-3D [Desombre et al., 2016; Hervouet, 2007; Lang et al., 2014]. Equation 3.1 deals with the conservation of mass, Equation 3.2 deals with the conservation of momentum and Equation 3.3 is an expression for the pressure at depth:

$$\frac{\partial u}{\partial x} + \frac{\partial v}{\partial y} + \frac{\partial w}{\partial z} = 0 \tag{3.1}$$

$$\begin{aligned} \frac{\partial u}{\partial t} + u\frac{\partial u}{\partial x} + v\frac{\partial u}{\partial y} + w\frac{\partial u}{\partial z} &= -g\frac{\partial Z_S}{\partial x} + \nu\Delta\left(u\right) + F_x \\ \frac{\partial v}{\partial t} + u\frac{\partial v}{\partial x} + v\frac{\partial v}{\partial y} + w\frac{\partial v}{\partial z} &= -g\frac{\partial Z_S}{\partial y} + \nu\Delta\left(v\right) + F_y \end{aligned} \tag{3.2}$$

$$p = p_{atm} + \rho_o g\left(Z_S - z\right) + \rho_o g\int_z^{Z_S} \frac{\Delta\rho}{\rho_o} dz \tag{3.3}$$

where u, v and w are the flow velocity (m/s) in the x, y and z Cartesian axes directions respectively (i.e. longitudinal, transverse and veritical orientations), t is time (s), g is the acceleration due to gravity (m/s^2), Z_S is the free surface elevation (m), z is the elevation above the bed (m), p and p_{atm} are the pressure and atmospheric pressure respectively (N/m^2), ρ_o and $\Delta\rho$ are the reference density and variation in density respectively (kg/m^3). F_x and F_y are source terms (m/s^2) which include; wind, Coriolis, bottom friction and other forces. The reader is

recommended to read the existing literature for further explanation of body force source terms such as bed friction, wind and Coriolis forces (see Gao [2008]), which have been omitted for brevity. Bottom friction and wind forces can have significant influence on shallow flows and are based on bed roughness and wind speed, respectively. The Coriolis force is an inertial force which acts on a body in motion within a rotating reference frame and influences fluid flows based on their global position and velocity. ν is the velocity diffusivity (m^2/s), also referred to as the coefficient of turbulent viscosity or the eddy viscosity. This may be considered an isotropic or anisotropic value, depending on the turbulence closure model used. Further information on the derivation of Equations 3.1 to 3.3 can be found in Hervouet [2007].

In many cases, where the flow is well mixed in the vertical direction and the dominant transport processes occur in the horizontal direction, Equations 3.1 and 3.2 can be integrated over the depth and simplified to obtain the depth-averaged Navier Stokes, or shallow water, equations. In such cases, flow is considered to only occur in the horizontal plane.

3.2.2 Advection-diffusion equation

The Advection-Diffusion Equation (ADE) is used to calculate the transport of a solute in a fluid, for example, salt (i.e. salinity modelling). It is implemented in TELEMAC to calculate tracer transport, which in the case of this study represents *E.Coli*. These were treated as mass conservative, passive numerical tracers (i.e. they do not influence the hydrodynamics), and bacteria-sediment interactions were ignored.

The ADE can be written in 3D and 2D, shown in their reduced forms in Equations 3.4 and 3.5 respectively, as applied in TELEMAC [Desombre et al., 2016; Hervouet, 2007; Lang et al., 2014]:

$$\frac{\partial c}{\partial t} + u\frac{\partial c}{\partial x} + v\frac{\partial c}{\partial y} + w\frac{\partial c}{\partial z} = \nu_T \Delta\left(c\right) + S_T \tag{3.4}$$

$$\frac{\partial c}{\partial t} + \overrightarrow{u} \cdot \overrightarrow{\nabla}(c) = \frac{1}{h} div\left(h\nu_T \overrightarrow{\nabla} c\right) + S_T \tag{3.5}$$

where c is the tracer concentration, t is time, h is the water depth, ν_T is the tracer diffusion coefficient (m^2/s) and S_T is the source or sink term, including both explicit and implicit terms.

Tracer decay is taken into account by a sink term which is commonly written as a first order decay equation [Chapra, 1997; Thomann and Mueller, 1987]:

$$S_{sink} = \frac{\partial c}{\partial t} = -kc \tag{3.6}$$

where k is the decay rate (1/d).

In the solution of Equations 3.4 and 3.5, source and sink terms are included as follows:

$$\begin{aligned} S_T &= S_{source} - S_{sink} \\ S_T &= S_{source} - kc \end{aligned} \tag{3.7}$$

3.2.3 Turbulent diffusion theory

Of particular interest in environmental studies is the calculation (or specification) of the velocity diffusivity (ν), otherwise referred to as the turbulent viscosity or the (kinematic) eddy viscosity, and the tracer diffusion coefficient (ν_T). Herein an explanation is given on the derivation of each and the differences, in particular the distinction between diffusion and dispersion, two terms which are misleadingly often used interchangeably in the literature.

3.2.3.1 Diffusion

Eddy viscosity, often referred to as turbulent viscosity, is influenced by turbulent and molecular diffusion (see Equation 3.8). However, the effects of molecular diffusion are negligible in comparison to those caused by turbulence and can therefore be ignored [Fischer, 1973] (see Equation 3.9).

$$\nu = \nu_{turbulent} + \nu_{molecular} \tag{3.8}$$

$$\nu = \nu_{turbulent} \tag{3.9}$$

The concept of turbulent viscosity arises due to the time-averaging of the turbulent velocity fluctuation terms in the derivation of the Navier Stokes equations. These represent the difference between the instantaneous and time-averaged velocity components in a flow:

$$\begin{aligned} u &= \overline{u} + u' \\ v &= \overline{v} + v' \\ w &= \overline{w} + w' \end{aligned} \tag{3.10}$$

where u, u' and $\overline{u}$ denote the instantaneous velocity, turbulent velocity fluctuation and time-averaged velocity in the x direction, respectively. This also applies to v and w in the y and z directions, respectively.

The same is true for a dissolved substance, or tracer, of concentration c:

$$c = \overline{c} + c' \tag{3.11}$$

Under the Reynolds stress assumption, the turbulent viscosity is defined as a

function of the shear stresses within a fluid (τ_{ij}). These are often expressed using tensor notation; for example, see Equation 3.12 for the expression in the x and y directions:

$$\tau_{ij} = \begin{bmatrix} \tau_{ii} & \tau_{ij} \\ \tau_{ji} & \tau_{jj} \end{bmatrix} = -\overline{u_i' u_j'} = - \begin{bmatrix} \overline{u_x' u_x'} & \overline{u_x' u_y'} \\ \overline{u_y' u_x'} & \overline{u_y' u_y'} \end{bmatrix} = - \begin{bmatrix} \overline{u'^2} & \overline{u'v'} \\ \overline{v'u'} & \overline{v'^2} \end{bmatrix} \tag{3.12}$$

where the overline (e.g. $\overline{uv}$), indicates time-averaging of the product term.

Under the Boussinesq assumption of eddy viscosity, these terms can be represented in a diffusive manner as follows (see Goldstein [1938]):

$$\begin{aligned} \overline{u'u'} &= -\nu \left(\frac{\partial u}{\partial x} + \frac{\partial u}{\partial x} \right) \\ \overline{u'v'} &= -\nu \left(\frac{\partial u}{\partial y} + \frac{\partial u}{\partial x} \right) \\ \overline{u'w'} &= -\nu \left(\frac{\partial u}{\partial z} + \frac{\partial v}{\partial x} \right) \end{aligned} \tag{3.13}$$

which represent the flux terms found on the right hand side of Equation 3.2: $\nu\Delta(u)$.

Extending Equations 3.12 and 3.13 to include a tracer of concentration c, as in the derivation of the ADE, this may also be expressed as follows [Sayre and Chang, 1968]:

$$\nu_z = \frac{\overline{-v'c'}}{\frac{\partial C}{\partial z}} \approx \frac{\overline{-u'v'}}{\frac{\partial U}{\partial z}} \approx \frac{-U^{*2}\frac{z}{h}}{\frac{\partial U}{\partial z}} \tag{3.14}$$

where ν_z is the eddy viscosity in the z direction and U^* is the shear velocity

(m/s), defined as:

$$U^* = \sqrt{\frac{\tau_0}{\rho}} = \sqrt{gRS_f} \tag{3.15}$$

where R is the hydraulic radius and S_f is the friction slope.

The eddy viscosity can be calculated either by direct solution of the Reynolds stresses or, more commonly, using one of a number of turbulence closure models. Of these, the two most commonly used methods in 3D hydro-environmental modelling studies are the $\kappa - \epsilon$ and Smagorinsky models. Using the Smagorinsky model, as in this study, ν is calculated by solving Equation 3.16 [Li and Wang, 2000; Smagorinsky, 1963]:

$$\nu = {C_S}^2 \Delta x \Delta y \sqrt{2\left(\frac{\partial u}{\partial x}\right)^2 + 2\left(\frac{\partial v}{\partial y}\right)^2 + \left(\frac{\partial u}{\partial y} + \frac{\partial v}{\partial x}\right)^2} \tag{3.16}$$

where C_S is the Smagorinsky constant; this is assigned a value of 0.1 in TELEMAC.

As discussed in previous chapters, it is common in hydro-environmental modelling studies to adopt a depth-averaged approach. In such instances, the eddy viscosity is also averaged over the depth. Assuming isotropic turbulence and a logarithmic velocity profile, Elder [1959] integrated Equation 3.14 over the depth to obtain the depth averaged eddy viscosity ($\overline{\nu}$), in the longitudinal flow direction [Sayre and Chang, 1968]:

$$\overline{\nu} = \frac{1}{h}\int_0^h \nu_z \mathrm{d}z = \frac{\kappa}{6} U^* h \tag{3.17}$$

This is also referred to as the coefficient of turbulent diffusion and was defined by Elder [1959] as:

$$\overline{\nu} = 0.167 \kappa U^* h \tag{3.18}$$

where κ is the von Karman coefficient, equal to 0.4.

Following the isotropic assumption, and assuming no side wall effects, the coefficient of turbulent diffusion in the transverse flow direction (ν_y) can also be defined:

$$\nu_x = \nu_y = \overline{\nu} \tag{3.19}$$

In experimental studies this value is often normalized for different flow conditions, as shown in Equation 3.20,

$$\epsilon = \frac{\overline{\nu}}{U^* h} \tag{3.20}$$

where ϵ is the non-dimensional coefficient of turbulent diffusion. To avoid potential confusion on behalf of the reader, note that although this symbol is often assigned to the eddy viscosity in the literature, this is not the case herein to maintain consistency throughout.

3.2.3.2 Dispersion

The tracer diffusion coefficient is influenced by two processes; turbulent diffusion and dispersion. While the turbulent diffusion term arises due to time-averaging of the turbulent velocity fluctuations, an additional dispersion term is introduced due to spatial-averaging of the velocity and concentration terms when deriving the ADE. This term is not necessary when solving the analytical solution. Note that dispersion occurs in the horizontal direction [Bowden, 1965], and is most prevalent in the longitudinal flow direction, hence the lateral and vertical directions are ignored herein.

Simplification through depth-averaging assumes the horizontal flow components to be uniform over the vertical. The depth-averaged flow components are; U in the x direction and V in the y direction. Similarly, the concentration of a dissolved tracer is assumed to be constant throughout the water column, rep-

resented by C. However, in reality a velocity and tracer concentration gradient exist. The latter is as a result of turbulent mixing between fluid layers of different velocities, causing tracer to be transported at different speeds throughout the water column [Bowden, 1965; Okubo, 1974].

It can therefore be said that the time-averaged velocity component and tracer concentration are the sum of the depth-averaged values and fluctuating components (u'' and c''):

$$\begin{aligned} \overline{u} &= U + u'' \\ \overline{c} &= C + c'' \end{aligned} \tag{3.21}$$

The substitution of Equation 3.21 into the ADE results in a mass flux term to describe this phenomenon:

$$\overline{\overline{u''c''}} = -\nu_x \frac{\partial c}{\partial x} \tag{3.22}$$

where ν_x is the the coefficient of longitudinal dispersion. The tracer diffusion coefficient is the sum of diffusive and dispersive effects such that:

$$\nu_T = \overline{\nu} + \nu_x \tag{3.23}$$

A number of models exist which define ν_T, however it is important to note that in the majority of hydro-environmental studies, only turbulence closure models such as $\kappa-\epsilon$ and Smagorinsky are used and longitudinal dispersion is ignored. The most commonly adopted method that includes dispersive effects is that proposed by Elder [1959], who showed that based on a logarithmic velocity profile and assuming isotropic turbulence, the tracer diffusion coefficients in the longitudinal and transverse flow directions (ν_{xT} and ν_{yT} respectively) are as given as follows:

$$\nu_x = 5.86U^*h$$
$$\nu_y = 0 \tag{3.24}$$

Combining Equations 3.18, 3.19, 3.23 and 3.24:

$$\nu_{xT} = 5.93U^*h$$
$$\nu_{yT} = 0.067U^*h \tag{3.25}$$

For further information on other equations based on different velocity profiles, see Bowden [1965]. Details of the treatment of diffusion and dispersion in TELEMAC are given in Section 3.3.3.

3.2.4 Bacterial decay kinetics

Of the methods available to calculate bacterial decay and summarised in Section 2.2, two were chosen for implementation in this study; those proposed by Mancini [1978] and Stapleton et al. [2007a]. Herein a description of each is given.

The former was chosen due to its widespread use and sensitivity to multiple parameters known to influence bacterial decay; in particular, light intensity and water depth (a proxy for light intensity).

The latter is less widely used, however was developed as a result of an extensive study conducted within the Severn Estuary, to determine the impact of turbidity and light intensity on bacterial decay. It is therefore considered more applicable to the study site due to the importance of sediment particle size and composition on decay, whereas the formula proposed by Mancini [1978] was based on data collated from the literature and ignores sediment effects.

3.2.4.1 Mancini decay function

Decay rate k is calculated as a function of light intensity, salinity and temperature as follows [Chapra, 1997; Mancini, 1978]:

$$k = k_T + k_i \tag{3.26}$$

$$k_T = [0.8 + 0.006(P_s)] * 1.07^{t-20} \tag{3.27}$$

$$k_i = \alpha \overline{I} \tag{3.28}$$

$$\overline{I} = \frac{I_a}{k_e h} \left[1 - e^{k_e h}\right] \tag{3.29}$$

where P_s is the percentage sea water, h is the water depth (m), I_a is the average daily light intensity (ln/h), $\overline{I}$ is the depth averaged light intensity, α is a proportionality constant and k_e is the light extinction coefficient (1/m). This is a function of suspended solids ss (mg/l), and can be written as follows Chapra [1997]:

$$k_e = 0.55ss \tag{3.30}$$

If salinity (C_{sal}) is given as a concentration (mg/l) rather than a percentage,

Equation 3.27 can be written as follows [Chapra, 1997]:

$$k_T = [0.8 + 0.02C_{sal}] * 1.07^{T-20} \tag{3.31}$$

Combining Equations 3.28 and 3.31 the decay rate can be written as:

$$k = [0.8 + 0.02C_{sal}] * 1.07^{T-20} + \frac{\alpha I_a}{k_e h}\left[1 - e^{k_e h}\right] \tag{3.32}$$

This equation is used for 2D (depth-averaged) implementation of the Mancini [1978] decay model as k as a function of the average light intensity over the fully mixed depth.

In TELEMAC-3D, the 3D mesh consists of the 2D mesh replicated over a specified number of sigma layers. This requires a minimum of 2 layers as the first and last layer are fixed at the bed and water surface respectively [Desombre et al., 2016].

Decay is based on the light intensity at each nodal depth, calculated using the Beer-Lambert law (see Equation 2.34) [Chapra, 1997].

In the case of finite volume methods, the average light penetrating over each layer would be used. This can be calculated using the layer averaged Beer-Lambert law (based on the mean value theorem for integrals):

$$\overline{I} = \frac{I_0}{k_e\left(z_{bottom} - z_{top}\right)}\left(e^{-k_e z_{top}} - e^{-k_e z_{bottom}}\right) \tag{3.33}$$

Depth-irradiance curves calculated using Equations 2.34 and 3.33 closely match, as shown in Figure 3.1:

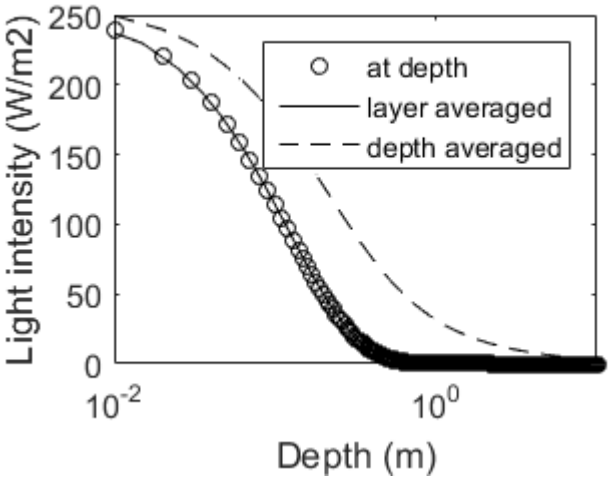

Figure 3.1: Comparison between irradiance at depth; calculated using Equations 2.34 (at depth), 3.33 (layer averaged); and depth averaged irradiance, using Equation 3.32, where k_e was calculated using Equation 2.37 and $ss = 84.82$ mg/l (see Section 5.3.2)

To calculate the decay rate at depth z, Equation 3.32 can be rewritten using Equation 2.34, as shown in Equation 3.34. Note that this does not consider variations in temperature or salinity throughout the water column.

$$k(z) = [0.8 + 0.02C_{sal}] * 1.07^{T-20} + \alpha I_0 e^{-k_e z} \tag{3.34}$$

3.2.4.2 Stapleton decay function

Decay rate is represented by a T_{90} value, the time taken for the concentration to reduce by 90% [Guillaud et al., 1997], which is related to the decay rate k as [Kashefipour et al., 2002b; Kay et al., 2005]:

$$T_{90} = \frac{2.303}{k} \tag{3.35}$$

Stapleton et al. [2007a] proposed that T_{90} can be calculated as a function of turbidity and light intensity, as follows:

$$T_{90} = T_{902} + (T_{901} - T_{90*1}) \tag{3.36}$$

$$T_{901} = \frac{ln10}{K_B * 60 * I} \tag{3.37}$$

$$T_{90*1} = \frac{ln10}{K_B * 60 * I^{exp}} \tag{3.38}$$

$$LogT_{902} = (0.0047 * Turbidity) + 0.677 \tag{3.39}$$

$$Turbidity = 139.479 * Log(ss) - 244.736 \pm 32.678 \tag{3.40}$$

where I is the sunlight intensity (W/m^2), I^{exp} is the fixed irradiance for the experiments (260±14 W/m^2), T_{901} is the sunlight dependent *Enterococci* mortality rate, T_{90*1} is the *Enterococci* mortality rate obtained from laboratory experiments, T_{902} is the turbidity related *Enterococci* mortality rate and $K_B = 1.1 \times 10^{-5}$ and ss is the suspended sediment concentration (mg/l).

While Stapleton et al. [2007a] only investigated the decay of *Enterococci*, the difference in magnitude of K_B to that of *E.coli* ($K_B = 1.3 \times 10^{-5}$), is insignificant and the same approach is considered applicable, as in this study.

For a 2D implementation of Equation 3.36 the sunlight intensity I in Equation 3.37 is calculated as the average light intensity over the water column (see Equation 3.29). For a 3D approach where the decay rate is calculated at each

nodal depth, light penetration was calculated using the Beer-Lambert law (see Equation 2.34).

3.3 TELEMAC model suite

This section briefly describes the salient features of the TELEAMC model suite, given its application herein in the macro-tidal environment of Swansea Bay, and the treatment given to the turbulent transport of pollutants. In this study the governing equations of mass and momentum transport were solved using linear and quasi-bubble solution methods respectively (see Equations 3.1 to 3.3), and the hydrostatic pressure hypothesis was assumed. For further information, see Lang et al. [2014] and Hervouet [2007].

3.3.1 Minimum water depth

It is commonplace in hydrodynamic models to specify a minimum water depth below which a cell or node is considered dry. However, this requires a threshold to be defined; for example 1 cm or 5 cm. Depending on the scheme used, this can break mass conservation. The TELEMAC suite of solvers does not contain such a limit and employs schemes to ensure mass and momentum conservation, including tracer mass conservation. In some cases the treatment can result in the generation of negative depths, however, these can be suppressed and corrected to ensure strictly positive values. This requires the model to distinguish between 'wet' and 'dry' elements, an issue of key importance when studying a site with large areas of intertidal flats such as Swansea Bay.

3.3.2 Wetting and drying

An element is considered dry, or partially dry, when the bed elevation of one node in that element exceeds the free surface of another. Similarly, an element is considered wet if the bed elevation of each node is lower than the free surface at all other nodes in that element. TELEMAC-2D allows the user to choose from two methods which are applied to the numerical treatment of dry (or partially dry)

elements. The first corrects the free surface gradient to prevent flow between dry elements, while the second excludes these elements from the computation. However, the latter can result in mass conservation errors and is not well suited to tidal flat problems. The former is recommended by the TELEMAC developers and has been used in this study. Similar treatments are available in TELEMAC-3D. Further details can be found in Hervouet [2007].

3.3.3 Turbulence

In TELEMAC-2D the user is presented with four options for modelling turbulence. Of these, only the Elder model accounts for differences in dispersion along and across the flow [Elder, 1959]. This allows the user to specify the non-dimensional longitudinal dispersion coefficient (this includes dispersion and turbulent diffusion effects), and the non-dimensional transverse diffusion coefficient (see Equations 3.24 and 3.25). The other available options are; a constant viscosity coefficient which lumps molecular viscosity, turbulent viscosity and dispersion; the $\kappa - \epsilon$ turbulence model and the Smagorinsky model [Smagorinsky, 1963] (see Equation 3.16).

TELEMAC-3D provides the choice of; a constant viscosity coefficient, Smagorinsky, $\kappa - \epsilon$ and $\kappa - \omega$ models. Note that no information has been given on the $\kappa - \epsilon$ and $\kappa - \omega$ models as they have not been used and therefore, being non-essential to the thesis, detailed explanations have been omitted for brevity.

3.4 Measurement of turbulent flow properties

This section briefly describes the theory and equations used in the particle tracking study detailed in Chapter 4.

3.4.1 Particle tracking and dispersion

Herein, the term 'particle' may refer to a range of buoyant objects, such as drogues, GPS trackers or other small items. Further details and specifics of previous studies can be found in the referenced literature.

3.4.1.1 Background theory

Except in proximity to a flow boundary, the dispersion of floating particles is governed by turbulent diffusion; for example, as defined by Elder [1959] in Equation 3.18. This assumes that the surface turbulence, causing particle dispersion, is homogeneous within parallel planes and requires particles to be beyond the influence of boundary effects [Engelund, 1969; Sayre and Chamberlain, 1964]. In comparison, a dissolved substance is also affected by vertical shear and turbulent fluctuations [Okubo, 1974; Sayre and Chamberlain, 1964; Sayre and Chang, 1968], resulting in longitudinal dispersion [Okubo, 1974]. However, shear dispersion does not act perpendicular to the flow direction and the transverse dispersion of floating particles is approximately equal to the transverse diffusion of dissolved tracers; both of which are governed by turbulent diffusion [Sayre and Chang, 1968].

Upon release, the transverse dispersion of a particle cloud increases in accordance with the third law in variance [Okubo, 1974, 1992] (see Equation 3.41) and the Richardson-Okubo power law [Okoye, 1970; Orlob, 1959; Sayre and Chamberlain, 1964; Sayre and Chang, 1968] (see Equation 3.42). For a rigid-boundary open channel flow, this represents the maximum value, which is a function of the limiting eddy size; governed by the channel geometry, flow rate, flow depth and friction parameters [Orlob, 1959; Sayre and Chamberlain, 1964].

$$\sigma_y^2 = \alpha_1 \epsilon t^3 \tag{3.41}$$

$$K_y = \alpha_2 \epsilon^{\frac{1}{3}} L_z^{\frac{4}{3}} \tag{3.42}$$

σ_y^2 is the relative position variance of the particle cloud in the transverse direction (m^2, see Equation 3.45), where σ is the standard deviation in particle position (m) [Batchelor, 1952; List et al., 1990], t is time (s) and ϵ is the rate of energy dissipation per mass of fluid. L is the characteristic length scale, which

depends on the experimental and analysis methods used and K_y is the coefficient of turbulent diffusion for floating particles (m^2/s), in the transverse flow direction.

3.4.1.2 Analysis of particle tracks

Stemming from the work by Taylor [1922], the relative dispersion of a particle cloud, herein called cloud dispersion, at time i can be calculated based on the position of each particle j using the method of moments (see Equations 3.43, 3.44 and 3.45) [Aoyagi et al., 2003; Cederwall, 1971; Han et al., 2016; List et al., 1990; Orlob, 1959; Sayre and Chamberlain, 1964; Sayre and Chang, 1968; Suara et al., 2017]. The total, longitudinal and transverse coefficients of turbulent diffusion for floating particles (K, K_x and K_y respectively) are calculated as the second order moments of the particle cloud distribution, with reference to the centroid of the particle cloud [Batchelor, 1952; Suara et al., 2017]. This assumes a constant value over the measured time interval and that the particles do not reach the channel side walls [Cederwall, 1971; Sayre and Chamberlain, 1964; Sayre and Chang, 1968].

$$K\left(t_i\right) = \frac{1}{2}\frac{\Delta\sigma_i^2}{\Delta t} \tag{3.43}$$

$$K_x\left(t_i\right) = \frac{1}{2}\frac{\Delta\sigma_{x_i}^2}{\Delta t} \tag{3.44}$$

$$K_y\left(t_i\right) = \frac{1}{2}\frac{\Delta\sigma_{y_i}^2}{\Delta t} \tag{3.45}$$

The variance in position of the particle group at time i (σ_i^2) is calculated using Equations 3.46, 3.47 and 3.48, and the centroid ($\overline{x_i}$,$\overline{y_i}$) using Equations 3.49 and

3.50:

$$\sigma_i^2 = \frac{\left(\sigma_{x_i}^2 + \sigma_{y_i}^2\right)}{2} \tag{3.46}$$

$$\sigma_{x_i}^2 = \frac{\sum_j \left(x_{ij} - \overline{x_i}\right)^2}{N-1} \tag{3.47}$$

$$\sigma_{y_i}^2 = \frac{\sum_j \left(y_{ij} - \overline{y_i}\right)^2}{N-1} \tag{3.48}$$

$$\overline{x_i} = \frac{\sum x_{ij}}{N} \tag{3.49}$$

$$\overline{y_i} = \frac{\sum y_{ij}}{N} \tag{3.50}$$

where N is the number of particles.

The skewness in particle distribution (S, dimensionless), is calculated as the third order moment [Cederwall, 1971]:

$$S_x = \frac{\frac{1}{N}\sum_j \left(x_{ij} - \overline{x_i}\right)^3}{{\sigma_{xi}^2}^{3/2}} \tag{3.51}$$

3.4.2 Characteristic parameters

Two parameters are commonly used to describe the level of turbulence within a flow field; the Turbulence Intensity (TI) and the Turbulent Kinetic Energy

(TKE). Turbulence Intensity is calculated using Equation 3.52, where u' is the root mean square of the turbulent velocity fluctuations (see Equations 3.53 and 3.54) and $\overline{u}$ is the time-averaged velocity (see Equations 3.10 and 3.55). This can also be calculated in each flow direction, whereby the velocity components are taken in the desired coordinate direction (see Equations 3.56, 3.57 and 3.58).

$$TI = \frac{u'}{\overline{u}} \tag{3.52}$$

$$u' = \sqrt{\frac{1}{3}\left(u'^2_x + u'^2_y + u'^2_z\right)} \tag{3.53}$$

$$u'_x = \sqrt{\frac{\sum_j \left(u'_{x_{ij}} - \overline{u'_{x_i}}\right)^2}{N}} \tag{3.54}$$

$$\overline{u} = \sqrt{\overline{u_x} + \overline{u_y} + \overline{u_z}} \tag{3.55}$$

$$TI_x = \frac{u'_x}{\overline{u_x}} \tag{3.56}$$

$$TI_y = \frac{u'_y}{\overline{u_y}} \tag{3.57}$$

$$TI_z = \frac{u'_z}{\overline{u_z}} \tag{3.58}$$

Turbulent Kinetic Energy is calculated using Equation 3.59, which is related to the turbulence intensity through Equations 3.53 and 3.60. The directional TKE components are calculated using Equations 3.61, 3.62 and 3.63.

$$TKE = \frac{1}{2}\left(\overline{u'_x{}^2} + \overline{u'_y{}^2} + \overline{u'_z{}^2}\right) \tag{3.59}$$

$$u' = \sqrt{\frac{2}{3}TKE} \tag{3.60}$$

$$TKE_x = \frac{1}{2}\overline{u'_x{}^2} \tag{3.61}$$

$$TKE_y = \frac{1}{2}\overline{u'_y{}^2} \tag{3.62}$$

$$TKE_z = \frac{1}{2}\overline{u'_z{}^2} \tag{3.63}$$

Chapter 4

Experimental and numerical model study of turbulent diffusion for steady flow conditions

4.1 Introduction

This chapter covers an experimental and numerical study that was carried out at the Sediment Laboratory, Department of Hydraulic Engineering, Tsinghua University, China, from September to December 2017. In order to determine the non-dimensional coefficient of turbulent diffusion for a range of flow conditions, the movement of floating particles was tracked across the surface of a straight, uniform channel. These experiments were cross-validated with hydrodynamic model simulations, run using TELEMAC-2D.

Key definitions used herein are as follows: ϵ is the non-dimensional coefficient of turbulent diffusion, as defined by Equation 3.20; K is the coefficient of turbulent diffusion for floating particles, substituted for $\overline{\nu}$ in Equation 3.20; and cloud dispersion refers to the lateral spreading of a floating particle group with time.

4.2 Particle tracking study

4.2.1 Apparatus and set-up

The experimental flume used in this study was a large flat bed flume, details of which are shown in Figures 4.1 and 4.2. The flume had a working length of 35 m and a full width of 3.5 m, with the main section reduced to 2.1 m, operational between 0.01 m^3/s and 0.1 m^3/s. A 19 by 4 array of 76 pressure sensors was permanently fixed within the flume bed. Due to the fixed bed gradient and contraction, all experiments were carried out using steady non-uniform flow conditions. The water depth could be adjusted up to a maximum of 30 cm and was controlled by an underflow sluice gate at the outlet. Two grilles obstructed the flow at the inlet to reduce turbulence, caused by pumping, and increased the homogeneity (see Figure 4.3).

(a) (b) (c)

Figure 4.1: Flume at the Department of Hydraulic Engineering, Tsinghua University (a); with matting on the bed (b) and (c)

The flume had a glass bottom and sides, with a contraction formed by plastic blocks. The Manning's coefficient of the flume was previously measured as n = 0.009. To increase the bed roughness to a value closer to those found in natural rivers and streams (see Chow [1959]), 5 mm thick rubber matting, with 5 mm triangular perforations, was placed on the flume bed and weighted down with

galvanized steel bars at 2 m intervals (see Figures 4.1 and 4.4).

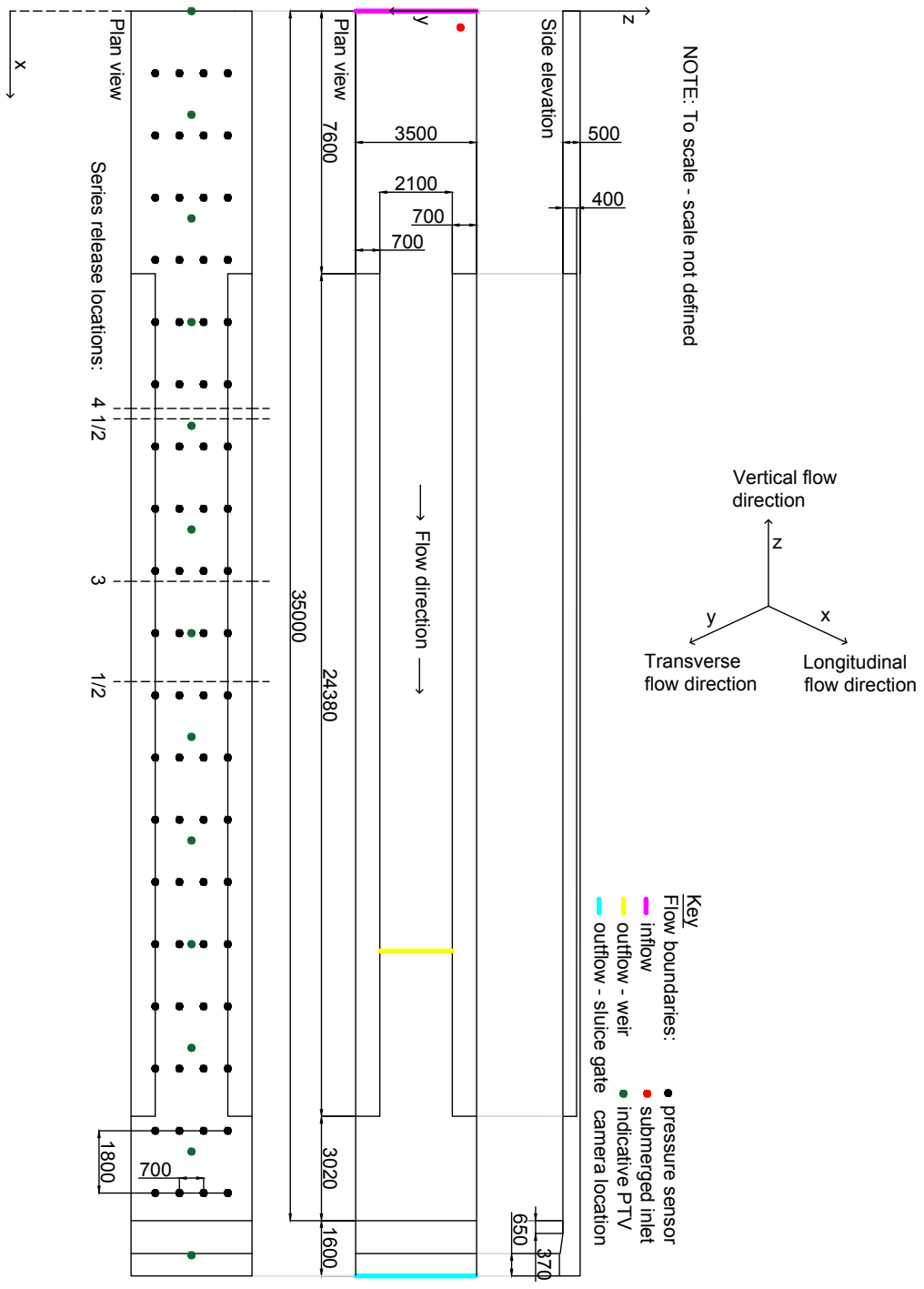

Figure 4.2: Plan view and side elevation of the flume at Tsinghua University

(a) (b) (c)

Figure 4.3: (a) Underflow sluice gate outlet, (b) flow control slats behind sluice gate and (c) flow control grille at flume inlet

Figure 4.4: Rubber matting placed on the bed of the flume to increase bed roughness

Flow measurements were made with a Nortek Vectrino sidelooking probe Acoustic Doppler Velocimeter (ADV). This was mounted on a mobile platform, as shown in Figure 4.5, allowing measurements to be taken at any flow depth and location.

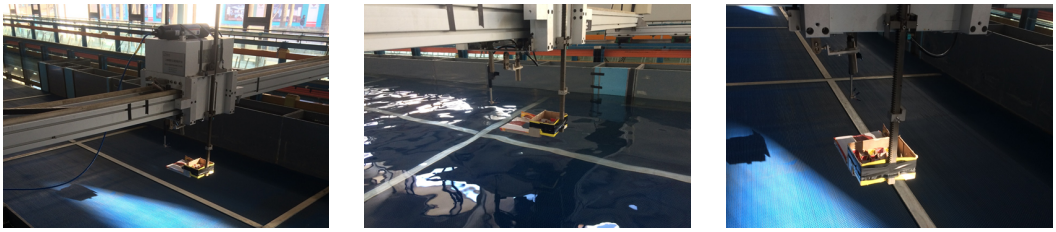

Figure 4.5: Nortek Vectrino ADV and particle dispenser on a mobile platform

A Particle Tracking Velocimetry (PTV) camera system was installed above, and along the length of the flume (see Figures 4.6 and 4.7). Due to limitations in the PTV analysis software (VDMS), it was only possible to use four adjacent cameras at once, covering approximately 10 m. Otherwise the particles would have been tracked over greater distances than presented in Section 4.2.3.

Figure 4.6: PTV camera system installed above flume

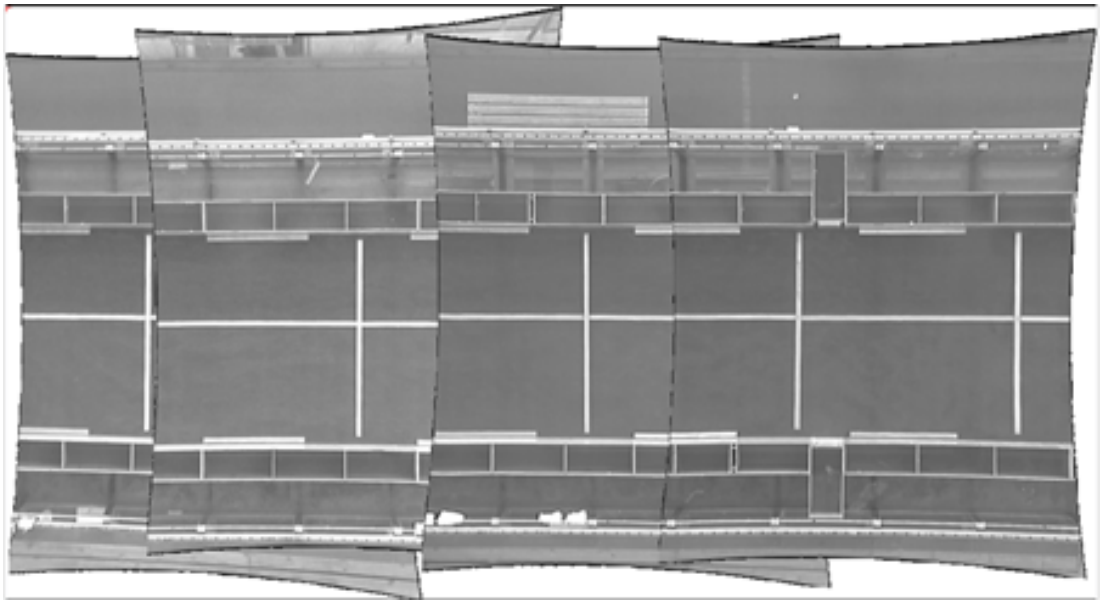

Figure 4.7: Example of the combined field of view (FOV) for the PTV camera array

4.2.2 Experimental methods

Four series of experiments were carried out, each of which included four flow cases. For each flow case, two particle release experiments were conducted using 20 particles and two using 40 particles. Plastic particles made of Polyvinyl chloride (PVC) of 10 mm diameter, and close to neutral buoyancy ($\rho = 900$ kg/m^3), were used (see Figure 4.8). Steady flow conditions were allowed to establish prior to particle release and the recording flow measurements.

(a) (b) (c)

Figure 4.8: PVC particle (a), (b) and dispenser (c)

Particles were released at the centreline of the channel from a 10 cm by 10 cm grid dispenser (see Figures 4.5 and 4.8) at a height of 10 cm, in order to reduce surface disturbances (see Weitbrecht et al. [2002]). Particles were distributed evenly among the divisions and released simultaneously on removal of the base, generating a random distribution. Their position on the water surface was tracked in time from the point of release, using the PTV system. Images were taken in batches of four, spaced at 0.2 s intervals, with 2 s between batches. This was due to software limitations which prevented continuous image capture at a fixed frame rate.

The bed roughness was calculated using Manning's equation [Okoye, 1970]:

$$U = \frac{1}{n} R^{\frac{2}{3}} S_f^{\frac{1}{2}} \tag{4.1}$$

where U is the depth-average velocity (m/s), R is the hydraulic radius (m), n is the Manning roughness coefficient and S_f is the friction slope (dimensionless). This was calculated using interpolation to fit a first order polynomial to the depth

readings taken using the centre two rows of pressure sensors (see Figure 4.2). Data from the outer two rows were ignored as a number of sensors were covered by the blocks forming the contraction.

ADV readings were taken using a profiler mounted on the same platform as the particle release tray (see Figure 4.5). A logarithmic velocity profile was assumed, following a $1/7^{\text{th}}$ power law:

$$u = U_{max}\left(\frac{z}{h}\right)^{\frac{1}{7}} \tag{4.2}$$

where u is the flow velocity (m/s) at elevation z (m) and the maximum velocity U_{max} occurs at the free surface. Integration between the bed ($z = 0$), and the water surface ($z = h$), yields Equations 4.3 and 4.4 for the magnitude and location of the mean velocity (U and z_U), respectively:

$$U = 0.875U_{max} \tag{4.3}$$

$$z_U = 0.4h \tag{4.4}$$

As such, depth-average values were taken as those recorded at 0.4h, and averaged over the centre third of the channel from readings taken at 70 cm, 105 cm and 145 cm across the width. Additional measurements were taken at the centre of the channel at; 0.2h, 0.6h and 0.8h; and at 0.4h, at 30 cm and 175 cm across the channel width.

The shear velocity ($U*$) was calculated using Equations 4.5 [Okoye, 1970; Sayre and Chamberlain, 1964]:

$$U* = \sqrt{gRS_f} \tag{4.5}$$

where ρ is the density of water (kg/m^3) and g is the acceleration due to gravity (m/s^2).

4.2.2.1 Series 1 and 2

The *in-situ* downstream underflow sluice gate was used to control the water level in the flume. Throughout the experiments a constant opening of 20 mm was maintained, such that the aspect ratio of the flow decreased with discharge.

Equation 4.6 was used to calculate the theoretical water level in the flume for each flow case to determine the near-steady flow conditions:

$$h_1 = \frac{1}{2g}\left(\frac{q}{C_D h_2 b}\right)^2 \tag{4.6}$$

where h_1 is the upstream water level (m), h_2 is the downstream water level (m), q is the discharge (m^2/s), b is the width (m), C_D is the coefficient of discharge (dimensionless) and g is acceleration due to gravity (m/s^2). This is valid for large h_1/h_2 ratios. The downstream water depth h_2 was assumed equivalent to the sluice opening h_0 and the coefficient of discharge was back-calculated as $C_D = 0.58$ after initial measurements were taken. Series 1 experiments were carried out with the flume in its original condition, with the rubber matting placed on the bed for Series 2.

Flow conditions and friction parameters are given in Tables 4.1, 4.2, 4.3 and 4.4. To ensure accuracy, the pressure sensors were recalibrated before commencing each series of particle release experiments. The differences in water levels between Series 1 and 2 for each flow rate can be attributed to differences in calibration.

In case of any influence of the flow contraction on cloud dispersion, the particles were released at 11.8 m and 19.4 m downstream of the flume inflow (4.2 m and 11.8 m downstream of the contraction, respectively; see Figure 4.2). The exact position was determined by the location of the power supply required for the ADV profiler.

Table 4.1: Bulk flow conditions for Series 1. Depth averaged along channel length, aspect ratio calculated for 2.1m width section of channel

Q (m^3/s)	**Depth** (m)	λ	**U** (m/s)	**Re**	**Fr**
0.06	0.122	17.256	0.250	2.6E+04	0.21
0.07	0.160	13.125	0.222	2.9E+04	0.17
0.08	0.202	10.412	0.197	3.2E+04	0.13
0.09	0.246	8.526	0.170	3.5E+04	0.11

Table 4.2: Series 1 friction parameters

Q (m^3/s)	**Sf**	τ_o (N/m^2)	**n**	**U*** (m/s)	**U*h** (m^2/s)
0.06	1.7E-04	0.187	0.013	0.0137	0.0017
0.07	6.4E-05	0.088	0.010	0.0094	0.0015
0.08	4.5E-05	0.075	0.011	0.0086	0.0017
0.09	1.6E-05	0.032	0.008	0.0056	0.0014

Table 4.3: Bulk flow conditions for Series 2. Depth averaged along the channel length, with the aspect ratio calculated for a 2.1 m width section of the channel

Q (m^3/s)	**Depth** (m)	λ	**U** (m/s)	**Re**	**Fr**
0.06	0.123	17.073	0.258	2.5E+04	0.21
0.07	0.159	13.183	0.220	2.9E+04	0.17
0.08	0.199	10.571	0.204	3.2E+04	0.14
0.09	0.248	8.463	0.182	3.5E+04	0.11

Table 4.4: Series 2 friction parameters

Q (m^3/s)	**Sf**	τ_o (N/m^2)	**n**	**U*** (m/s)	**U*h** (m^2/s)
0.06	5.3E-04	0.568	0.023	0.0238	0.0029
0.07	3.9E-04	0.531	0.025	0.0231	0.0037
0.08	1.7E-04	0.279	0.021	0.0167	0.0033
0.09	1.4E-04	0.271	0.023	0.0165	0.0041

4.2.2.2 Series 3 and 4

For each flow case the aspect ratio remained constant. The water level was maintained at a depth of 0.2 m using a number of downstream rectangular weirs located at 27.63 m (see Figure 4.9). The *in-situ* sluice gate was fully opened so that the flow downstream of the weir was unobstructed. The weir height was calculated for each flow case using Equation 4.7 [Horton, 1907] (see Table 4.5),

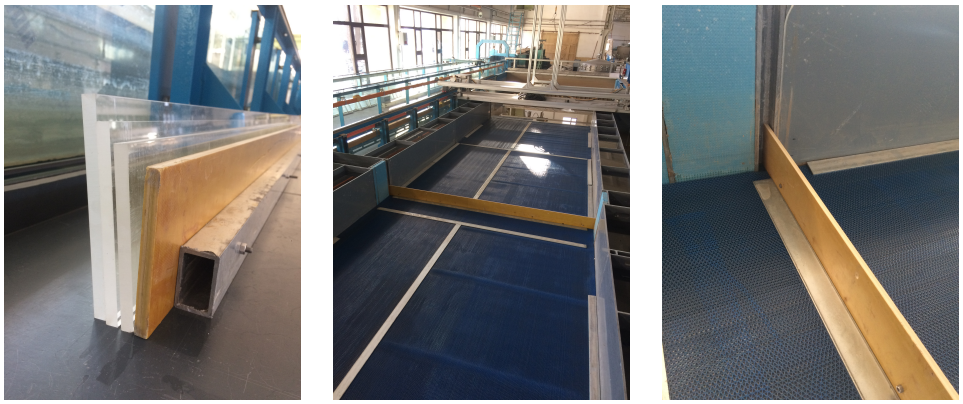

Figure 4.9: Weirs for water level control

$$q = \frac{2}{3} C_D b h_c^{\frac{3}{2}} \sqrt{2g}$$
$$h_w = h - h_c \tag{4.7}$$

where h is the flow depth (0.2 m), h_c is the water head above the weir crest, h_w is the weir height, $C_D = 0.65$ [ISO, 1980].

As in Series 1 and 2, two sets of experiments were carried out using this configuration. In Series 3 the particles were released at 16.5 m, further upstream of that in Series 1 and 2 due to position of the weir in the PTV FOV. In Series 4 the particles were released at 11.5 m. Vortices caused by the contraction were observed to have dissipated at this distance and the proximity of the release near the contraction was considered to be insignificant.

Flow conditions and friction parameters are given in Tables 4.6 and 4.7.

Table 4.5: Calculation of weir heights; see Equation 4.7

Q (m^3/s)	**h (m)**	**h_c (m)**	**h_w (m)**
0.04	0.2	0.046	0.154
0.06	0.2	0.061	0.139
0.08	0.2	0.073	0.127
0.10	0.2	0.085	0.115

Table 4.6: Bulk flow conditions for Series 3 and 4. Depth averaged along the channel length, with the aspect ratio calculated for a 2.1 m width section of the channel

Q (m^3/s)	**Depth (m)**	**λ**	**U - S3 (m/s)**	**U - S4 (m/s)**	**Re**	**Fr**
0.04	0.208	10.091	0.096	0.100	1.6E+04	0.06
0.06	0.203	10.343	0.149	0.155	2.4E+04	0.10
0.08	0.206	10.183	0.199	0.206	3.2E+04	0.13
0.10	0.205	10.269	0.250	0.254	4.0E+04	0.16

Table 4.7: Series 3 and 4 friction parameters

Q (m^3/s)	**Sf**	**τ_o (N/m^2)**	**n**	**U* (m/s)**	**U*h (m^2/s)**
0.04	5.6E-05	0.096	0.025	0.0098	0.0020
0.06	1.6E-04	0.264	0.027	0.0162	0.0033
0.08	2.4E-04	0.414	0.026	0.0203	0.0042
0.10	2.8E-04	0.477	0.022	0.0219	0.0045

4.2.3 Results

4.2.3.1 Series 1 and 2

Plots of the particle cloud variance with time are shown in Figure 4.10 for Series 1, q = 0.06 m^3/s for a release of 40 particles. Skewness values in particle distribution range between -0.24 and 0.43. Data are only shown for the fourth image from each batch for clarity. A first order polynomial was fitted to the data series and the coefficients of turbulent diffusion calculated using Equations 3.43, 3.44 and 3.45 as half of the gradient.

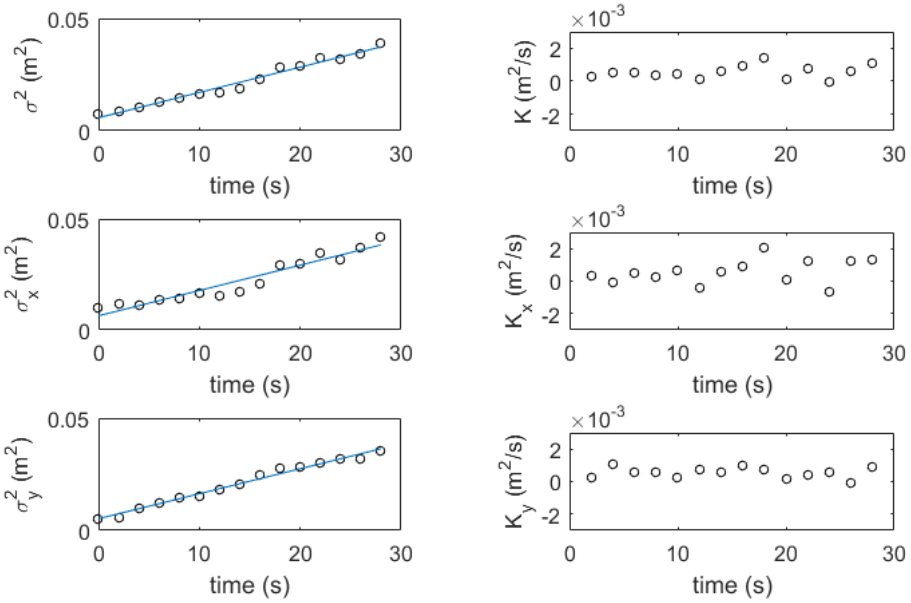

(a) (b)

Figure 4.10: Plot of variance (a) and non-dimensional turbulent diffusion coefficient (b) for Series 1, q = 0.06 m^3/s, 40 particle release. Subscripts x and y denote variables in the longitudinal and lateral flow directions respectively

Additional plots for this and other flow series have been omitted for brevity. However, it is important to note that not all experiments showed such clear trends, hence the reason for repetition. For example, Figure 4.11; Series 1, q = 60l/s, 20 particle release, shows skewness values ranging between -0.75 and 1.72.

The cause and significance of this is discussed in Section 4.2.4.

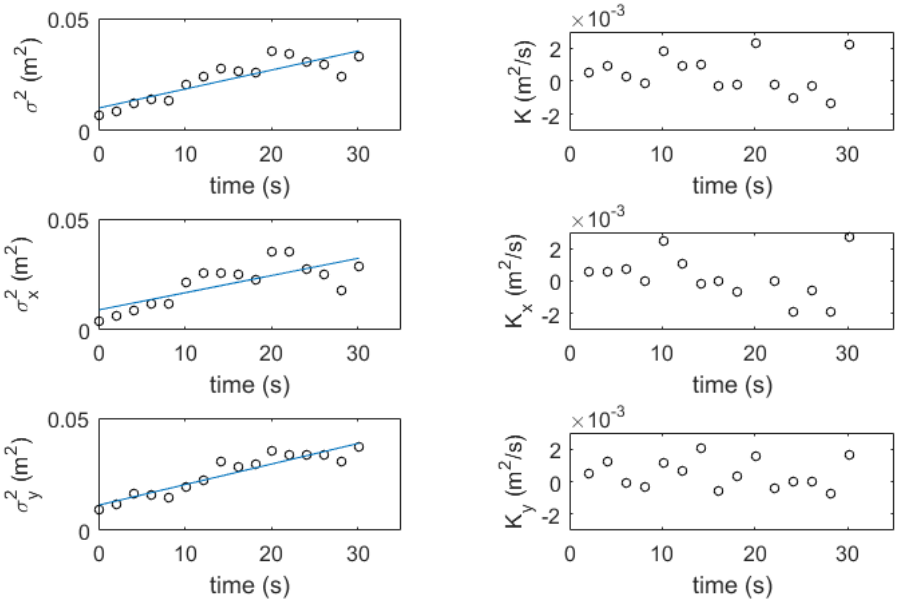

(a) (b)

Figure 4.11: Plot of variance (a) and non-dimensional turbulent diffusion coefficient (b) for Series 1, q = 0.06 m^3/s, 20 particle release. Subscripts x and y denote variables in the longitudinal and lateral flow directions respectively

Plots showing changes in the dimensional and non-dimensional coefficients of turbulent diffusion between flow cases are shown in Figures 4.12, 4.13, 4.14 and 4.15. Tabular data are given in Appendix A, Table 1. Plots of friction velocity, turbulence intensity (TI), and turbulent kinetic energy (TKE), are shown in Figures 4.16 and 4.17. The accompanying data are given in Appendix A, Tables 3 and 4.

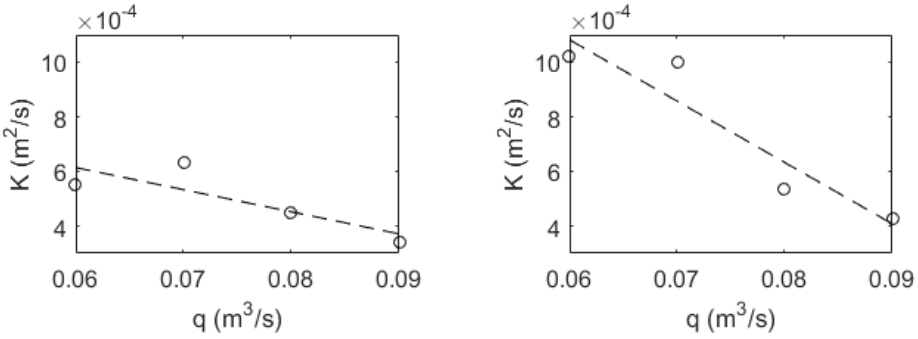

Figure 4.12: Particle cloud diffusion coefficients for each flow case in Series 1 (a) and 2 (b)

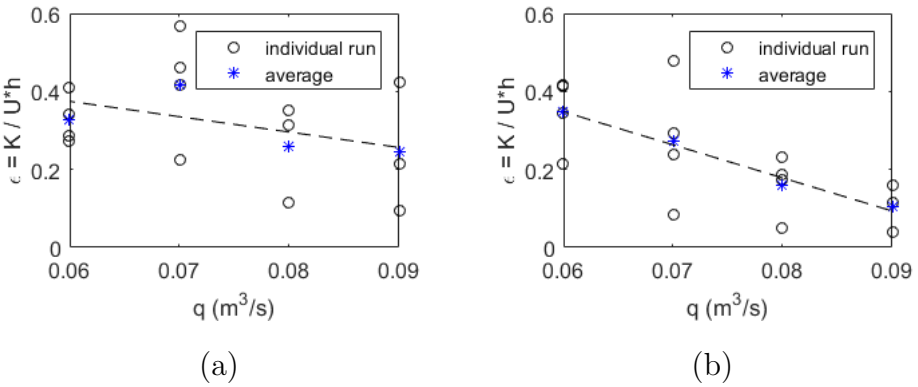

Figure 4.13: Plot of the total non-dimensional turbulent diffusion coefficient and flow for all Series 1 (a) and 2 (b) runs

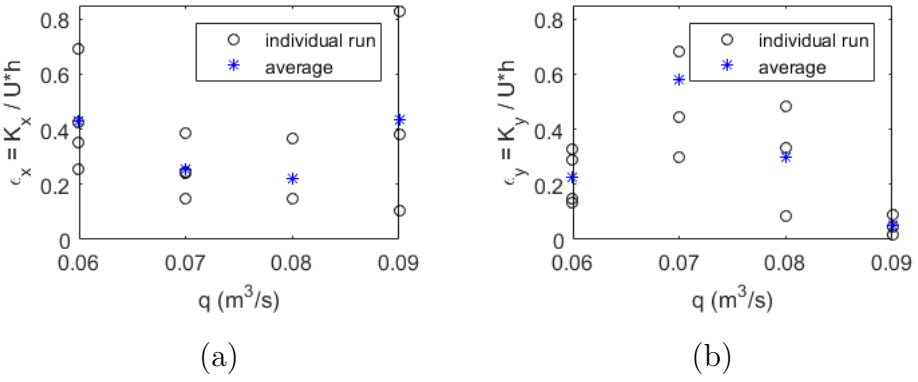

Figure 4.14: Plot of the non-dimensional turbulent diffusion coefficient in the x (a) and y (b) directions against flow for all Series 1 runs

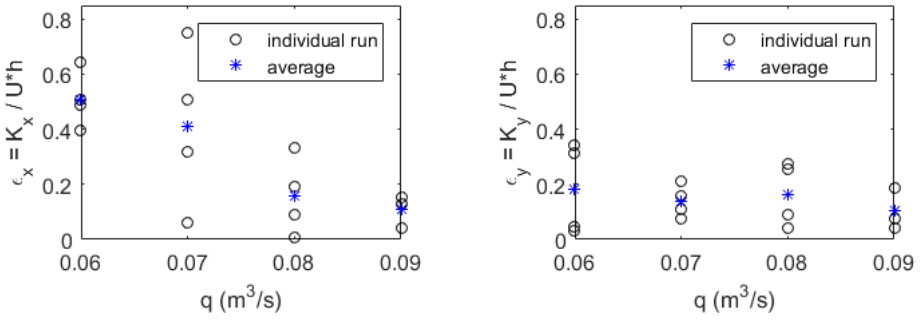

Figure 4.15: Plot of non-dimensional turbulent diffusion coefficient in the x (a) and y (b) directions against flow for all Series 2 runs

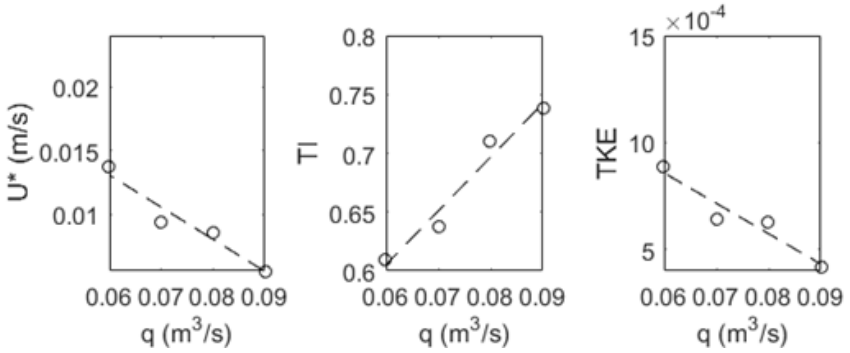

Figure 4.16: Friction velocity, turbulence intensity and turbulent kinetic energy for each flow case in Series 1

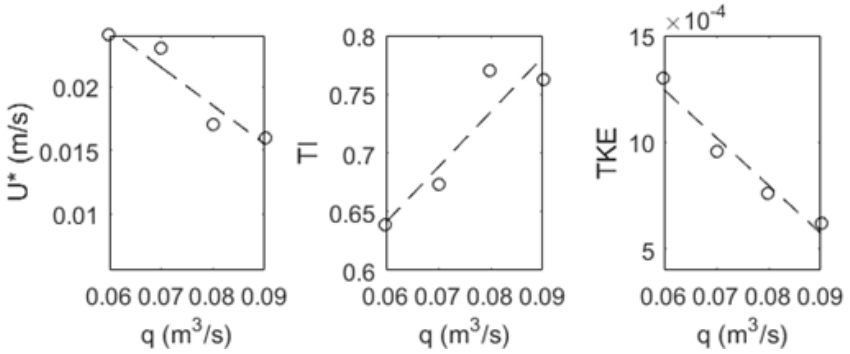

Figure 4.17: Friction velocity, turbulence intensity and turbulent kinetic energy for each flow case in Series 2

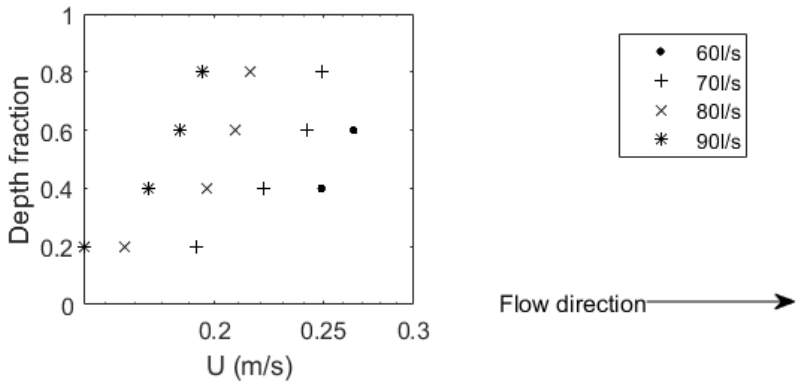

Figure 4.18: Series 1 longitudinal velocity profile taken over the depth at the centreline of the channel, immediately upstream of release locations

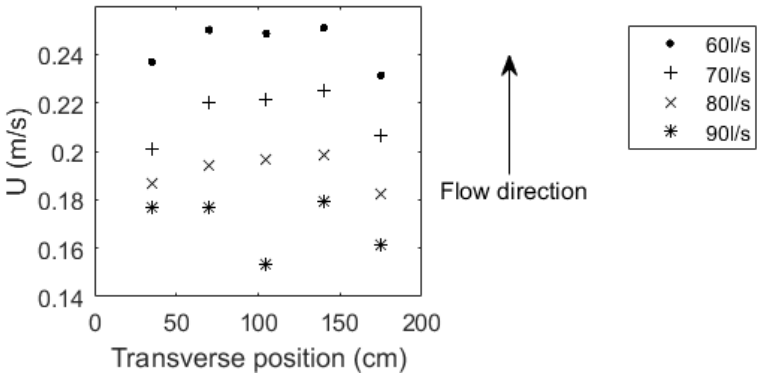

Figure 4.19: Series 1 transverse velocity profile taken across the width at 0.4d, immediately upstream of release locations

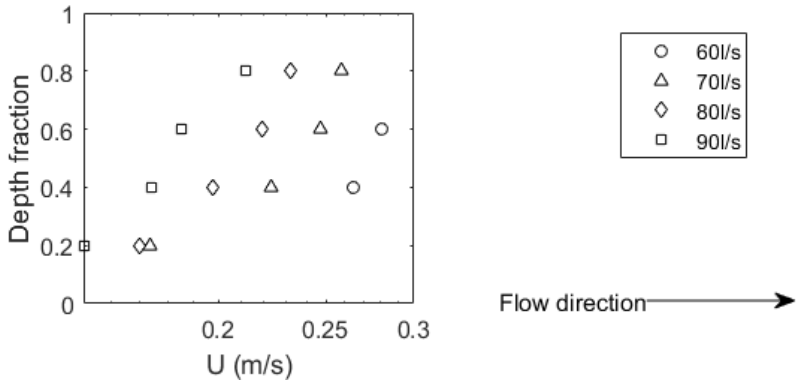

Figure 4.20: Series 2 longitudinal velocity profile taken over the depth at the centreline of the channel, immediately upstream of release locations

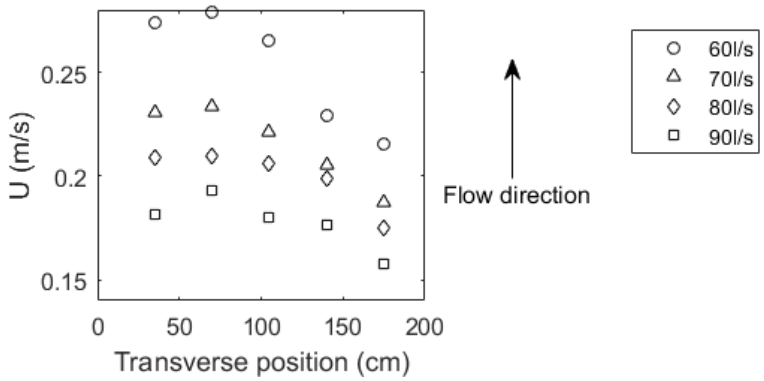

Figure 4.21: Series 2 transverse velocity profile taken across the width at 0.4d, immediately upstream of release locations

4.2.3.2 Series 3 and 4

Plots of the particle cloud variance with time are shown in Figure 4.22 for Series 4, q = 40 l/s for a release of 20 particles. The skewness values in the particle distribution range between -0.48 and 0.73. Directional values are provided in Appendix A, Tables 5 and 6. For each flow case the friction and turbulence parameters are shown in Figures 4.28 and 4.29.

It is of note that the uniform trend in variance shown in Figure 4.22 is not representative of all runs. In a number of cases the transverse cloud variance initially increased at a faster rate before plateauing. See Figure 4.23, Series 4, q = 0.06 m^3/s, 40 particle release. For these cases the non-dimensional coefficient of turbulent diffusion was calculated in the same manner as previously, however, a number of important points are made on this matter in Section 4.2.4 which discuss the validity of this method.

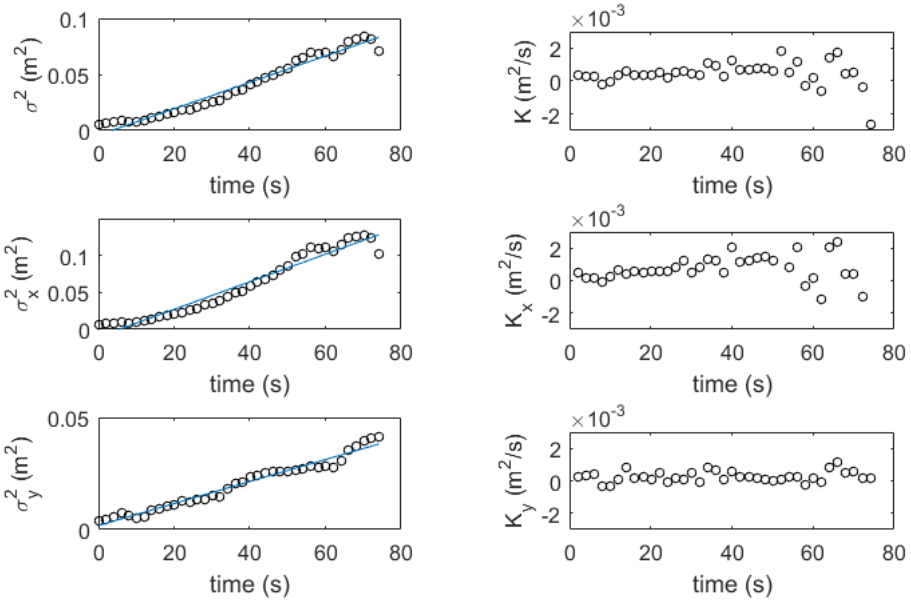

(a) (b)

Figure 4.22: Plot of variance (a) and the non-dimensional turbulent diffusion coefficient (b) for Series 4, q = 0.04 m^3/s, 20 particle release. Subscripts x and y denote variables in the longitudinal and lateral flow directions respectively

Plots showing the change in the non-dimensional coefficient of turbulent diffusion for the various flow cases are shown in Figures 4.24, 4.25, 4.26 and 4.27. Tabular data are given in Appendix A, Table 2. Plots of the friction velocity, turbulence intensity and turbulent kinetic energy are shown in Figures 4.28 and 4.29. Accompanying tables are given in Appendix A, Tables 5 and 6. Velocity profile plots recorded upstream of the Series 3 and 4 release locations are shown in Figures 4.30 and 4.31.

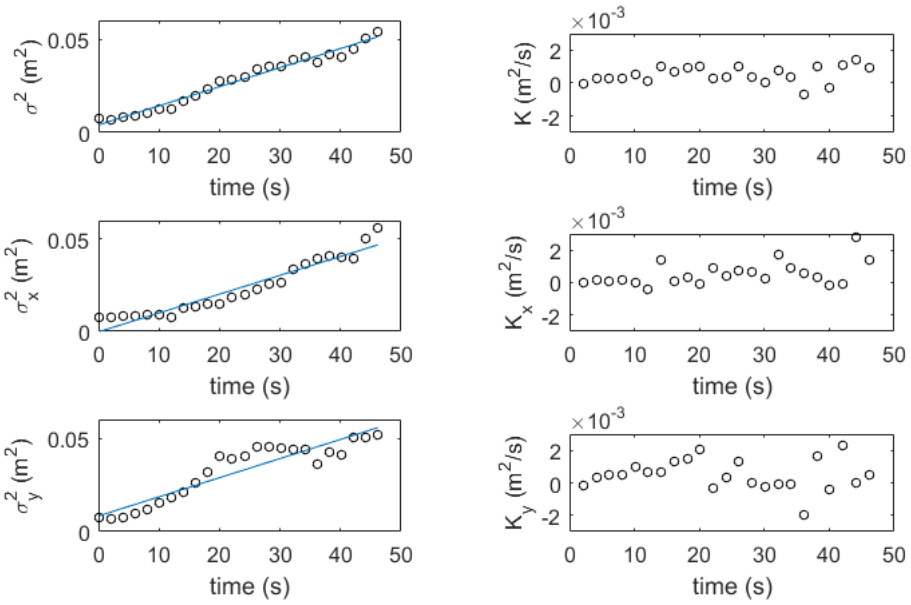

(a) (b)

Figure 4.23: Plot of variance (a) and the non-dimensional turbulent diffusion coefficient (b) for Series 4, q = 0.06 m^3/s, 40 particle release. Subscripts x and y denote variables in the longitudinal and lateral flow directions respectively

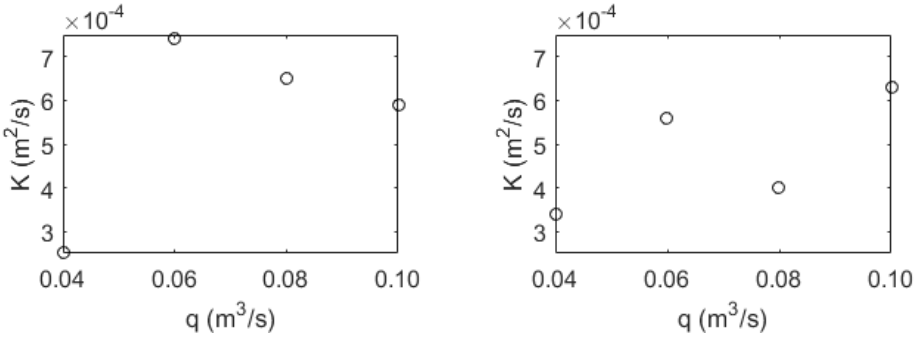

(a) (b)

Figure 4.24: Particle cloud diffusion coefficients for each flow case in Series 3 (a) and 4 (b)

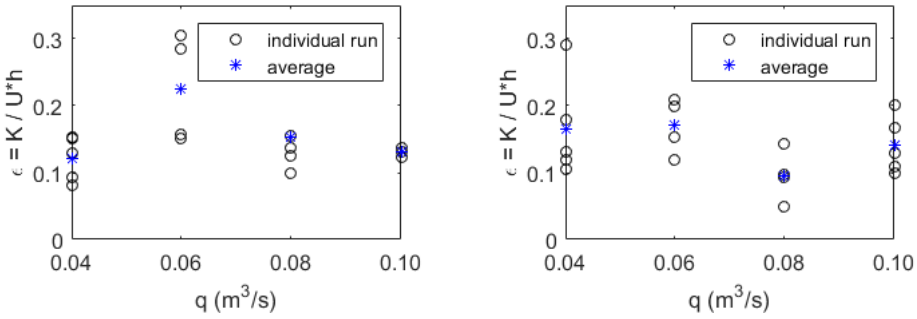

(a) (b)

Figure 4.25: Plot of the total non-dimensional turbulent diffusion coefficient and flow depth for all Series 3 (a) and 4 (b) runs

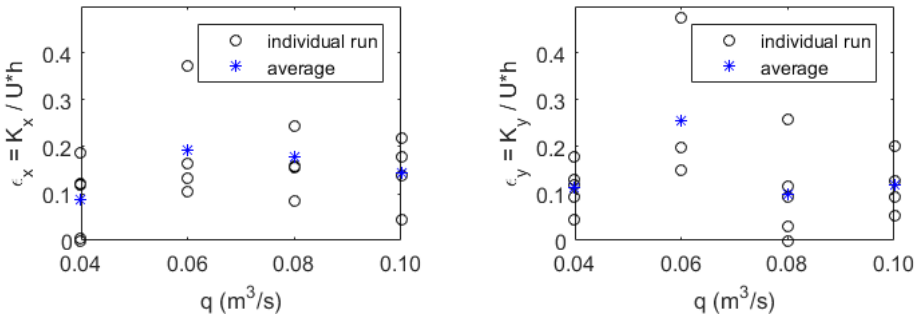

(a) (b)

Figure 4.26: Plot of the non-dimensional turbulent diffusion coefficient in the x (a) and y (b) directions against flow depth for all Series 3 runs

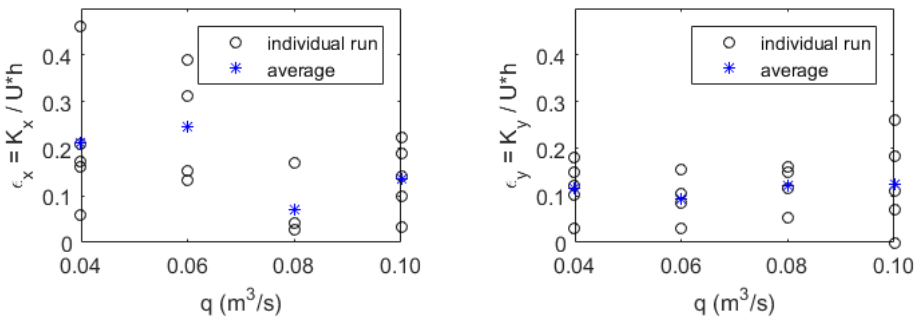

(a) (b)

Figure 4.27: Plot of the non-dimensional turbulent diffusion coefficient in the x (a) and y (b) directions against flow depth for all Series 4 runs

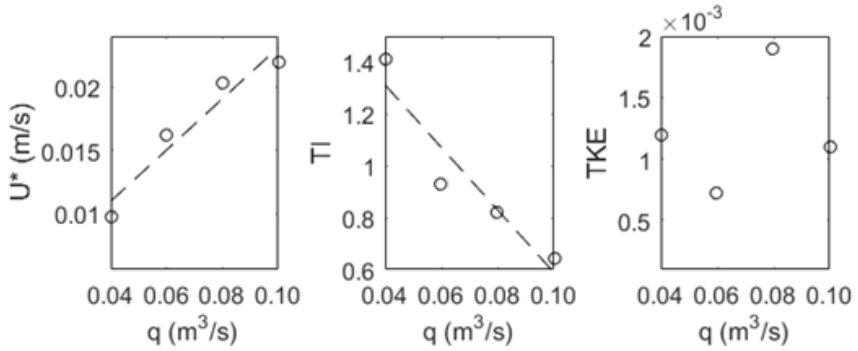

Figure 4.28: Friction velocity, turbulence intensity and turbulent kinetic energy for each flow case for Series 3

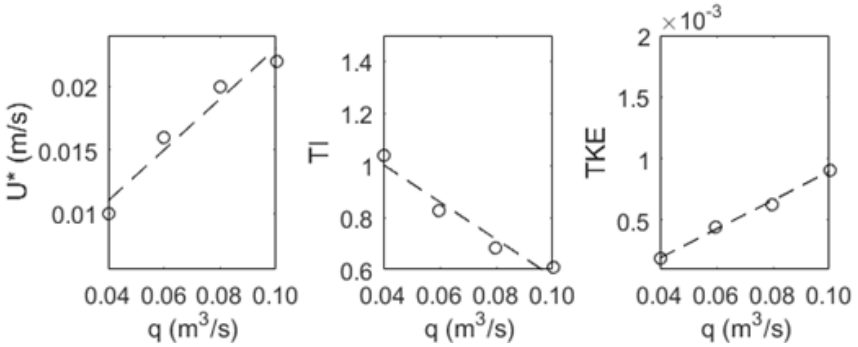

Figure 4.29: Friction velocity, turbulence intensity and turbulent kinetic energy for each flow case for Series 4

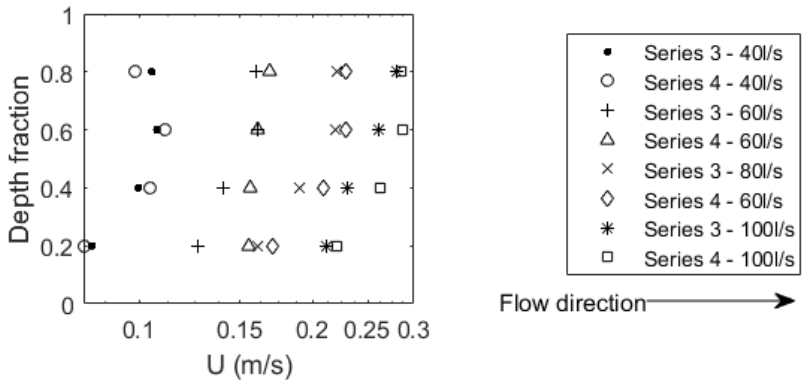

Figure 4.30: Longitudinal velocity profile taken over the depth along the centre-line of the channel, immediately upstream of release locations

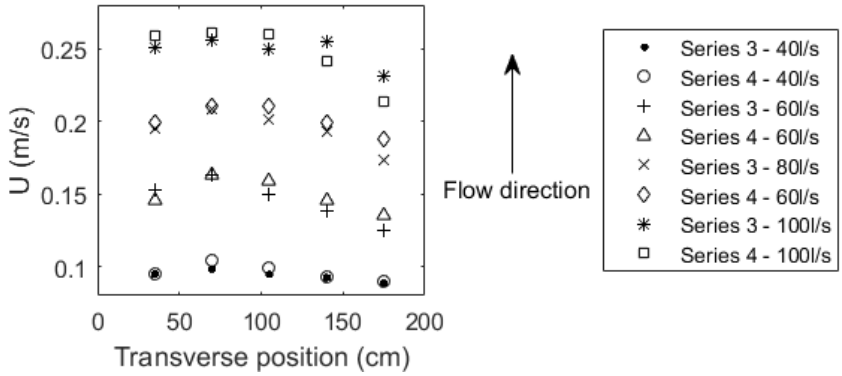

Figure 4.31: Longitudinal velocity profile taken across the width at 0.4d, immediately upstream of release locations

4.2.4 Discussion

While the following section refers primarily to the plots shown in Section 4.2.3, results from all experiments carried out using both 20 and 40 particles were used during analysis.

4.2.4.1 Series 1 and 2

It can be seen in Figures 4.12 and 4.13 that there is an increase in K from Series 1 to 2, with an associated reduction in ϵ for all flow cases, except q = 0.06 m^3/s. Possible reasons for this discrepancy will be discussed later in this section. Tabular values are given in Appendix A, Table 1. From Series 1 to Series 2, an reduction in the average value of ϵ from 0.322 to 0.221 was observed, with an increase in the average value of K from 4.91×10^{-4} m^2/s to 7.45×10^{-4} m^2/s. Given the similarity in the flow conditions between the two series, this can be explained by the increased bed roughness. This caused an increase in both the turbulence; as shown by an increase in the turbulence intensity (see Figures 4.16 and 4.17); and the shear velocity (see Tables 4.2 and 4.4, Figures 4.16 and 4.17).

In Figures 4.16 and 4.17, a reduction in the shear velocity and increase in the turbulence intensity with flow rate is shown. The increase in depth with flow rate causes a reduction in the flow velocity and thereby the friction velocity (see Tables 4.1 and 4.3). This relative reduction in the velocity and invariance in the

turbulence structure increases the turbulent intensity. Similarly, the reduction in flow velocity is responsible for the reduction in the turbulent kinetic energy.

Also apparent is the reduction in K and ϵ with increasing flow rate, in both Series 1 and 2, confirming the previously explained relationship with the shear velocity. Figure 4.14 demonstrates this relationship to be significantly more pronounced in the transverse direction in Series 1, whereas Figure 4.15 demonstrates this relationship to be significantly more pronounced in the longitudinal direction in Series 2. This may also be attributed to changes in the turbulent kinetic energy, where a strong inverse relationship with flow rate was observed in the longitudinal direction in Series 2. In Series 1 however, no clear relationship was observed in the longitudinal direction. This suggests that the aspect ratio of the flow; a proxy for the effect of secondary currents, led to the increased lateral diffusion [Okoye, 1970] and the observed reduction in ϵ with flow rate. However, it is not possible to draw conclusions from these data alone and further experiments are required (see discussion of Series 3 and 4).

In considering the directional non-dimensional turbulent diffusion coefficients, there is a clear distinction between the series. In Series 1 the observed reduction in the total diffusion coefficient can be attributed to the trend in the transverse direction, with no clear trend apparent in the flow direction. The opposite is observed in Series 2. Is it suggested that this is due to the prevalence of the transverse diffusion in Series 1, caused by secondary flows. In comparison with Series 2, the increased bed roughness is more influential, resulting in increasing the turbulence in the flow direction.

Measurements of the directional turbulence intensity (TI) are shown in Appendix A, Tables 3 and 3, which show greater TI readings in the transverse direction and invariant values in the longitudinal direction for Series 1.

For Series 2, the TI values are significantly higher in the longitudinal direction when compared to Series 1, yet the values are similar in the transverse direction. However, it is counter-intuitive to suggest an increase in turbulence intensity is responsible for a reduction in dispersion; and the value of ϵ. It is suggested that this is due to the magnitude of the turbulent kinetic energy. When Series 2 is compared with Series 1, the magnitude of the TKE in the longitudinal direction is significantly higher than the corresponding values in the transverse direction, and

span a greater range. The floating particles used in this study were not neutrally buoyant and a transfer of energy (i.e. work done) was required to move them. It is therefore suggested that the decrease in the TKE with flow rate was responsible for the reduction in cloud dispersion and ϵ. This does not disregard the influence of turbulence intensity, but highlights that the turbulent kinetic energy is more significant in this case.

4.2.4.2 Series 3 and 4

Before analysing the results obtained during Series 3 and 4 it is necessary to consider the effect of the downstream weir on the flow velocity profiles and turbulent diffusion parameters at each location. Profiles of the stream-wise velocity component over the depth and across the flow are shown in Figures 4.30 and 4.31. For each flow case in Series 3 they are shown to be similar, but lower than those in Series 4, causing a reduction in the Series 3 turbulence intensity measurements. This is thought to be due to a local increase in the flow velocity in the proximity of the neck of the flume.

As shown in Figure 4.29, the uniform trend in the TKE for Series 4 suggests that the Series 3 TKE measurements may be erroneous, as no trend is evident (see Figure 4.28). Alternately, it is suggested that the trend in total TKE for Series 3 is dependent on the TKE in the vertical direction, where greater readings were recorded for flow rates q = 0.04 m^3/s and q = 0.08 m^3/s, compared to q = 0.06 m^3/s and q = 0.1 m^3/s. TKE measured in the longitudinal and transverse directions have similar magnitudes. This indicates the presence of secondary currents at the location of Series 3 measurements (16.5 m), but not for those in Series 4 (11.5 m).

As shown in Figure 4.31, the transverse velocity profile for both series was asymmetrical, due by the presence of a transverse flow component (V); when q = 100 l/s, V = 0.02 m/s at 0.4d. It is suggested that this was either due to; the location of the inlet pipe in the corner of the flume (see Figure 4.2), or the Coriolis effect, which Coz [2019] has shown to be influential on the flow in the flume. This asymmetry was also observed in Series 1 and 2 (see Figures 4.19 and 4.21).

Due to the differences observed in velocity and turbulence measurements for Series 3 and 4 and the differences in the measured K values (see Figure 4.24), both series are discussed herein.

As seen in Figures 4.28 and 4.29, opposite trends are observed between the; friction velocity, turbulence intensity and turbulent kinetic energy; and flow rate in Series 3 and 4 compared with Series 1 and 2 (see Figures 4.16 and 4.17 respectively).

This suggests a the same to be true for ϵ, however, as shown in Figures 4.24, 4.25, 4.26 and 4.27, there is no discernible relationship between the dimensional and non-dimensional turbulent diffusion coefficients and flow rate. Of interest is the similar variance in the turbulent kinetic energy measured for Sereis 3 (see Figure 4.28), and the dimensional diffusion coefficient measured for Series 4 (see Figure 4.24). The comparison is valid, since the particles released in Series 4 were tracked to a distance of 21 m, thus confirming the relationship between the turbulent kinetic energy and diffusion, as suggested in the analysis of Series 1 and 2.

Considering the aspect ratio of the flow (λ): in all Series 3 and 4 flow cases λ was unchanged (see Table 4.6), compared to Series 1 and 2 where λ decreased with flow rate (see Tables 4.1 and 4.3). In Series 1 and 2, the reduction in ϵ with λ (see Figure 4.13), was due to a reduction in the lateral turbulence scale as the flow depth increased relative to the fixed width (see [Okoye, 1970]). This was more influential than the proposed relationship with turbulent kinetic energy. Hence in Series 3 and 4, when the aspect ratio was fixed, there was a relative invariance in the induced secondary currents in the flow and the observed changes in ϵ could be attributed to changes in the shear velocity, turbulence intensity or turbulent kinetic energy.

4.2.4.3 Further considerations

This section briefly describes potential sources of noise and uncertainty in the experimental data and provides an indication of methods on which future studies could improve.

PTV system errors

As seen in Figures 4.10, 4.11, 4.22 and 4.23, the difference in the particle cloud dispersion between consecutive image batches images is non-uniform (i.e. $\Delta\sigma$ and K vary with time). It is suggested that this is due to inaccuracies in the particle detection system, explained as follows.

The PTV camera system identified particles based on changes in total light intensity, observable due to differences in the reflectivity of water and the PVC particles. Prior to each particle release it was necessary to calibrate the background light intensity (i.e. that reflected of the surface of the water). However, changes in the cloud cover during a run caused this to deviate from the calibrated value (due to fluctuations in the light entering the laboratory windows) thereby preventing the system from identifying all particles in each frame. Similar interference was caused by glare from surface ripples, and in Series 2, 3 and 4, while the increase in reflected light intensity from the metal strips was registered in calibration, this still caused intermittent interference when particles passed above. It was possible to remove some of these effect in post-processing, but not entirely.

Particle separation distance

Particles were released in an initial random distribution beneath the dispenser. In situations where the initial separation distance between two particles was small (i.e. less than a particle diameter), or when two particles collided, they had a tendency to form a clump and were detected as a single particle. It is thought that this was due to surface tension and the lack of a surface coating on the particles preventing this from occurring (see Weitbrecht et al. [2002]). In addition, when clumps did not form the PTV system was often incapable of distinguishing between particles in close proximity, further reducing the number of particles detected.

As a result of the above, and the PTV system errors, approximately half of the particles were registered in each frame after image processing, and those which were varied from one frame to the next, causing the irregularly in particle position variance described. The effect of this is investigated in Section 4.3, though given the uniform trends observed in Figures 4.10, 4.11, 4.22 and 4.23 it is not considered significant.

Noisy data

When comparing the range of calculated ϵ values for each flow case within an experiment, there is a considerable variation, which is considered to be 'noise' in the underlying data trend. A number of reasons for this are proposed.

Firstly, as previously mentioned, particles with small separation distances had a tendency to clump. It is known that eddies smaller than a particle will have little effect on it's turbulent motion [Cederwall, 1971]. As such, in cases where clumping occurred it is reasonable to assume that the dispersion of the clumps should be different to that of the surrounding particles, which may also be responsible for the variation in cloud dispersion between releases.

It is also known that the initial separation of a particle group has an effect on the relative dispersion [Batchelor, 1952]. The larger the initial separation, the larger the range of turbulent structures (i.e. eddies) that can influence the dispersion of each particle, and vice versa. Combined with the previous points made, differences in the initial release pattern between experiments may also be responsible for increased or decreased cloud dispersion for multiple particle releases, for the same flow conditions.

It was noticed that for some runs in Series 3 and 4, the lateral cloud variance initially increased at a faster rate before plateauing (see Figure 4.23). It is possible that this may be due to some of the uncertainties discussed thus far, but given the relatively common occurrence of this pattern compared to Series 1 and 2, where it was not observed, another explanation is proposed.

Particle retention time

The measured stream-wise velocities for Series 3 and 4 flow cases q = 0.04 m^3/s and q = 0.06 m^3/s were significantly lower than those for flow cases q = 0.08 m^3/s and q = 0.1 m^3/s or in Series 1 and 2, q = 0.06 m^3 (see Tables 4.1, 4.3 and 4.6). Therefore, in these experiments the time taken for particles to cross the PTV FOV, herein called the retention time, was longer.

It is possible to calculate the dispersion of a particle cloud based on either the time elapsed since release or the distance from the release point (see Equations 3.41 and 3.42). Thus it can be reasoned that the dispersion of a particle cloud increases with retention time. In those experiments in Series 3 and 4 with reduced

velocity and increased retention time, it is proposed that some particles came within close enough proximity for the side wall to influence their position, thereby preventing further dispersion.

Although the effect discussed was observed at all flow cases in Series 3 and 4, it was more common for q = 0.04 m^3/s and q = 0.06 m^3/s, adding validity to this theory. However, it was not possible to investigate this further and it was therefore not considered during the analysis. A first order polynomial was used to calculate the diffusion coefficient, based on all data collected, instead of using only the initial segment with an apparent greater rate of spread.

It is understood that the coefficient of lateral diffusion tends towards a constant value at increasing distance from the source, after initially obeying and transitioning from the Richardson-Okubo power law [Orlob, 1959; Sayre and Chamberlain, 1964]. Due to the large initial particle separation distances (relative to the channel size) this limiting value is reached instantaneously, resulting in the linear trend in the dispersion, as shown in Figures 4.10, 4.11, 4.22 and 4.22. This confirms the method used to calculate a constant value for the turbulent diffusion coefficient for the channel.

4.2.5 Summary and conclusions

A series of experiments were conducted in a 2.1 m x 35 m open channel flume to monitor changes in the non-dimensional turbulent diffusion coefficient with shear velocity, turbulence intensity, turbulent kinetic energy and aspect ratio of the flow. Experiments were conducted using bed roughness values of n = 0.010 and n = 0.022 for flow rates between q = 0.04 m^3/s and q = 0.1 m^3/s. Floating PVC particles were released in groups of 20 and 40 and their position tracked using a PTV system installed above the flume. The key findings of this study are summarised as follows:

- Increased bed roughness causes greater particle cloud dispersion. In the cases considered this resulted in a reduction in the non-dimensional turbulent diffusion coefficient, due to an increase in the shear velocity while flow depth remained invariant.

- It has been shown that the turbulent kinetic energy is positively correlated with the dispersion of floating particles.
- There is a positive correlation between the non-dimensional turbulent diffusion coefficient and the aspect ratio of the flow due to the action of secondary currents.

While there is clear evidence to support these conclusions there are inconsistencies associated with the data collection method, leading to variances in the results. Further experiments using the existing set-up are desirable to significantly increase the quantity of data collected, or an alternative particle tracking method of increased accuracy should be used. In addition, similar experiments should be repeated using a dissolved tracer, using concentration tracking methods such as a flourometer or image analysis. This would allow the study of longitudinal dispersion, which is of more practical interest and has a significantly larger influence on pollutant dispersion in estuarine and coastal environments.

4.3 Numerical study

4.3.1 Set-up

Two models were set up using the depth-averaged finite element software TELEMAC-2D [Hervouet, 2007] to simulate each of the experimental configurations described in Section 4.2.2. These models replicated a sluice gate control and weir control, herein called model 1 and model 2, respectively (see Figures 4.32 and 4.33). In both cases a mesh resolution of 0.05 m was used with a time step of 0.05 s. Constant discharges and water levels (as given in Tables 4.1, 4.3 and 4.5), were used for the inflow and outflow boundary conditions for models 1 and 2, respectively. Model 1 was run to replicate Series 1 and 2, and model 2 run to replicate Series 3 and 4. In each case the initial water level was set to equal the outflow boundary condition.

Figure 4.32: Computational mesh of flume for sluice gate control. Dimensions given in m

Figure 4.33: Computational mesh of flume, reduced in length to weir boundary. Dimensions given in m

The Elder turbulence model was used which allows the user to specify the non-dimensional turbulent diffusion coefficient (ϵ) in the x and y directions (see Equation 3.18). Assuming isotropy, for each run series the average measured value of ϵ was assigned in both directions (see Table 4.8); the same value was assigned for Series 3 and 4.

Table 4.8: Value of the non-dimensional turbulent diffusion coefficient assigned for each numerical run series

Series	$\boldsymbol{\epsilon}$
1	0.32
2	0.23
3	0.15
4	0.15

4.3.2 Particle tracking

The particle tracking experiments described in Section 4.2 were replicated using the functionality in TELEMAC to simulate drogue dispersion. Particles (drogues), released into the model are transported in the horizontal plane in the x and y coordinate directions, with the depth of release and vertical velocity not being considered. The Lagrangian trajectory of the particles is calculated by

interpolation of the velocity from the surrounding mesh point values, at the start of the time step, and the displacement calculated accordingly [Hervouet, 2007]. Both models were run for a sufficient length of time to allow steady flow to be established prior to particle release.

To replicate the random scatter of particles generated in the flume releases (see Section 4.2.2), the initial coordinates were generated randomly for 40 particles, within a 10 cm by 10 cm area centred on the release location. A different initial scatter pattern was generated for each model run.

4.3.3 Results

4.3.3.1 Hydrodynamic simulation

The calculated hydrodynamic and friction parameters for each flow case in each series are shown in Tables 4.9 and 4.10, against the flume discharge.

Table 4.9: Series 1 (a) and 2 (b) flow and friction parameters

(a)

Q (m^3/s)	**Depth (m)**	**U* (m/s)**	**U*h (m^2/s)**
0.06	0.1363	0.0095	0.0013
0.07	0.1632	0.0091	0.0015
0.08	0.2005	0.0081	0.0016
0.09	0.2465	0.0072	0.0018

(b)

Q (m^3/s)	**Depth (m)**	**U* (m/s)**	**U*h (m^2/s)**
0.06	0.1351	0.0224	0.0030
0.07	0.1668	0.0203	0.0034
0.08	0.2045	0.0183	0.0037
0.09	0.2492	0.0163	0.0041

Table 4.10: Series 3 and 4 flow and friction parameters

Q (m^3/s)	**Depth (m)**	**U* (m/s)**	**U*h (m^2/s)**
0.04	0.2016	0.0094	0.0019
0.06	0.2035	0.0139	0.0028
0.08	0.2062	0.0183	0.0038
0.10	0.2117	0.0223	0.0047

4.3.3.2 Particle tracking and dispersion

As discussed in Section 4.2.3, the positions of up to half of the particles in each experiment were not recorded by the PTV system. To determine the effect of this on the calculated diffusion coefficients, two methods of analysis were used to evaluate the numerical results. Firstly, for each case the cloud variance and diffusion coefficient were calculated using the positions of all 40 particles (see Figure 4.34), in the same manner as described in Section 4.2.3.

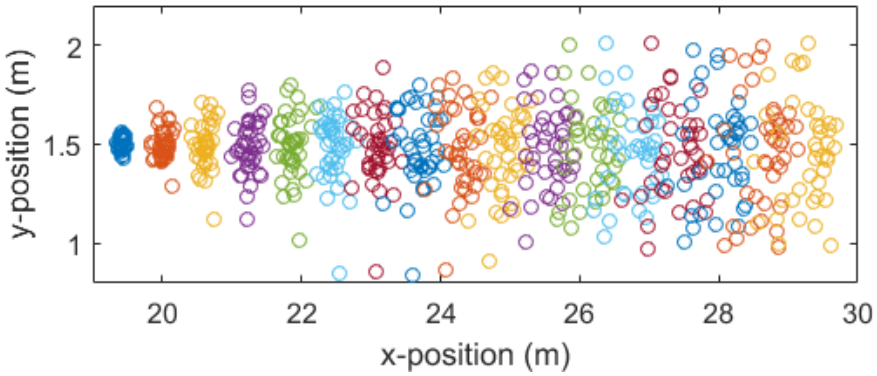

Figure 4.34: Plot of particle positions at 2 s intervals, for Series 2, q = 0.06 m^3/s, using the original data, where adjacent colours represent different points in time

In addition, for the same data set half of the particles were randomly removed at each time step, such that it was not guaranteed that a particle was detected from one image to the next. The cloud variance and diffusion coefficient were calculated using the reduced particle field (see Figure 4.35). Hereafter these two methods and data series are referred to as 'original' and 'random', respectively.

4.3.4 Results

Figure 4.36 presents a comparison between the calculated variance statistics for a flow case in Series 2 using the original and random analysis methods. Similar plots for other flow cases and series have been omitted for brevity.

For each flow case in Series 1 and 2 the calculated dimensional and non-dimensional diffusion coefficients are shown in Figures 4.37 and 4.38. Those for Series 3 and 4 are shown in Figures 4.39 and 4.40.

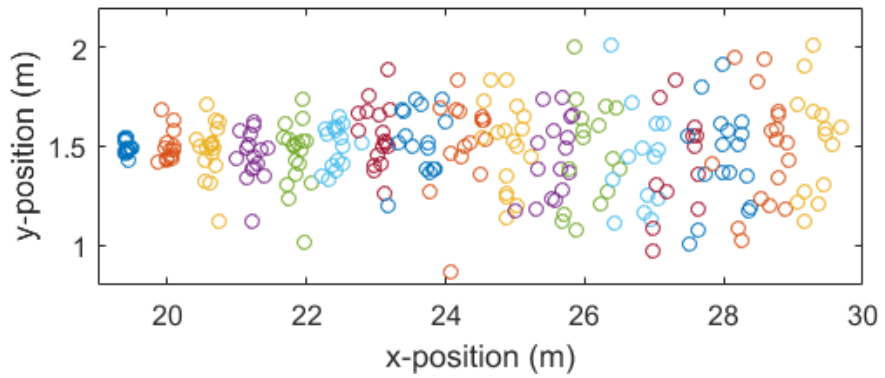

Figure 4.35: Plot of particle positions at 2 s intervals, for Series 2, q = 0.06 m^3/s, using the random data, where adjacent colours represent different points in time

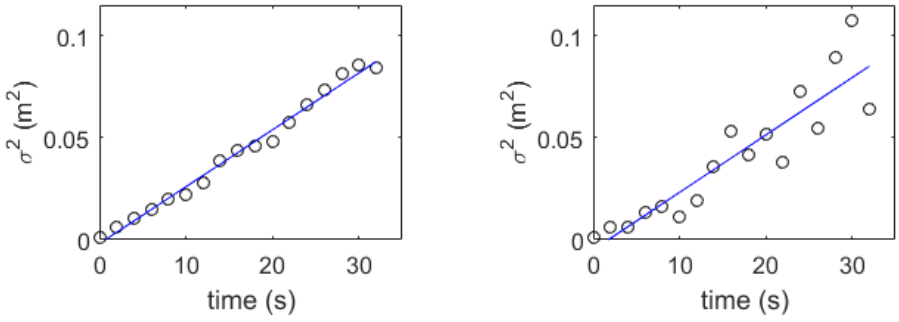

(a) (b)

Figure 4.36: Plot of drogue cloud variance for Series 2, q = 0.06 m^3/s using the original and random data; (a) and (b) respectively

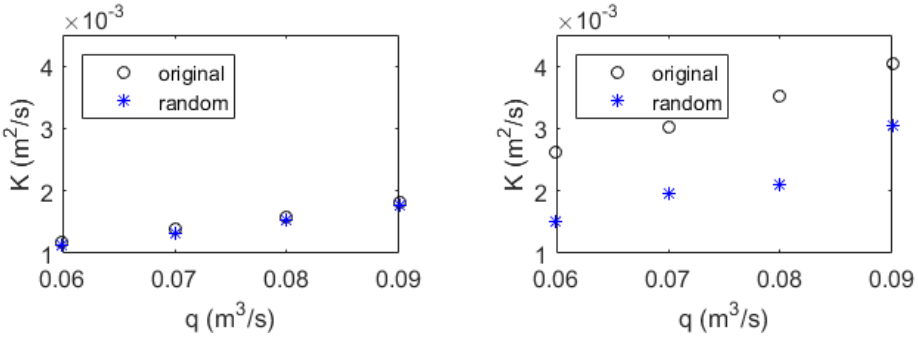

(a) (b)

Figure 4.37: Plot of dimensional turbulent diffusion coefficient for all Series 1 and 2 runs; (a) and (b) respectively

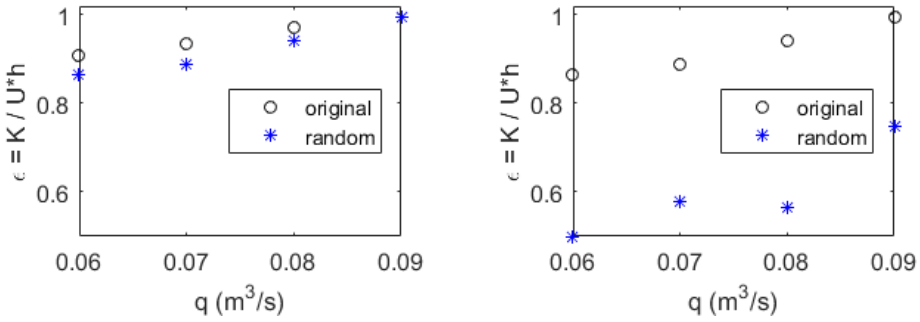

(a) (b)

Figure 4.38: Plot of non-dimensional turbulent diffusion coefficient for all Series 1 and 2 runs; (a) and (b) respectively

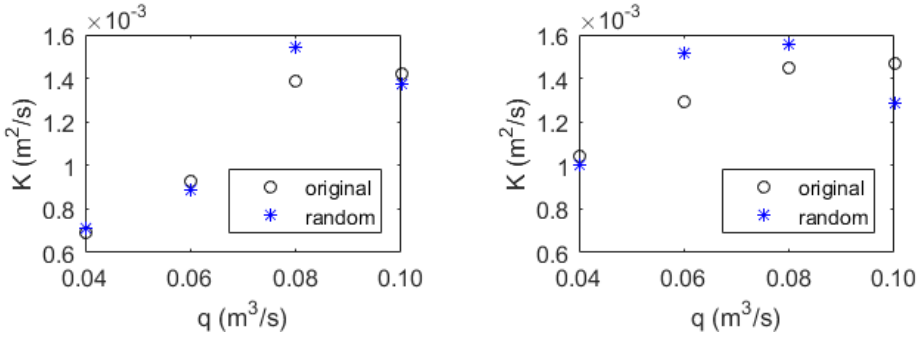

(a) (b)

Figure 4.39: Plot of dimensional turbulent diffusion coefficient for all Series 3 and 4 runs; (a) and (b) respectively

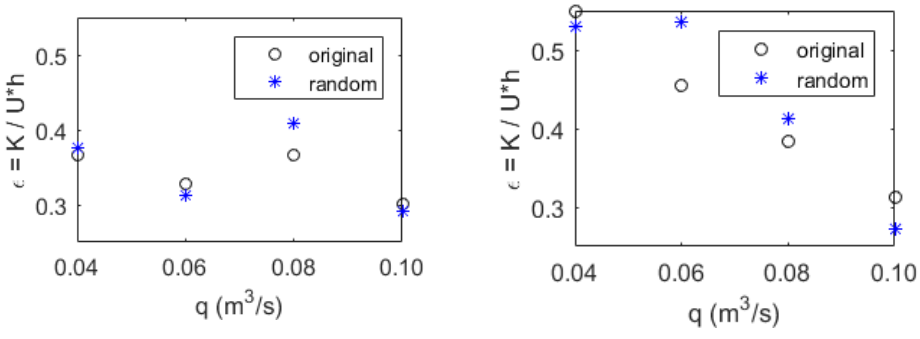

(a) (b)

Figure 4.40: Plot of non-dimensional turbulent diffusion coefficient for all Series 3 and 4 runs; (a) and (b) respectively

Tables 4.11 and 4.12 show a comparison between the average non-dimensional turbulent diffusion coefficients for each flow case and the minimum and maximum calculated skewness values in particle position.

Table 4.11: Average non-dimensional turbulent diffusion coefficient for all Series 1 and 2 runs; (a) and (b) respectively

(a)

Series	**K/U*h**	**K_x/U*h**	**K_y/U*h**	**Sk_{min}**	**Sk_{max}**
Original	0.959	1.183	0.736	-0.658	0.727
Random	0.922	1.110	0.735	-1.623	1.467

(b)

Original	0.922	1.110	0.735	-1.186	0.804
Random	0.598	0.720	0.476	-1.588	1.248

Table 4.12: Average non-dimensional turbulent diffusion coefficient for all Series 3 and 4 runs; (a) and (b) respectively

(a)

Series	**K/U*h**	**K_x/U*h**	**K_y/U*h**	**Sk_{min}**	**Sk_{max}**
Original	0.340	0.359	0.322	-0.568	1.060
Random	0.347	0.374	0.321	-1.087	1.758

(b)

Original	0.425	0.558	0.292	-1.194	0.551
Random	0.437	0.570	0.304	-2.017	1.110

4.3.5 Discussion and comparison with experimental data

As expected, it can be seen from Table 4.9 that for Series 1 and 2, the water depth and shear velocity calculated for each flow case are of a similar magnitude

to the values measured experimentally (see Tables 4.2 and 4.4), and follow the same relationship with flow rate. This is also the case for Series 3 and 4 (see Tables 4.7 and 4.10), which confirms that TELEMAC is an accurate model for predicting hydrodynamics in the current case study.

It can also be seen that values of U*h were calculated to be of a similar magnitude to those measured experimentally, however in Series 1 and 2, a uniform trend was predicted with flow rate, which was not observed experimentally. This can be attributed to errors in water level measurements, which were known to be a potential source of uncertainty due to; sensor inaccuracy, calibration errors, and whether a true steady state flow state was established prior to data collection.

It can be seen in Figure 4.36 that while there is more scatter in the variance of the random, vis-a-vis the original data, the trend is similar. This is reflected in the increased skewness of the random data (see Tables Tables 4.11 and 4.12), and the similarity in the dimensional and non-dimensional diffusion coefficients calculated using the two analysis methods, as shown in Figures 4.38 and 4.40, respectively. However, an exception is seen for Series 2, despite the skewness values being calculated as lower than for Series 1, 2 or 3 (see Tables 4.11 and 4.12), which highlights a potential source of error in the experimental data.

4.3.5.1 Series 1 and 2

As shown in Figure 4.37 and observed experimentally, there is an increase in K in Series 2 due to the increase in bed friction and shear velocity. Similarly, it can be seen in Figure 4.38 that there is a reduction in ϵ, which can be attributed to the lower value assigned when setting up the turbulence model (see Table 4.8), and the increase in shear velocity. However, in both cases a positive relationship was flow rate is predicted, whereas the opposite was seen experimentally, for which two explanations are proposed.

Firstly, while the experimental data suggested that the specified value of ϵ should decrease with flow rate, the same value was used for each flow case due to uncertainty in the observed trend. However, that a positive relationship with flow rate is predicted, despite the constant value assigned to ϵ, suggests that more importantly, it is the use of a 2D model and the choice of turbulence model which

are responsible.

It has been confirmed by experiment that as suggested by Okoye [1970], there is a positive correlation between ϵ and the aspect ratio of the flow, due to the action of secondary currents. However it is not possible to predict secondary currents when using a depth-averaged model and it is therefore suggested that either; it is necessary to use a 3D model in order to calculate the impact of secondary flows on turbulent diffusion and particle dispersion, or that the non-dimensional diffusion coefficient should be written as suggested by Okoye [1970] to account for the assumptions and inherent limitations of 2D simulations. That is, as a function of shear velocity, depth and aspect ratio:

$$\epsilon = \Phi(\lambda) \tag{4.8}$$

where Φ is an unknown function.

4.3.5.2 Series 3 and 4

It can be seen in Figure 4.39 that in Series 3 and 4, K was positively correlated with flow rate. However, as indicated by the random data, the removal of particles during analysis was sufficient to mask the true data trend. This increase in turbulent diffusion with flow rate can be attributed to increased levels of turbulence as the flow speed increased, as confirmed experimentally.

The reduction in ϵ with flow rate observed in Series 4 (see Figure 4.40 (b)), was due to the increase in shear velocity with flow speed. In contrast, no trend can be seen in the Series 3 data (see Figure 4.40 (a)), due to the less pronounced trend in K with flow rate seen in Figure 4.39 (a). This confirms that despite efforts to reduce the downstream and upstream impacts of the flow contraction and weir on the experimental data collected in Series 3 and 4, respectively, this was not possible.

4.3.5.3 Further considerations

It can be seen from Tables 4.11 and 4.12 that in all flow series, on average, ϵ_x was calculated to be larger than ϵ_y, whereas no trend was observed experimentally. As there is no further relationship between ϵ_x, ϵ_y and skewness, this can be attributed to the inability of the 2D model to simulate secondary currents in the flume, which would result in a more homogeneous turbulence field, less aligned with the primary flow direction.

It can also be seen that in all flow series, the calculated values of ϵ were several orders of magnitude larger than those observed experimental and specified (see Figures 4.38 and 4.40 and Table 4.8). Furthermore, it can be seen in Figures 4.37 and 4.39 that the calculated values of K were of a similar order of magnitude larger than those observed. This indicates that in the configuration used for this study, TELEMAC-2D over-predicts the movement of surface particles. While it is not discussed in detail herein, it is suggested that this may be due to particle-particle interactions, such as clumping, or due to other influences such as particle weight, buoyancy and shape, which are not considered in TELEMAC.

4.3.6 Summary and conclusions

In summary, the numerical simulations proved to be a reliable representation of the experiments undertaken, cross-validating and confirming the inverse relationship between ϵ and shear velocity and the positive correlation between ϵ and the aspect ratio of the flow.

However, it is suggested than when using a depth-averaged model to predict the motion of surface particles, or drogues, the turbulence model should be modified as proposed by Okoye [1970] to take into account the impact of secondary currents.

Chapter 5

Development of water quality model

5.1 Introduction

This chapter focusses on the development of two models of Swansea Bay, UK, using TELEMAC-2D and TELEMAC-3D. In each case, multiple modelling approaches have been taken and their performance compared. Further comparison has been made between the use of a 2D or 3D model, and recommendations made as to that deemed most suitable. The results of a comprehensive bathing water assessment, made using the most suitable model, are discussed in Chapter 6.

5.2 Study Site

Swansea Bay is a well mixed macro-tidal inlet situated in the north of the Severn Estuary, UK [Ahmadian et al., 2013; Bakar et al., 2016]. It is approximately 13 km wide at the mouth and contains two bathing waters; Swansea Bay and Aberafan (see Figures 5.1 and 5.2), both of which received a good rating in the most recent bathing water assessment period, and was chosen for this study due to the large quantity of environmental data available.

The primary rivers flowing into the bay are the Rivers Tawe and Neath, the catchments of which include the following land uses; common land, grassland, woodland and forestry, urban and industrial.

Figure 5.1: Location of bathing waters (BW) within Swansea Bay, Severn Estuary, UK: BW1 - Swansea Bay, BW2 - Aberafan

Figure 5.2: Swansea Bay, bacterial source inputs (red dots) and locations of interest

The bay is subject to 85 inputs, as shown in Figure 5.3a, 47 of which were included within the TELEMAC models: 28 Primary and 19 secondary surface water and sewage discharges were recorded at 15 minute intervals during the 2011 bathing season (May to September), for for the Smart Coasts - Sustainable Communities project (herein referred to as Smart Coasts [Aberystwyth University and University College Dublin, 2018]. Within the same project all primary sources

were predicted from October to November 2012 at 15 minute intervals; predictions were not made for combined sewer overflow (CSO) spills. FIO measurement records were available at the positions shown in Figure 5.3b on 15th November 2012 (a spring tide), and at BW1 for the 2011 bathing season.

Of these, BW1 and BW2 transects are used to monitor Swansea Bay and Aberafan for the rBWD, respectively: samples are taken at a depth of 0.5 m [Bedri et al., 2016; Bomminayuni, 2015]. Over the tidal cycle, tidal flats are exposed up to a distance of 1500 m from shore, preventing measurements being taken at any one location but along the sampling transects shown; herein referred to as the Designated Sampling Point (DSP) for each bathing water.

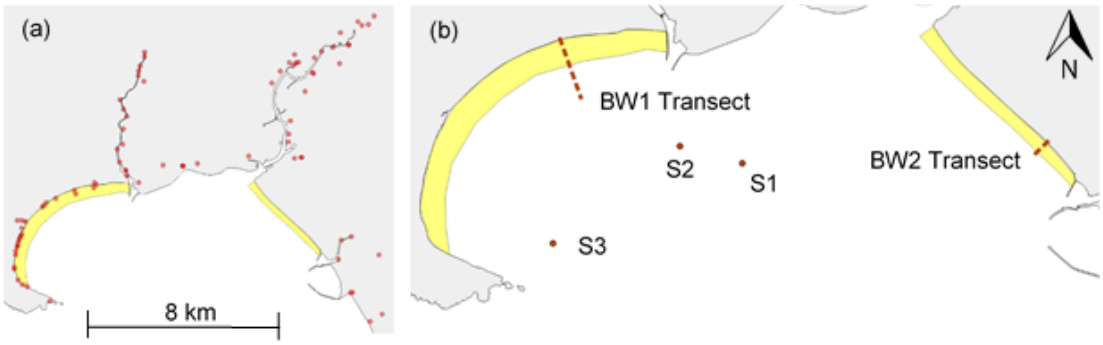

Figure 5.3: (a) Location of bacterial inputs (b) Location of monitoring points and transects

5.3 Model details

5.3.1 Set-up

Two computational meshes of the Severn Estuary were created, one each for the 2D and 3D models, with differences in the region of Swansea Bay (see Figure 5.4). The 3D domain comprised of a 2D mesh repeated over 5 uniformly distributed sigma layers.

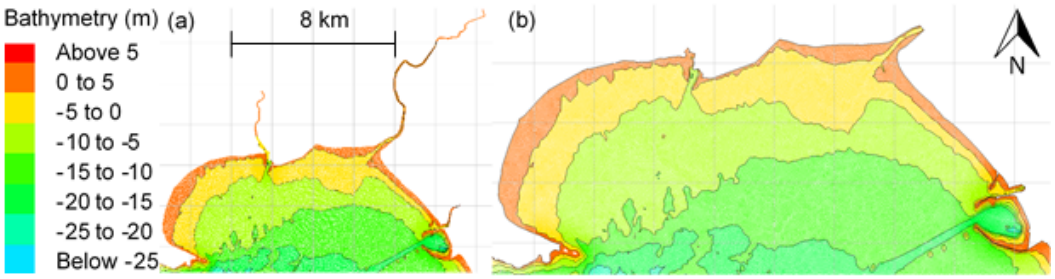

Figure 5.4: 2D (a) and 3D (b) unstructured computational meshes of Swansea Bay. Bathymetry relative to mean sea level (MSL)

Bacterial sources were included as concentration (cfu/100 ml)-time series. Source locations within each domain are shown in Figures 5.5 and 5.6 respectively, with source details (including lumped sources), given in Appendix B.2, Table 7.

To remove the need for coupling with a 1D model, the 2D model was extended up the River Tawe and to the tidal limits of the Rivers Afan and Neath. However, these reaches were excluded from the 3D model to reduce unnecessary vertical refinement in regions where 3D effects were of no concern. Note that at the time of writing, coupling between the latest release of TELEMAC-3D (v7p3r2), and the 1D river model TELEMAC-MASCARET, was not possible. In the 3D model, the bacterial source inputs distributed within each reach were lumped into a single source point, whereas those in the 2D model retained their true position.

Both meshes covered the extent of the Severn Estuary up to the tidal limit at Gloucester (see Figure 5.7). The mesh size in Swansea Bay was determined based on sensitivity testing. Stapleton et al. [2007a] found that a coarse grid (600 m by 600 m), was incapable of capturing localised features such as pollutant plume shape. However, bathymetry data of Swansea Bay was available at a maximum resolution of 30 m [The University of Edinburgh, 2016a,b], enforcing a lower limit on the grid size. Two computational meshes were developed; using a 25 m and 50 m mesh in Swansea Bay, increasing at a uniform rate of 1.2 to 1000 m in the Severn Estuary. At the resolutions tested the model was found to be insensitive to mesh size and a 50 m grid size was used within Swansea Bay to increase computational efficiency.

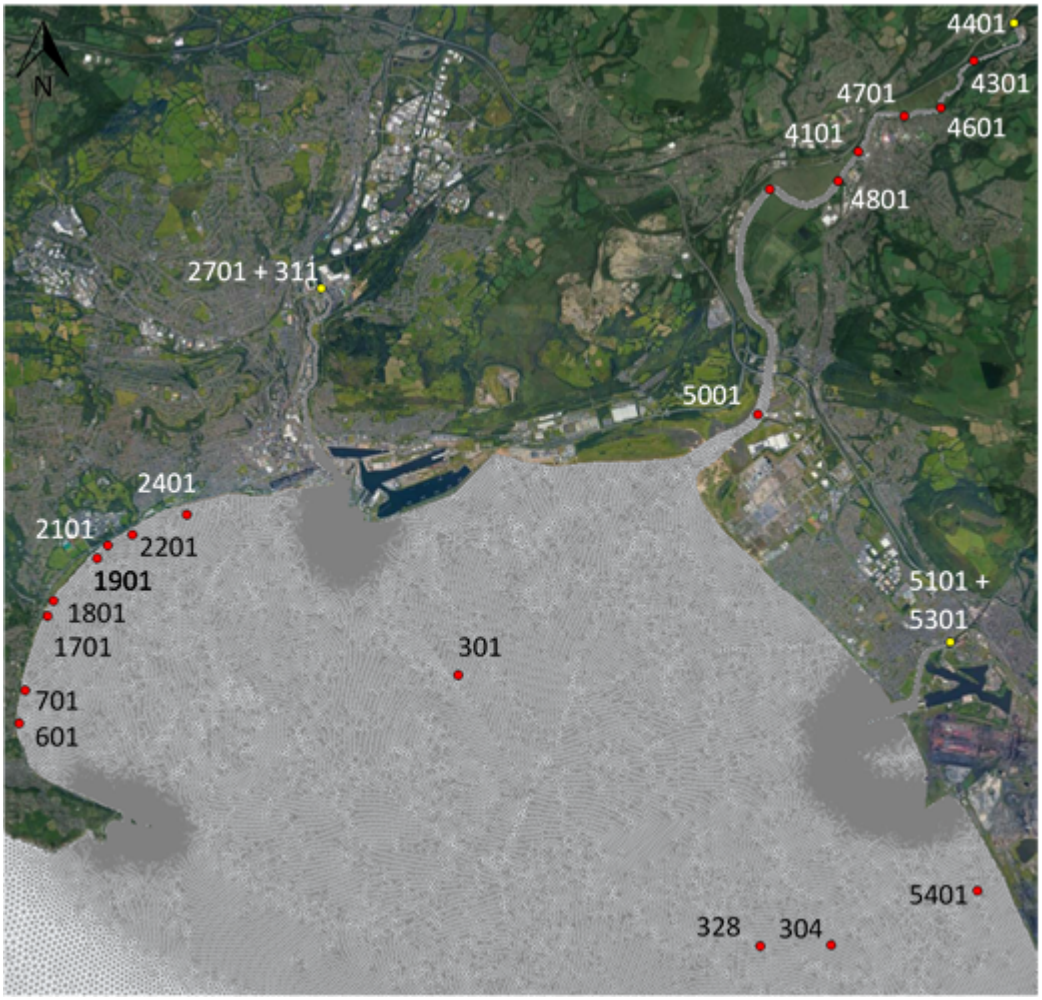

Figure 5.5: Primary input locations of bacterial sources within the 2012 2D domain of Swansea Bay; point sources (red dots) and boundary conditions (yellow dots)

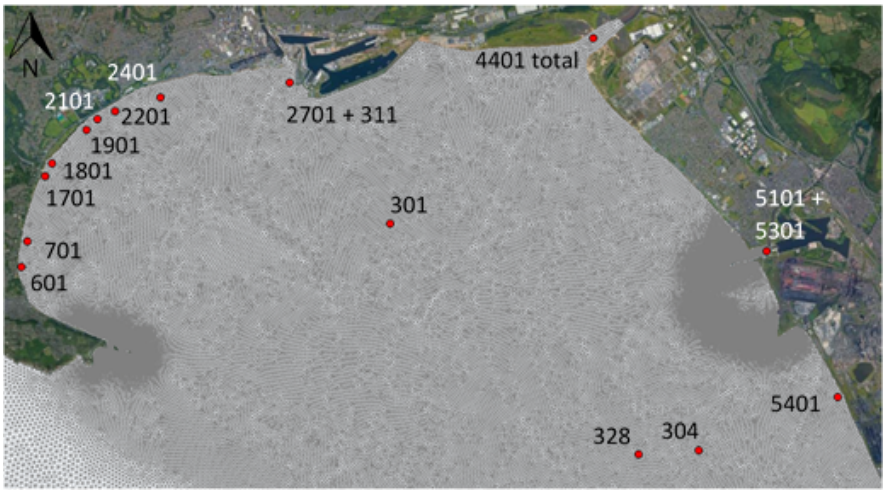

Figure 5.6: Primary input locations of bacterial sources within to 2012 3D domain

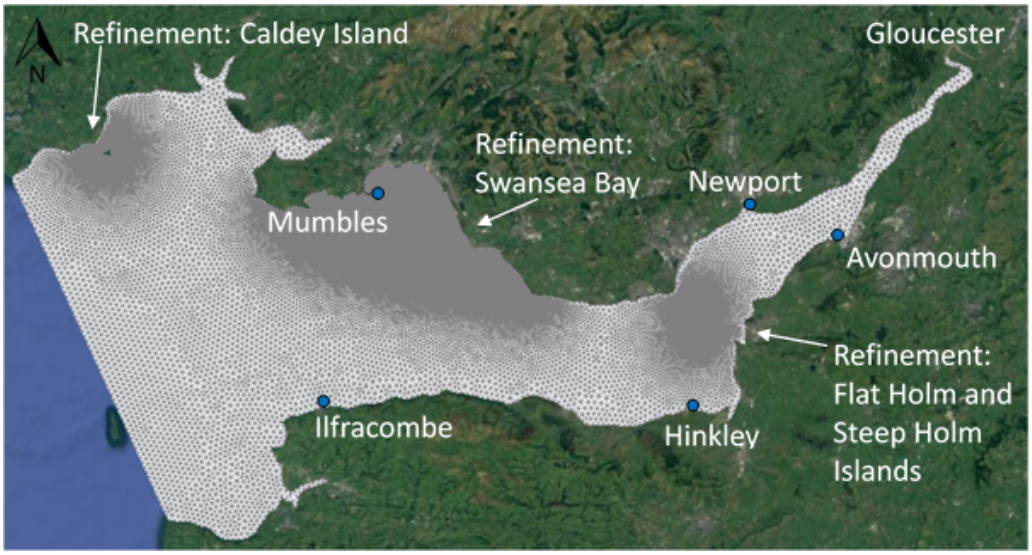

Figure 5.7: Extents of the unstructured computational mesh within the Severn Estuary and water level monitoring locations

Bathymetry data was obtained from EDINA Digimap, relative to chart datum (CD), at a 30 m grid resolution [The University of Edinburgh, 2016a,b]. Water levels at the open boundary were known relative to mean sea level (MSL), thus it was necessary to convert the bathymetry data from CD to MSL. Chart datum is commonly defined as the level of the lowest astronomical tide (LAT), and changes with location. The difference between CD and MSL was known throughout the domain at a grid resolution of 50 m in intertidal estuarine zones and 1000 m elsewhere (see Figure 5.8). These values were interpolated within, and extrapolated at the edges, of the domain using natural and linear methods respectively, allowing each datum to be adjusted from CD to MSL by a unique value. In addition to these changes, the bathymetry was manually adjusted in the river reaches where the data obtained from EDINA was unavailable and incorrect.

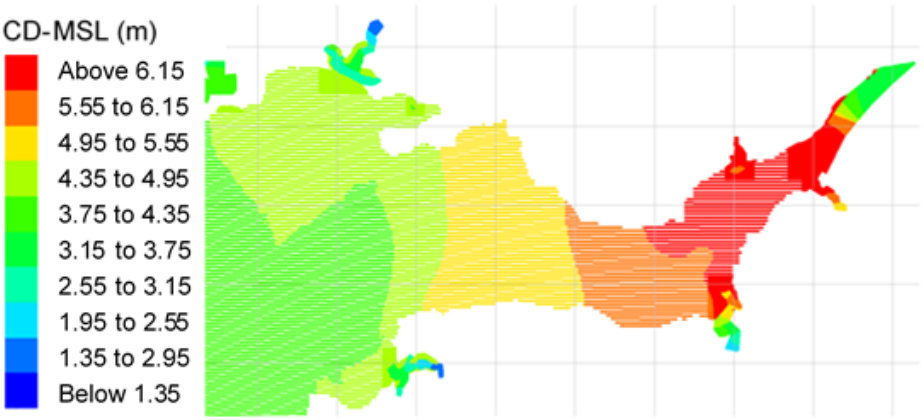

Figure 5.8: Difference between chart datum (CD) and mean sea level (MSL) throughout the model domain

Further refinement to the mesh was made within Swansea Bay to capture shoreline complexities. The domain boundary in this region was more detailed than elsewhere and was created by modifying a UK coastline shapefile (provided by the OpenStreetMap project [Topf and Hormann, 2016]), using satellite imagery from Google Maps and Admirality Charts 1161 and 1179.

An open boundary with a tidal water level series was imposed along the westward edge of the domain where the Severn Estuary meets the Celtic Sea; a constant water level was applied along the length of the boundary. Hourly data was

obtained from the National Oceanography Centre Continental Shelf Model (CS3) [The National Oceanography Centre, 2018].

For each simulation a cold start initial condition was used; aligned with high tide, constant water level and zero velocity flow conditions were specified throughout the domain.

Test runs were carried out during model development to determine the significance of the Coriolis effect on model predictions. While water level predictions were found to be insensitive to the inclusion of the Coriolis term, improvements were seen in the predicted velocities. Therefore, the Coriolis coefficient was included as a model parameter.

5.3.1.1 Tawe Barrage

The Tawe barrage is a partially submerged weir separating the River Tawe and Swansea Bay, which allows the intrusion of salt water when the tide level is above that of the crest, and controls the river flow at other times. A fish pass is located adjacent to the structure (see Figure 5.9). While the 2D model included the barrage geometry and the dredged region on the downstream / southern (tidal) side, the 3D model did not extend beyond this point or include the barrage geometry.

Figure 5.9: Tawe barrage and fish pass during different tidal phases

Admirality chart 1161 shows the region on the seaward side of the barrage dredged to a depth of -4.9 m, relative to CD (last recorded in 1999). Details of the Tawe Barrage were obtained from a plan produced by W.S.Atkins & Partners (see Figure 5.10). The primary and secondary weirs have crest heights of 3.55

m and 3.05 m respectively, with downstream stilling basins at -4.0 m and -5.7 m respectively, relative to Ordnance Datum (OD).

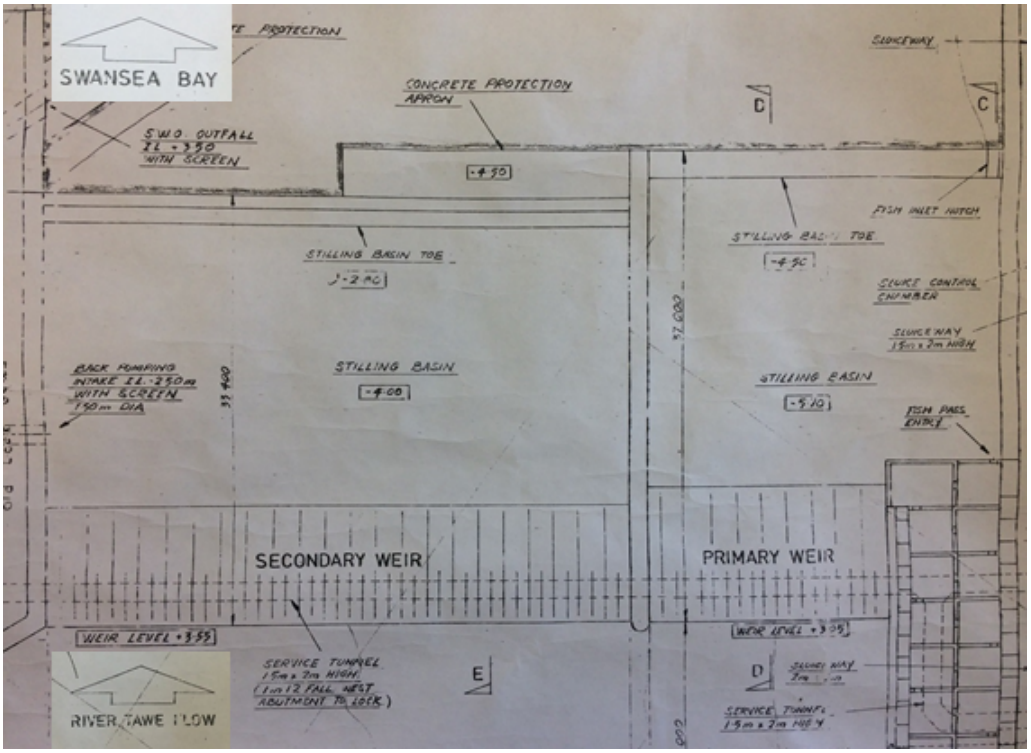

Figure 5.10: Design drawing of River Tawe Barrage, produced by W.S.Atkins & Partners (30/01/87)

The difference between CD and OD in Swansea Bay is -5.0 m [The National Oceanography Centre, 2016], and the difference between OD and MSL is approximately 0.3 m (see Section 5.3.3). Due to the large difference in elevation between the weir crest and dredged region (circa. 13 m), it was considered infeasible to model this region and accurately represent the bathymetry without causing numerical instability, or significantly reducing the grid size. TELEMAC includes a broad crested weir function, however this was found to increase the computation time significantly. The preferred solution method was to define the barrage geometry as shown in Figure 5.10, but gradually increase the bed elevation upstream and downstream to the crest. A bed elevation of -4.9 m, relative to MSL / OD, was specified in the region below the stilling basin (see Figure 5.11). This is below the water level at low tide in Swansea Bay and was not considered to

have an adverse effect on pollutant transport.

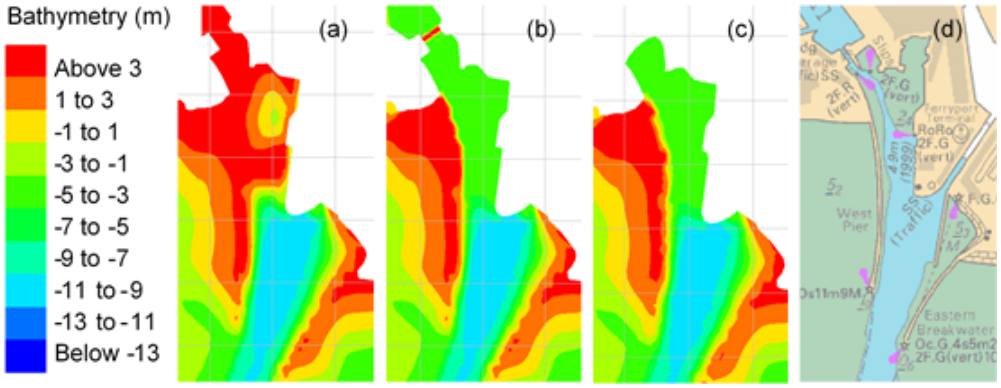

Figure 5.11: Bathymetry in the vicinity of the Tawe Barrage; (a) original, (b) 2D model including the Tawe Barrage and adjusted for dredging, (c) 3D model adjusted for dredging, (d) Admirality chart 1161

5.3.1.2 River reaches

The 2D mesh was extended 3 km up the Tawe River to the Natural Resoruces Wales (NRW) gauging station at Morfa. A water level and discharge boundary condition was prescribed using data provided by NRW and the Smart Coasts project [Aberystwyth University and University College Dublin, 2018]. Bathymetry data was unavailable for this region and was approximated as follows.

The online gauge at Morfa shows the lowest recorded level as 2.71 m [Natural Resources Wales, 2018a]. Google Maps and LiDAR data provided by NRW [Natural Resources Wales and Welsh Government, 2018] was used to measure the mean water surface gradient between Ynystanglws gauging station and Morfa, Morfa and the Tawe Barrage, as 1/1000 m (bed slope, S = 0.001). The datums used at Ynystanglws and Morfa were unknown, as was the bed level. Records show that during the model simulation period (on 13/11/12), the level at Morfa varied between 3.0 m and 3.5 m. Simultaneously, the discharge at the Tawe Barrage was between 20 m^3/s and 30 m^3/s. The discharge at Morfa was calculated

using Equation 5.1,

$$Q = UA = \frac{1}{n} A R^{\frac{2}{3}} \sqrt{S} \tag{5.1}$$

where q is the discharge (m^3/s), U is the mean current speed (m/s), A is the flow area (m^2), n is the Manning's number, R is the hydraulic radius (m) and S is the bed slope (dimensionless).

Assuming a Mannings value of n = 0.030 (for a clean, straight, main channel; see Chow [1959]), a bed slope parallel to that of the water surface (S = 0.001), a channel width of 30 m (measured from satellite imagery), a bed level of 2.5 m (relative to MSL / OD) and a water depth of 1.0 m (i.e. gauge reading = 3.5 m), a value of 30 m^3/s was calculated. This was in agreement with the discharge over the Tawe Barrage, thus the bathymetry within the Tawe was generated assuming a bed level of 2.5 m at Morfa and a linear bed slope of S = 0.001 (see Figure 5.12).

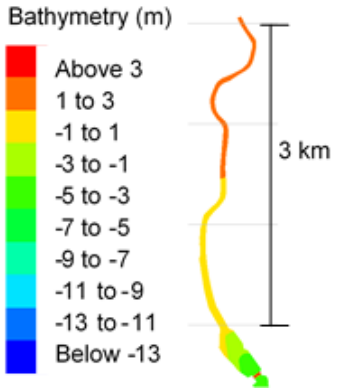

Figure 5.12: River Tawe bathymetry used in the 2D model, relative to MSL / OD

The bathymetries of the Rivers Afan and Neath were known at the estuary mouths but unavailable upstream to the tidal limits, which are at 2 km and 11 km, respectively. In both cases the tidal limit is a weir; at Green Park and Tonna, respectively. Based on the known bed profile at the mouth of each river a V shaped channel was assumed along their length up to the tidal limits (see

Figure 5.13).

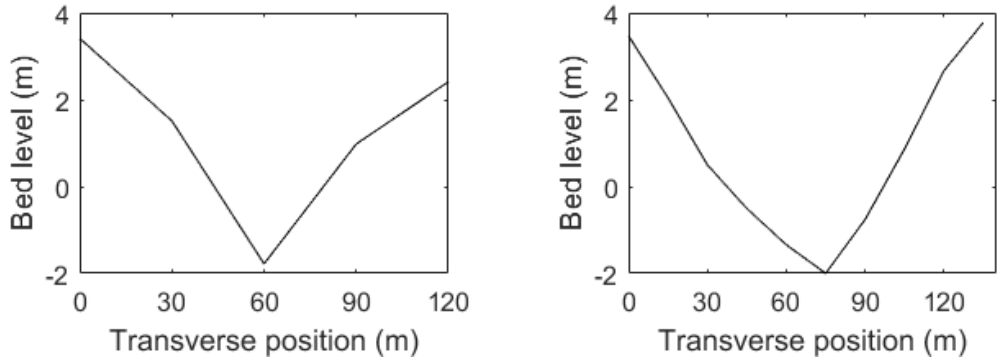

(a) (b)

Figure 5.13: Transverse bed profile of the Rivers Afan (a), and Neath (b), at the respective estuary mouth. Bathymetry relative to MSL and drawn facing upstream

The bed slope of each river was assumed parallel to the water surface slope, measured as 0.0025 and 0.003, respectively. The bank gradient, along the river length, was obtained from inspection of LiDAR data and measured as 0.002 to 0.003 in both cases.

Inflow boundary conditions comprising of of discharge and water level were prescribed at the tidal limits. The bed level of the most upstream nodes in each reach were adjusted to 5.0 m; above the highest astronomical tide (HAT) in Swansea Bay in 2011 and 2012, with a constant inflow water depth of 0.5 m prescribed (see Figure 5.14). Although the inflow depth was unknown and variable over the simulation period, the tidal limits were considered far enough upstream to allow the flow time to settle before reaching the river mouth.

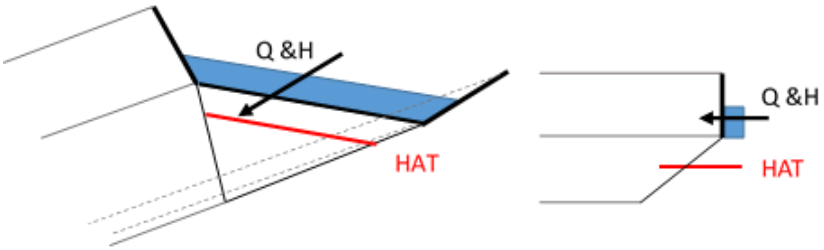

Figure 5.14: Schematic of modified bed topography at the tidal limits of the Rivers Afan and Neath

5.3.2 Parameter selection

Swansea Bay is well mixed [Ahmadian et al., 2013] and variations in temperature and salinity throughout the water column were therefore not considered. Instead, constant values of 15 °C and 32 ppt were used, respectively, as detailed in previous studies [Aberystwyth University and University College Dublin, 2018; White et al., 2014]. While surveys have shown variations in suspended sediment concentration throughout the water column [White et al., 2014], data is sparse and a constant value of 84.82 mg/l (24.2 NTU; see Equation 3.40), was assumed based on measurements taken nearby at Langland Bay and Porthcawl by Stapleton et al. [2007b]. Equations 3.32 and 3.34 can therefore be considered a function of light intensity and water depth (see Figure 5.15). Light intensity is also a proxy for water depth due to Equation 2.34.

It should be noted that measurements taken in the 2011 Smart Coasts survey [Aberystwyth University and University College Dublin, 2018] show that the turbidity varied between 2 NTU and 3180 NTU over the bathing season, with mean and median values of 178 NTU and 77 NTU, respectively. This variation may have been due to changes in wave and wind conditions or sediment loads in the estuaries flowing in to Swansea Bay. However, details of the survey conditions are unknown and it is therefore recognised that assuming a constant value is a simplification, but accepted as a model limitation.

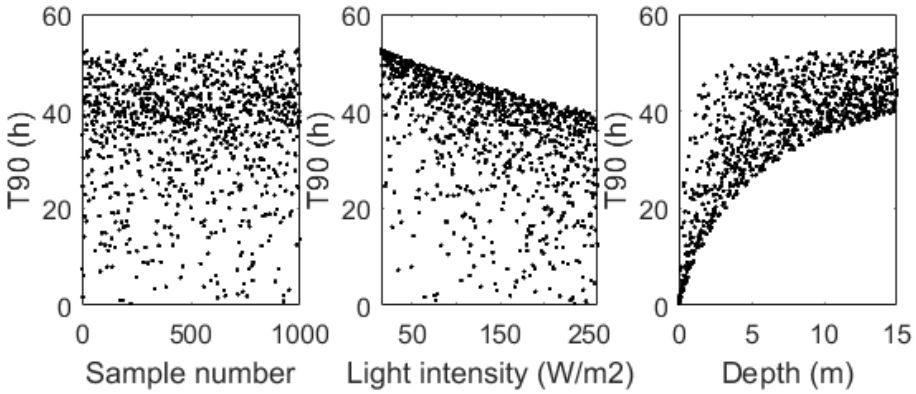

Figure 5.15: Sensitivity analysis of Equation 3.32 to light intensity and water depth, using latin hypercube sampling. Water depth varied up to the maximum natural (i.e. not dredged) depth in Swansea Bay (see Figure 5.4)

It is known that increased surface shear induced by wind can affect dispersion in shallow water [Bedri et al., 2011; Moulinec et al., 2011]. However, wind conditions at water level were unknown for the time periods covered by the model simulations and wind velocity was therefore omitted as a model parameter to uncertainty.

A sine function, convering the range 0 to π, was used to represent the variation in light intensity over daylight hours (06:00 to 18:00), as proposed by Boye et al. [2014] (see Figure 5.16). During the summer months, light intensity in the Severn Estuary is known to vary between 0 and 260 W/m^2 [Stapleton et al., 2007a]. Data recorded over the 2012 simulation period shows an average daily maximum of 170 W/m^2 (see Figure 5.17). Night time values were recorded at 0.15 W/m^2. However, a lower limit of 15 W/m^2 was used, as discussed in Section 5.4. Additional simulations were run using measured irradiance data, collected at 15 minute intervals, to determine the benefit of using high temporal resolution data.

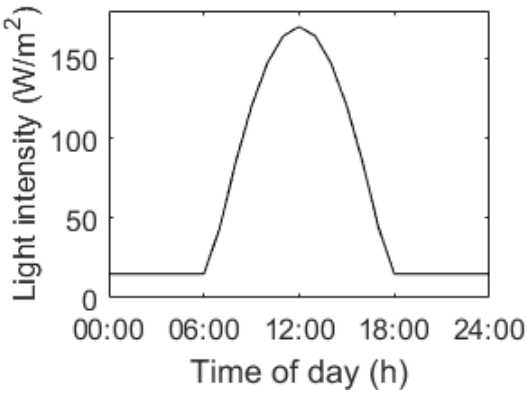

Figure 5.16: Light intensity function over the day

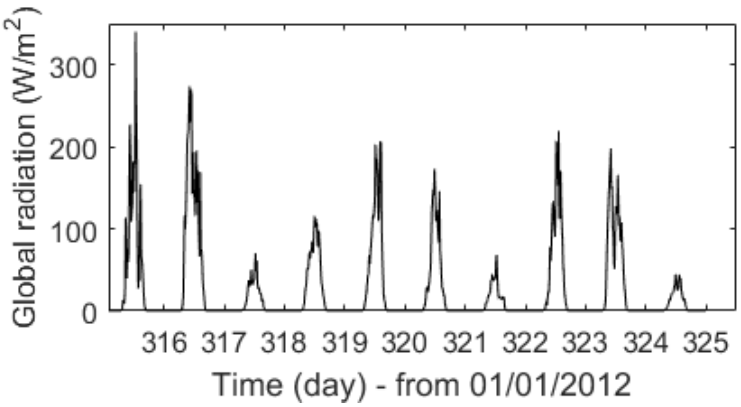

Figure 5.17: Light intensity in Swansea Bay, measured at 15 minute intervals from 11/11/12 to 19/11/12 [Aberystwyth University and University College Dublin, 2018]

5.3.3 Calibration and validation

Model calibration was carried out using tide gauge records provided by the British Oceanographic Data Centre (BODC), at four sites throughout the Severn Estuary and Bristol Channel; Hinkley, Ilfracombe, Mumbles and Newport [British Oceanographic Data Centre, 2016] (see Figure 5.7), over a spring-neap tidal cycle.

As the BODC provides water level records relative to CD, these were adjusted to OD using conversion values provided by the National Tidal and Sea Level Facility [The National Oceanography Centre, 2016]. For each monitoring location these values were; -5.90 m, -4.80 m, -5.00 m and -5.81 m, respectively. Further conversion from OD to MSL was required for comparison with model results. Adjustments were made based on the MSL observed over the simulation period. At each location these were; -0.32 m, -0.48 m, -0.40 m and -0.58 m, respectively.

A constant Manning's coeffiecent was used throughout the model domain. Based on the range of suggested rougnness values presented in Chow [1959], water levels were calibrated by testing values of 0.02, 0.025 and 0.03; suitable for excavated or dredged channels, and clean, straight main channels. The model was found to have low sensitivity to the bed roughness and a value of 0.025 was selected as that producing the best fit.

Plots comparing measured and predicted water levels using a Manning's value of n = 0.025 are shown in Figures 5.18, 5.19, 5.20 and 5.21, alongside root mean square error (RMSE) and Nash Sutcliffe efficiency (NSE) values. Note that the missing measured data in Figure 5.20 (from day 320 to 322), reflects a gap in the BODC data record. It can be seen that the model consistently over and under-predicts high and low tides, respectively, as reflected in the RMSE values. This was believed to be due to an error in the water level time series applied at the open sea boundary, however was of little concern due to the high NSE values.

Predicted velocities were validated against data gathered during an Acoustic Doppler Current Profiler (ADCP) survey of Swansea Bay from 21/07/2012 to 28/08/2012 at locations shown in Figure 5.22 [Aberystwyth University and University College Dublin, 2018]. The survey was carried out using a bed mounted Nortek Aquapro; system details are shown in Table 5.1 [EMU Limited, 2012]. Val-

idation plots of depth-averaged current speed and direction at locations L2 and L4 are shown in Figures 5.23, 5.24, 5.25 and 5.26. Current direction is presented with respect to due north. Additional plots have been omitted for brevity.

Table 5.1: Swansea Bay ADCP survey deployment setup

Instrument height	0.7 m
Current and water level profile interval	600 s
Cell size	0.5 m
Current and water level average interval	60 s
Blanking distance	0.5 m

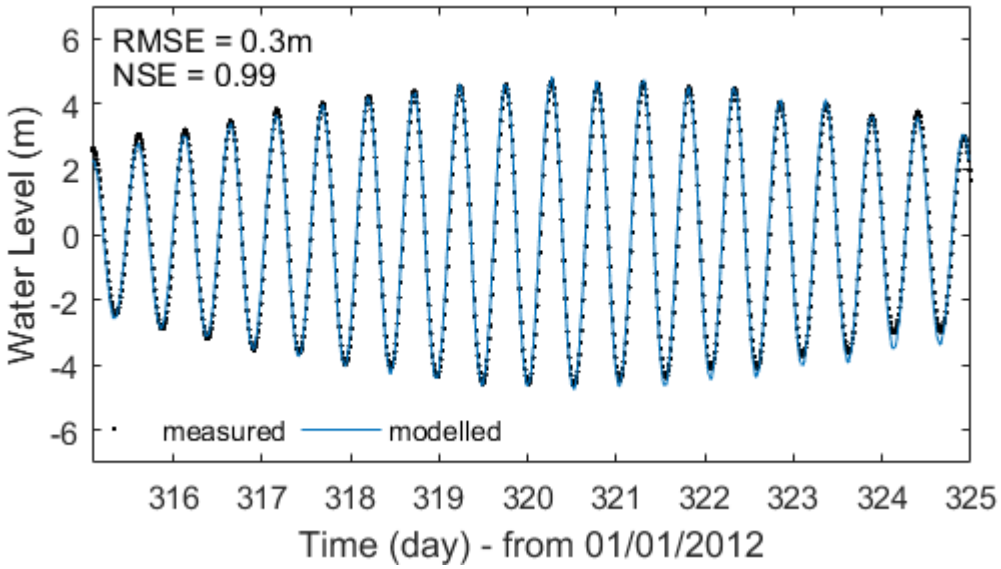

Figure 5.18: Plot of calibrated water levels measured at Ilfracombe (51.22°N, 4.11°W), adjusted relative to MSL, n = 0.025

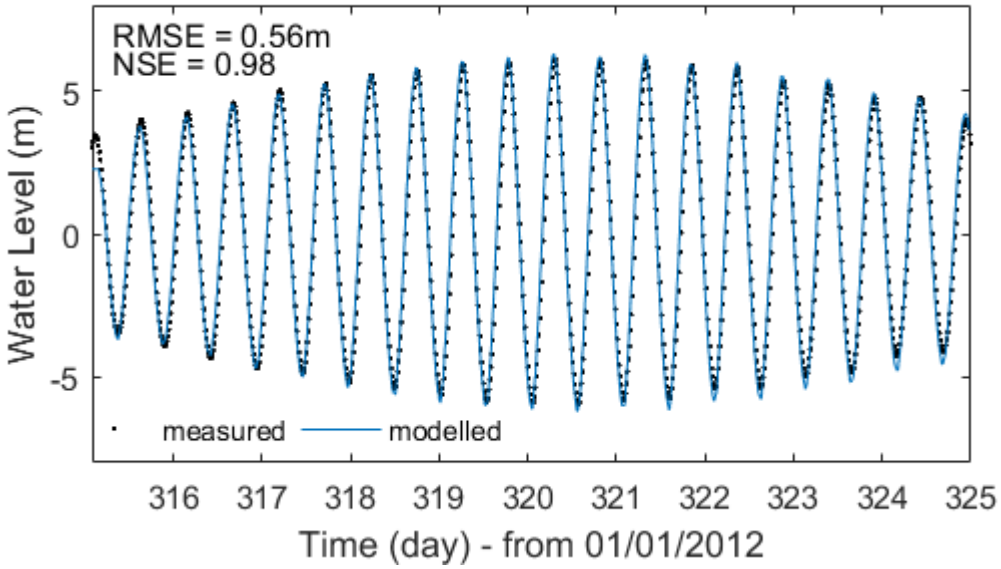

Figure 5.19: Plot of calibrated water levels measured at Hinkley (51.22°N, 3.13°W), adjusted relative to MSL, n = 0.025

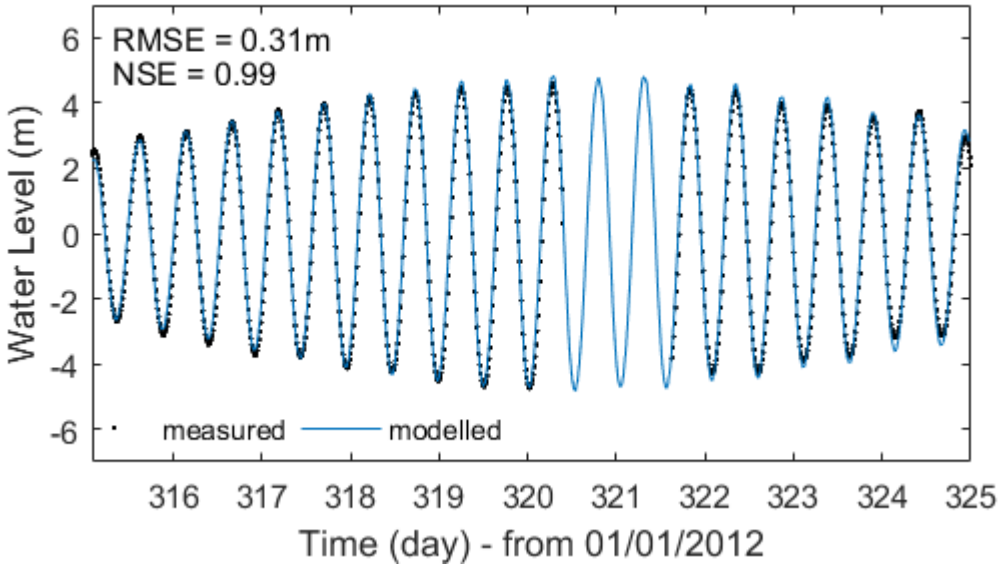

Figure 5.20: Plot of calibrated water levels measured at Mumbles (51.57°N, 3.96°W), adjusted relative to MSL, n = 0.025

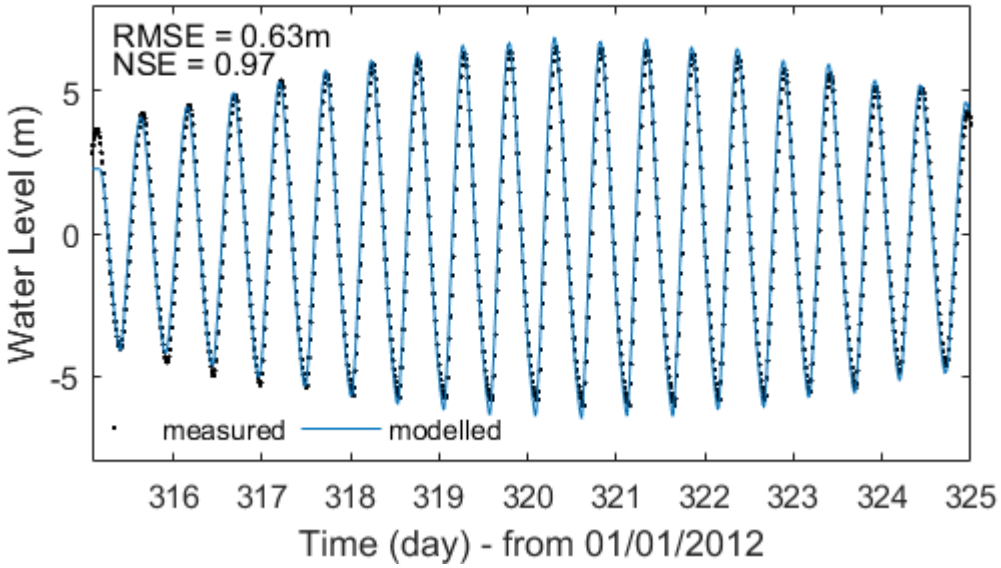

Figure 5.21: Plot of calibrated water levels measured at Newport (51.55°N, 2.99°W), adjusted relative to MSL, n = 0.025

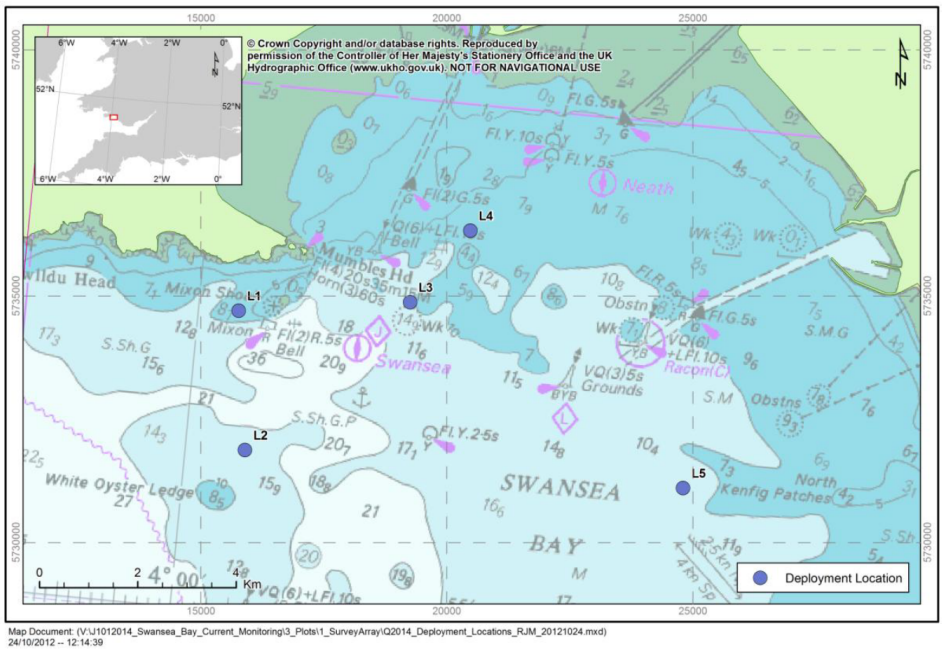

Figure 5.22: ADCP survey locations in Swansea Bay

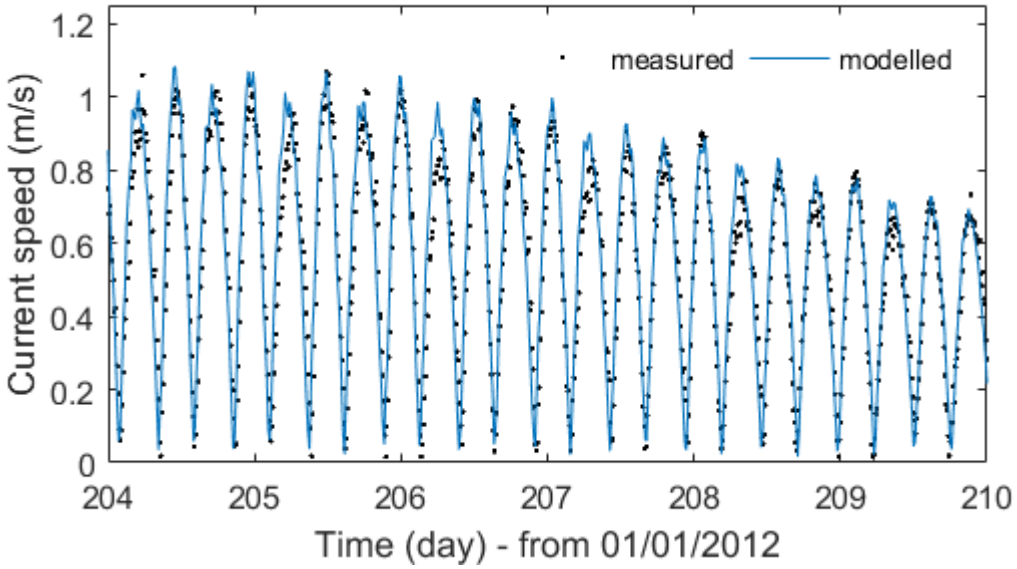

Figure 5.23: Plot of validated current speed near Swansea Bay at location L2 (51°31.78′N, 003°58.96′W)

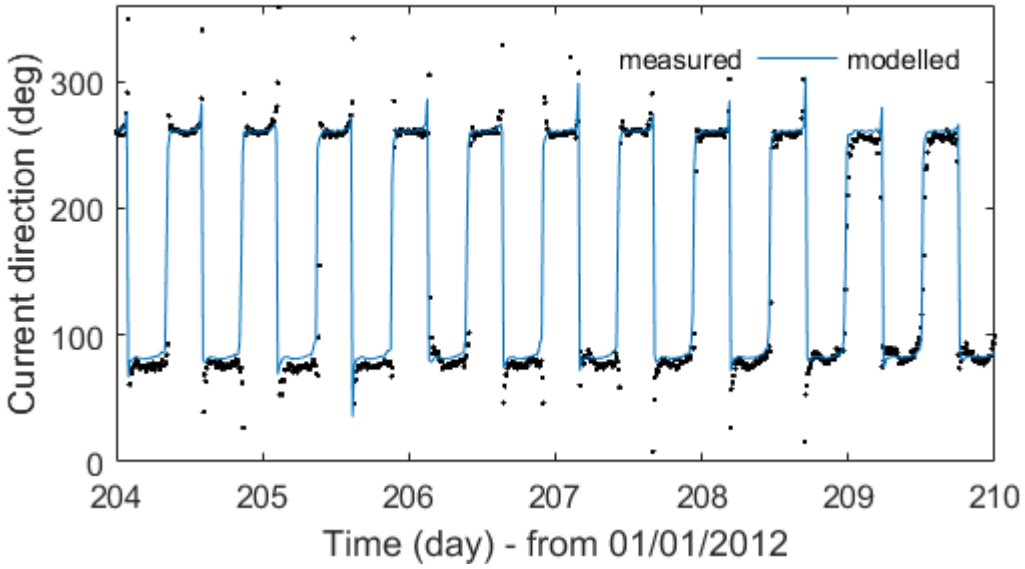

Figure 5.24: Plot of validated current direction near Swansea Bay at location L2 (51°31.78′N, 003°58.96′W)

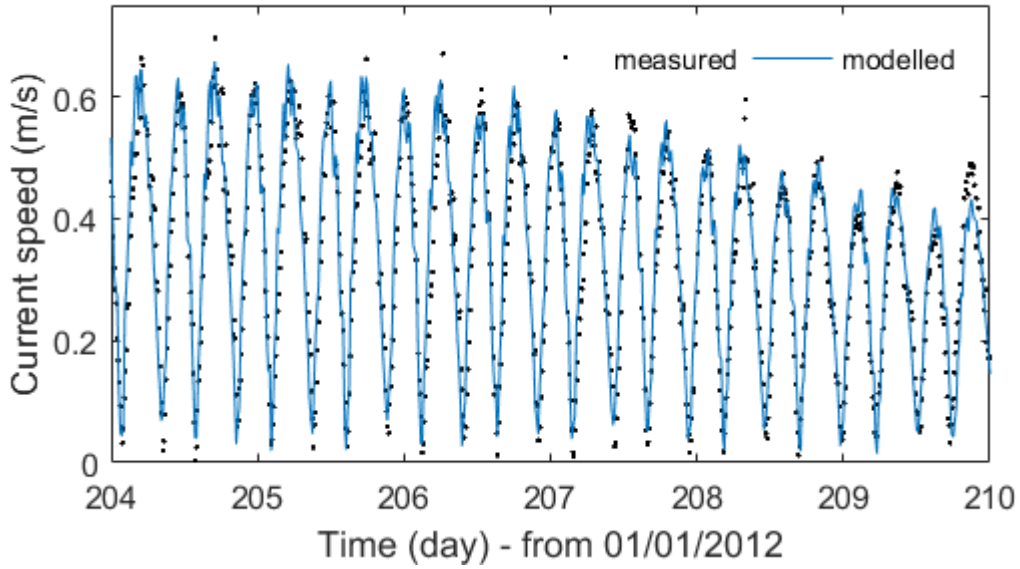

Figure 5.25: Plot of validated current speed in Swansea Bay at location L4 (51°34.85′N, 003°51.25′W)

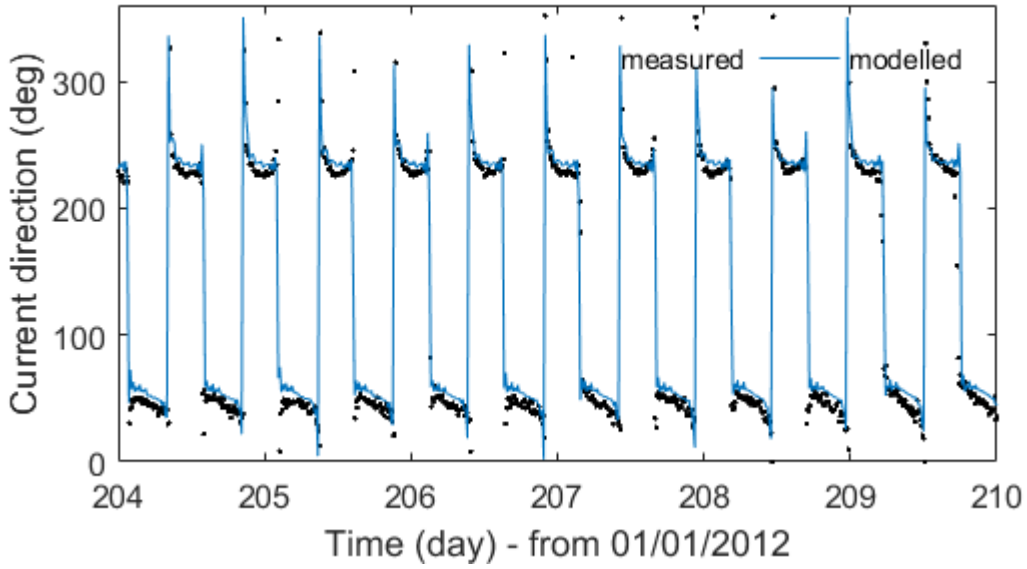

Figure 5.26: Plot of validated current direction in Swansea Bay at location L4 (51°34.85′N, 003°51.25′W)

Plots of measured and predicted water levels in the Rivers Neath and Tawe are shown in Figures 5.27 and 5.28, respectively, using data obtained from Natural Resources Wales [2018b] and Aberystwyth University and University College Dublin [2018].

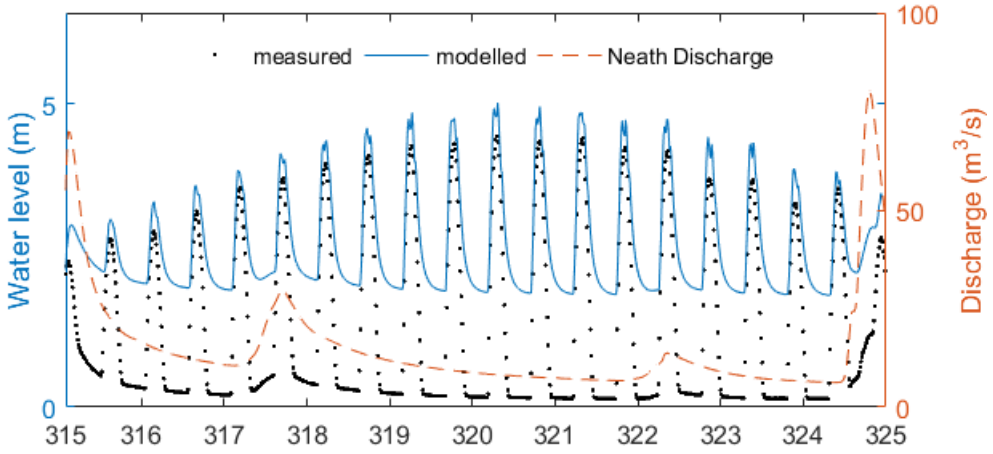

Figure 5.27: Plot of the measured and predicted water levels at Neath Tidal gauging station relative to MSL, with overlay of river discharge

As seen in Figure 5.27, except during peak flow events, the water level in the Neath is predominantly determined by tidal influence. Furthermore, high tides are consistently over-predicted, which was though to be due to an error in the open sea boundary condition. However, this could not be confirmed as the reference datum at the NRW gauging station Neath Tidal was not provided. The 2 m difference at low tide may be attributed to incorrect bathymetry, however, as the bed elevation was unknown, it was not possible to determine the measured flow depth and therefore accurately determine the flow characteristics.

The NRW Tawe Fish Pass gauge is located immediately upstream of the fish pass and barrage, and water levels are recorded relative to CD. Therefore, the data presented in Figure 5.28 has been adjusted to MSL using the difference at the nearby BODC station; Mumbles.

It can be seen that during the hours of tidal influence, water levels are well predicted, however, a difference between the measured and predicted water levels can be seen during low water. This is due to use of the bed smoothing configu-

ration in TELEMAC; required to prevent numerical instabilities which arose as a result of the large gradient from the barrage crest to base. This caused a reduction in crest elevation, and therefore, during times of no tidal influence, water level.

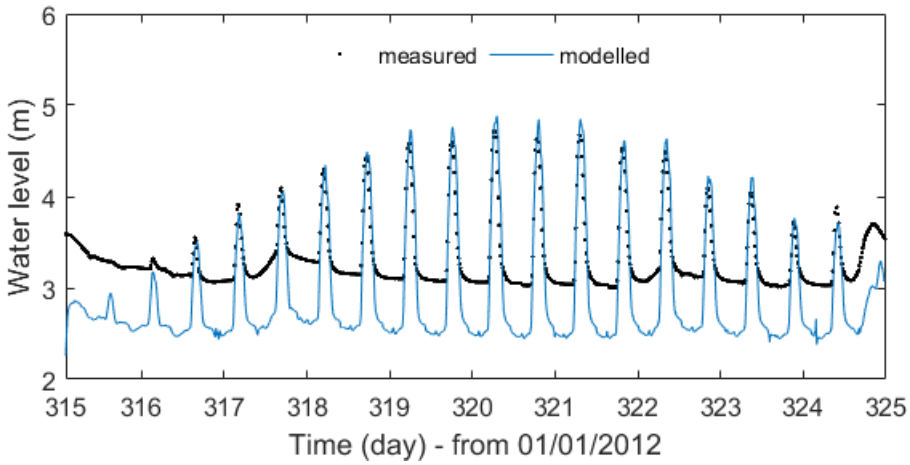

Figure 5.28: Plot of the measured and predicted water levels at the Tawe Fish Pass relative to MSL

As an alternative to bed smoothing, the geometry may have been more precisely defined and the barrage modelled as a dyke. However, it was not possible to correctly model the flow without a significant reduction in the mesh size, as at times, the small water depth caused a choke in the flow (see Figure 5.29).

This was not done to avoid an increase in computation time and use of the bed smoothing configuration was accepted since correct discharge was ensured over the barrage. Any errors in the predicted flow velocity over the barrage were considered insignificant, as in reality a stilling basin is installed downstream of the barrage. Furthermore, the main scope of this study is to model bacterial processes within Swansea Bay, with a focus on the rBWD DSPs, and it was deemed unnecessary to pursue this matter further due to the distance between the barrage and the closest DSP.

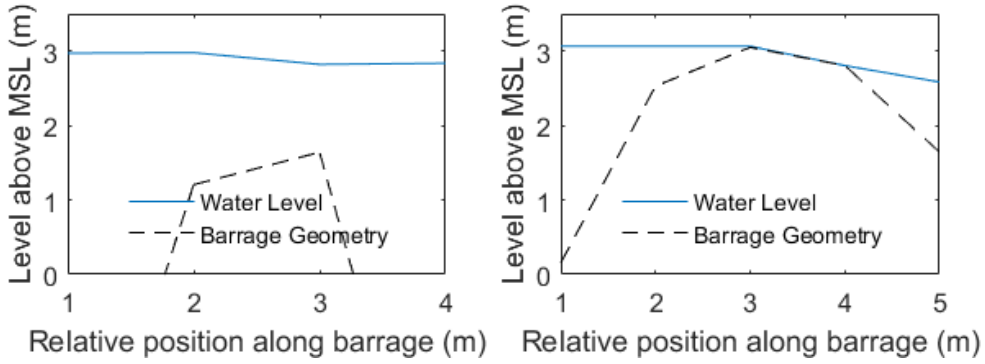

(a) (b)

Figure 5.29: Crest geometry of Tawe Barrage; smoothed allowing flow (a), dyke refinement causing a choke (b)

5.3.4 Model configuration

Details of the configurations used for the 2D and 3D models are shown in Table 5.2.

In the 2D model a time step of 2.5 s was required to satisfy the Courant-Friedrichs-Lewy (CFL) condition (i.e. a Courant number of 1) [Courant et al., 1967]. An adaptive time step was used which enabled TELEAMC to adjust the time step from the specified value based on the default acceptable deviation from the target Courant number.

However, this functionality was not available in TELEMAC-3D. A time step of 1.0 s was required when running the 3D model to prevent numerical instabilities introduced when including the Coriolis term.

The Smagorinsky turbulence model [Smagorinsky, 1963] is recommended for large scale marine domains [Lang et al., 2014] and was used in similar studies [Bedri et al., 2013, 2014a, 2015; Gourgue et al., 2013]. It was therefore selected as an initial choice. Further comparison with other turbulence models is discussed in Section 5.5.

In the absence of any data on the diffusion and dispersion of tracers in Swansea Bay, the coefficient of tracer diffusion was set at 1×10^{-6}, to prevent the introduction of errors due to a poor choice of value. This the default setting in TELEMAC [Desombre et al., 2016]. Though this paremeter can have a significant impact on

tracer transport, it has been shown that when the mesh is 5 m to 100 m, there is negligible difference in model predictions for values below 1×10^{-1} [Smolders et al., 2015].

Table 5.2: Comparison of salient model parameters between 2D and 3D model

	2D Model	**3D Model**
Number of nodes (horizontal)	142533	133341
Number of elements (horizontal)	281440	264237
Number of vertical layers	1	5
Number of nodes (total)	142533	666705
Number of elements (total)	281440	1321185
Maximum element size (m)	1000	1000
Minimum element size (m)	5	10
Minimum water depth (m)	0	0
Time step (s)	2.5	1.0
Horizontal turbulence model	Smagorinsky	Smagorinsky
Vertical turbulence model	N/A	Smagorinsky
Manning's n	0.025	0.025
Coefficient of tracer diffusion	1×10^{-6}	1×10^{-6}

5.4 Comparison of bacterial modelling techniques

This section describes modifications made to the TELEMAC source code. Version v7p3r2 was used as the latest release at the time of writing. Future releases may require alternative approaches due to changes in the source code structure or the relevant subroutines.

Further information on the TELEMAC source code beyond what is described can be found on the TELEMAC website (see Electricité de France [2018]).

5.4.1 2D

To modify the decay function within TELEMAC-2D, the subroutine `difsou.f` was edited. The decay rate is defined by a T_{90} value, prescribed by the user in the configuration file using the keyword: "`COEFFICIENT 1 FOR LAW OF TRACERS DEGRADATION`".

5.4.1.1 Constant T_{90} decay rate

Based on sampling over the feasible parameter range using the Mancini [1978] equation, it has been shown that the maximum T_{90} value experienced within the domain is close to 50 h (see Section 5.3.2). For this reason, a constant T_{90} value of 50 h was used as a 'control' decay rate to which any modifications could be compared.

5.4.1.2 Mancini decay function

Figure 5.30 outlines the method used to implement Equation 3.32. The source code is given in Appendix B.1, Listing 1. Additional points of note are as follows.

At each time step TELEMAC stores a value for the decay rate at all nodes in the mesh. Values are calculated based on the water depth at each node and the depth-averaged light intensity. This gives a temporally and spatially varying decay function.

Calculation of the depth-averaged light intensity requires division by the water depth (see Equation 3.29), which has a minimum value of 0 m, and results in values approaching infinity as the water depth approaches zero. To overcome this a depth limit of 0.05 m was used, below which the decay rate was calculated as that at a depth of 0.05 m.

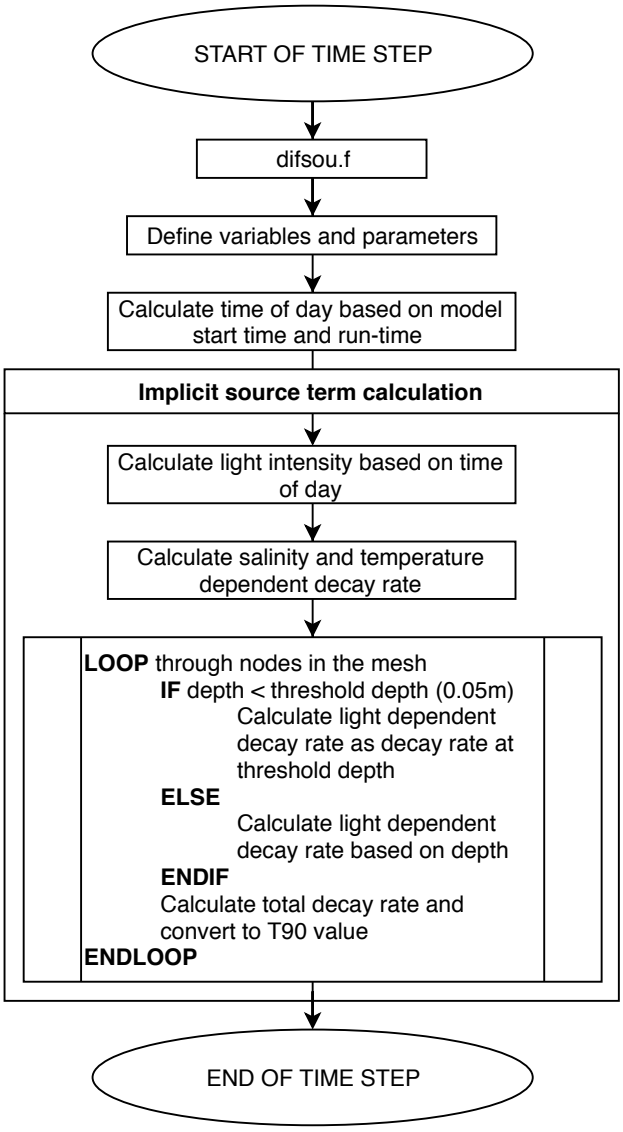

Figure 5.30: Flow chart showing implementation of the Mancini [1978] decay equation in TELEMAC-2D

5.4.1.3 Stapleton decay function

Figure 5.31 outlines the method used to implement Equations 3.36 to 3.40. The steps prior to implicit source term calculation are as in Figure 5.30 and have been removed for brevity. The source code is given in Appendix B.1, Listing 2. Additional points of note are as follows.

A threshold depth for decay of 0.05 m was implemented, as in the Mancini [1978] model, to aid in comparison between the two.

A lower limit of 15 W/m^2 was placed on light intensity to prevent the T_{90} value tending towards infinity as depth and I approach zero (see Equation 3.37). This is equal to 10 times the recorded night time irradiation in Swansea Bay (see Figure 5.17).

Equations 3.36 to 3.40 are only valid when the observed light intensity is equal to, or below, that used experimentally (260±14 W/m^2). To ensure this an upper limit of 260±14 W/m^2 was placed on measured irradiance data.

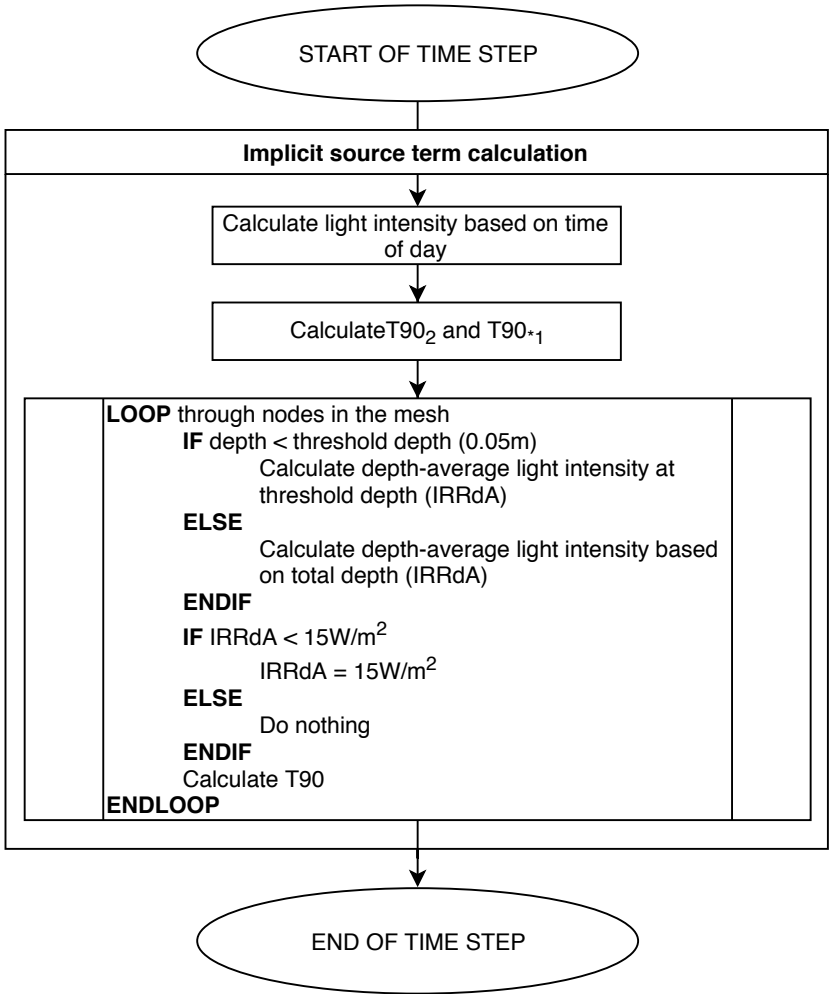

Figure 5.31: Flow chart showing implementation of the Stapleton et al. [2007a] decay equation in TELEMAC-2D

5.4.2 3D

The v7p3r2 release of TELEMAC-3D does not support modelling of a non-conservative tracer, and to include a T_{90} decay function, the subroutine `source_trac.f` was modified as shown in Appendix B.1, Listing 3. This provides an example of a day / night decay function on which the changes described below were based.

As described in Sections 3.2.4.1 and 3.2.4.2, two methods were used when implementing the Mancini [1978] and Stapleton et al. [2007a] decay equations; depth-averaged and depth-staggered functions. Flow charts comparing the two methods are shown in Figures 5.32 and 5.33 respectively. While each method was written in a separate subroutine, they have been shown side by side for comparison and brevity. Fortran code for each method can be found in Appendix B.1, Listings 4, 5, 6 and 7. The points made previously, in relation to implementing each function in TELEMAC-2D, are also valid. In Figure 5.33, all steps prior to the source term calculation have been omitted for brevity as they are the same as shown in Figure 5.32.

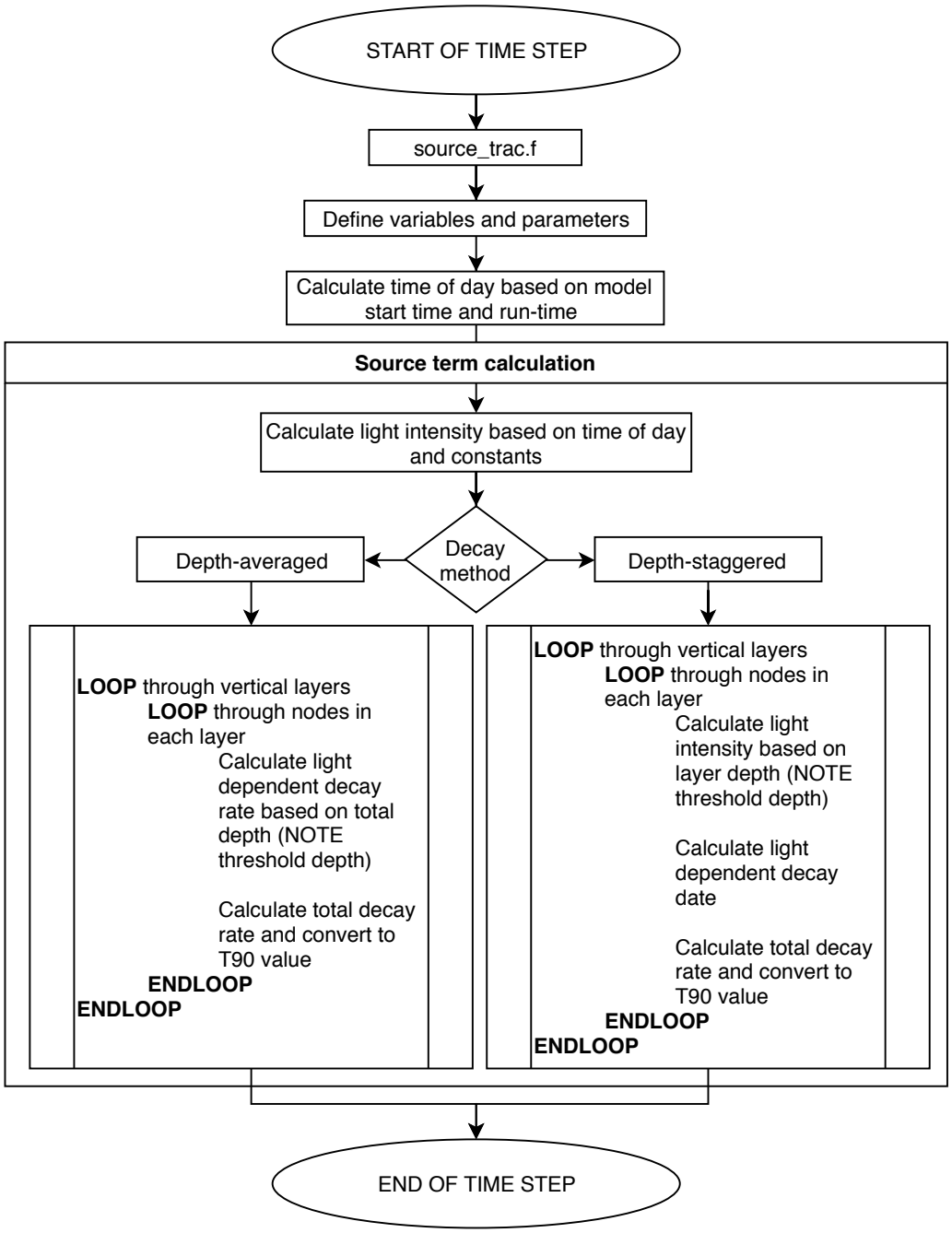

Figure 5.32: Flow chart showing implementation of the Mancini [1978] decay equation in TELEMAC-3D

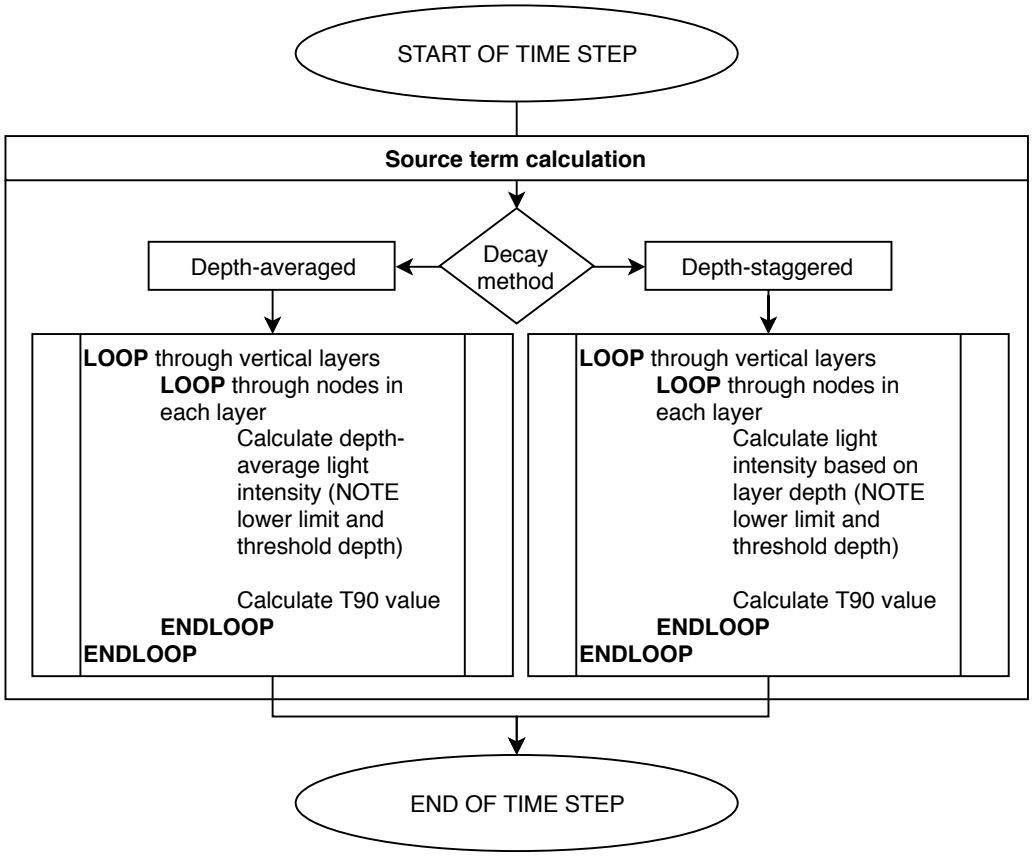

Figure 5.33: Flow chart showing implementation of the Stapleton et al. [2007a] decay equation in TELEMAC-3D

5.5 Results and discussion

Herein, model performance is assessed using *E.coli* records from 15th November 2012. A more in depth assessment of model predictions is made using *E.coli* and *Enterococci* records taken throughout the 2011 bathing season in Chapter 6.

5.5.1 2D

5.5.1.1 Effect of distributed river sources

Having extended the 2D model domain to the tidal limit of the River Neath, it is possible to compare the effect of modelling each point source individually, or lumping all sources into a single input at the boundary inflow. Shown in Figure 5.34, the modelled concentration (conc.) at the estuary mouth is lower during peak events when using distributed sources, though largely the same.

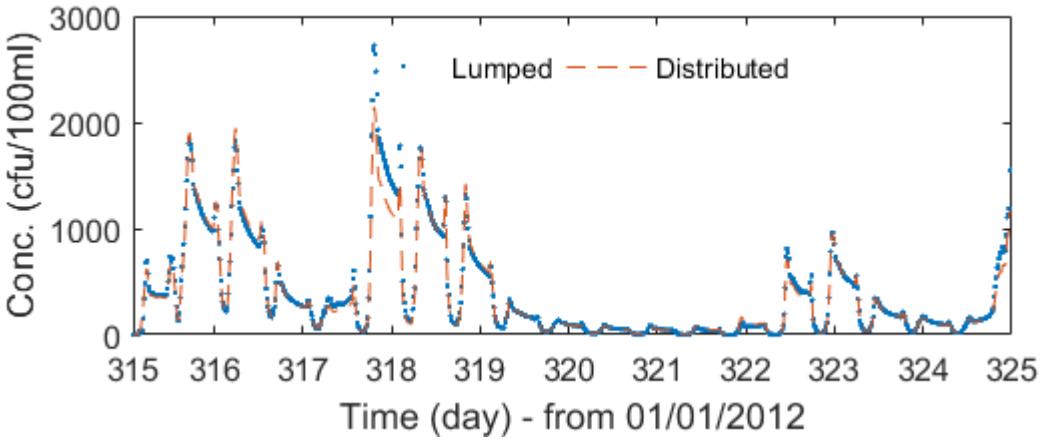

Figure 5.34: *E.coli* concentration plot showing comparison of distributed and lumped sources in the River Neath at estuary mouth

In comparison, the difference is more significant upstream, as seen at Neath Tidal in Figure 5.35; during peak flow events the response of the distributed source model is dampened compared to the lumped source 'pulse' release. Although the bacterial concentration profile along the river reach is of limited interest in this study, distributed sources were used in all 2D model runs discussed hereafter.

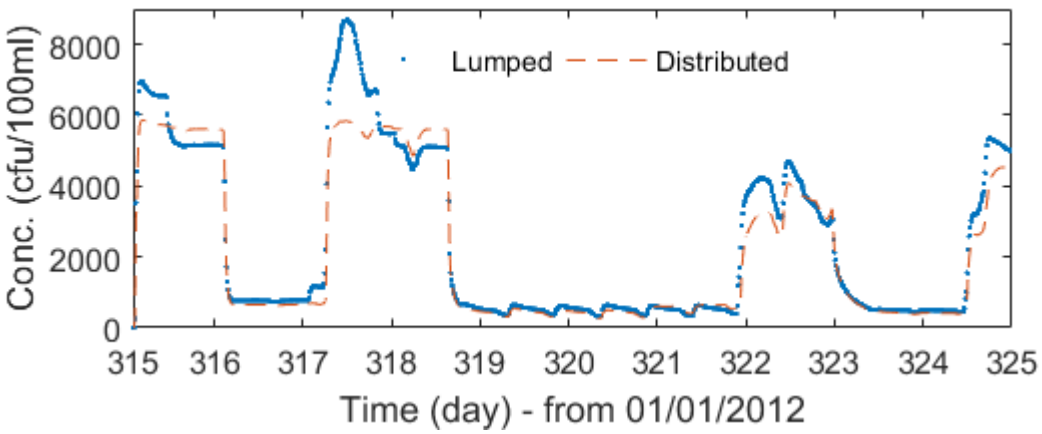

Figure 5.35: *E.coli* concentration plot showing comparison of distributed and lumped sources in the River Neath at Neath Tidal gauging station

5.5.1.2 Comparison of bacterial decay models

Figures 5.36 and 5.37 present comparisons between the performance of the three bacterial decay models, implemented within the 2D model, at the DSPs for Swansea Bay and Aberafan bathing waters, respectively. Additional plots showing predictions at sites S2 and S3 are shown in Appendix B.2, Figures 1 and 2, respectively.

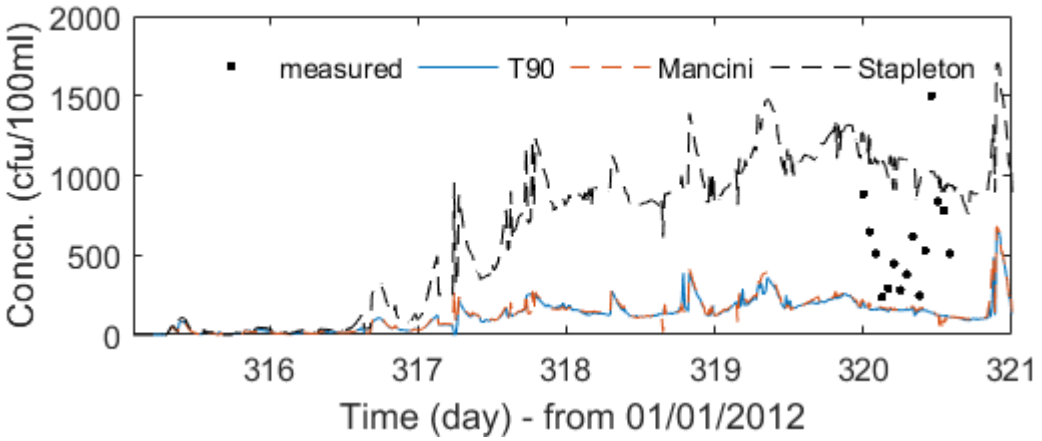

Figure 5.36: Comparison between the measured and predicted *E.coli* concentrations at the Swansea Bay DSP using three decay functions in the 2D model; T_{90} = 50 h constant, Mancini [1978] and Stapleton et al. [2007a]

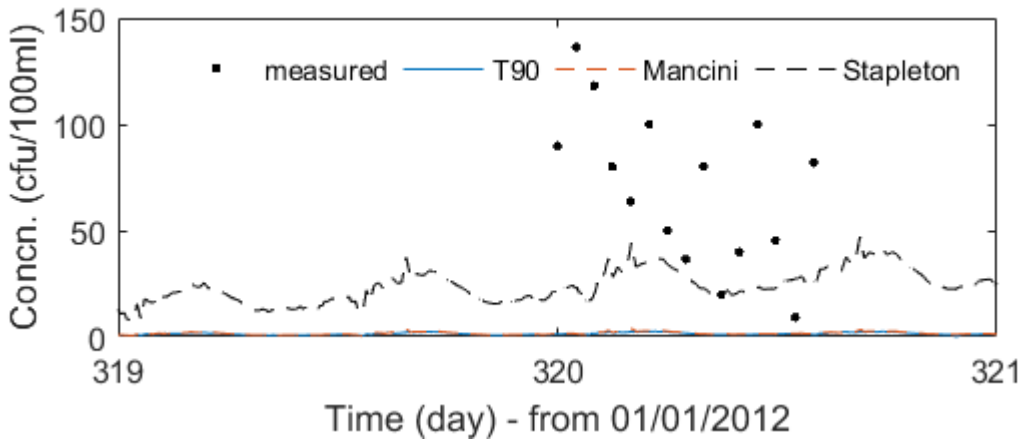

Figure 5.37: Comparison between the measured and predicted *E.coli* concentrations at Aberafan beach using three decay functions in the 2D model; T_{90} = 50 h constant, Mancini [1978] and Stapleton et al. [2007a]

It can be seen that only the function proposed by Stapleton et al. [2007a] provides predictions that are of a similar magnitude to the measured data. In comaprison, the function proposed by Mancini [1978] and a constant T_{90} value of 50 h significantly under predict concentrations at both locations. Predictions made at the other sample locations within Swansea Bay show the same relationship; see Appendix B.2, Figures 1 and 2 for predictions at sites S2 and S3.

This difference in model performace can be explained by examining the variation in decay rate calculated by each function throughout a typical day; shown in Figure 5.38. Considering the most offshore transect point along the Swansea Bay DSP, it can be seen that for the majority of the time, the calculated T_{90} values are larger when using the Stapleton et al. [2007a] function. Of note is the large night time T_{90} value of 220 h, exponentially decreasing to 8 h at midday. In comparison, the values predicted using the Mancini [1978] function do not exceed 30 h and fall to 0 h in the day. Also seen is the dependence of the Mancini [1978] model on water level and light intensity, whereas the Stapleton et al. [2007a] model is a function of light intensity only.

Comparing the magnitude of observed and predicted bacterial concentrations between Swansea Bay and Aberafan, lower values are given for the latter in both cases. This due to input bacterial concentrations being lower in the River

Neath compared to the River Taff, which influence Aberafan and Swansea Bay respectively.

It can also be seen in Figures 5.36 and 5.37 that the *E.coli* concentrations predicted using the Mancini [1978] decay function follow similar patterns to that using the Stapleton et al. [2007a] model, but of a smaller magnitude. This suggests that the temporal variation at a point is primarily dependent on correct hydrodynamic simulation and the magnitude of bacterial inputs, whereas the magnitude is dependent on the decay model chosen. Note that the model results discussed thus far use predicted bacterial inputs. The effect of accurate source loading is investigated further, using measured input data, in Chapter 6.

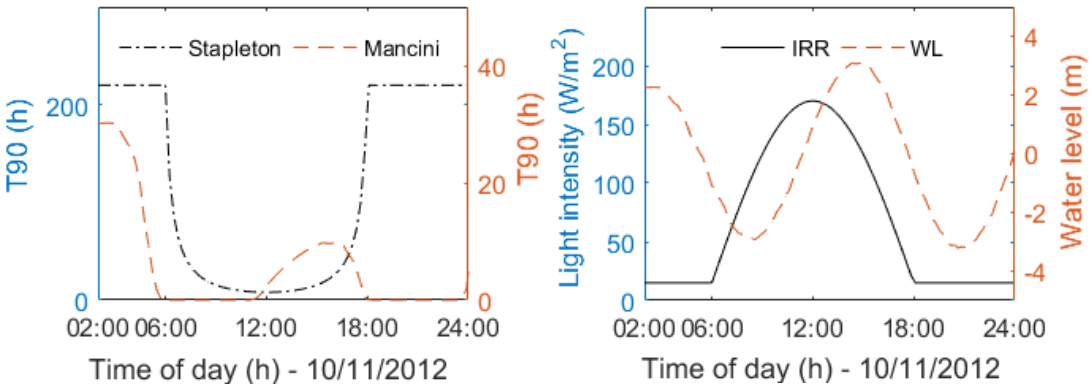

Figure 5.38: Comparison between the decay rate calculated at the most offshore Swansea Bay DSP transect point using Stapleton et al. [2007a] and Mancini [1978] decay models (a), in relation to irradiance (IRR) and water level (WL) (b)

5.5.1.3 Spatial variability

As discussed in Section 5.2, monitoring at the Swansea Bay and Aberafan DSPs is done along a transect. As such, two methods have been used to compare measured and predicted data. Firstly, the predictions shown in Figures 5.36 and 5.37 are taken at the shallowest transect point greater than or equal to the sampling depth (0.5 m). Thus the line plots shown correspond to multiple locations. Alternatively, using the Stapleton et al. [2007a] decay function, the

predicted concentrations at all points along each transect are plotted in Figures 5.39 and 5.40. For comparison, the predicted concentration at each point along the Swansea Bay DSP transect is shown in Appendix B.2, Figure 3. The spikes seen in Figure 5.40 are due to the node drying out and the concentration reaching zero.

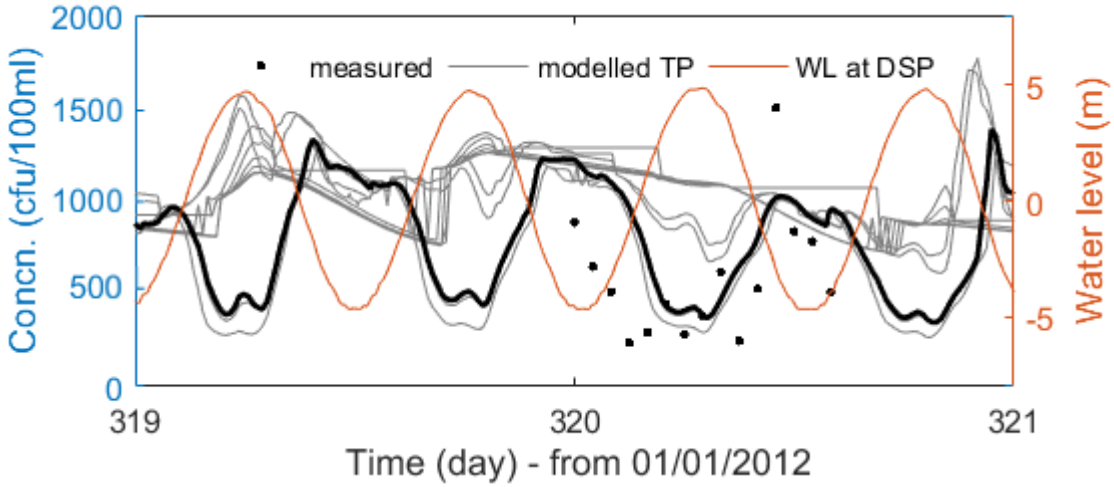

Figure 5.39: Comparison between the measured and predicted *E.coli* concentrations at each monitoring location along the Swansea Bay DSP transect (TP), using the Stapleton et al. [2007a] decay function in the 2D model. Plotted alongside the predicted water level at the most offshore monitoring location

It can be seen in Figures 5.39 and 5.40 that at any point in time, there are significant spatial differences in the predicted *E.coli* concentrations at each transect point, with a range of up to half the magnitude of the highest predicted concentration. The point which is considered a best fit to the measured data has been highlighted. It is suggested that because of this spatial variance (also seen in Figure 5.41), when modelling it may be prudent to take samples at multiple locations to ascertain potential 'safe' and 'no go' zones. In addition, it highlights a potential limitation of the model to accurately calculate processes which take place at a high spatial resolution. These points will be discussed further in Chapter 6.

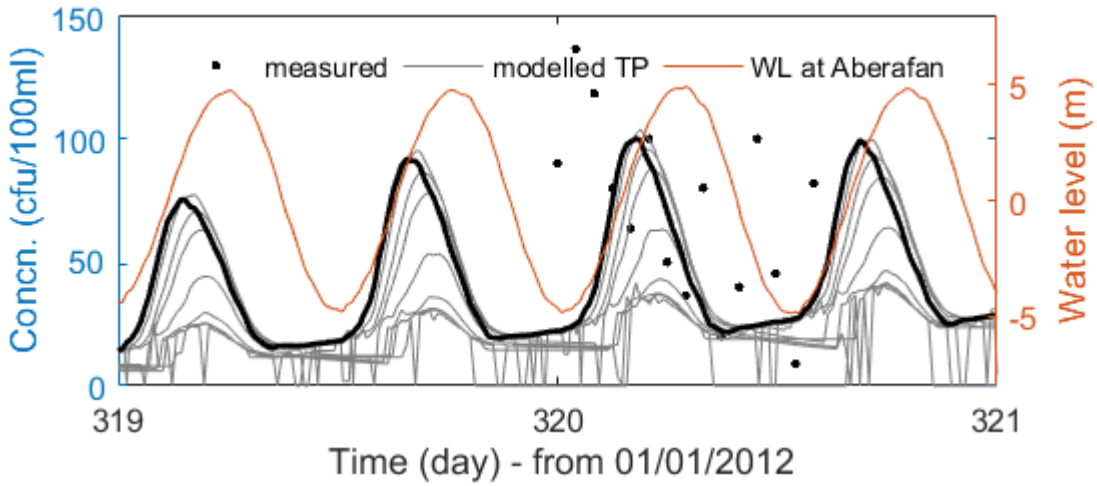

Figure 5.40: Comparison between the measured and predicted *E.coli* concentrations at each monitoring location along the Aberafan DSP transect (TP), using the Stapleton et al. [2007a] decay function in the 2D model. Plotted alongside predicted water level at the most offshore monitoring location

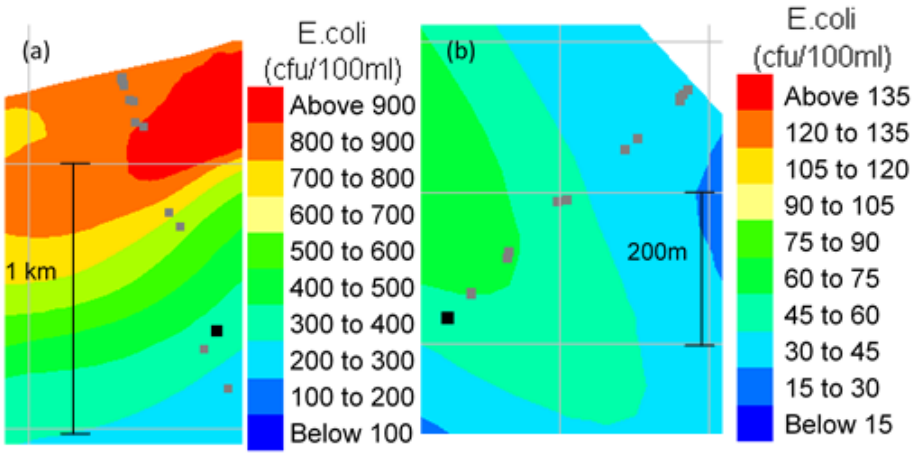

Figure 5.41: Surface plots of the predicted *E.coli* concentration along the DSP transects, using the Stapleton et al. [2007a] decay function in the 2D model at 15/11/12 19:11:57 (high tide); (a) Swansea Bay, (b) Aberafan

In addition, Figure 5.39 shows a diurnal pattern in the predicted *E.coli* concentration at the Swansea Bay DSP, with lower concentrations at high tide. There is, however, disagreement between measured and predicted data, suggesting that there may be other influential factors not yet considered.

Considering the Aberafan DSP (see Figure 5.40), although the Stapleton et al. [2007a] model predicts *E.coli* concentrations within range of the observations, there is significant variation between the two. The lack of a clear temporal pattern in the measured data may indicate irregularities in the sampling procedure or naturally occurring variance in *E.coli* concentrations within the locality. In order to explore these points further it is necessary to look at a longer data record; as is done in see Chapter 6.

Comparing the Mancini [1978] and Stapleton et al. [2007a] decay models, it can be seen in Figures 5.42 and 5.43 that both models predict different spatial concentration distributions within Swansea Bay. The Mancini [1978] decay model predicts reduced concentrations in shallow water regions due to the dependence of Equation 3.29 on depth (see Figures 5.15 and 5.38). This is of significance when studying regions such as Swansea Bay, with a shallow beach gradient and large areas of intertidal flats, exposed to wetting and drying; it emphasises the importance of using multiple assessment locations when processing model predictions made using the Mancini [1978] decay model.

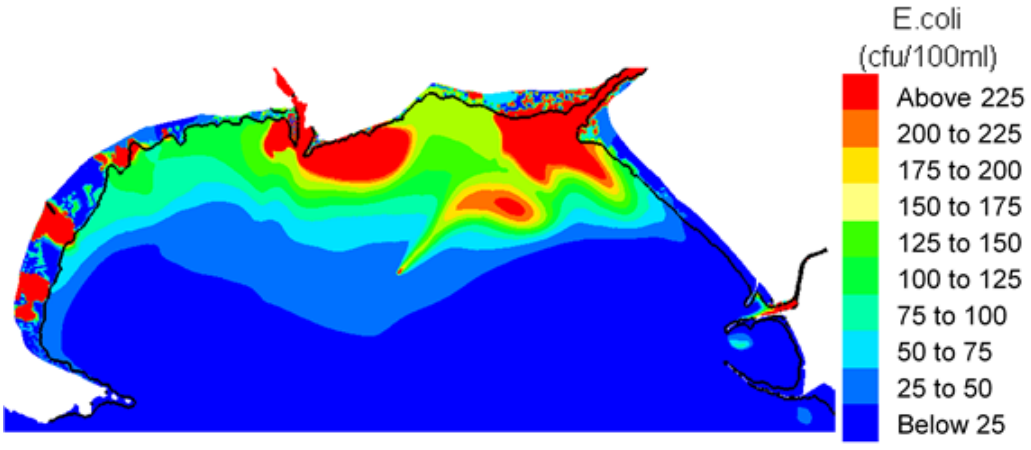

Figure 5.42: Surface plots of the predicted *E.coli* concentration throughout Swansea Bay using the Mancini [1978] decay function in the 2D model, at 15/11/12 16:00 (mid-tide). Water line (0.05 m depth) represented by black line

As previously discussed, TELEMAC calculates water depth absolutely without a threshold, hence the regions of water less than 0.05 m deep with an *E.coli* concentration. For the purpose of this study these can be ignored and considered 'dry', as they present an unrealistic picture of pollution distribution. Possible causes include errors in the model bathymetry and the static location of the source points on the beach (see Section 5.6). However, these regions could provide an indication of higher *E.coli* concentrations within beach sand which may be useful for predicting the risk of infection to beach users.

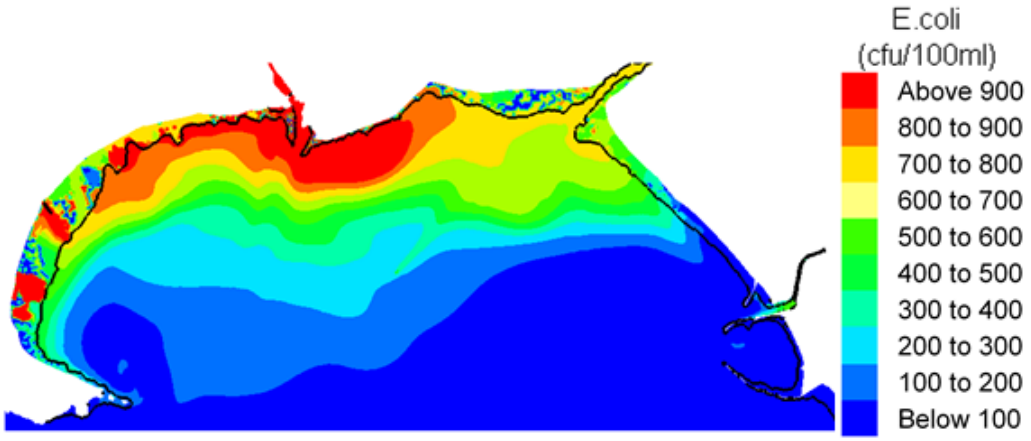

Figure 5.43: Surface plots of the predicted *E.coli* concentration throughout Swansea Bay using the Stapleton et al. [2007a] decay function in the 2D model, at 15/11/12 16:00 (mid-tide). Water line (0.05 m depth) represented by black line

5.5.2 3D

5.5.2.1 Variation of decay rate with depth

Figure 5.44 presents a comparison between the 3D model *E.coli* concentration predictions at the Swansea Bay DSP. As in the 2D model, use of the Mancini [1978] decay function results in lower predicted concentrations, while those made using the Stapleton et al. [2007a] function are of the same magnitude as the measured data. It can also be seen that in the case of both the Mancini [1978] and Stapleton et al. [2007a] decay models, lower concentrations were predicted

when using the depth-staggered function. The same observations can be made when comparing measurements and predictions at other locations in Swansea Bay; for example, see Appendix B.2 Figure 4 for a comparison at S2. Note that all 3D results presented herein have been averaged over the vertical layers to provide an indication of concentration throughout the water column, rather than in a single layer.

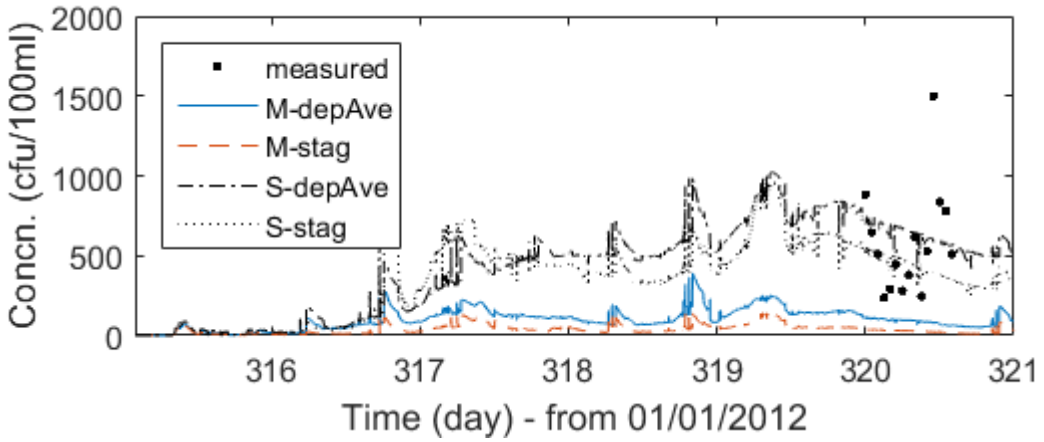

Figure 5.44: Comparison between the measured and predicted 3D model predictions of *E.coli* concentrations at the Swansea Bay DSP using depth-averaged (depAve) and staggered (stag) functions with the Mancini [1978] (M) and Stapleton et al. [2007a] (S) decay models

The difference between the depth-averaged and depth-staggered decay model predictions can be explained as follows. Consider Equation 5.2, a simplified form of Equation 3.4, reduced to 1D in the vertical with zero vertical velocity. In this case the problem is reduced to one controlled by diffusion between layers, and decay. This can be further reduced to Equation 2.2 by setting the tracer diffusion term to zero.

$$\frac{\partial C}{\partial t} = \frac{\partial}{\partial z}\left(\nu_T \frac{\partial C}{\partial z}\right) - kC \tag{5.2}$$

The analytical solution of Equation 2.2 is given in Equation 5.3:

$$C(t) = C_0 e^{-kt} \tag{5.3}$$

where $C(t)$ is the concentration at time t, C_0 is the concentration at time $t = 0$ and k is the decay rate (1/d).

For a simple 5 layer problem with a node spacing of 1 m, we look at the decay of an initial tracer concentration of 1000 (dimensionless), over 2 days. Equation 5.2 was solved using time step of 1 minute and finite different methods; a first order forward difference scheme in time and a second order central difference scheme in space. The boundary value problem was solved at the surface and bed by introducing phantom layers with a value equal to the adjacent real boundary. The parameters in Equations 3.32 and 3.34 were set as those used in the Swansea Bay model (see Section 5.3.2). Light intensity was fixed at 260 W/m^2.

As can be seen in Figure 5.45 (a), there is good agreement between the analytical and finite difference solutions when calculating decay as a depth-staggered parameter, setting the tracer diffusion term to zero, thus confirming the method is sound. The data plotted in Figure 5.45 (a) is also presented in Appendix B.2, Tables 8, 9,10 and 11 for information. As shown in see Appendix B.2, Tables 9 and 12, it can be seen that changing the tracer diffusion term to 1×10^{-6}, as in the Swansea Bay model, has negligible difference on the concentration in each layer.

Comparing the use of depth-staggered and depth-averaged decay functions, it can be seen in Figure 5.45 (b) and Appendix B.2, Tables 12 and 14 that the overall concentration in the water column is less when a depth-staggered approach was used. This is because the exponentially larger decay rate in the surface layers causes a greater reduction in concentration than at depth. Figure 5.46 compares the decay rates calculated over a depth of 5 m using each approach, and the Mancini [1978] model, which highlights this point further.

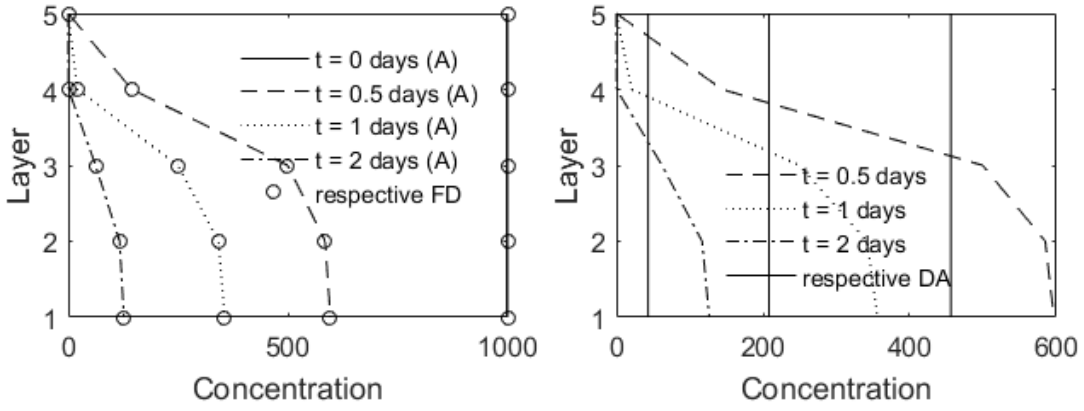

(a) b

Figure 5.45: Solution of simplified 5 layer decay problem; (a) comparison between analytical and finite difference (FD) solutions using a depth-staggered decay rate, where $\nu_T = 0$; (b) comparison between depth-averaged (DA) and staggered solutions

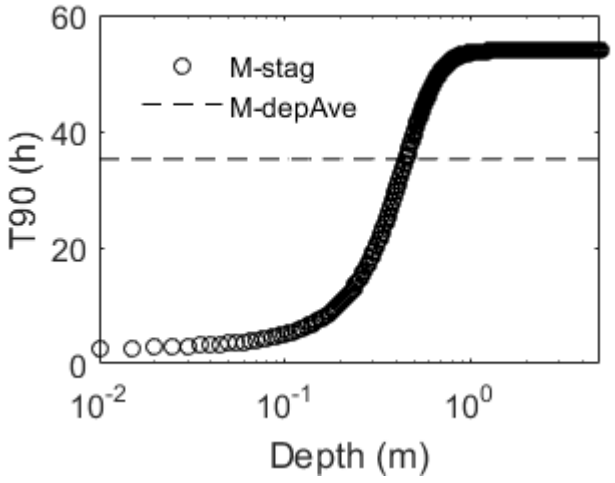

Figure 5.46: Comparison of Equations 3.32 and 3.34; depth-staggered and depth-averaged decay rates respectively

To emphasise the effect of diffusion, ν_T can be increased to a value of unity and removed from Equation 5.2. It can be seen from Appendix B.2, Tables 12, 13, 14 and 15 that this results in higher concentrations in the surface layers, reduced concentrations at depth and a reduction in total concentration in the water column. This is due to increased transport of tracer from the regions of high concentration at depth, to lower concentration at the surface. Tracer in the surface layers continues to decay at a faster rate, increasing the concentration gradient and hence the movement of tracer between layers.

This interchange between layers will be further increased by including the velocity term in Equation 5.2, where there is upward flow, such as in Swansea Bay and in the vicinity of long sea outfall diffusers with a vertical orientation.

5.5.2.2 Comparison with 2D model results

Figures 5.47, 5.48, 5.49 and 5.50 provide a comparison between the 2D and 3D model predictions of *E.coli* concentration in Swansea Bay. To enable direct comparison between the two, the depth-averaged decay approach is presented for the 3D model. For information, a comparison at site S2 is shown in Appendix B.2 Figure 5.

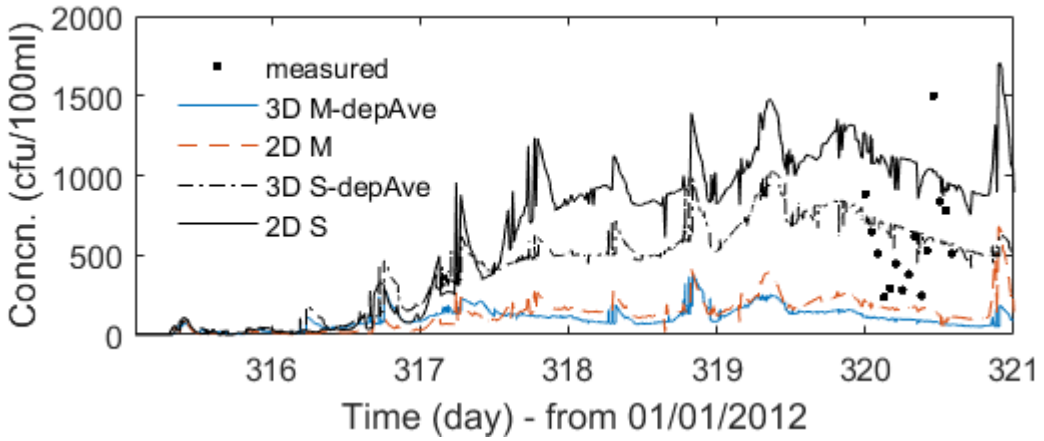

Figure 5.47: Comparison between the measured, 2D and 3D model predictions of *E.coli* concentrations at the Swansea Bay DSP, using the Mancini [1978] (M) and Stapleton et al. [2007a] (S) decay functions

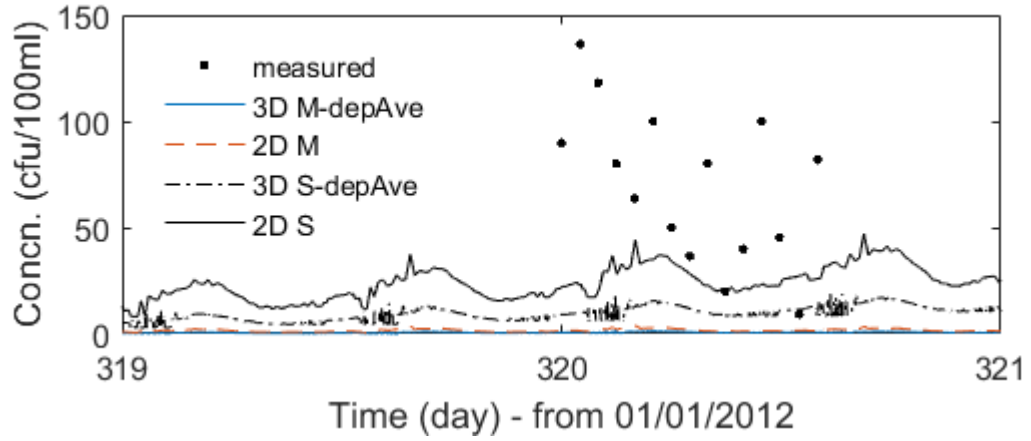

Figure 5.48: Comparison between the measured, 2D and 3D model predictions of *E.coli* concentrations at the Aberafan DSP, using the Mancini [1978] (M) and Stapleton et al. [2007a] (S) decay functions

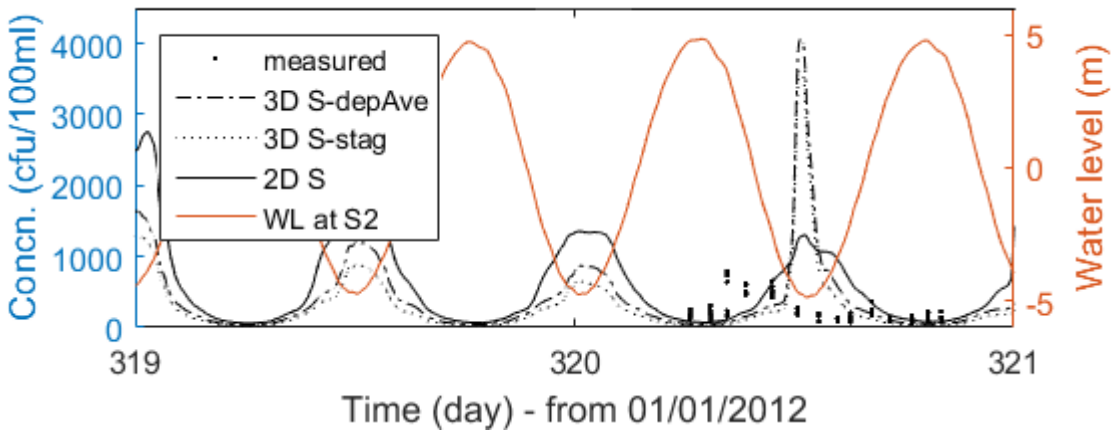

Figure 5.49: Comparison between the measured, 2D and 3D model predictions of *E.coli* concentrations at site S2; Mancini [1978] (M) and Stapleton et al. [2007a] (S)

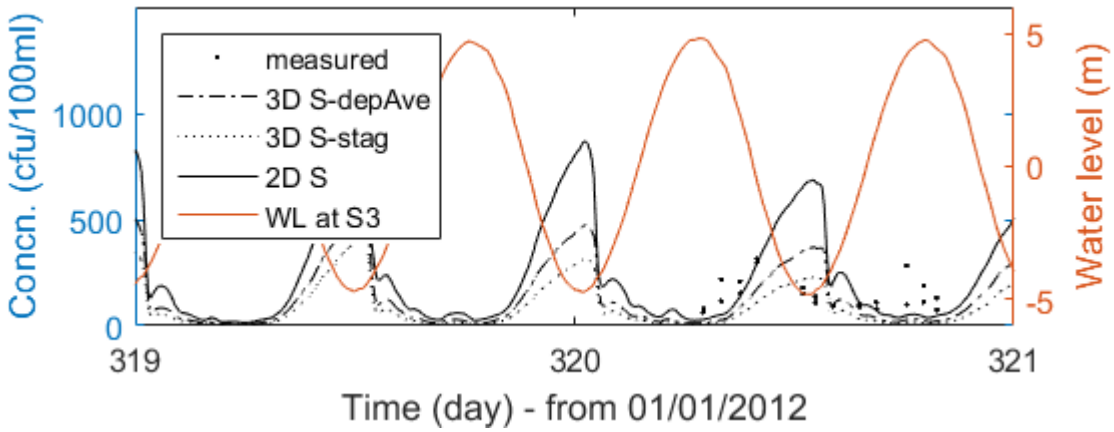

Figure 5.50: Comparison between the measured, 2D and 3D model predictions of *E.coli* concentrations at site S3; Mancini [1978] (M) and Stapleton et al. [2007a] (S)

It can be seen that in all cases using the same decay function, the 2D model predicts higher concentrations than the 3D model. Furthermore, while both the 2D and 3D models predict *E.coli* concentrations within the range of measured data at the Swansea Bay DSP, the 2D model predictions are more similar in magnitude and the 3D model under predicts concentrations at the Aberafan DSP. These observations can be attributed to the inclusion of the Rivers Neath and Tawe in the 2D model, whereas they were excluded from the 3D model, and can be explained by looking at Figures 5.51 and 5.52.

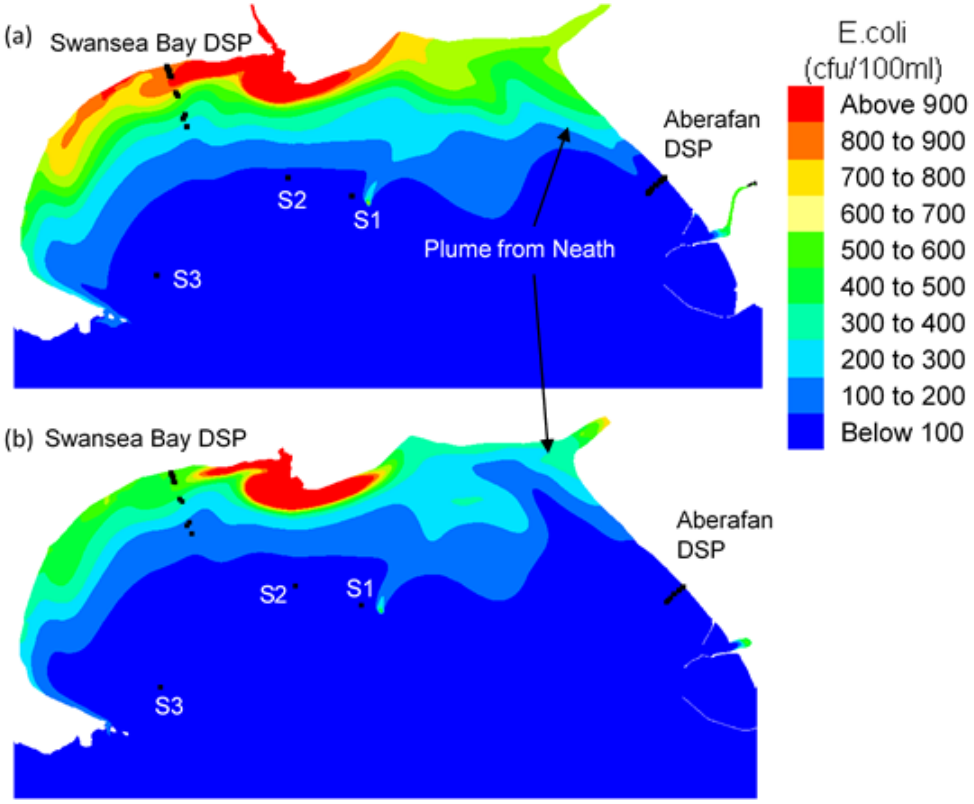

Figure 5.51: Comparison of the predicted *E.coli* concentration distribution in Swansea Bay, at 15/11/12 19:16 (HT), using the Stapleton et al. [2007a] decay function in the 2D (a) and 3D (b) models. Depth-averaged decay function used in the 3D model

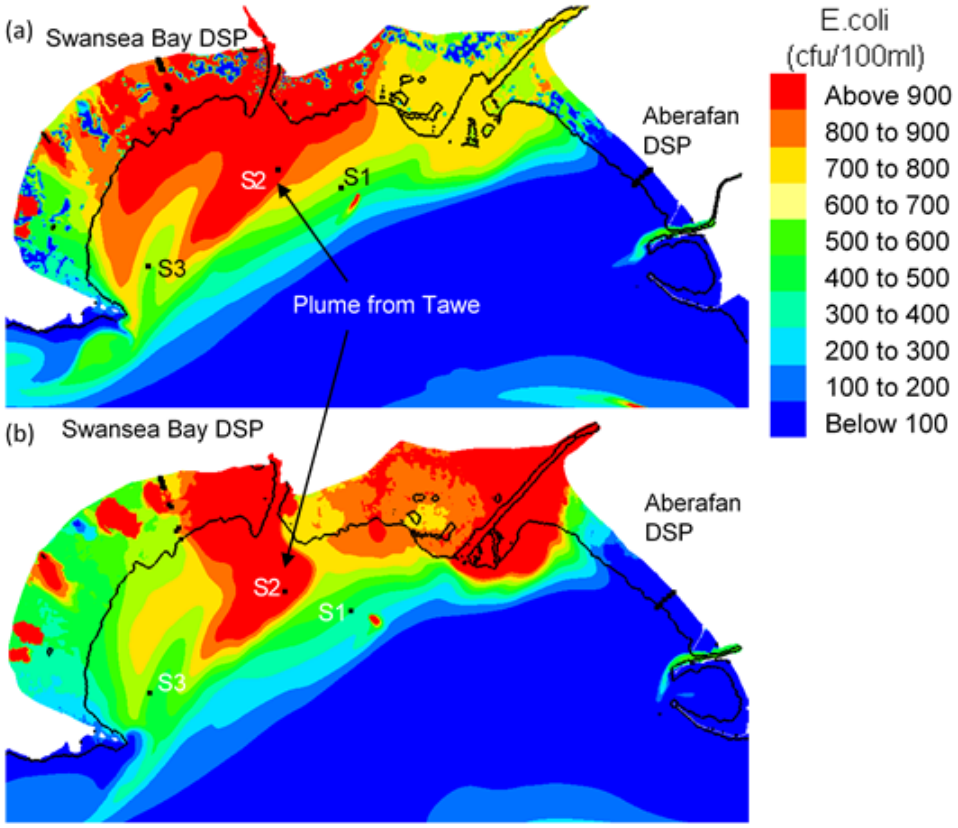

Figure 5.52: Comparison of the predicted *E.coli* concentration distribution in Swansea Bay, at 15/11/12 12:09 (LT), using the Stapleton et al. [2007a] decay function in the 2D (a) and 3D (b) models. Depth-averaged decay function used in the 3D model

Based on the location of the model *E.coli* inputs (see Figures 5.5 and 5.6), it can be reasoned that the plume from the River Neath is responsible for the water quality at the Aberafan DSP. Whereas the Neath is included within the 2D model, it is represented as a point source at the river mouth in the 3D model, without an assigned velocity. In this case the flow speed is greatly reduced and the plume does not extend far enough into the bay on the ebb tide (see 5.52), to be directed along Aberafan beach on the flood tide (see Figure 5.51). This is also true at the Swansea Bay DSP, where the 2D model predicts higher concentrations than the 3D model, which represents the Tawe barrage as a point *E.coli* source. In both cases the 3D model is incapable of correctly calculating the advection of *E.coli*. This highlights the importance of including the momentum of bacterial

inputs, either by assigning a velocity to point sources or linking 1D river models and the 3D coastal model, with momentum transfer between domains.

With regard to the predicted concentration at site S2 (see Figure 5.49), the spike on 15/11/12 (day 320) is due to a difference in the shape of the plume from the Tawe Barrage. In the 3D model it is smaller and of higher concentration compared to that in the 2D model, which is distributed over a larger region and of lower concentration.

5.5.3 Temporal variation in light intensity

Figures 5.53 and 5.54 provide a comparison between the use of a sinusoidal light intensity function and measured, sub-hourly data to calculate decay, when using the Stapleton et al. [2007a] decay function.

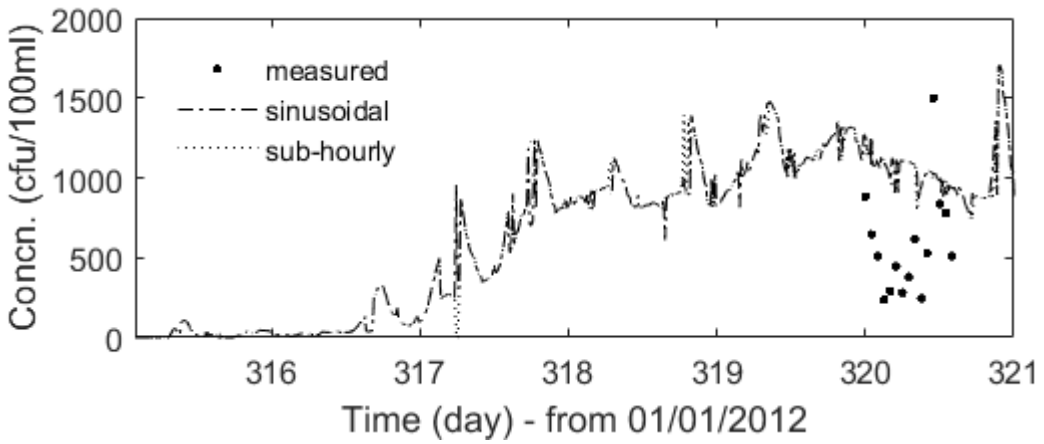

Figure 5.53: Comparison between the use of a sinusoidal light intensity function and sub-hourly measured data in the 2D model, using the Stapleton et al. [2007a] decay function

It can be seen that there is a negligible difference in the 2D model results while a clear difference can be seen in the 3D model; that run using sub-hourly measured data predicts higher concentrations than that using a sinusiudal function. However, both models predict a similar magnitude and temporal variation in *E.coli* concentration, suggesting that if sub-hourly data is unavailable, it is sufficient to assume a sinusoidal daylight function of average peak intensity for

short simulation periods. Results are omitted for the depth-averaged 3D decay model as no difference is observed, as with the 2D model. This is due to the calculation of differential decay rates throughout the water column when using the staggered approach, which makes the surface layers more sensitive to changes in light intensity.

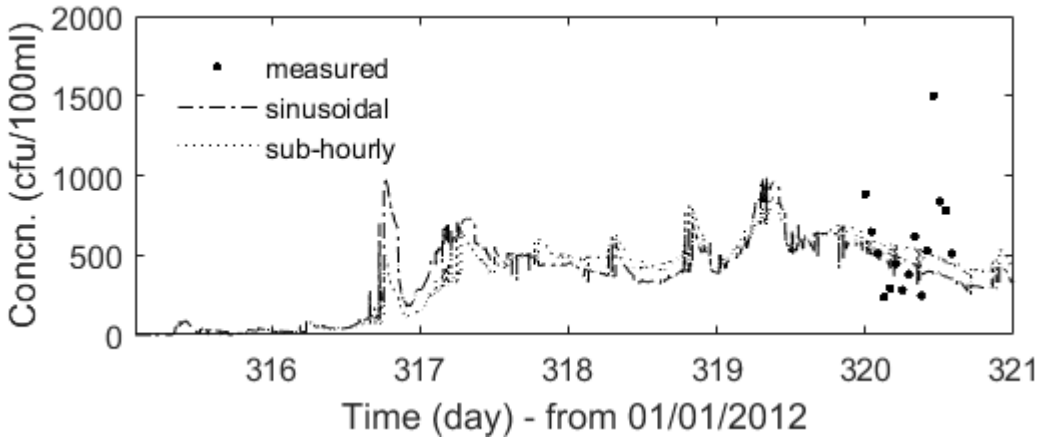

Figure 5.54: Comparison between the use of a sinusoidal light intensity function and sub-hourly measured data in the 3D model, using the depth-staggered Stapleton et al. [2007a] decay function

Two explanations are proposed to account for the difference between the use of a sinusoidal function or measured data. From comparison between Figures 5.16 and 5.17, it can be seen that the sinusoidal function over-predicts light intensity throughout the day, leading to faster decay rates. It is therefore suggested that a sine function, covering the range -$pi/2$ to $3\pi/2$, may provide a better representation of the measured data. In addition, the difference between the two models is greatest following days of below average sunlight. This is due to over prediction of the decay rate when imposing the same peak light intensity each day, as was done when using the sinusoidal function.

The above is also true when using the Mancini [1978] decay function, however plots have been omitted here for brevity. These are shown in Appendix B.2, Figures 6 and 7).

5.5.4 Comparison of turbulence models

The model simulations discussed so far were run using the Smagorinsky turbulence model. Figures 5.55 and 5.56 provide a comparison between predicetd *E.coli* concentrations using each of the four options available to model turbulence within TELEMAC. The longitudinal and transverse dispersion coefficients of the Elder model were set to 6 and 0.6 respectively, as recommended in the TELEMAC user manual (see Lang et al. [2014]).

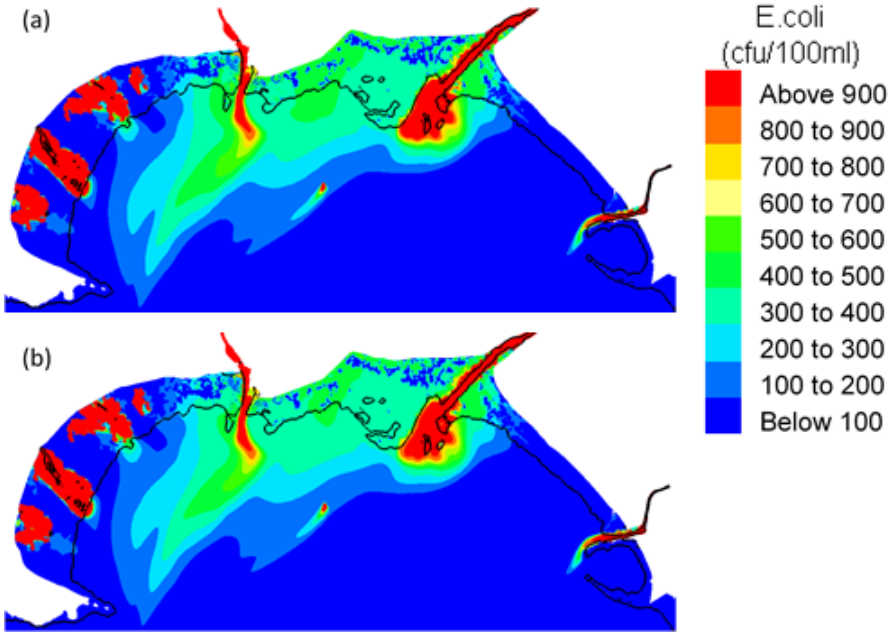

Figure 5.55: Comparison of the predicted *E.coli* concentration distribution in Swansea Bay at 12/11/12 10:14 (LT) in Swansea Bay using a constant decay rate of T_{90} = 50 h. Turbulence models; (a) constant viscosity and (b) Elder model

It can be see that in each case there are minor differences in the *E.coli* concentration distribution throughout Swansea Bay in close proximity to the plume edge, however, predictions are mostly the same. Similar invariance between the different turbulence models is observed at a smaller scale, using the TELEMAC model discussed in Chapter 4 (see Figure 5.57).

In this test case, tracer was released from the midsection of a straight, shallow, flat bottomed channel at a constant flow rate and concentration of 0.01 m^3/s and 999 (dimensionless) respectively. The flow depth and flow rate were set as 0.21

m and 0.05 m^3/s respectively.

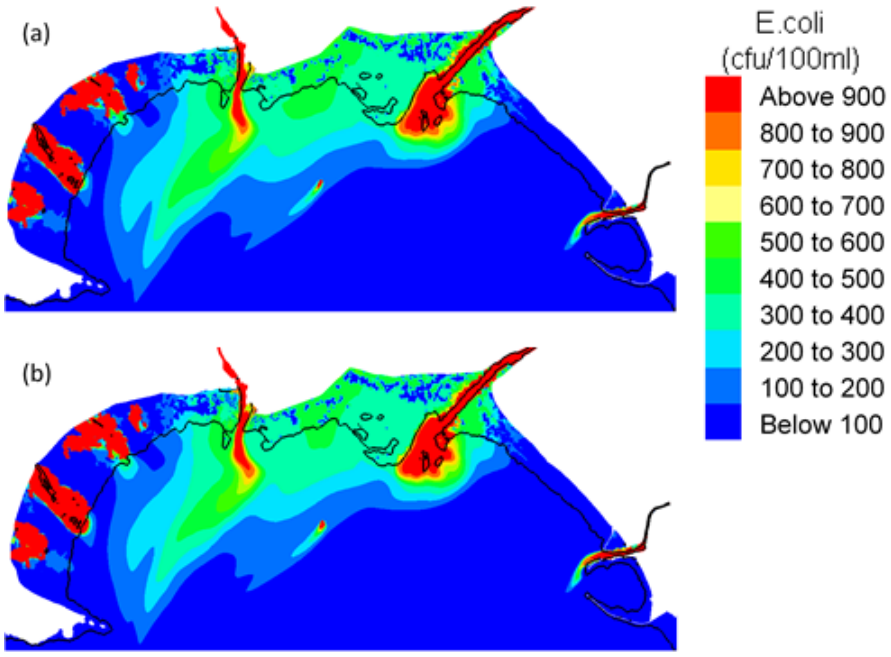

Figure 5.56: Comparison of the predicted *E.coli* concentration distribution in Swansea Bay at 12/11/12 10:14 (LT) in Swansea Bay using a constant decay rate of $T_{90} = 50$ h. Turbulence models; (a) $\kappa - \epsilon$ model and (b) Smagorinsky model

However, significant differences are observed when using the Elder model. This is due to the predominantly uni directional flow, which emphasises the non-dimensional dispersion coefficients specified by the user. The effect is less evident in the model of Swansea Bay due to constant changes in flow direction throughout the tidal cycle. As such the Smagorinsky model is used henceforth.

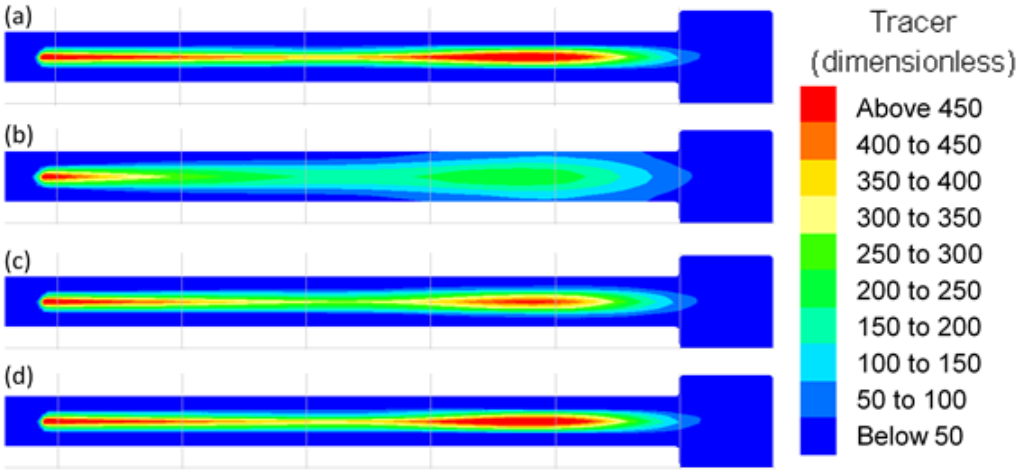

Figure 5.57: Comparison between turbulence models in a straight uniform flat bottomed channel; (a) constant viscosity, (b) Elder model, (c) $\kappa - \epsilon$ model and (d) Smagorinsky model

5.5.5 Computational efficiency

Although not the primary purpose of this study, it is of interest to the wider modelling community to comment on the performance of TELEMAC. All models in this study were run on the HPC Wales Cardiff cluster, on which more information can be found online (see HPC Wales [2018]). Table 5.3 compares the computational requirements and performance of the 2D and 3D models. While the 3D model contained 5 times the number of mesh nodes than in the 2D model, and the computational power doubled, the total run time increased by a factor of 1.8.

It should be noted that the number of CPU cores required for each model was not optimised as HPC resources were not a limiting factor. However, this may have resulted in under-performance in both cases. This is because TELEMAC divides the model global domain into sub-domains based on the number of CPU cores used, and data exchange is made between sub-domains at the end of each time step. A point is reached where the number of sub-domains is too large relative to the size of the global domain and the time to job completion is slowed due to increased sub-domain communication.

Nonetheless, TELEAMC is highly optimised for parallel computing and rec-

ommended by the author. Initial model development was made using v6p2r3 and though no comparison is presented herein, a significant performance improvement was noticed when transitioning to v7p2r3.

Table 5.3: Comparison of CPU use and run time between 2D and 3D models from 10/11/2012 - 17/11/2012

	2D Model	3D Model
Number of mesh nodes (total)	142533	666705
Number of mesh elements (total)	281440	1321185
Number of HPC nodes	4	8
Number of CPU cores per HPC node	16	16
Total number of CPU cores	64	128
Elapsed time to completion	0h 50min	1h 30min

5.6 Improved representation of beach sources

So far the bacterial sources shown in Figure 5.2 have been implemented as stationary point sources. Therefore, in the models discussed so far, because the minimum water depth in TELEMAC is 0 m, when these sources are released on the beach the contaminated water spreads over a large area in a thin film (i.e. of a depth less than 1 cm, up to 1×10^{-5} m; for example see Figure 5.52. While inaccurate, this is necessary to ensure mass conservation. In reality, these inputs form small streams in the beach sand which run from the source point to the tide line (see Figure 5.58). The spreading described is due to the coarse grid resolution which does not allow the streams to be modelled. To do so would result in a significant reduction in mesh size to 1 m or less, and an increase in computational requirements and run time.

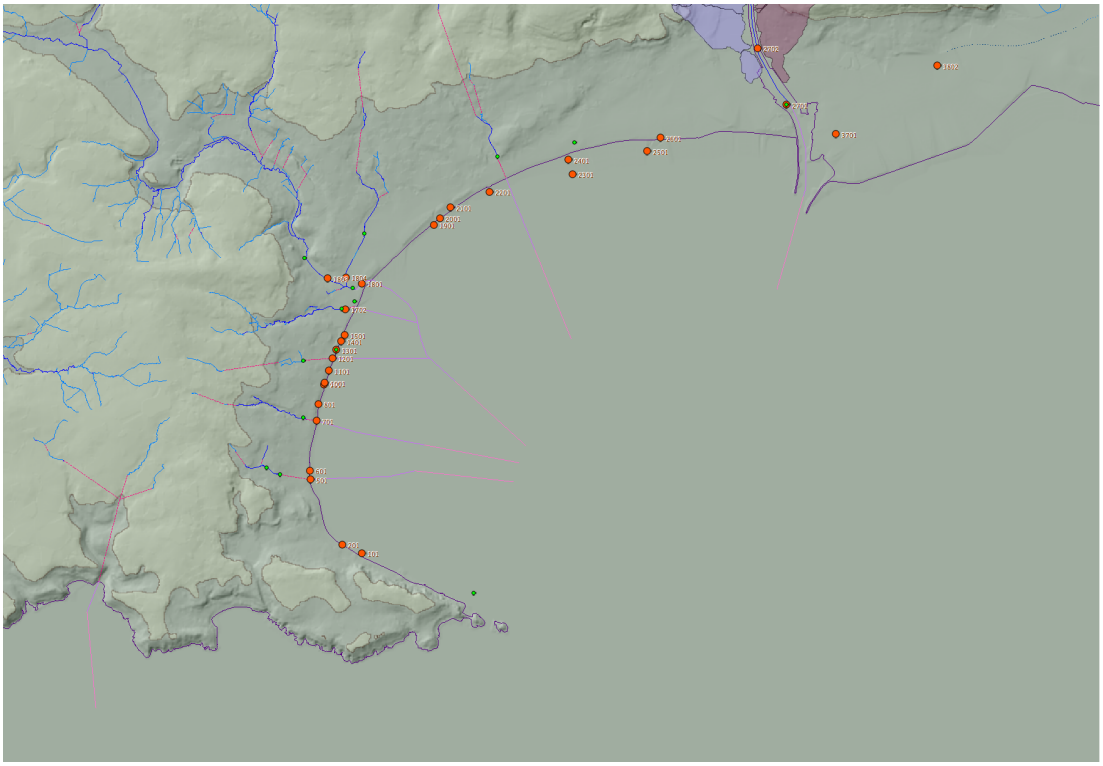

Figure 5.58: Stream tracks of beach sources along Swansea Bay; purple lines and red dots respectively

Alternatively, the method proposed herein treats each source point as a transect running to the low water line. Each transect is represented by multiple source points which discharge the same volume of water and concentration of bacteria (see Figure 5.59). The source release location is changeable to ensure release is always at a point below the water line, mimicking transport within a stream.

To ensure mass conservation, modifications to the TELEMAC source code only permit one point to discharge per time step; that which is closest to, and below, the waterline. This method of improved source representation has been implemented in TELEMAC-2D, with modifications made to `debsce.f` and `trsce.f`, to control source discharge and tracer concentration respectively.

An illustration of this source representation is shown in Figure 5.60, which demonstrates release at four different tidal phases. A similar approach was used by Feng et al. [2015] who developed a microbial transport model accounting for loading from beach sand and storm water runnoff at a beach in Florida, U.S.

However, in this study the model was reduced to a 1D case for a single lumped source, solved using finite difference methods. The grid followed a transect perpendicular to the straight uniform shoreline, which was assumed to representative of the beach.

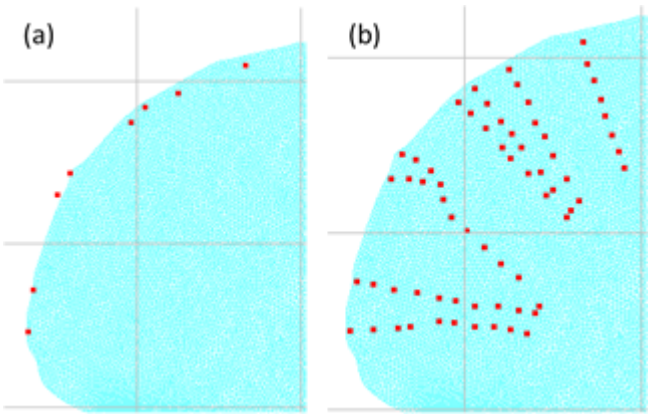

Figure 5.59: Static source points at the outlet location and respective source transects along Swansea Bay beach; (a) and (b) respectively

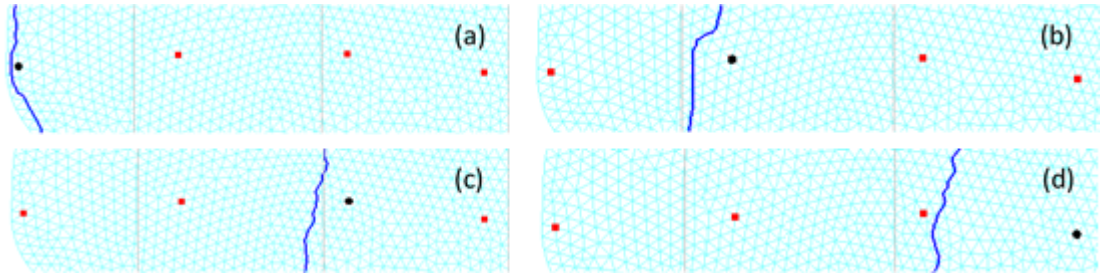

Figure 5.60: Illustration of improved source representation; blue line = threshold depth (0.05 m), red squares = transect points, black circle = source release point

An important point to consider when implementing this method is the treatment of sources when using multiple CPUs; i.e. parallel computing. When a job is distributed across multiple cores the domain is divided by this number into sub-domains, and each core carries out the computations for a single sub-domain. At the start of the computation the initial conditions are known throughout the domain and all sub-domains, and at the end of a time step information is shared across sub-domain boundaries. However, within a time step, processors only retain information on the sub-domains they are allocated. This is important in

the case where a source transect spans across two or more sub-domains and is overcome using Message Passing Interface (MPI) programming.

Consider the following example; a single transect with 10 points which span across two sub-domains (see Figure 5.61). Points 1:5, in sub-domain 1, are dealt with by procecssor 1, and points 6:10, in sub-domain 2, are dealt with by processor 2. The pseudocode in Figure 5.62 describes the action of each processor during one time step and highlights the data exchange between them.

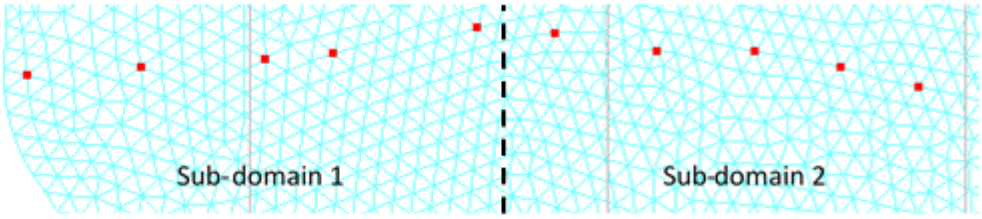

Figure 5.61: Source transect made of 10 points equally distributed across two sub-domains

Prior to MPI communication, processors 1 and 2 only have access to information at points 1:5 and 6:10, respectively. After MPI communication, using the function `MPI_ALLREDUCE`, both processors have access to information at all points, 1:10, along the transect. Each processor is then able to execute the remaining code to ensure the transect point, with the minimum depth above the pre-defined threshold (0.05 m), releases. Release at all other points along the transect is set to zero for that time step. Example Fortran code is given in Appendix B.1, Listing 8.

Previous analyses have shown the 2D model, using the Stapleton et al. [2007a] decay function, to best predict *E.coli* concentrations at both DSPs and throughout Swansea Bay (see Section 5.5). In addition, the use of measured light intensity data, instead of a representative sine function, was shown to have an impact on the magnitude of predicted concentrations, at no additional computational cost. As such, the method of improved source representation was implemented alongside the Stapleton et al. [2007a] decay function in TELEMAC-2D, using variable light intensity. Two simulations were run; using threshold depths of 0.05 m and 0.5 m.

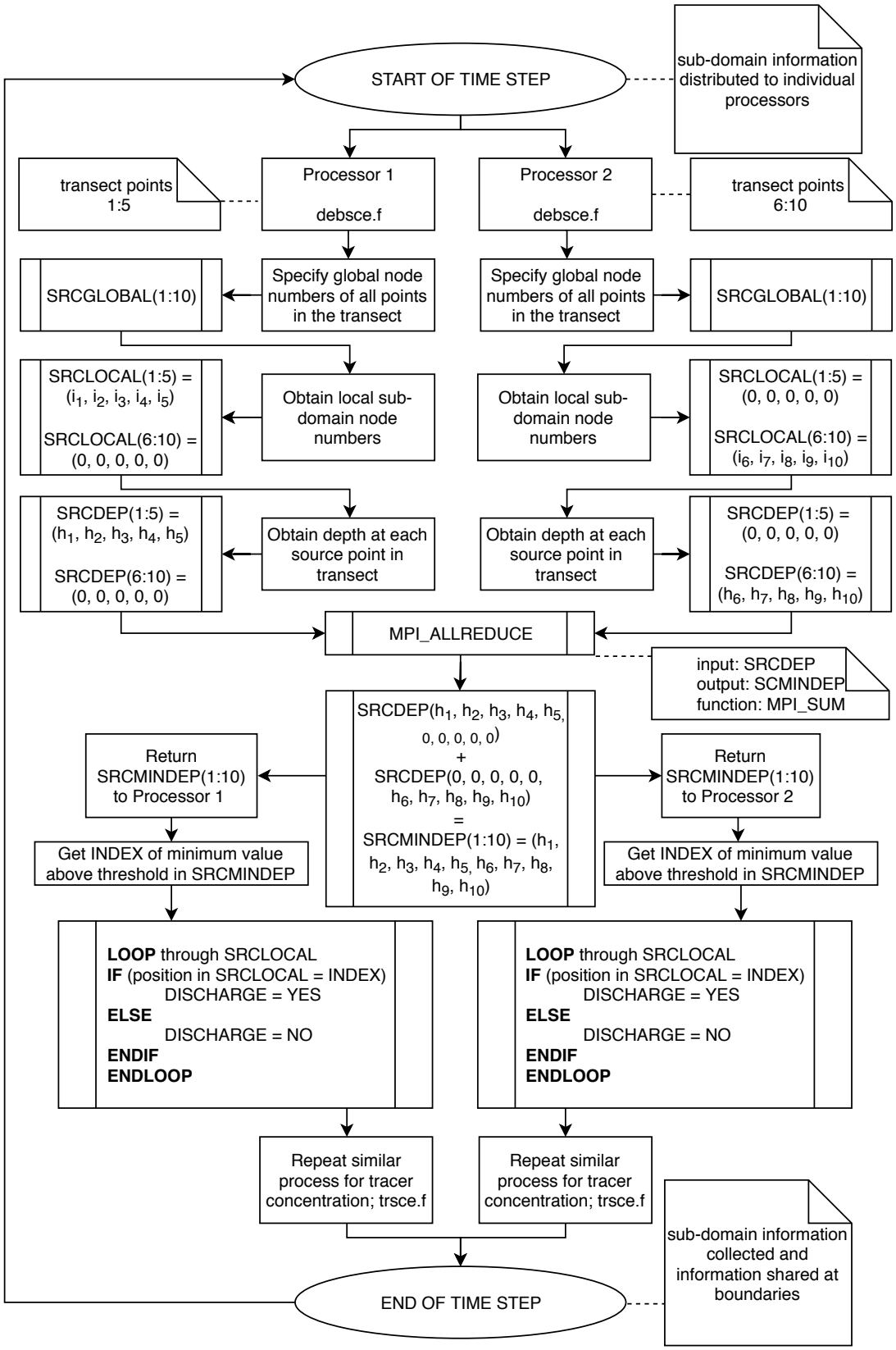

Figure 5.62: Flow chart showing implementation of the improved source representation method in TELEMAC-2D

5.6.1 Results and discussion

Plots comparing the measured and predicted *E.coli* concentrations at the Swansea Bay DSP and site 3, using the static and improved source release models, are shown in Figures 5.63 and 5.64.

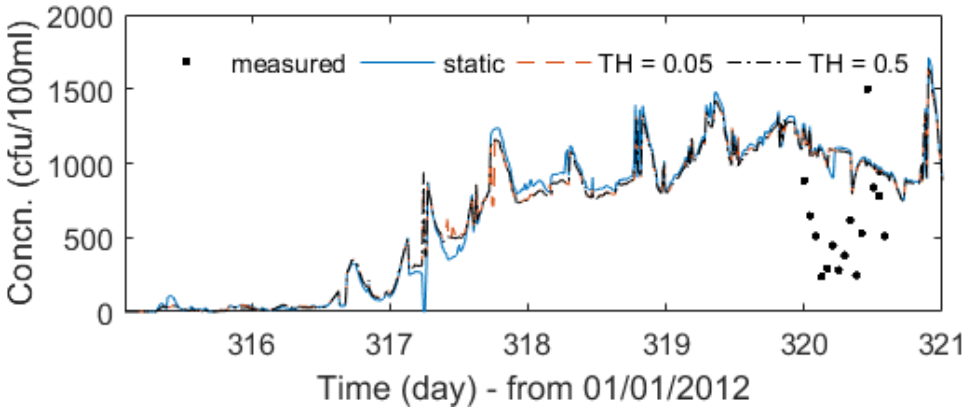

Figure 5.63: Comparison between the predicted *E.coli* concentrations at the Swansea Bay DSP, using static sources, and improved source representation with two threshold depths (TH)

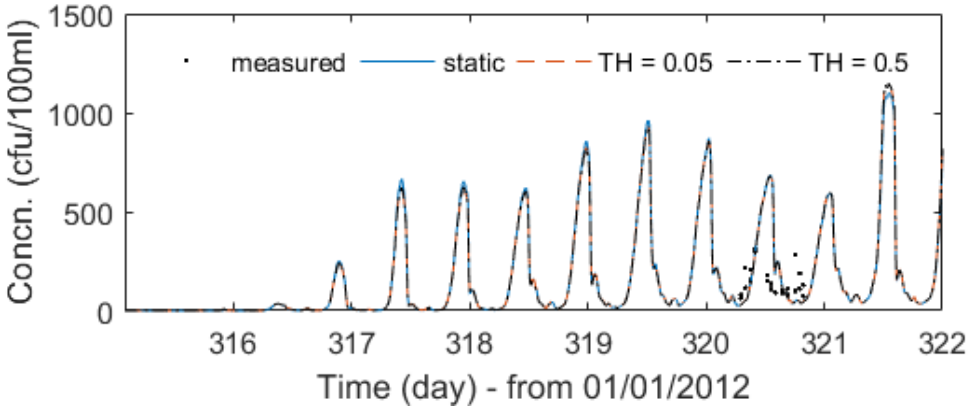

Figure 5.64: Comparison between the predicted *E.coli* concentrations at site S3, using static sources, and improved source representation with two threshold depths (TH)

It can be seen that using the improved model has a minor impact, and though differences are evident, they are not significant enough to warrant the choice of one

method over the other. The most noticeable differences are seen at the Swansea Bay DSP, where it can be seen that for the majority of the simulation, using the improved source model results in lower concentrations. This is due to increased dilution as the tracer is released into deeper water. While it is not possible to discern a difference between the two improved source models using different threshold depths, it can be seen in Figure 5.65 that if all release locations are moved to a point below the low tide line, *E.coli* concentrations in the nearshore region are under predicted throughout the tidal cycle, due to increased dilution. This indicates that correctly modelling the beach sources is important in order to accurately predict the dynamics governing bacterial transport.

It is therefore suggested that the apparent invariance between the static and improved source release models seen in Figures 5.63 and 5.64, is due to the distance of the DSP and site 3 from the source locations. In contrast, if the surface concentration distribution is considered, there are clear differences when comparing the two approaches over a tidal cycle (see Figure 5.65). At high tide there are elevated concentrations in the static discharge model and the *E.coli* plume extends along a greater length in the west of Swansea Bay. During the ebb tide the differences become more pronounced as the plume spreads over a large beach area above the water line. In comparison, the predicted concentrations in the improved source model are greatly reduced and the plume below the water line is of reduced size. There are also small regions of high *E.coli* concentration immediately below the waterline, in the vicinity of the source points, which have more serious implications on the predicted risk to bathers.

With regard to the *E.coli* distribution above the water line, this will have a greater implication if beach sand is considered a diffuse bacterial source and sink, in a similar manner to how Bakar et al. [2017] modelled inter-tidal marshland in the Loghour Estuary, UK. Furthermore, these regions may aid in correct prediction of the location of 'safe' and 'no go zones', on the beach and in the water, which is of utmost importance when disseminating bathing water information to beach goers, as advised by the rBWD.

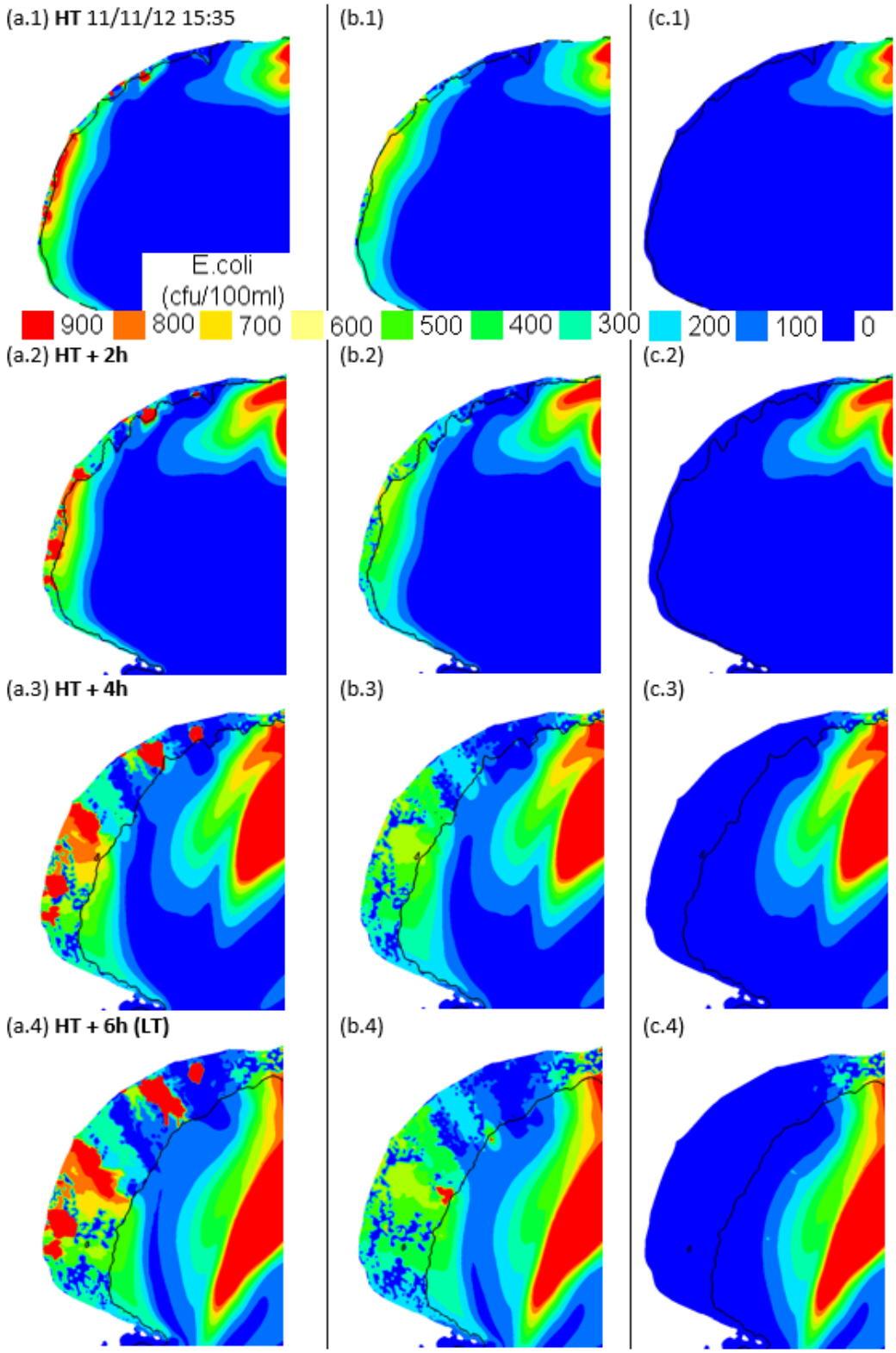

Figure 5.65: Comparison of the predicted *E.coli* concentration distribution in Swansea Bay, using the 2D model with static sources, improved source representation (TH = 0.05), and deep water sources; (a), (b) and (c), respectively

5.7 Summary and conclusions

Two computational models, one 2D and one 3D, were set up using the hydrodynamic solver TELEMAC to simulate the transport and decay of *E.coli* in Swansea Bay and compare a range of modelling approaches. In each case, two bacterial decay functions were implemented; those proposed by Mancini [1978] and Stapleton et al. [2007a]. Two methods were used when implementing these in the 3D model; a depth-averaged approach, where a constant decay rate was used throughout the water column, and a depth-staggered approach, where the decay rate was calculated to vary with depth.

In all cases the decay model proposed by Stapleton et al. [2007a] was found to provide the best predictions of the *E.coli* concentration throughout the domain, with those predicted by the 2D model the most accurate. In particular this was due to the larger night time decay rate predicted when using the Stapleton et al. [2007a] function. However, while different in magnitude, the temporal response predicted when using each function was similar, confirming the importance of correct hydrodynamic simulation and bacterial inputs. The 3D model was found to under predict bacterial concentrations due to the inclusion of the Rivers Neath and Tawe as point sources, without momentum conservation.

The under prediction of bacterial concentrations when using the Mancini [1978] decay model was due to the calculation of faster bacterial decay rates, as a result of the dependence of the decay equation on water depth. This has a significant impact in large intertidal regions of shallow bed gradient, such as Swansea Bay, and resulted in a significant difference in the predicted spatial *E.coli* concentration distribution, compared to when using the Stapleton et al. [2007a] model. In comparison, as the suspended sediment concentraton was assumed constant, the Stapleton et al. [2007a] decay model was only sensitive to light intensity.

Of the two methods used to calculate decay throughout the water column in the 3D model, the depth-staggered approach was found to predict lower bacterial concentrations, due to the exponential decrease in light intensity with depth and the associated effect on the decay rate. It is therefore suggested that in studies where it is necessary to adopt a 3D modelling approach, a depth-staggered decay

model should be used as it provides a more accurate representation of the spatial variation in bacterial die-off.

In addition, the use of measured light intensity data to calculate bacterial decay, assigned at 15 minute intervals, was compared to using a sinusoidal function (over the range 0 to π), to represent the daily variation in light intensity. This was found to have an impact when using the 3D depth-staggered model, however the difference observed was of a small magnitude and it is therefore suggested that if sub-hourly data is unavailable, it is sufficient to assume a sinusoidal daylight function of average peak intensity for short simulation periods. A function covering the range -$\pi/2$ to $3\pi/2$ is recommended as the most realistic representation of the temporal variation in light intensity throughout a typical day. A negligible difference was observed in the 3D depth-averaged, and 2D models.

Using the 2D model, an improved method of representing beach sources was developed to mimic the streams found on Swansea Bay beach. Rather than being considered stationary, the sources were moved along a transect throughout the simulation, to ensure they discharged just below the waterline. This provided more accurate predictions of the spatial distribution of *E.coli* within the domain, with the most significant effects noticed above and near the waterline, such as zones of elevated bacterial concentration where the beach streams enter the water. In addition it highlights the limitations of using TELEMAC to model static beach sources on shallow gradient beaches subject to wetting and drying throughout the tidal cycle.

Chapter 6

Hydro-environmental modelling of Swansea Bay

6.1 Model details and application

6.1.1 Scope of study

Having developed a computational model capable of predicting the *E.coli* concentration throughout Swansea Bay in Chapter 5 (the 2D model with improved source representation, using the Stapleton et al. [2007a] decay function), this chapter is focussed on the application and assessment of the model over the 2011 bathing season. It addresses a number of points which were raised during model development and provides a more comprehensive and critical assessment of model performance. This was possible as bacterial inputs were measured over this period, compared to the predicted input data used for 2012.

In addition, in Chapter 5 *E.coli* concentrations were measured at the DSP. This chapter investigates the robustness of this method and whether a more widespread approach to sampling is required when assessing compliance with the rBWD. For example; is a single DSP good enough, or are there certain areas of non-compliance that lifeguards can be advised on when designating 'safe' and 'no-go' bathing zones?

6.1.2 Set-up

The model was run from 12th July to 4th August 2011, and 5th August to 30th September 2011, using measured source input data collected for the Smart Coasts project [Aberystwyth University and University College Dublin, 2018]. Due to the considerable variation in recorded light intensity over this period, measured data was used as a model input; obtained from the meteorological monitoring station in Cwm Level Park, Swansea [City and County of Swansea, 2018] (see Figures 6.1 and 6.2; covering 12th July to 4th August 2011 and 5th August to 30th September 2011, respectively). However, there was a gap in the data record from 4th July to 5th July 2011, hence the period from 12th July to 30th September 2011 was not modelled continuously.

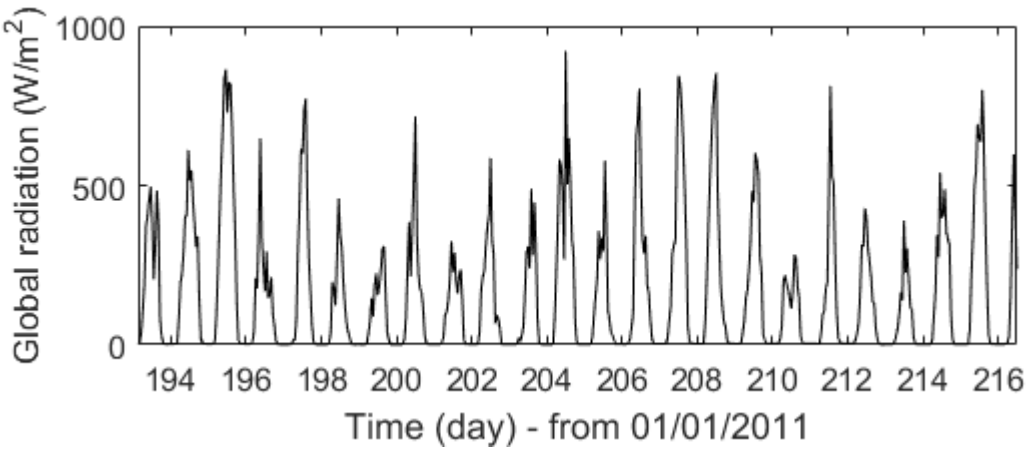

Figure 6.1: Light intensity in Swansea, measured at Cwm Level Park in hourly intervals from 12/07/11 to 04/08/11

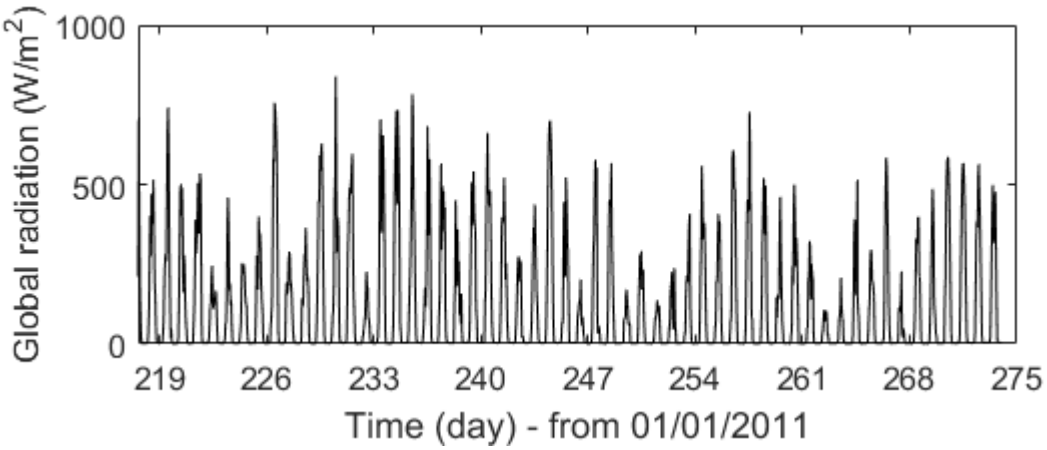

Figure 6.2: Light intensity in Swansea, measured at Cwm Level Park in hourly intervals from 05/08/11 to 30/09/11

E.coli concentration data, measured during the Smart Coasts project [Aberystwyth University and University College Dublin, 2018], was only available at the Swansea Bay DSP. Therefore, focus is placed on the Swansea Bay bathing water in the west of the domain (see Figure 5.2).

6.1.3 Parameter selection

Due to the large tidal range in Swansea Bay (between 5 m and 10 m; see Figure 5.20), resulting in a well mixed environment [Ahmadian et al., 2013], a constant suspended sediment concentration of 84.82 mg/l was assumed in Chapter 5, based on measurements taken nearby at Langland Bay and Porthcawl by Stapleton et al. [2007b]. However, this reduces Equations 3.36 to 3.40 to a function of light intensity only, implying that the equations are insensitive to changes in in turbidity.

The plot shown in Figure 6.3 illustrates the difference in predicted bacterial concentrations at the Swansea Bay DSP over the range of suspended sediment concentrations recorded in Swansea Bay by White et al. [2014]. It can be seen that there is a negligible difference in concentration, whereas it is reasonable to hypothesise that turbidity would be positively correlated with bacterial concentration, due to increased light attenuation causing a reduction in decay.

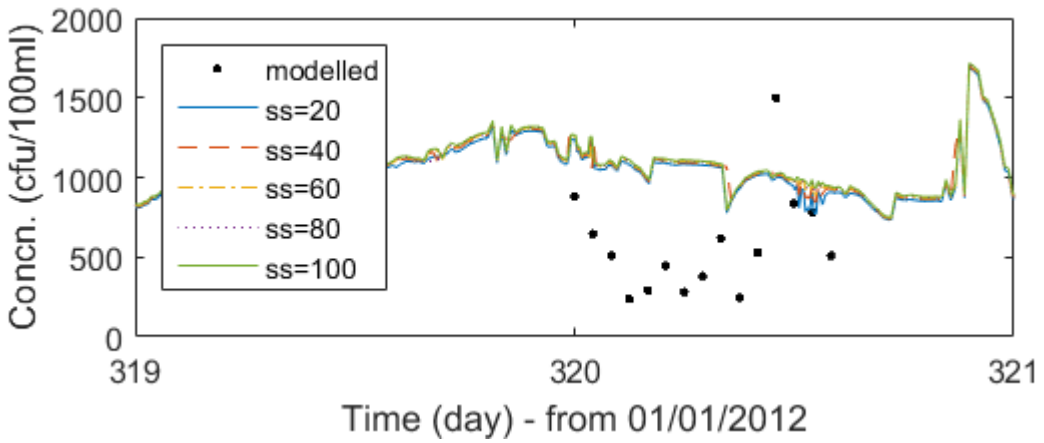

Figure 6.3: Comparison of the predicted *E.coli* concentrations at the Swansea Bay DSP for a range of suspended sediment (ss) concentrations (mg/l); using the Stapleton et al. [2007a] decay function in the 2D model

It is suggested that the reason for this insensitivity is due to the rapid attenuation of light with depth (see Figure 6.4), such that the lower light intensity limit and decay rate are reached at shallow depths (i.e. less than 1 m; see Section 5.4). Therefore, beyond a threshold depth (i.e. the Secchi-depth, see Equation 2.36), determined by the light intensity and light attenuation coefficient, the decay rate is invariant and independent of turbidity (see Figure 6.5).

Given the limited availability of turbidity data for Swansea Bay there is a high degree of uncertainty associated with any detailed sediment modelling. As such, the insensitivity of the model shown in Figure 6.4 was accepted at sufficient to justify the chosen parametrisation (ss = 84.82 mg/l). While not adopted in this thesis, the following section describes a proposed update to the representation of light attenuation in shallow water models, which it is suggested may increase model accuracy.

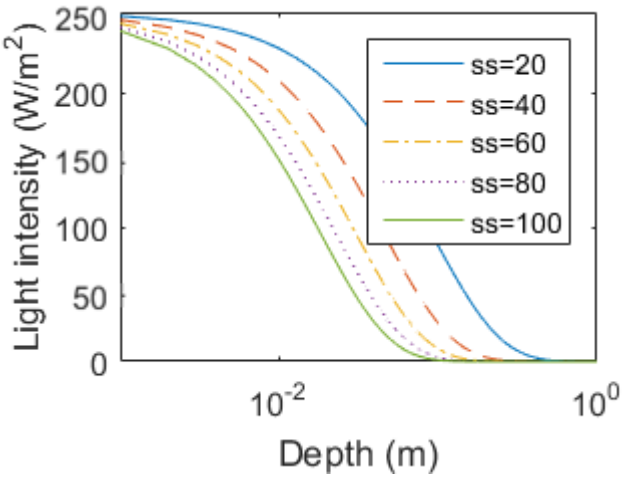

Figure 6.4: Attenuation of light with depth for for a range of suspended sediment (ss) concentrations (mg/l), where $I = 260$ W/m^2 and k_e was calculated using Equation 2.37

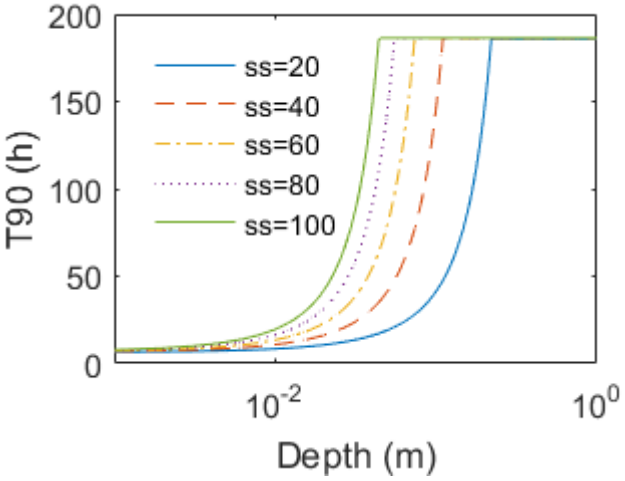

Figure 6.5: Effect of light attenuation on change in T_{90} value with depth for for a range of suspended sediment (ss) concentrations (mg/l), using the Stapleton et al. [2007a] decay function, where $I = 260$ W/m^2 and k_e was calculated using Equation 2.37

6.2 Schematisation of light attenuation

White et al. [2014] observed an increase in suspended sediment concentration with depth in Swansea Bay; 10 mg/l to 15 mg/l recorded at the surface and 50 mg/l to 100 mg/l at depth, though no further information was given. This relationship can be explained through the action of particle settling and bed shear causing localised disturbances. Figure 6.4 demonstrates both the attenuation of light with depth and the positive correlation between turbidity and the degree of attenuation. It is therefore suggested that where a turbidity profile is present, the equation for light attenuation should be adjusted to account for the relationship with depth.

Based on Equation 2.37 and assuming linear relationship with depth, this is written as:

$$k_e = 0.55(ss_0 + f(z)) \tag{6.1}$$

where is the ss_0 is the suspended sediment concentration at the surface, (mg/l), z is the depth below the surface (m), k_e is the light attenuation coefficient and $f(z)$ is a function representing the relationship between suspended sediment concentration and depth.

For implementation in a 2D model, assuming a linear relationship between suspended sediment concentration and depth, the depth-averaged light extinction coefficient is calculated using the mean value theorem for integrals and written as:

$$\overline{k_e} = 0.55ss_0 + 0.275mh \tag{6.2}$$

where h is the depth of water and m is the suspended sediment-depth gradient (mg/l/m). This yields the same value of k_e as if Equation 2.37 and the depth-average sediment concentration were used in the first instance. However, if measurements show the suspended sediment profile to vary non-linearly with

depth then this may prove beneficial in creating a pseudo-3D sediment model, with applications in 2D and 3D models, reducing time and computational resource requirements.

6.3 Methodology

6.3.1 Spatial assessment

E.coli concentration data was recorded throughout the 2011 bathing season at 30 minute intervals from 07:00 to 16:00, at the Swansea Bay DSP [Aberystwyth University and University College Dublin, 2018]. Sample locations are shown in Figure 6.6 (a), while Figure 6.6 (b) shows the nearest mesh nodes used for analysis. Based on the findings discussed in Chapter 5, in order to account for spatial variability in model predictions, these have been further reduced to three points along the transect; at the high (H), mid (M), and low (L) tide extents, as shown in Figure 6.6 (c).

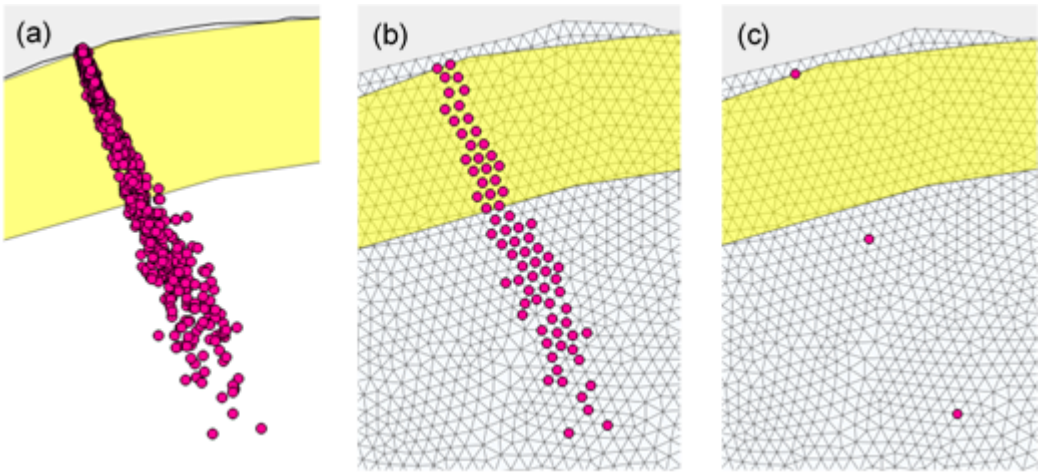

Figure 6.6: FIO sampling locations throughout the 2011 bathing season (a) [Aberystwyth University and University College Dublin, 2018], and the respective 2D mesh nodes and assessment points; (b) and (c)

In addition, Swansea Bay has been divided into 5 compliance / bathing zones in order to determine the cross-shore variability in bathing water quality and

identify regions of higher concentration which if swum in will increase the risk of bathers falling ill. These have been further divided into high, mid, and low extents, as with the DSP, which is located in Zone 4 (see Figure 6.7).

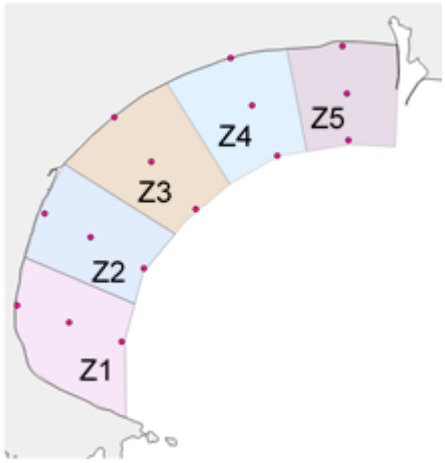

Figure 6.7: Swansea Bay compliance / bathing zones 1 to 5 (Z1 to Z5) and their respective analysis points (pink dots)

6.3.2 Predictive performance

An effective method for evaluating the performance of a predictive model is the use of a contingency table (see Table 6.1), which compares a predicted value with a pre-defined threshold (such as the rBWD limits) [Bedri et al., 2016; Bennett et al., 2013; García-Alba et al., 2018]. In relation to bathing water quality, this can be used to advise on management practices and health risks [Bedri et al., 2016].

Performance metrics which are derived from this table and are used herein to quantify model performance are defined in Table 6.2, on which further information is given by Bennett et al. [2013].

Table 6.1: Contingency table [Bedri et al., 2016; Bennett et al., 2013]

		Measured > Threshold		
		Yes	No	
Predicted > Threshold	Yes	True Positive (TP)	False Positive (FP)	Predicted Yes
	No	False Negative (FN)	True Negative (TN)	Predicted No
		Measured Yes	Measured No	Total

Table 6.2: Performance metrics derived from Table 6.1 [Bedri et al., 2016; Bennett et al., 2013]

Metric	**Formula**	**Range**	**Ideal value**
Accuracy	$\frac{TP+TN}{Total}$	0 - 1	1
Bias score	$\frac{TP+FP}{TP+FN}$	0 - ∞	1
Hit rate	$\frac{TP}{TP+FN}$	0 - 1	1
False alarm rate	$\frac{FP}{FP+TN}$	0 - 1	0
Success index	$\frac{1}{2}\left(\frac{TP}{TP+FN}+\frac{TN}{Total}\right)$	0 - 1	1
Threat score	$\frac{TP}{TP+FN+FP}$	0 - 1	1

6.4 Results and Discussion

6.4.1 Swansea Bay DSP

Model predictions of the *E.coli* concentration at the Swansea Bay DSP throughout the bathing season are shown in Figures 6.8 and 6.9. In each plot, the modelled lines represent predictions at the mesh nodes shown in Figure 6.6 (b).

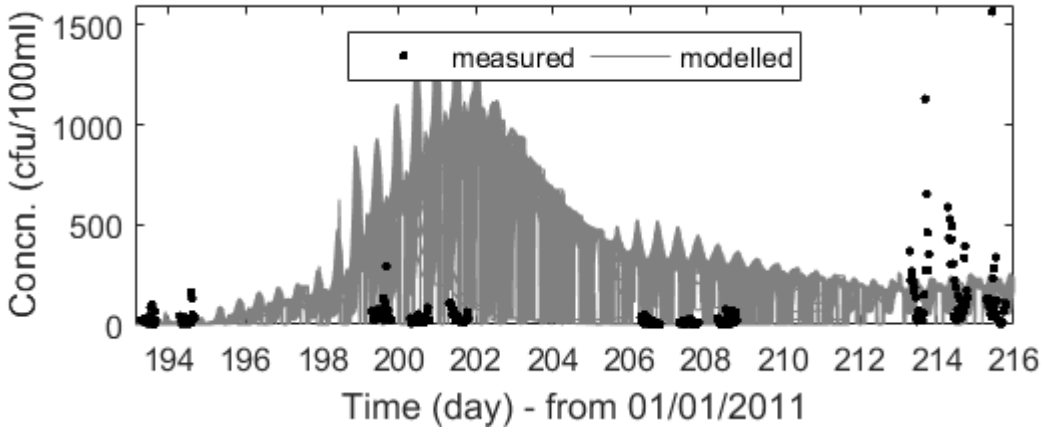

Figure 6.8: Comparison between the measured and predicted *E.coli* concentrations at all mesh nodes along the Swansea Bay DSP from 12th July to 4th August 2011

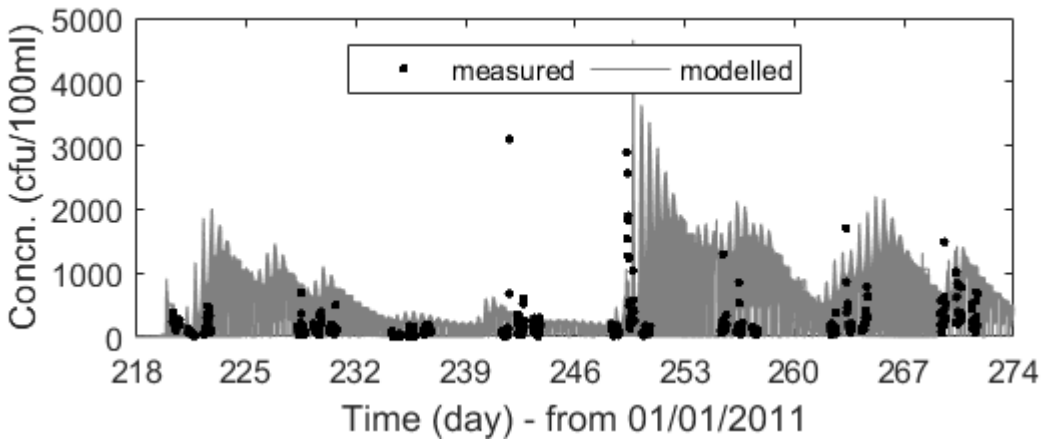

Figure 6.9: Comparison between the measured and predicted *E.coli* concentrations at all mesh nodes along the Swansea Bay DSP from 5th August to 30th September 2011

It can be seen that there is significant variability in the predicted *E.coli* concentration between nodes which makes model performance unclear. Therefore, to aid comparison with the measured data, Figures 6.10 and 6.11 present predictions given at the same time as the sample data. The performance metrics, calculated using the rBWD 'excellent' limit (250 cfu/100 ml), are shown in Table 6.3, while the contingency table values are given in Appendix B.2, Tables 16 and 17.

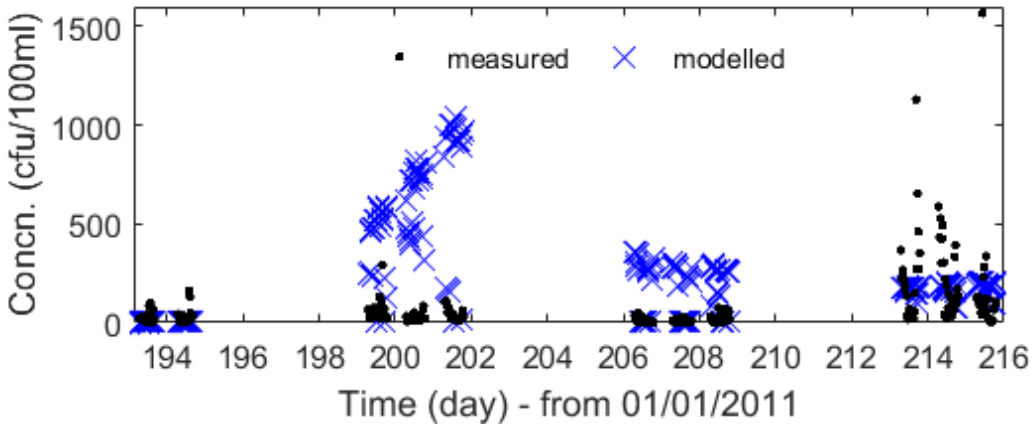

Figure 6.10: Comparison between the measured and predicted *E.coli* concentrations at the Swansea Bay DSP from 12th July to 4th August 2011

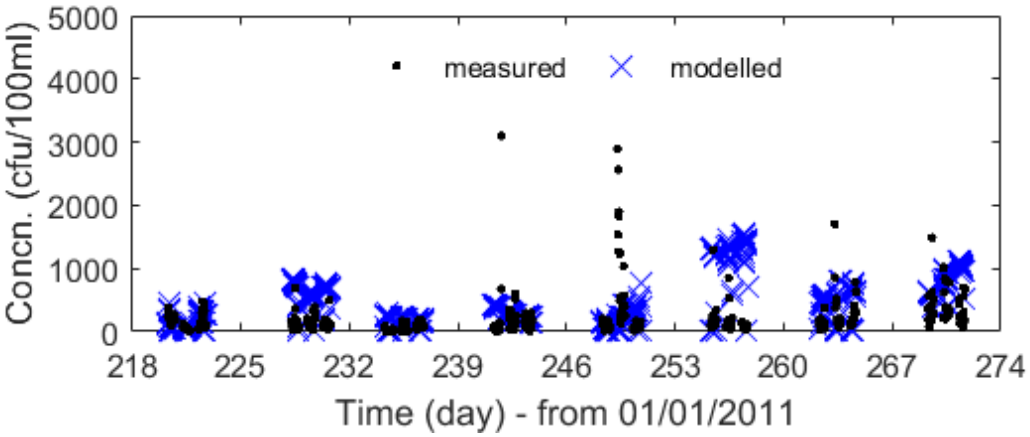

Figure 6.11: Comparison between the measured and predicted *E.coli* concentrations at the Swansea Bay DSP from 5th August to 30th September 2011

Similarly, having acknowledged that there is spatial variability in predictions along the DSP transect, such that modelled concentrations do not always spatially or temporally align with measured values (see Chapter 5), Figures 6.12 and 6.13 present predictions taken at the wet mesh node closest in magnitude to the sample data (herein called the Minimum Magnitude method), which is expected to improve the performance metrics. The performance metrics, calculated using the rBWD 'excellent' limit, are shown in Table 6.3, while the contingency table values are given in Appendix B.2, Tables 18 and 19.

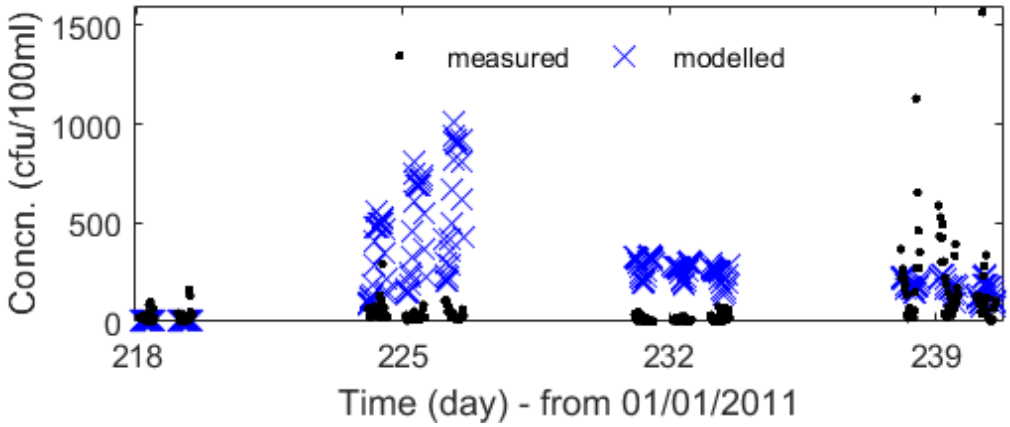

Figure 6.12: Comparison between the measured and predicted *E.coli* concentrations closest in magnitude to the sampled data at the Swansea Bay DSP, from 12th July to 4th August 2011, using a threshold depth of 0.05 m

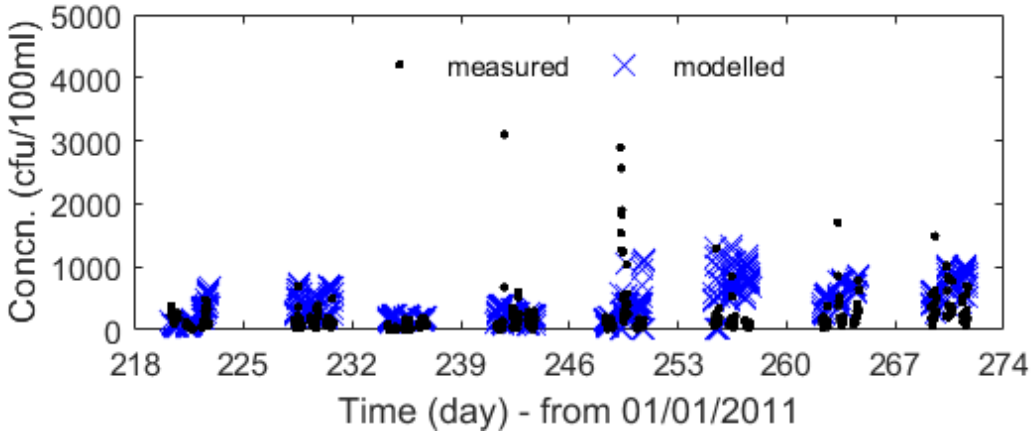

Figure 6.13: Comparison between the measured and predicted *E.coli* concentrations closest in magnitude to the sampled data at the Swansea Bay DSP, from 5th August to 30th September 2011, using a threshold depth of 0.05 m

Table 6.3: Performance metrics for Figures 6.10, 6.11, 6.12 and 6.13, calculated using the rBWD 'excellent' limit

Date / Metric	**12th Jul to 4th Aug**		**5th Aug to 30th Sept**	
	Figure 6.10	**Figure 6.12**	**Figure 6.11**	**Figure 6.13**
Accuracy	0.6	0.5	0.5	0.6
Bias score	4.6	4.8	2.8	2.8
Hit rate	0.0	0.0	0.6	0.9
False alarm rate	0.4	0.4	0.5	0.5
Success index	0.3	0.3	0.5	0.7
Threat score	0.0	0.0	0.2	0.3

As shown in Table 6.3, the middling accuracy and false alarm rate scores for all runs suggest that model performance is generally poor, with equal probability of correctly, or incorrectly, predicting exceedance events. This is confirmed by the low threat score in all cases. A hit rate of 0 for the model run from July to August, compared to 0.6 and 0.9 for that from August to September, confirms that the latter demonstrates better predictive performance. This is also confirmed by the larger success index values. A bias score greater than 1 indicates that the models have a tendency to overestimate event magnitude.

It can be seen from Figures 6.10 and 6.12, and Table 6.3, that in the model run from July to August, contrary to the hypothesis, using the Minimum Magnitude method of analysis caused a reduction in the accuracy value. It is suggested that this was due to the two methods sampling results at different mesh nodes, either side of the threshold depth of 0.05 m. This suggests that a higher mesh resolution would provide greater accuracy when predicting results to compare with samples where the position and time of collection are known. Model performance was improved for the period from August to September, suggesting that performance metrics are more reliable when calculated over a longer duration, or using an increased number of predictions. However, model performance remained poor. As the model input data was measured over this period, it confirms that the model was incapable of correctly simulating all processes which determine the *E.coli* concentration over this period

It is suggested that poor model performance may be due to limitations of the

Stapleton et al. [2007a] decay equation. As shown in Figures 6.1 and 6.2, the light intensity is often greater than the upper limit of 260 W/m^2 (see Section 5.3.1). Therefore, the model is incapable of correctly predicting *E.coli* decay at at light intensities greater than 260 W/m^2, leading to an under prediction of decay rates and an over prediction of bacterial levels. This is confirmed by the greater hit rate and lower threat score of the model run from August to September; the input light intensity time series contained lower peak values than from July to August (see Figures 6.1 and 6.2), thus the model under predicted bacterial decay by a lesser extent.

In addition, it may be the case that poor model performance when tested on data from 2011 is that the data from 2012 used for model calibration was not suitably representative of conditions in 2011.

In order to assess the model performance at a higher temporal resolution, Figures 6.14, 6.15 and 6.16 present the predicted *E.coli* concentration versus the measured concentration at the Swansea Bay DSP over periods of three consecutive days. Results are shown at three fixed locations along the transect, as shown in Figure 6.6 (c). The elevations of each point; H, M and L, are; 3.85 m, -3.22 m and -5.0 m, respectively (relative to Ordnance Datum). Plots of the predicted *E.coli* concentration at the nearest mesh node at the time of sampling for the same time periods are shown in Figures 6.17, 6.18 and 6.19.

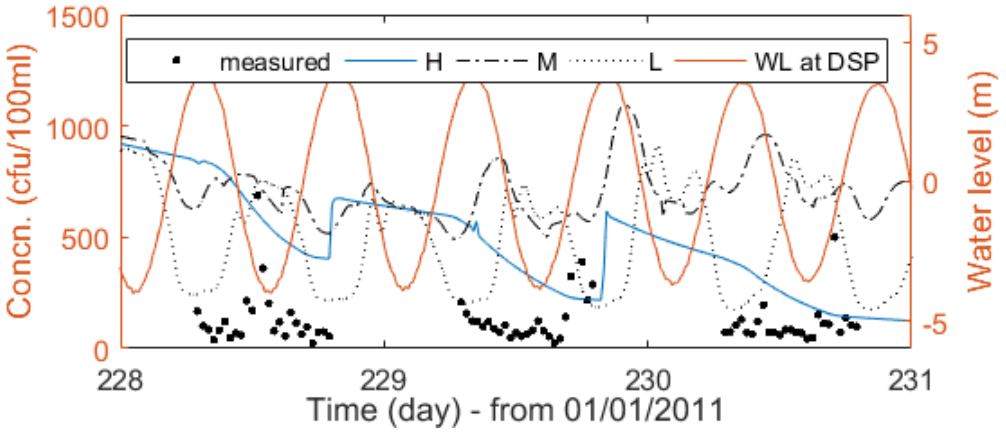

Figure 6.14: Comparison between the measured and predicted *E.coli* concentrations along the Swansea Bay DSP transect at the; high (H), mid (M) and low (L) sampling locations, with respect to water level

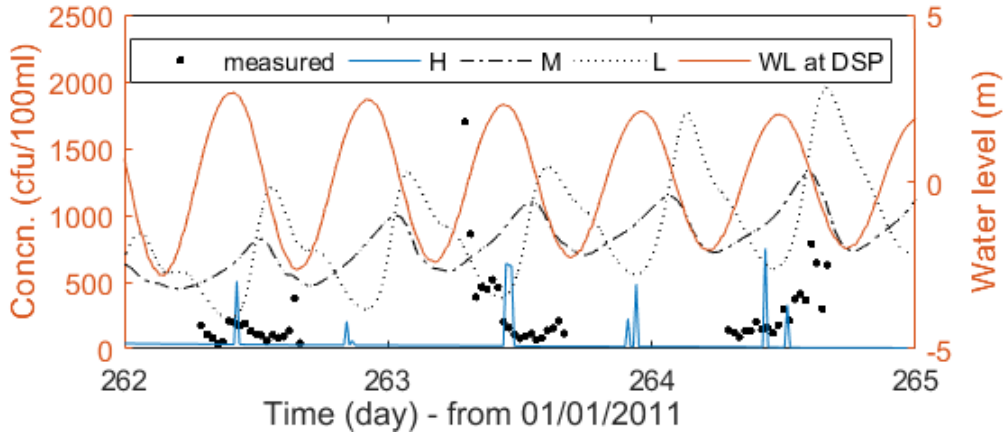

Figure 6.15: Comparison between the measured and predicted *E.coli* concentrations along the Swansea Bay DSP transect at the; high (H), mid (M) and low (L) sampling locations, with respect to water level

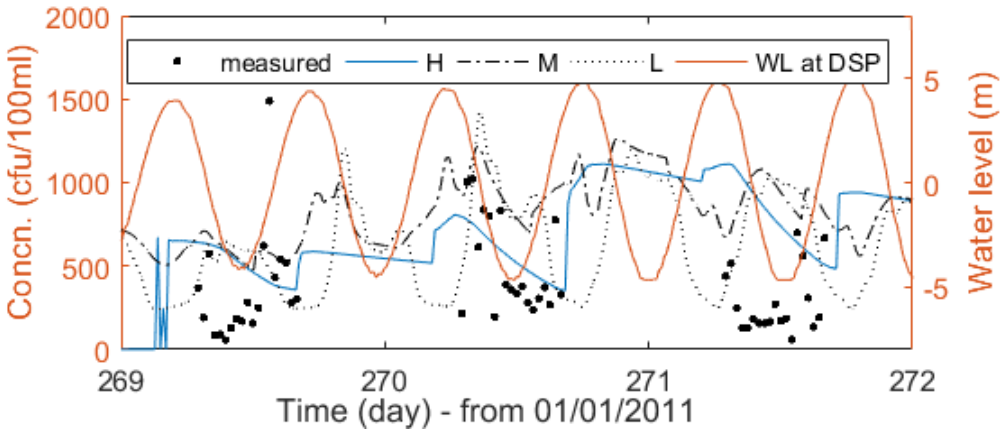

Figure 6.16: Comparison between the measured and predicted *E.coli* concentrations along the Swansea Bay DSP transect at the; high (H), mid (M) and low (L) sampling locations, with respect to water level

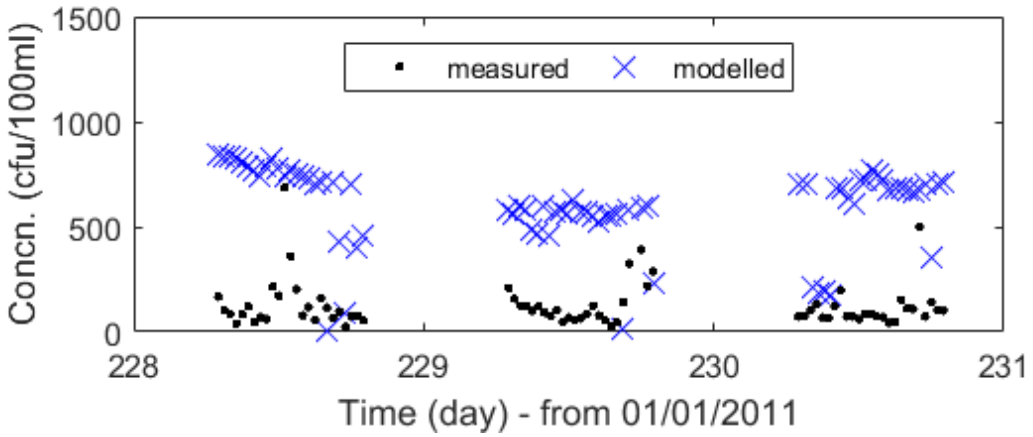

Figure 6.17: Comparison between the measured and predicted *E.coli* concentrations at the Swansea Bay DSP

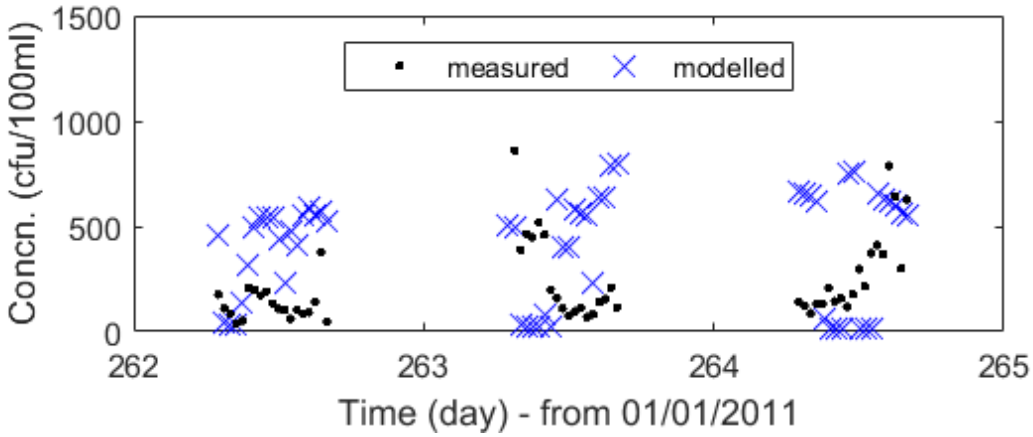

Figure 6.18: Comparison between the measured and predicted *E.coli* concentrations at the Swansea Bay DSP

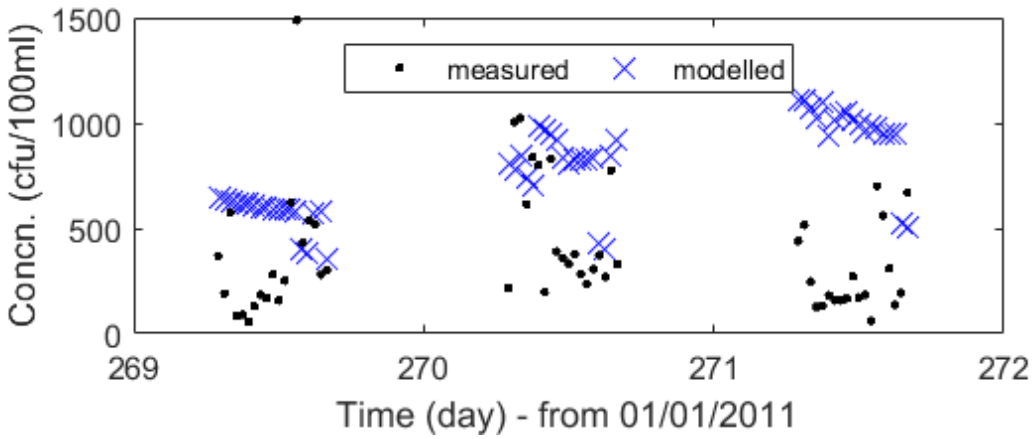

Figure 6.19: Comparison between the measured and predicted *E.coli* concentrations at the Swansea Bay DSP

It can be seen from Figures 6.14 to 6.19 that while the model is capable of predicting *E.coli* concentrations of a similar magnitude to the measured data, there is a high degree of sub-daily temporal variability that is not predicted by the model. It can also be seen that at the low tide sampling point, the predicted *E.coli* concentration is strongly linked to the tidal cycle, with a greater range of predicted values, and elevated concentrations predicted during low tide. Similarly, concentrations at the mid-tide point are elevated during the mid-tide phase, confirming the cyclic convection of a pollutant plume over the tidal cycle, as discussed in Chapter 5. However, the range of predicted concentration values is smaller than at the low tide point, and the concentration is predominantly greater, both of which are due to the inshore advection of pollutants of the flood tide.

It should be noted that the predicted concentrations plotted at the high tide sampling location are misleading. The bed elevation at this point is 3.86 m (reative to MSL), thus below this value the beach is dry. As discussed in Chapter 5, the prediction of non-zero concentration values when this occurs is due to TELEMAC permitting depth values above 0 m, resulting in the prediction of small depths of stagnant water. The bed elevation at the mid and low tide locations are -3.22 m and -5.08 m, respectively, and therefore, this issue is minimised.

Having established the relationship between the predicted concentration and

tidal phase, in order to investigate the model sensitivity the other influential parameters, Figures 6.20 to 6.22 present the predicted concentration with respect to the following model inputs; River Tawe flow rate, River Tawe bacterial concentration, and light intensity. Of the three time periods shown in Figures 6.14 to 6.19, the 25th to 29th September is shown as both the measured and predicted *E.coli* concentrations exhibit a greater degree of variability.

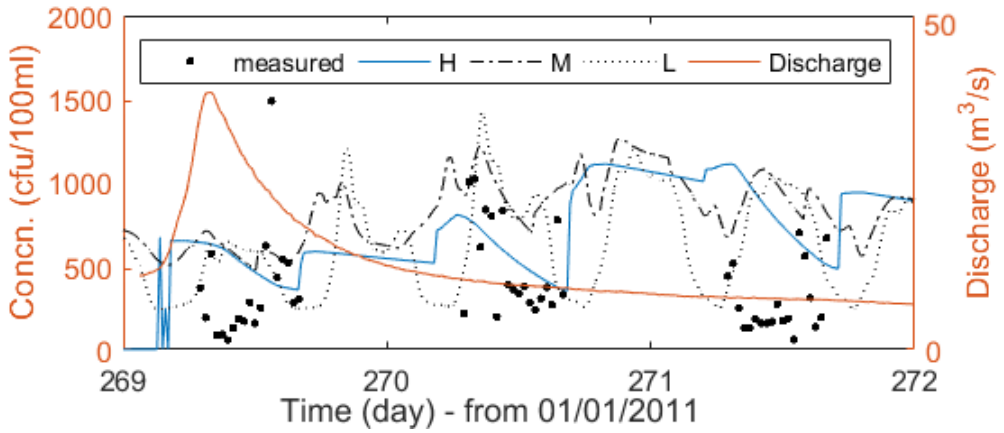

Figure 6.20: Comparison between the measured and predicted *E.coli* concentrations along the Swansea Bay DSP transect at the; high (H), mid (M) and low (L) sampling locations, with respect to the River Tawe discharge

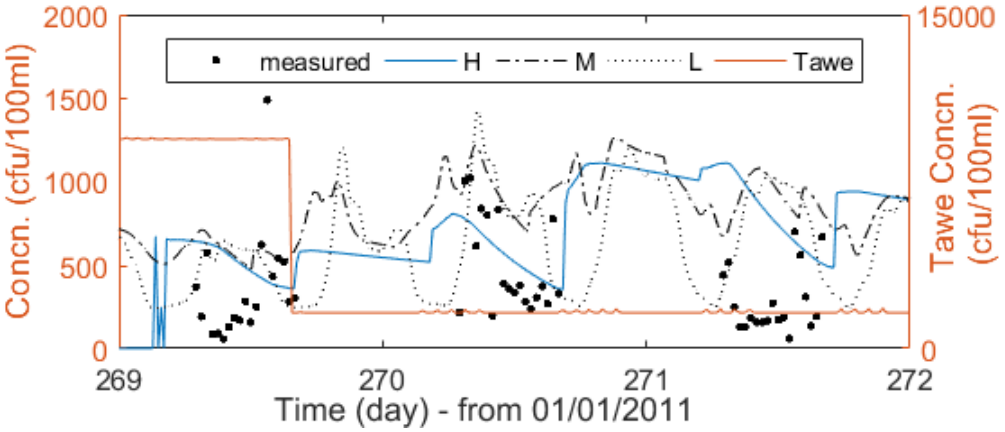

Figure 6.21: Comparison between the measured and predicted *E.coli* concentrations along the Swansea Bay DSP transect at the; high (H), mid (M) and low (L) sampling locations, with respect to the River Tawe *E.coli* concentration

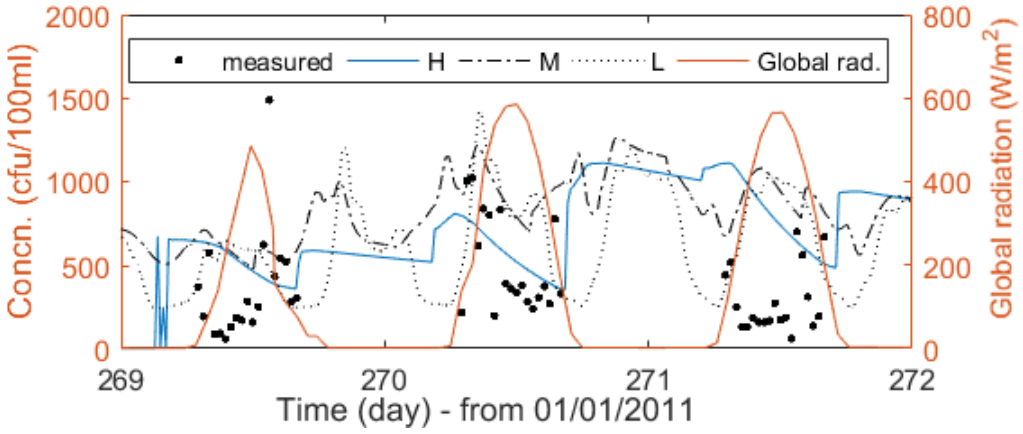

Figure 6.22: Comparison between the measured and predicted *E.coli* concentrations along the Swansea Bay DSP transect at the; high (H), mid (M) and low (L) sampling locations, with respect to input light intensity

Figures 6.20 and 6.21 present the measured discharge and bacterial concentration in the River Tawe used as model inputs. It can be seen that the elevated inflow discharge and bacterial concentration on day 269 results in an increase in the predicted *E.coli* concentration at the DSP. However, due to the difference in temporal scales that determine the riverine regime and sub-daily bacterial decay, there is no high-resolution temporal correlation between the two.

It can be seen in Figure 6.22 that over the period observed, the light intensity varies throughout the day in a saw tooth / sinusoidal manner, with peak values of between 500 W/m^2 and 600 W/m^2 at midday. However, while the measured data exhibits a trend of low bacterial concentrations around midday, the model predictions do not. It is proposed that this is due to the insensitivity of the model to light intensities greater that 260 W/m^2, such that the peak daily decay rate was not reached over the observed period, and the tidal influence was therefore dominant.

In addition, it can be seen from Figures 6.14 to 6.16, and Figure 6.22 that there are significant hourly variations in the measured bacterial concentrations that do not correlate with variations in light intensity. It is therefore suggested that while light intensity is known to be strongly linked to bacterial decay, there may be other processes within Swansea Bay which are also responsible for the observed

hourly variations in bacterial concentration. Since these have been excluded from the model, this may be partly responsible for the poor model performance.

These may include; turbidity, wave attenuation and surf zone processes, and wind effects. It is suggested that these may impact bacterial levels as follows. Wave attenuation processes cause an increase in bed sediment disturbances, resulting in increased sediment levels within the surf zone. The increase in turbidity and the subsequent attenuation of radiation may be a contributing factor in causing fluctuations in bacterial concentration not accounted for in the model. Furthermore, the disturbance of bed sediments may act as a bacterial source, locally increasing and causing temporal and spatial fluctuations in concentration [Yang, 2005]. Increased surface shear induced by wind may also have an influence in shallow water, inducing greater flow velocities and causing increased dispersion [Bedri et al., 2011; Moulinec et al., 2011].

Rainfall and wave measurements are indicative of the prevailing meteorological conditions and enable better interrogation of model results to highlight processes and inputs not captured. However, such data was not available over the observed period and this was therefore not possible.

6.4.2 Beach Zone Compliance

Table 6.4 presents a comparison between the number of predicted exceedance events at each of the locations in the compliance zones shown in Figure 6.7. Events were calculated using the rBWD 'excellent' limit when the water depth at each location exceeded a threshold depth of 0.05 m. Therefore, points were not sampled when the beach was 'dry'.

Table 6.4: (a) Predicted number of rBWD exceedance events between the 5th August and 30th September at each compliance location in Swansea Bay; (b) percentage of time during which the rWBD 'excellent' limit is exceeded at each location

(a)

	Z1	**Z2**	**Z3**	**Z4**	**Z5**
H	259	1012	239	184	1036
M	1776	2044	2363	3495	4747
L	2052	2430	2970	3865	3722

(b)

	Z1	**Z2**	**Z3**	**Z4**	**Z5**
H	63	72	72	77	95
M	51	67	67	72	90
L	37	44	51	67	93

It can be seen from Table 6.4 (b) that the percentage of time during which the rBWD 'excellent' limit is exceeded progressively increases from Zone 1 to Zone 5. This is due to the impact of the River Tawe on the bacterial concentration at the DSP (which is situated in Zone 4), as discussed on Chapter 5. At the high tide sampling location, the predicted percentage of exceedances in Zones 1 and 5 are lower and higher than average, respectively, while values are similar in Zones 2 to 4. This indicates that at high tide, the DSP is representative of Zones 2 to 3. However, while DSP samples may show acceptable bacterial levels, samples taken in Zone 5 may not. Conversely, while DSP samples may show unacceptable bacterial levels, samples taken in Zone 1 may not.

In all zones, the percentage of time during which the rBWD limit is exceeded is reduced with distance offshore. This is due to the offshore transport and increased dilution of pollutants on the ebb tide [Feng et al., 2015].

At the low tide sampling location, the DSP is not representative of any zones as the predicted percentage of exceedances progressively increases from Zone 1 to Zone 5, and lower at all locations during low tide. This suggests that the risk of bathers falling ill is reduced from Zone 5 to Zone 1, confirming that a flexible approach may be taken to beach management via the designation of safe and unsafe zones based on water quality.

6.5 Summary and conclusions

In this chapter, the hydro-environmental model of Swansea Bay developed in Chapter 5 (the 2D model with improved source representation, using the Stapleton et al. [2007a] decay function), was applied to predict *E.coli* concentrations throughout the 2011 bathing season, using measured light intensity and bacterial inputs. Model performance was assessed using the contingency table and performance metrics method.

It was found that despite the good model performance shown in Chapter 5, the model was incapable of predicting hourly variations in *E.coli* concentration, as seen in the sampled data, and for the majority of the simulation, over-predicted concentrations. It is proposed that the inclusion of sediment, wave, and wind processes in the nearshore zone will better capture these fluctuations.

Furthermore, it is suggested that the over prediction of bacterial concentrations was due to the under prediction of bacterial decay rates, as a result of the upper limit placed on light intensity, defined in the Stapleton et al. [2007a] equation. As such, the model exhibited greater sensitivity to the tidal phase.

The spatial variability in *E.coli* concentrations within Swansea Bay was investigated by dividing the bathing water into five compliance zones. It was shown that the dominant advective process governing bacterial transport is the cyclic motion of pollutants over the tidal cycle. This causes higher bacterial concentrations to be predicted during the high, and flood, tide, and vice versa on the low, and ebb tide.

Furthermore, there is notable cross-shore variability in *E.coli* concentration, which is greater during low tide, confirming an adaptive approach to beach management should be taken when designating safe and unsafe bathing zones.

Chapter 7

Conclusions and outlook

Summary and conclusions

This thesis has focused on studying the mechanisms which govern the fate and transport of pollutants in shallow waters, specifically, in estuarine and coastal environments. The work covered in Chapters 4 to 6 can be divided into two major topics; an experimental study of turbulent diffusion carried out at Tsinghua University, China, and a numerical study of *E.coli* transport and decay in Swansea Bay, UK.

The purpose of the investigation into turbulent diffusion was to develop current understanding of the mechanisms which govern pollutant transport in riverine and estuarine environments. The conclusions, discussed below, will assist in the prediction of floating pollutant transport, which facilitates the application of targeted mitigation measures.

Using a straight, shallow, flat bottom flume, a range of experiments were carried out in which the bed roughness and flow rate were varied. The position of a group of floating PVC particles was tracked from release, using a PTV system installed vertically above the flume. By calculating the change in particle group variance over time it was possible to calculate the dimensional and non-dimensional coefficients of turbulent diffusion for each set of flow conditions. In addition, a numerical study was carried out using TELEMAC-2D to cross-validate the experimental results. Based on the outcomes of both the experimental and numerical studies, the following conclusions were made:

- It was observed experientially that increased bed roughness is positively correlated with particle group dispersion. This phenomenon was also replicated by the TELEMAC-2D model, confirming the importance of including spatially variable bed roughness values in numerical models, where applicable.

- It was shown that the levels of turbulent kinetic energy within the experimental flow regimes were positively correlated with the dispersion of floating particles. This may assist in estimating pollutant transport along rivers in data sparse regions, if turbulence measurements can be taken.

- It was also found that turbulent diffusion is positively correlated with the aspect ratio of a flow, due to the action of secondary currents. However, it was not possible to replicate this in TELEAMC-2D. It is therefore suggested that when using a 2D model to predict pollutant transport in riverine environments, the turbulence model should be modified to account for the effect of secondary currents on lateral diffusion.

The study of Swansea Bay investigated a variety of methods commonly used in the numerical simulation of bacterial fate and transport at a high temporal resolution. The performance of the spatially and temporally variable bacterial decay models proposed by Mancini [1978] and Stapleton et al. [2007a] was tested in both 2D and 3D hydro-environmental models, using the open source TELEMAC software suite. In doing so, the use of hourly measured solar radiation data as a model input, to predict bacterial decay, was compared with the use of a simplified sinusoidal approximation of the observed daily variation in radiation intensity.

In addition, two new modelling techniques were developed within the TELEMAC solver, using MPI programming. To the knowledge of the author, this is the first research study to propose these methods, which are; a depth-varying bacterial decay model, for application in a 3D hydraulic model, and the implementation of non-stationary beach source points in a 2D model.

Having established the most suitable approach for modelling Swansea Bay, the preferred method was applied in a detailed bathing water assessment of the 2011 bathing season. This enabled an assessment of the revised Bathing Waters Di-

rective (rBWD) monitoring procedure to determine whether a single Designated Sampling Point (DSP) is representative of the whole bathing water.

The main conclusions from this body of work are summarised as follows:

- In a study of the 2012 bathing season, the bacterial decay model proposed by Stapleton et al. [2007a] was found to better predict the concentration of *E.coli* in Swansea Bay than the model proposed by Mancini [1978]. This was due to the prediction of lower night time decay rates when using the former.

- There has been a degree of uncertainty regarding the predicted decay values, whether they were erroneous and if the Stapleton et al. [2007a] model was representative the bacterial processes within Swansea Bay. If true then the apparent accuracy of the [Stapleton et al., 2007a] model, when applied to the 2012 bathing season, could have been due to the under prediction of night time decay rates. If lower night time decay rates are applied, this could result in similar concentration predictions to those calculated when using the [Mancini, 1978] model.

- In this case, the under prediction of bacterial concentrations when using the Mancini [1978] model could have been due to the exclusion of wind effects, surf zone and sediment processes. The exlusion of these processes may have also contributed to the poor performance of the Stapleton et al. [2007a] model when applied to the 2011 bathing season.

- The decay model proposed by Mancini [1978] was found to be particularly sensitive to water depth and predicted reduced bacterial concentrations in shallow regions. This resulted in the prediction of a different spatial concentration distribution of *E.coli* to that predicted using the Stapleton et al. [2007a] model, which was found to be less sensitive to changes in water depth and had reduced sensitivity to changes in light intensity. This was due to the rapid attenuation of light in the water column caused by the high turbidity levels in Swansea Bay, and an upper limit on the range of light intensity values over which the equation is applicable. This limit was often

exceeded in the input data series and as a result, predicted concentrations were primarily influenced by the tidal cycle.

- It was found that the 2D model predicted greater bacterial concentrations at the Swansea Bay and Aberafan DSPs than the 3D model. This was due to the inclusion of the Rivers Tawe and Neath as point inputs with no flow velocity in the latter, causing reduced advection, whereas the rivers were modelled to their tidal limit in the former. This confirms the importance of ensuring momentum conservation at non-static source boundaries.

- The newly developed, 3D depth variable decay model predicted lower bacterial concentrations than a depth-averaged decay model. This was due to the exponential decrease in bacterial decay with depth inducing a concentration distribution throughout the water column, thereby increasing diffusion from regions of high to low concentration. This approach is recommended as being a more realistic representation of bacterial processes and it is suggested that it should be used in 3D modelling studies.

- Using a sinusoidal approximation of the daily variation light intensity (with a peak value taken as the average of the measured peak daily intensity), is suitable in 2D and 3D modelling studies when a depth-averaged decay model is applied. In these cases, no difference was observed in the predicted bacterial concentration to those predicted when using hourly measured radiation data as a model input. However, it was found that when using a 3D depth variable decay rate, the model was sensitive to higher temporal resolution irradiance inputs and therefore, these should be used if possible.

- It was found that using the newly developed method of representing beach sources as non-stationary inputs improves predictions of bacterial concentrations in the nearshore zone and is a viable alternative to high spatial resolution modelling of source tracks in this region.

- The final outcome of this study was the confirmation of significant spatial and temporal variability in the predicted bacterial concentrations in Swansea Bay. Greater bacterial concentrations in proximity to the waterline were predicted during high tide, and vice versa at low tide. Greater

variance in the predicted bacterial concentration was also observed offshore, compared to reduced variance in proximity to the high tide line. Therefore, the sampled bacterial concentration may be related to the time of measurement during rBWD monitoring.

- Furthermore, due to the location of the River Tawe in the north-east of Swansea Bay bathing water, bacterial concentrations are predicted to reduce with distance from the river mouth. It is therefore proposed that an adaptive approach should be taken when designating safe bathing zones as the risk of bathers falling ill is reduced in the southern end of the bathing water and during low tide.

Recommendations for operation and future work

Based on the outcomes of the research presented in this thesis, it is apparent that further work is required to develop deterministic models capable of predicting sub-daily temporal variations in bacterial concentration suitable for practical applications.

However, the following conclusions can be drawn which enable researchers, engineers and beach mangers to apply this research in the operation of Swansea Bay and other bathing waters:

- In the case of large beaches such as Swansea Bay, bacterial levels and water quality can vary significantly along their length. Therefore, the classification of bathing waters based on sampling at a single point should be reassessed.

- In 3D modelling studies, a depth variable decay rate should be applied to better reflect the effect of light attenuation on bacterial decay. In 2D studies, artificially increased bacterial decay rates may be required to compensate for this.

- Where applicable, source momentum must be included and conserved as omission can lead to the under prediction of bacterial concentrations.

- Modellers should consider the use of spatially variable beach sources when studying shallow gradient beaches in macro-tidal environments. If found to be too computationally intensive then sensitivity analysis should be carried out to determine the impact of opting to use a simplified stationary source approach.

- The decay equation proposed by Mancini [1978] has limitations when studying turbid, shallow depth intertidal habitats due to the dependence of the equation on water depth. This can lead to over prediction of decay rates and sensitivity analysis should therefore be carried out to determine its suitability.

- The use of a sinusoidal function to represent daily variations in light intensity in hydro-bacterial models is a suitable simplification when data is unknown at a higher resolution than the maximum daily intensity.

The following recommendations have been made to indicate topics which, in the opinion of the author, are promising lines of study. Had more time been available, these would have been pursued. They will also address many of the assumptions and limitations previously described.

- Given the well mixed nature of Swansea Bay, this study has assumed a constant suspended sediment profile throughout the water column. However, in regions where sediment concentration profiles exist, such as estuarine environments, it may be of interest for future studies to develop an equation for light attenuation (and by proxy, bacterial decay) based on this profile. This will enable more accurate calculation of depth variable or depth-averaged decay rates, reducing time and computational requirements that would otherwise be spent developing and calibrating a sediment model.

- The development of a numerical source apportionment model would enable the immediate and accurate identification of the primary pollution sources at a specific location. For example, in environments such as Swansea Bay, where diffuse agricultural pollution is mixed with combined sewer overflow discharges and those from a long sea outfall. This would also enable the use

of more specific bacterial inputs, such as the type of animal in catchments which support multiple species of livestock, facilitating targeted pollution identification, and control measures.

- The degree to which sediment-bacteria interactions affect bacterial levels is currently not very clear and it is therefore of interest to investigate this further. This includes the representation of beach sand as a bacterial source. It is suggested that these processes, combined with surf and wind effects, may be responsible for the high degree of temporal variation in bacterial concentrations observed within a day, currently not captured by the numerical model developed herein. Accurate prediction of these variations may lead to the use of a real-time deterministic model to advise the public of bathing conditions, in accordance with the rBWD.

- A detailed statistical analysis of measured bacterial data in Swansea Bay, in addition to other influential variables such as; rainfall, river flows, temperature, salinity, turbidity, wind and wave conditions, may better inform on the covariance between parameters and indicate processes which are under represented in the current model schematisation.

- Similar laboratory experiments to the particle tracking study described, however, using a dissolved tracer, would enable the calculation of the non-dimensional turbulent diffusion coefficient to greater accuracy, and provide a good measure for validating the results presented herein. In addition this would enable the study of the longitudinal dispersion coefficient under similar conditions.

- Such a study would also facilitate in the development of an empirical equation to describe the relationship between the aspect ratio of a flow and the non-dimensional turbulent diffusion coefficient.

Appendices

A Experimental and numerical model study of turbulent diffusion for steady flow conditions

Table 1: Series 1 (a) and 2 (b) Average non-dimensional coefficients of turbulent diffusion as shown in Figure 4.13

(a)

Q	ϵ	ϵ_x	ϵ_y
0.06	0.328	0.431	0.226
0.07	0.418	0.256	0.580
0.08	0.260	0.220	0.300
0.09	0.244	0.436	0.051

(b)

Q	ϵ	ϵ_x	ϵ_y
0.06	0.347	0.510	0.184
0.07	0.273	0.409	0.137
0.08	0.161	0.157	0.164
0.09	0.104	0.107	0.102

Table 2: Series 3 (a) and 4 (b) Average non-dimensional coefficients of turbulent diffusion as shown in Figure 4.25

(a)

Q	ϵ	ϵ_x	ϵ_y
0.04	0.121	0.086	0.113
0.06	0.224	0.194	0.255
0.08	0.154	0.178	0.100
0.10	0.132	0.145	0.118

(b)

Q	ϵ	ϵ_x	ϵ_y
0.04	0.165	0.213	0.117
0.06	0.171	0.247	0.094
0.08	0.095	0.070	0.121
0.10	0.141	0.137	0.125

Table 3: Series 1 ADV turbulence measurements; (a) turbulence intensity (b) turbulent kinetic energy

(a)

Q	**TI**	**TIx**	**TIy**	**TIz**
0.06	0.610	0.100	2.238	2.378
0.07	0.637	0.092	2.074	3.259
0.08	0.710	0.100	2.447	4.962
0.09	0.738	0.100	2.106	3.355

(b)

TKE	**TKEx**	**TKEy**	**TKEz**
8.9E-04	3.1E-04	9.4E-05	4.9E-04
6.4E-04	2.1E-04	9.9E-05	3.3E-04
6.3E-04	1.9E-04	6.8E-05	3.7E-04
4.2E-04	1.5E-04	6.5E-05	2.1E-04

Table 4: Series 2 ADV turbulence measurements; (a) turbulence intensity (b) turbulent kinetic energy

(a)

Q	**TI**	**TIx**	**TIy**	**TIz**
0.06	0.666	0.134	2.133	3.276
0.07	0.774	0.146	1.778	2.931
0.08	0.746	0.138	3.666	2.798
0.09	0.723	0.101	1.999	3.994

(b)

TKE	**TKEx**	**TKEy**	**TKEz**
1.4E-03	5.9E-04	1.6E-04	6.1E-04
1.3E-03	5.0E-04	1.2E-04	6.8E-04
8.6E-04	4.0E-04	1.1E-04	3.5E-04
4.7E-04	1.7E-04	7.9E-05	2.2E-04

Table 5: Series 3 ADV turbulence measurements; (a) turbulence intensity (b) turbulent kinetic energy

(a)

Q	**TI**	**TIx**	**TIy**	**TIz**
0.04	1.411	0.131	2.900	2.167
0.06	0.928	0.130	1.601	5.190
0.08	0.819	0.120	2.056	3.001
0.10	0.643	0.125	1.896	4.529

(b)

TKE	**TKEx**	**TKEy**	**TKEz**
1.2E-03	7.9E-05	3.3E-05	1.1E-03
7.2E-04	1.8E-04	5.7E-05	4.8E-04
1.9E-03	2.9E-04	8.3E-05	1.5E-03
1.1E-03	4.9E-04	1.5E-04	4.3E-04

Table 6: Series 4 ADV turbulence measurements; (a) turbulence intensity (b) turbulent kinetic energy

(a)

Q	**TI**	**TIx**	**TIy**	**TIz**
0.04	1.037	0.109	1.360	5.010
0.06	0.826	0.117	1.569	3.454
0.08	0.682	0.107	1.820	3.197
0.10	0.607	0.111	1.501	2.318

(b)

TKE	**TKEx**	**TKEy**	**TKEz**
1.9E-04	5.9E-05	2.2E-05	1.1E-04
4.5E-04	1.7E-04	4.2E-05	2.4E-04
6.3E-04	2.5E-04	8.2E-05	3.1E-04
9.1E-04	4.0E-04	1.2E-04	3.9E-04

B Development of water quality model

B.1 Example Fortran code

Listing 1: Example Fortran code for the implementation of the Mancini [1978] decay equation in TELEMAC-2D

```
!                      *****************
                       SUBROUTINE DIFSOU
!                      *****************
!
     &(TEXP,TIMP,YASMI,TSCEXP,HPROP,TN,TETAT,NREJET,ISCE,
       DSCE,TSCE,
     & MAXSCE,MAXTRA,AT,DT,MASSOU,NTRAC,FAC,NSIPH,ENTSIP,
       SORSIP,
     & DSIP,TSIP,NBUSE,ENTBUS,SORBUS,DBUS,TBUS,NWEIRS,
       TYPSEUIL,
     & N_NGHB_W_NODES,NDGA1,NDGB1,TWEIRA,TWEIRB)
!
!***********************************************************
! TELEMAC2D   V7P2
!***********************************************************
!
!brief    PREPARES THE SOURCES TERMS IN THE DIFFUSION
   EQUATION
!+                FOR THE TRACER.
!
!warning  BEWARE OF NECESSARY COMPATIBILITIES FOR HPROP,
   WHICH
!+             SHOULD REMAIN UNCHANGED UNTIL THE
   COMPUTATION OF THE
!+             TRACER MASS IN CVDFTR
!
!previous history removed for brevity
!
```

```
!history  J KING (CU)
!+        2018
!+        V7P2
!+   Decay rate calculates based on Mancini (1978)
   equation
!
!~~~~~~~~~~~~~~~~~~~~~~~~~~~~~~~~~~~~~~~~~~~~~~~~~~~~~~~~~~~~
!| AT                |-->| TIME IN SECONDS
!| DBUS              |-->| DISCHARGE OF TUBES.
!| DSCE              |-->| DISCHARGE OF POINT SOURCES
!| DSIP              |-->| DISCHARGE OF CULVERT.
!| DT                |-->| TIME STEP
!| ENTBUS            |-->| INDICES OF ENTRY OF TUBES IN
   GLOBAL NUMBERING
!| ENTSIP            |-->| INDICES OF ENTRY OF PIPE IN GLOBAL
    NUMBERING
!| FAC               |-->| IN PARALLEL :
!|                   |   | 1/(NUMBER OF SUB-DOMAINS OF THE
   POINT)
!| HPROP             |-->| PROPAGATION DEPTH
!| ISCE              |-->| NEAREST POINTS OF DISCHARGES
!| MASSOU            |<--| MASS OF TRACER ADDED BY SOURCE
   TERM
!| MAXSCE            |-->| MAXIMUM NUMBER OF SOURCES
!| MAXTRA            |-->| MAXIMUM NUMBER OF TRACERS
!| NBUSE             |-->| NUMBER OF TUBES
!| NREJET            |-->| NUMBER OF POINT SOURCES.
!| NSIPH             |-->| NUMBER OF CULVERTS
!| NTRAC             |-->| NUMBER OF TRACERS
!| NWEIRS            |-->| NUMBER OF WEIRS
!| SORBUS            |-->| INDICES OF TUBES EXITS IN GLOBAL
   NUMBERING
!| SORSIP            |-->| INDICES OF PIPES EXITS IN GLOBAL
```

```
!   NUMBERING
!| TBUS              |-->| VALUES OF TRACERS AT TUBES
    EXTREMITY
!| TETAT             |-->| COEFFICIENT OF IMPLICITATION FOR
    TRACERS.
!| TEXP              |-->| EXPLICIT SOURCE TERM.
!| TIMP              |-->| IMPLICIT SOURCE TERM.
!| TN                |-->| TRACERS AT TIME N
!| TSCE              |-->| PRESCRIBED VALUES OF TRACERS AT
    POINT SOURCES
!| TSCEXP            |<--| EXPLICIT SOURCE TERM OF POINT
    SOURCES
!|                   |   | IN TRACER EQUATION, EQUAL TO:
!|                   |   | TSCE - ( 1 - TETAT ) TN
!| TSIP              |-->| VALUES OF TRACERS AT CULVERT
    EXTREMITY
!| TWEIRA            |-->| VALUES OF TRACERS ON SIDE A OF
    WEIR
!| TWEIRB            |-->| VALUES OF TRACERS ON SIDE B OF
    WEIR
!| TYPSEUIL          |-->| TYPE OF WEIRS (IF = 2, WEIRS
    TREATED AS SOURCES POINTS)
!| YASMI             |<--| IF YES, THERE ARE IMPLICIT SOURCE
    TERMS
!~~~~~~~~~~~~~~~~~~~~~~~~~~~~~~~~~~~~~~~~~~~~~~~~~~~~~~~~~~~~
!
      USE BIEF
      USE DECLARATIONS_TELEMAC
      USE INTERFACE_PARALLEL
      USE DECLARATIONS_TELEMAC2D, ONLY: LOITRAC, COEF1TRAC
          , QWA, QWB,
     &    MAXNPS,U,V,UNSV2D,V2DPAR,VOLU2D,T1,T2,T3,T4,T5,T6,
          T7,T8,T9,T10,
```

```
     &   T11, T12, MESH, MSK,
     &   IELMU, S, NPOIN, CF, H, SECCURRENTS, SEC_AS, SEC_DS, SEC_R
         , IND_T, LT,
     &   ICONVFT, OPTADV_TR, PATMOS, LISTIN, GRAV, ZF, DEBUG,
         IND_S, MASKEL,
     &   MARDAT, MARTIM, LAMBD0, PHI0,
     &   WNODES_PROC, WNODES
      USE DECLARATIONS_WAQTEL, ONLY: FORMRS, O2SATU, ADDTR,
          WAQPROCESS,
     &   WATTEMP, RSW, ABRS, RAYEFF
      USE INTERFACE_WAQTEL
!
      USE DECLARATIONS_SPECIAL
      IMPLICIT NONE
!
!-----------------------------------------------------------------------
!
      INTEGER          , INTENT(IN)    :: ISCE(*), NREJET,
          NTRAC
      INTEGER          , INTENT(IN)    :: NSIPH, NBUSE,
          NWEIRS
      INTEGER          , INTENT(IN)    :: N_NGHB_W_NODES
      INTEGER          , INTENT(IN)    :: ENTSIP(NSIPH),
          SORSIP(NSIPH)
      INTEGER          , INTENT(IN)    :: ENTBUS(NBUSE),
          SORBUS(NBUSE)
      INTEGER          , INTENT(IN)    :: MAXSCE, MAXTRA,
          TYPSEUIL
      INTEGER          , INTENT(IN)    :: FAC(*)
      LOGICAL          , INTENT(INOUT) :: YASMI(*)
      DOUBLE PRECISION , INTENT(IN)    :: AT, DT, TETAT, DSCE
          (*)
      DOUBLE PRECISION , INTENT(IN)    :: DSIP(NSIPH), DBUS
```

```
     (NBUSE)
      DOUBLE PRECISION , INTENT(IN)    :: TSCE(MAXSCE,
     MAXTRA)
      DOUBLE PRECISION , INTENT(INOUT) :: MASSOU(*)
      TYPE(BIEF_OBJ)   , INTENT(IN)    :: TN,HPROP,TSIP,
     TBUS
      TYPE(BIEF_OBJ)   , INTENT(IN)    :: TWEIRA,TWEIRB
      TYPE(BIEF_OBJ)   , INTENT(IN)    :: NDGA1,NDGB1
      TYPE(BIEF_OBJ)   , INTENT(INOUT) :: TSCEXP,TEXP,TIMP
!
!-----------------------------------------------------------------
!
      INTEGER I,K,IR,ITRAC,N,INDIC,NTRA
      LOGICAL DISTRI
!
      DOUBLE PRECISION DEBIT,TRASCE
      DOUBLE PRECISION DENOM,NUMER,NORM2,SEC_RMAX,RMAX
!
      DOUBLE PRECISION H1,H2,TRUP,TRDO,AB,DZ
      DOUBLE PRECISION, PARAMETER :: EPS=1.D-6
!
      INTRINSIC SQRT
!
!-----------------------------------------------------------------
!
      DOUBLE PRECISION OSECS,OFRAC,TFRAC,NDAYS,FRACD
      DOUBLE PRECISION SUNRISE,SUNSET,MIDDAY
      DOUBLE PRECISION IRR,EXT
      DOUBLE PRECISION, PARAMETER :: IRRNIGHT = 15.D0
      DOUBLE PRECISION, PARAMETER :: IRRDAY = 170.D0
      DOUBLE PRECISION T90
      DOUBLE PRECISION DEK,DKi,DKs,DKt,RNGE
      DOUBLE PRECISION, PARAMETER :: ALFA = 1.D0
```

```
      DOUBLE PRECISION, PARAMETER :: SS = 84.82D0
      DOUBLE PRECISION, PARAMETER :: SAL = 32.D0
      DOUBLE PRECISION, PARAMETER :: TEMP = 15.D0
      DOUBLE PRECISION, PARAMETER :: PI=4.D0*ATAN(1.D0)
      DOUBLE PRECISION, PARAMETER :: DKTHRESH = 0.05D0
!
!-----------------------------------------------------------------
!
!     MODEL START TIME AT 0200H - CALCULATE INITIAL
   FRACTIONAL TIME OF DAY
!
      OSECS = 7200.D0
      OFRAC = OSECS/86400.D0
      TFRAC = AT/86400.D0
      NDAYS = INT(TFRAC)
      FRACD = TFRAC-NDAYS+OFRAC
      IF (FRACD.GT.1.D0) THEN
          FRACD = FRACD - 1.D0
      END IF
!
!-----------------------------------------------------------------
!
!     SECONDARY CURRENTS WILL BE TREATED APART
!
      NTRA=NTRAC
      IF(SECCURRENTS) NTRA=NTRA-1
!
!-----------------------------------------------------------------
!
!     EXPLICIT SOURCE TERMS
!
      DO ITRAC=1,NTRA
        CALL OS( 'X=0      ',X=TSCEXP%ADR(ITRAC)%P)
```

```
          CALL OS('X=0          ',X=TEXP%ADR(ITRAC)%P)
          MASSOU(ITRAC) = 0.D0
        ENDDO
!
!-----------------------------------------------------------------
!       INITIALIALIZATION OF YASMI
        IF(LT.EQ.1)THEN
          DO ITRAC=1,NTRA
            IF(LOITRAC(ITRAC).EQ.0) THEN
              YASMI(ITRAC)=.FALSE.
            ELSEIF(LOITRAC(ITRAC).EQ.1) THEN
              YASMI(ITRAC)=.TRUE.
            ELSE
              IF(LNG.EQ.1) WRITE(LU,*) 'DIFSOU : LOI NON
                PROGRAMMEE'
              IF(LNG.EQ.2) WRITE(LU,*) 'DIFSOU : LAW NOT
                IMPLEMENTED'
              CALL PLANTE(1)
              STOP
            ENDIF
          ENDDO
!         WHEN COUPLING WITH WAQTEL, PREPARE IMPLICIT SOURCE
    TERMS
!
          IF(INCLUS(COUPLING,'WAQTEL')) THEN
            CALL YASMI_WAQ(NTRA,YASMI)
          ENDIF
        ENDIF
!
!       IMPLICIT SOURCE TERMS (DEPENDING ON THE LAW CHOSEN)
!
        DO ITRAC=1,NTRA
          IF(LOITRAC(ITRAC).EQ.1) THEN
```

```
!           MANCINI LAW
            SUNRISE = (6.D0*3600.D0)/86400.D0
            MIDDAY = (12.D0*3600.D0)/86400.D0
            SUNSET = (18.D0*3600.D0)/86400.D0
            RNGE = IRRDAY - IRRNIGHT
            IF ((FRACD.GT.SUNRISE).AND.(FRACD.LT.SUNSET))
               THEN
              IRR = RNGE*SIN(PI*(FRACD-SUNRISE)/MIDDAY)
     &                + IRRNIGHT
            ELSE
              IRR = IRRNIGHT
            END IF
!           CONVERT TO LANGLEY/HR
            IRR = IRR/11.63D0
            EXT = 0.55D0*SS
            DKs = 0.8D0 + (0.02D0*SAL)
            DKt = DKs*(1.07D0**(TEMP-20.D0))
            DO I=1,HPROP%DIM1
!             LIMIT HPROP TO PREVENT DIVISION BY ZERO: T90
    = INF
              IF (HPROP%R(I)<DKTHRESH) THEN
                          DKi = ALFA*IRR*(1.D0-EXP(-EXT*
                              DKTHRESH))/
     &                              (EXT*DKTHRESH)
              ELSE
!             DECAY CALCULATED NORMALLY
                          DKi = ALFA*IRR*(1.D0-EXP(-EXT*HPROP%
                              R(I)))/(EXT*HPROP%R(I))
              END IF
              DEK = DKi + DKt
              T90 = 2.3D0*24.D0/DEK
                          TIMP%ADR(ITRAC)%P%R(I) = (-2.3D0
                              /T90/3600.D0)*HPROP%R(I)
```

```
            ENDDO
          ENDIF
        ENDDO
!
!  END OF USER MODIFICATIONS, REMAINDER OF FILE REMOVED
   FOR BREVITY
!
!-----------------------------------------------------------------------
```

Listing 2: Example Fortran code for the implementation of the Stapleton et al. [2007a] decay equation in TELEMAC-2D

```
!                        ****************
                         SUBROUTINE DIFSOU
!                        ****************
!
     &(TEXP,TIMP,YASMI,TSCEXP,HPROP,TN,TETAT,NREJET,ISCE,
       DSCE,TSCE,
     & MAXSCE,MAXTRA,AT,DT,MASSOU,NTRAC,FAC,NSIPH,ENTSIP,
       SORSIP,
     & DSIP,TSIP,NBUSE,ENTBUS,SORBUS,DBUS,TBUS,NWEIRS,
       TYPSEUIL,
     & N_NGHB_W_NODES,NDGA1,NDGB1,TWEIRA,TWEIRB)
!
!***********************************************************
! TELEMAC2D   V7P2
!***********************************************************
!
!brief    PREPARES THE SOURCES TERMS IN THE DIFFUSION
   EQUATION
!+                FOR THE TRACER.
!
!warning  BEWARE OF NECESSARY COMPATIBILITIES FOR HPROP,
   WHICH
!+             SHOULD REMAIN UNCHANGED UNTIL THE
   COMPUTATION OF THE
!+             TRACER MASS IN CVDFTR
!
!previous history removed for brevity
!
!history  J KING (CU)
!+        2018
!+        V7P2
```

```
!+   Decay rate calculates based on Stapleton (2007b)
   equation
!
!~~~~~~~~~~~~~~~~~~~~~~~~~~~~~~~~~~~~~~~~~~~~~~~~~~~~~~~~~~~~
!| AT                |-->| TIME IN SECONDS
!| DBUS              |-->| DISCHARGE OF TUBES.
!| DSCE              |-->| DISCHARGE OF POINT SOURCES
!| DSIP              |-->| DISCHARGE OF CULVERT.
!| DT                |-->| TIME STEP
!| ENTBUS            |-->| INDICES OF ENTRY OF TUBES IN
   GLOBAL NUMBERING
!| ENTSIP            |-->| INDICES OF ENTRY OF PIPE IN GLOBAL
    NUMBERING
!| FAC               |-->| IN PARALLEL :
!|                   |   | 1/(NUMBER OF SUB-DOMAINS OF THE
   POINT)
!| HPROP             |-->| PROPAGATION DEPTH
!| ISCE              |-->| NEAREST POINTS OF DISCHARGES
!| MASSOU            |<--| MASS OF TRACER ADDED BY SOURCE
   TERM
!| MAXSCE            |-->| MAXIMUM NUMBER OF SOURCES
!| MAXTRA            |-->| MAXIMUM NUMBER OF TRACERS
!| NBUSE             |-->| NUMBER OF TUBES
!| NREJET            |-->| NUMBER OF POINT SOURCES.
!| NSIPH             |-->| NUMBER OF CULVERTS
!| NTRAC             |-->| NUMBER OF TRACERS
!| NWEIRS            |-->| NUMBER OF WEIRS
!| SORBUS            |-->| INDICES OF TUBES EXITS IN GLOBAL
   NUMBERING
!| SORSIP            |-->| INDICES OF PIPES EXITS IN GLOBAL
   NUMBERING
!| TBUS              |-->| VALUES OF TRACERS AT TUBES
   EXTREMITY
```

```
!| TETAT            |-->| COEFFICIENT OF IMPLICITATION FOR
   TRACERS.
!| TEXP             |-->| EXPLICIT SOURCE TERM.
!| TIMP             |-->| IMPLICIT SOURCE TERM.
!| TN               |-->| TRACERS AT TIME N
!| TSCE             |-->| PRESCRIBED VALUES OF TRACERS AT
   POINT SOURCES
!| TSCEXP           |<--| EXPLICIT SOURCE TERM OF POINT
   SOURCES
!|                  |   | IN TRACER EQUATION, EQUAL TO:
!|                  |   | TSCE - ( 1 - TETAT ) TN
!| TSIP             |-->| VALUES OF TRACERS AT CULVERT
   EXTREMITY
!| TWEIRA           |-->| VALUES OF TRACERS ON SIDE A OF
   WEIR
!| TWEIRB           |-->| VALUES OF TRACERS ON SIDE B OF
   WEIR
!| TYPSEUIL         |-->| TYPE OF WEIRS (IF = 2, WEIRS
   TREATED AS SOURCES POINTS)
!| YASMI            |<--| IF YES, THERE ARE IMPLICIT SOURCE
   TERMS
!~~~~~~~~~~~~~~~~~~~~~~~~~~~~~~~~~~~~~~~~~~~~~~~~~~~~~~~~~~~~
!
      USE BIEF
      USE DECLARATIONS_TELEMAC
      USE INTERFACE_PARALLEL
      USE DECLARATIONS_TELEMAC2D, ONLY: LOITRAC, COEF1TRAC
          , QWA, QWB,
     &    MAXNPS,U,V,UNSV2D,V2DPAR,VOLU2D,T1,T2,T3,T4,T5,T6,
          T7,T8,T9,T10,
     &    T11,T12,MESH,MSK,
     &    IELMU,S,NPOIN,CF,H,SECCURRENTS,SEC_AS,SEC_DS,SEC_R
          ,IND_T,LT,
```

```
      &   ICONVFT,OPTADV_TR,PATMOS,LISTIN,GRAV,ZF,DEBUG,
          IND_S,MASKEL,
      &   MARDAT,MARTIM,LAMBD0,PHI0,
      &   WNODES_PROC,WNODES
       USE DECLARATIONS_WAQTEL,ONLY: FORMRS,O2SATU,ADDTR,
           WAQPROCESS,
      &   WATTEMP,RSW,ABRS,RAYEFF
       USE INTERFACE_WAQTEL
!
       USE DECLARATIONS_SPECIAL
       IMPLICIT NONE
!
!-----------------------------------------------------------------
!
       INTEGER              , INTENT(IN)    :: ISCE(*),NREJET,
           NTRAC
       INTEGER              , INTENT(IN)    :: NSIPH,NBUSE,
           NWEIRS
       INTEGER              , INTENT(IN)    :: N_NGHB_W_NODES
       INTEGER              , INTENT(IN)    :: ENTSIP(NSIPH),
           SORSIP(NSIPH)
       INTEGER              , INTENT(IN)    :: ENTBUS(NBUSE),
           SORBUS(NBUSE)
       INTEGER              , INTENT(IN)    :: MAXSCE,MAXTRA,
           TYPSEUIL
       INTEGER              , INTENT(IN)    :: FAC(*)
       LOGICAL              , INTENT(INOUT) :: YASMI(*)
       DOUBLE PRECISION     , INTENT(IN)    :: AT,DT,TETAT,DSCE
           (*)
       DOUBLE PRECISION     , INTENT(IN)    :: DSIP(NSIPH),DBUS
           (NBUSE)
       DOUBLE PRECISION     , INTENT(IN)    :: TSCE(MAXSCE,
           MAXTRA)
```

```
      DOUBLE PRECISION , INTENT(INOUT) :: MASSOU(*)
      TYPE(BIEF_OBJ)   , INTENT(IN)    :: TN,HPROP,TSIP,
     &    TBUS
      TYPE(BIEF_OBJ)   , INTENT(IN)    :: TWEIRA,TWEIRB
      TYPE(BIEF_OBJ)   , INTENT(IN)    :: NDGA1,NDGB1
      TYPE(BIEF_OBJ)   , INTENT(INOUT) :: TSCEXP,TEXP,TIMP
!
!-----------------------------------------------------------------
!
      INTEGER I,K,IR,ITRAC,N,INDIC,NTRA
      LOGICAL DISTRI
!
      DOUBLE PRECISION DEBIT,TRASCE
      DOUBLE PRECISION DENOM,NUMER,NORM2,SEC_RMAX,RMAX
!
      DOUBLE PRECISION H1,H2,TRUP,TRDO,AB,DZ
      DOUBLE PRECISION, PARAMETER :: EPS=1.D-6
!
      INTRINSIC SQRT
!
!-----------------------------------------------------------------
!
      DOUBLE PRECISION OSECS,OFRAC,TFRAC,NDAYS,FRACD
      DOUBLE PRECISION SUNRISE,SUNSET,MIDDAY
      DOUBLE PRECISION IRR,EXT,TURB,RNGE,IRRNEW
      DOUBLE PRECISION, PARAMETER :: IRRNIGHT = 15.D0
      DOUBLE PRECISION, PARAMETER :: IRRDAY = 170.D0
      DOUBLE PRECISION T90,T90EXP,T901,T902
      DOUBLE PRECISION, PARAMETER :: ALF = 1.D0
      DOUBLE PRECISION, PARAMETER :: SS = 84.82D0
      DOUBLE PRECISION, PARAMETER :: PI=4.D0*ATAN(1.D0)
      DOUBLE PRECISION, PARAMETER :: DKTHRESH = 0.05D0
!
```

```
!-----------------------------------------------------------------------
!
!       FRACTIONAL TIME OF DAY
!
        OSECS = 7200.D0
        OFRAC = OSECS/86400.D0
        TFRAC = AT/86400.D0
        NDAYS = INT(TFRAC)
        FRACD = TFRAC-NDAYS+OFRAC
        IF (FRACD.GT.1.D0) THEN
            FRACD = FRACD - 1.D0
        END IF
!
!-----------------------------------------------------------------------
!
!       SECONDARY CURRENTS WILL BE TREATED APART
!
        NTRA=NTRAC
        IF(SECCURRENTS) NTRA=NTRA-1
!
!-----------------------------------------------------------------------
!
!       EXPLICIT SOURCE TERMS
!
        DO ITRAC=1,NTRA
          CALL OS( 'X=0          ',X=TSCEXP%ADR(ITRAC)%P)
          CALL OS( 'X=0          ',X=TEXP%ADR(ITRAC)%P)
          MASSOU(ITRAC) = 0.D0
        ENDDO
!
!-----------------------------------------------------------------------
!       INITIALIALIZATION OF YASMI
        IF(LT.EQ.1)THEN
```

```
          DO ITRAC=1,NTRA
            IF(LOITRAC(ITRAC).EQ.0) THEN
              YASMI(ITRAC)=.FALSE.
            ELSEIF(LOITRAC(ITRAC).EQ.1) THEN
              YASMI(ITRAC)=.TRUE.
            ELSE
              IF(LNG.EQ.1) WRITE(LU,*) 'DIFSOU : LOI NON
                PROGRAMMEE'
              IF(LNG.EQ.2) WRITE(LU,*) 'DIFSOU : LAW NOT
                IMPLEMENTED'
              CALL PLANTE(1)
              STOP
            ENDIF
          ENDDO
!         WHEN COUPLING WITH WAQTEL, PREPARE IMPLICIT SOURCE
    TERMS
!
          IF(INCLUS(COUPLING,'WAQTEL')) THEN
            CALL YASMI_WAQ(NTRA,YASMI)
          ENDIF
        ENDIF
!
!       IMPLICIT SOURCE TERMS (DEPENDING ON THE LAW CHOSEN)
!
        DO ITRAC=1,NTRA
          IF(LOITRAC(ITRAC).EQ.1) THEN
!           STAPLETON LAW
            SUNRISE = (6.D0*3600.D0)/86400.D0
            MIDDAY = (12.D0*3600.D0)/86400.D0
            SUNSET = (18.D0*3600.D0)/86400.D0
            RNGE = IRRDAY - IRRNIGHT
            IF ((FRACD.GT.SUNRISE).AND.(FRACD.LT.SUNSET))
              THEN
```

```
            IRR = RNGE*SIN(PI*(FRACD-SUNRISE)/MIDDAY)
     &            + IRRNIGHT
          ELSE
            IRR = IRRNIGHT
          END IF
          IF (IRR.GT.260.D0) THEN
            IRR = 260.D0
          END IF
          EXT = 0.55D0*SS
          TURB = 139.479D0*LOG10(SS) - 244.736D0
          T902 = 10.D0**((0.0047D0*TURB) + 0.677D0)
          T90EXP = LOG(10.D0)/(0.000011D0*260.D0*60.D0)
!         DEPTH AVERAGED DECAY - BASED ON DEPTH AVERAGED
!         LIGHT INTENSITY OVER THE WATER COLUMN
          DO I=1,HPROP%DIM1
!           DEPTH AVERAGED BEER-LAMBERT LAW
            IRRNEW = ALF*IRR*(1.D0-EXP(-EXT*HPROP%R(I)))/
     &                                    (EXT*HPROP%R(I))
            IF (IRRNEW.LT.15.D0) THEN
              IRRNEW = 15.D0
            END IF
                    T901 = LOG(10.D0)/(0.000011D0*IRRNEW
                       *60.D0)
                    T90 = T902 + T901 - T90EXP
!           LIMIT DEPTH FOR DECAY RATE
            IF (HPROP%R(I)<DKTHRESH) THEN
!             CALCULATE DEPTH AVERAGED IRR AT THRESHOLD
   AND DEPTH
!             AVERAGED DECAY BASED ON THIS
!             DEPTH AVERAGED BEER-LAMBERT LAW:
              IRRNEW = ALF*IRR*(1.D0-EXP(-EXT*DKTHRESH))/
     &                        (EXT*DKTHRESH)
              T901 = LOG(10.D0)/(0.000011D0*IRRNEW*60.D0)
```

```
                T90 = T902 + T901 - T90EXP
              ELSE
!               T90 = T90
              END IF
                                TIMP%ADR(ITRAC)%P%R(I) = (-2.3D0/
                                  T90/3600.D0)*HPROP%R(I)
            ENDDO
          ENDIF
        ENDDO
!
!  END OF USER MODIFICATIONS, REMAINDER OF FILE REMOVED
   FOR BREVITY
!
!-------------------------------------------------------------
```

Listing 3: Example Fortran code for the inclusion of tracer decay in TELEMAC-3D

```
!                       **********************
                        SUBROUTINE SOURCE_TRAC
!                       **********************
     &  (LT)
!
!
!*************************************************
! TELEMAC3D   V7P1
!*************************************************
!
!brief    PREPARES SOURCE TERMS FOR DIFFUSION OF TRACERS.
!
!previous history removed for brevity
!
!history  J KING (CU)
!+        2018
!+        V7P2
!+   Inclusion of exponential decay rate (T90 decay)
!
!~~~~~~~~~~~~~~~~~~~~~~~~~~~~~~~~~~~~~~~~~~~~~~~~~~~~~
!| LT                |-->| ITERATION NUMBER
!~~~~~~~~~~~~~~~~~~~~~~~~~~~~~~~~~~~~~~~~~~~~~~~~~~~~~
!
      USE BIEF
      USE DECLARATIONS_TELEMAC, ONLY : COUPLING
      USE DECLARATIONS_TELEMAC3D
!     HEAT EXCHANGE WITH ATMOSPHERE
      USE EXCHANGE_WITH_ATMOSPHERE
      USE DECLARATIONS_WAQTEL, ONLY : NEBU, ZSD, WAQPROCESS,
     &    RAYEFF
      USE INTERFACE_WAQTEL
```

```
      USE INTERFACE_TELEMAC3D, EX_SOURCE_TRAC => SOURCE_TRAC
!
      USE DECLARATIONS_SPECIAL
      IMPLICIT NONE

!-----------------------------------------------------------------------
!
      INTEGER, INTENT(IN)             :: LT
!-----------------------------------------------------------------------
!
!-----------------------------------------------------------------------
!
      INTEGER ITRAC
      DOUBLE PRECISION DUMM(2)
!
!       INTEGER IPLAN, I, J
!       DOUBLE PRECISION TREEL, SAL, RO, LAMB, RAY_SOL, LATITUDE
    , LONGITUDE
!       DOUBLE PRECISION KD
!
!-----------------------------------------------------------------------
!
      INTEGER IPOIN3, IPOIN2, IPLAN, SURF
      DOUBLE PRECISION OSECS, OFRAC, TFRAC, NDAYS, FRACD
      DOUBLE PRECISION SUNRISE, SUNSET
      DOUBLE PRECISION, PARAMETER :: T90NIGHT=50.D0
      DOUBLE PRECISION, PARAMETER :: T90DAY=50.D0
      DOUBLE PRECISION T90
      DOUBLE PRECISION, PARAMETER :: PI=4.D0*ATAN(1.D0)
!
!-----------------------------------------------------------------------
!
!       FRACTIONAL TIME OF DAY
```

```
!
      OSECS = 7200.D0
      OFRAC = OSECS/86400.D0
      TFRAC = AT/86400.D0
      NDAYS = INT(TFRAC)
      FRACD = TFRAC-NDAYS+OFRAC
      IF (FRACD.GT.1.D0) THEN
          FRACD = FRACD - 1.D0
      END IF
!
!-----------------------------------------------------------------------
!
!     SETS SOURCE TERMS TO ZERO
!
      IF(NTRAC.GE.1) THEN
!
!       CALL OS ( 'X=C     ' , X=S0TA  , C=0.D0 )
!       CALL OS ( 'X=C     ' , X=S1TA  , C=0.D0 )
!
!       SOURCE TERMS SIMPLY MARKED
!
!       BEWARE, PUT Q INSTEAD OF 0 IN TYPR IF NOT NIL
!
        DO ITRAC=1,NTRAC
          S0TA%ADR(ITRAC)%P%TYPR='0'
          S1TA%ADR(ITRAC)%P%TYPR='Q'
        ENDDO
        SUNRISE = (6.D0*3600.D0)/86400.D0
        SUNSET = (18.D0*3600.D0)/86400.D0
        IF ((FRACD.GT.SUNRISE).AND.(FRACD.LT.SUNSET)) THEN
            T90 = T90DAY
        ELSE
            T90 = T90NIGHT
```

```
        END IF
        DO IPOIN2=1,NPOIN2
            DO IPLAN=1,NPLAN
              IPOIN3=IPOIN2+(IPLAN-1)*NPOIN2
              S1TA%ADR(1)%P%R(IPOIN3) = 2.3D0/T90/3600.D0
            END DO
        END DO
!
!  END OF USER MODIFICATIONS, REMAINDER OF FILE REMOVED
   FOR BREVITY
!
!*************************************************
```

Listing 4: Example Fortran code for the inclusion of the Mancini [1978] decay equation in TELEMAC-3D using a depth-averaged approach

```
!                       **********************
                        SUBROUTINE SOURCE_TRAC
!                       **********************
     &  (LT)
!
!
!*****************************************************
! TELEMAC3D   V7P1
!*****************************************************
!
!brief     PREPARES SOURCE TERMS FOR DIFFUSION OF TRACERS.
!
!previous history removed for brevity
!
!history  J KING (CU)
!+        2018
!+        V7P2
!+   Inclusion of Mancini (1978) depth-averaged decay rate
    (T90 decay)
!
!~~~~~~~~~~~~~~~~~~~~~~~~~~~~~~~~~~~~~~~~~~~~~~~~~~~~~~~~~
!| LT                |-->| ITERATION NUMBER
!~~~~~~~~~~~~~~~~~~~~~~~~~~~~~~~~~~~~~~~~~~~~~~~~~~~~~~~~~
!
      USE BIEF
      USE DECLARATIONS_TELEMAC,ONLY : COUPLING
      USE DECLARATIONS_TELEMAC3D
!     HEAT EXCHANGE WITH ATMOSPHERE
      USE EXCHANGE_WITH_ATMOSPHERE
      USE DECLARATIONS_WAQTEL,ONLY : NEBU,ZSD,WAQPROCESS,
          RAYEFF
```

```
      USE INTERFACE_WAQTEL
      USE INTERFACE_TELEMAC3D, EX_SOURCE_TRAC =>SOURCE_TRAC
!
      USE DECLARATIONS_SPECIAL
      IMPLICIT NONE

!-----------------------------------------------------------------
!
      INTEGER, INTENT(IN)             :: LT
!-----------------------------------------------------------------
!
!-----------------------------------------------------------------
!
      INTEGER ITRAC
      DOUBLE PRECISION DUMM(2)
!
!       INTEGER IPLAN, I, J
!       DOUBLE PRECISION TREEL, SAL, RO, LAMB, RAY_SOL, LATITUDE
    , LONGITUDE
!       DOUBLE PRECISION KD
!
!-----------------------------------------------------------------
!
      INTEGER IPOIN3, IPOIN2, IPLAN, SURF
      DOUBLE PRECISION OSECS, OFRAC, TFRAC, NDAYS, FRACD
      DOUBLE PRECISION SUNRISE, SUNSET, MIDDAY
      DOUBLE PRECISION IR, EXT
      DOUBLE PRECISION, PARAMETER :: IRRNIGHT = 15.D0
      DOUBLE PRECISION, PARAMETER :: IRRDAY = 170.D0
      DOUBLE PRECISION T90
      DOUBLE PRECISION DEK, DKi, DKs, DKt, LAYDEP, RNGE
      DOUBLE PRECISION, PARAMETER :: ALF = 1.D0
      DOUBLE PRECISION, PARAMETER :: SS = 84.82D0
```

```
      DOUBLE PRECISION, PARAMETER :: SAL = 32.D0
      DOUBLE PRECISION, PARAMETER :: TMP = 15.D0
      DOUBLE PRECISION, PARAMETER :: PI=4.D0*ATAN(1.D0)
      DOUBLE PRECISION, PARAMETER :: DKTHRESH = 0.05D0
!
!-----------------------------------------------------------------------
!
!     FRACTIONAL TIME OF DAY
!
      OSECS = 7200.D0
      OFRAC = OSECS/86400.D0
      TFRAC = AT/86400.D0
      NDAYS = INT(TFRAC)
      FRACD = TFRAC-NDAYS+OFRAC
      IF (FRACD.GT.1.D0) THEN
          FRACD = FRACD - 1.D0
      END IF
!
!-----------------------------------------------------------------------
!
!     SETS SOURCE TERMS TO ZERO
!
      IF(NTRAC.GE.1) THEN
!
!       CALL OS ( 'X=C       ' , X=S0TA , C=0.D0 )
!       CALL OS ( 'X=C       ' , X=S1TA , C=0.D0 )
!
!       SOURCE TERMS SIMPLY MARKED
!
!       BEWARE, PUT Q INSTEAD OF 0 IN TYPR IF NOT NIL
!
        DO ITRAC=1,NTRAC
          S0TA%ADR(ITRAC)%P%TYPR='0'
```

```
            S1TA%ADR(ITRAC)%P%TYPR='Q'
          ENDDO
!         MANCINI LAW
          SUNRISE = (6.D0*3600.D0)/86400.D0
          MIDDAY = (12.D0*3600.D0)/86400.D0
          SUNSET = (18.D0*3600.D0)/86400.D0
          RNGE = IRRDAY - IRRNIGHT
          IF ((FRACD.GT.SUNRISE).AND.(FRACD.LT.SUNSET)) THEN
              IR = RNGE*SIN(PI*(FRACD-SUNRISE)/MIDDAY)
     &                + IRRNIGHT
          ELSE
              IR = IRRNIGHT
          END IF
!         CONVERT TO LANGLEY/HR
          IR = IR/11.63D0
          EXT = 0.55D0*SS
          DKs = 0.8D0 + (0.02D0*SAL)
          DKt = DKs*(1.07D0**(TMP-20.D0))
!         DEPTH AVERAGED CALCULATION OF DECAY BASED ON
    CHANGE IN
!         IR OVER THE WATER COLUMN
          DO IPOIN2=1,NPOIN2
              DO IPLAN=1,NPLAN
                IPOIN3=IPOIN2+(IPLAN-1)*NPOIN2
!               DECAY CONDITION DEPENDS ON H > / < THRESHOLD
                IF (H%R(IPOIN2)>DKTHRESH)THEN
!               DEPTH AVERGAED BEER-LAMBERT LAW
                DKi = ALF*IR*(1.D0-EXP(-EXT*H%R(IPOIN2)))/
     &                                    (EXT*H%R(IPOIN2))
                          ELSE
!               DECAY dAve DKi AT THRESHOLD
!                 DEPTH AVERGAED BEER-LAMBERT LAW
                  DKi = ALF*IR*(1.D0-EXP(-EXT*DKTHRESH))/
```

```
      &                                        (EXT*DKTHRESH)
                        ENDIF
                    DEK = DKi + DKt
                    T90 = 2.3D0*24.D0/DEK
                    S1TA%ADR(1)%P%R(IPOIN3) = 2.3D0/T90/3600.D0
                END DO
            END DO
!
        ENDIF
!
!   END OF USER MODIFICATIONS, REMAINDER OF FILE REMOVED
    FOR BREVITY
!
!*************************************************
```

Listing 5: Example Fortran code for the inclusion of the Mancini [1978] decay equation in TELEMAC-3D using a staggered approach

```
!                       **********************
                        SUBROUTINE SOURCE_TRAC
!                       **********************
     &  (LT)
!
!
!*****************************************************
! TELEMAC3D   V7P1
!*****************************************************
!
!brief     PREPARES SOURCE TERMS FOR DIFFUSION OF TRACERS.
!
!previous history removed for brevity
!
!history  J KING (CU)
!+        2018
!+        V7P2
!+   Inclusion of Mancini (1978) staggered decay rate (T90
    decay)
!
!~~~~~~~~~~~~~~~~~~~~~~~~~~~~~~~~~~~~~~~~~~~~~~~~~~~~~~~~~
!| LT                |-->| ITERATION NUMBER
!~~~~~~~~~~~~~~~~~~~~~~~~~~~~~~~~~~~~~~~~~~~~~~~~~~~~~~~~~
!
      USE BIEF
      USE DECLARATIONS_TELEMAC,ONLY : COUPLING
      USE DECLARATIONS_TELEMAC3D
!     HEAT EXCHANGE WITH ATMOSPHERE
      USE EXCHANGE_WITH_ATMOSPHERE
      USE DECLARATIONS_WAQTEL,ONLY : NEBU,ZSD,WAQPROCESS,
          RAYEFF
```

```
      USE INTERFACE_WAQTEL
      USE INTERFACE_TELEMAC3D, EX_SOURCE_TRAC =>SOURCE_TRAC
!
      USE DECLARATIONS_SPECIAL
      IMPLICIT NONE

!-----------------------------------------------------------------
!
      INTEGER, INTENT(IN)             :: LT
!-----------------------------------------------------------------
!
!-----------------------------------------------------------------
!
      INTEGER ITRAC
      DOUBLE PRECISION DUMM(2)
!
!       INTEGER IPLAN, I, J
!       DOUBLE PRECISION TREEL, SAL, RO, LAMB, RAY_SOL, LATITUDE
    , LONGITUDE
!       DOUBLE PRECISION KD
!
!-----------------------------------------------------------------
!
      INTEGER IPOIN3, IPOIN2, IPLAN, SURF
      DOUBLE PRECISION OSECS, OFRAC, TFRAC, NDAYS, FRACD
      DOUBLE PRECISION SUNRISE, SUNSET, MIDDAY
      DOUBLE PRECISION IR, EXT
      DOUBLE PRECISION, PARAMETER :: IRRNIGHT = 15.D0
      DOUBLE PRECISION, PARAMETER :: IRRDAY = 170.D0
      DOUBLE PRECISION T90
      DOUBLE PRECISION DEK, DKi, DKs, DKt, LAYDEP, RNGE
      DOUBLE PRECISION, PARAMETER :: ALF = 1.D0
      DOUBLE PRECISION, PARAMETER :: SS = 84.82D0
```

```
      DOUBLE PRECISION, PARAMETER :: SAL = 32.D0
      DOUBLE PRECISION, PARAMETER :: TMP = 15.D0
      DOUBLE PRECISION, PARAMETER :: PI=4.D0*ATAN(1.D0)
      DOUBLE PRECISION, PARAMETER :: DKTHRESH = 0.05D0
!
!-----------------------------------------------------------------------
!
!     FRACTIONAL TIME OF DAY
!
      OSECS = 7200.D0
      OFRAC = OSECS/86400.D0
      TFRAC = AT/86400.D0
      NDAYS = INT(TFRAC)
      FRACD = TFRAC-NDAYS+OFRAC
      IF (FRACD.GT.1.D0) THEN
          FRACD = FRACD - 1.D0
      END IF
!
!-----------------------------------------------------------------------
!
!     SETS SOURCE TERMS TO ZERO
!
      IF(NTRAC.GE.1) THEN
!
!       CALL OS ( 'X=C       ' , X=S0TA , C=0.D0 )
!       CALL OS ( 'X=C       ' , X=S1TA , C=0.D0 )
!
!       SOURCE TERMS SIMPLY MARKED
!
!       BEWARE, PUT Q INSTEAD OF 0 IN TYPR IF NOT NIL
!
        DO ITRAC=1,NTRAC
          S0TA%ADR(ITRAC)%P%TYPR='0'
```

```
            S1TA%ADR(ITRAC)%P%TYPR='Q'
          ENDDO
!         MANCINI LAW
          SUNRISE = (6.D0*3600.D0)/86400.D0
          MIDDAY = (12.D0*3600.D0)/86400.D0
          SUNSET = (18.D0*3600.D0)/86400.D0
          RNGE = IRRDAY - IRRNIGHT
          IF ((FRACD.GT.SUNRISE).AND.(FRACD.LT.SUNSET)) THEN
              IR = RNGE*SIN(PI*(FRACD-SUNRISE)/MIDDAY)
     &                + IRRNIGHT
          ELSE
              IR = IRRNIGHT
          END IF
!         CONVERT TO LANGLEY/HR
          IR = IR/11.63D0
          EXT = 0.55D0*SS
          DKs = 0.8D0 + (0.02D0*SAL)
          DKt = DKs*(1.07D0**(TMP-20.D0))
!         IR VALUE VARIABLE WITH DEPTH (AND BETWEEN LAYERS)
          DO IPOIN2=1,NPOIN2
              DO IPLAN=1,NPLAN
                IPOIN3=IPOIN2+(IPLAN-1)*NPOIN2
!               DECAY CONDITION DEPENDS ON H > / < THRESHOLD
                IF (H%R(IPOIN2)>DKTHRESH)THEN
!               DECAY CALCULATED BASED ON LAYER DEPTH
                                  SURF = IPOIN2+(NPLAN-1)*NPOIN2
!                 ACCOUNT FOR WATER SURFACE BEING ABOVE /
   BELOW 0.0 DATUM
                  LAYDEP=(ZPROP%R(IPOIN3)-ZPROP%R(SURF))
                     *(-1.D0)
                                      DKi = ALF*IR*EXP(-EXT*
                                        LAYDEP)
!                 LIMIT DKi TO PREVENT EXTREMELY LARGE VALUE
```

```
    : LIM=1s
!                   DUE TO DEPTH THRESHOLD THIS LOOP IS
   OBSOLETE
                                IF (DKi>198979.2D0) THEN
                                    DKi = 198720.D0
                                  ELSE
!                     DKi = DKi
                              END IF
                                  ELSE
!                 DECAY dAve DKi AT THRESHOLD
!                   DEPTH AVERGAED BEER-LAMBERT LAW
                    DKi = ALF*IR*(1.D0-EXP(-EXT*DKTHRESH))/
     &                                    (EXT*DKTHRESH)
                                  ENDIF
                  DEK = DKi + DKt
                  T90 = 2.3D0*24.D0/DEK
                  S1TA%ADR(1)%P%R(IPOIN3) = 2.3D0/T90/3600.D0
                END DO
            END DO
!
        ENDIF
!
!  END OF USER MODIFICATIONS, REMAINDER OF FILE REMOVED
   FOR BREVITY
!
!*************************************************
```

Listing 6: Example Fortran code for the inclusion of the Stapleton et al. [2007a] decay equation in TELEMAC-3D using a depth-averaged approach

```
!                       **********************
                        SUBROUTINE SOURCE_TRAC
!                       **********************
     &  (LT)
!
!
!*****************************************************
! TELEMAC3D   V7P1
!*****************************************************
!
!brief     PREPARES SOURCE TERMS FOR DIFFUSION OF TRACERS.
!
!previous history removed for brevity
!
!history  J KING (CU)
!+        2018
!+        V7P2
!+   Inclusion of Stapleton (2007b) depth-averaged decay
   rate (T90 decay)
!
!~~~~~~~~~~~~~~~~~~~~~~~~~~~~~~~~~~~~~~~~~~~~~~~~~~~~~~~~
!| LT                |-->| ITERATION NUMBER
!~~~~~~~~~~~~~~~~~~~~~~~~~~~~~~~~~~~~~~~~~~~~~~~~~~~~~~~~
!
      USE BIEF
      USE DECLARATIONS_TELEMAC,ONLY : COUPLING
      USE DECLARATIONS_TELEMAC3D
!     HEAT EXCHANGE WITH ATMOSPHERE
      USE EXCHANGE_WITH_ATMOSPHERE
      USE DECLARATIONS_WAQTEL,ONLY : NEBU,ZSD,WAQPROCESS,
          RAYEFF
```

```
      USE INTERFACE_WAQTEL
      USE INTERFACE_TELEMAC3D, EX_SOURCE_TRAC =>SOURCE_TRAC
!
      USE DECLARATIONS_SPECIAL
      IMPLICIT NONE

!-----------------------------------------------------------------------
!
      INTEGER, INTENT(IN)             :: LT
!-----------------------------------------------------------------------
!
!-----------------------------------------------------------------------
!
      INTEGER ITRAC
      DOUBLE PRECISION DUMM(2)
!
!       INTEGER IPLAN, I, J
!       DOUBLE PRECISION TREEL, SAL, RO, LAMB, RAY_SOL, LATITUDE
    , LONGITUDE
!       DOUBLE PRECISION KD
!
!-----------------------------------------------------------------------
!
      INTEGER IPOIN3, IPOIN2, IPLAN, SURF
      DOUBLE PRECISION OSECS, OFRAC, TFRAC, NDAYS, FRACD
      DOUBLE PRECISION SUNRISE, SUNSET, MIDDAY
      DOUBLE PRECISION IRR, EXT, TURB, RNGE, IRRNEW
      DOUBLE PRECISION, PARAMETER :: IRRNIGHT = 15.D0
      DOUBLE PRECISION, PARAMETER :: IRRDAY = 170.D0
      DOUBLE PRECISION T90, T90EXP, T901, T902, LAYDEP
      DOUBLE PRECISION, PARAMETER :: ALF = 1.D0
      DOUBLE PRECISION, PARAMETER :: SS = 84.82D0
      DOUBLE PRECISION, PARAMETER :: PI=4.D0*ATAN(1.D0)
```

```
      DOUBLE PRECISION, PARAMETER :: DKTHRESH = 0.05D0
!
!-----------------------------------------------------------------
!
!       FRACTIONAL TIME OF DAY
!
      OSECS = 7200.D0
      OFRAC = OSECS/86400.D0
      TFRAC = AT/86400.D0
      NDAYS = INT(TFRAC)
      FRACD = TFRAC-NDAYS+OFRAC
      IF (FRACD.GT.1.D0) THEN
          FRACD = FRACD - 1.D0
      END IF
!
!-----------------------------------------------------------------
!
!       SETS SOURCE TERMS TO ZERO
!
      IF(NTRAC.GE.1) THEN
!
!         CALL OS ( 'X=C       ' , X=S0TA , C=0.D0 )
!         CALL OS ( 'X=C       ' , X=S1TA , C=0.D0 )
!
!         SOURCE TERMS SIMPLY MARKED
!
!         BEWARE, PUT Q INSTEAD OF 0 IN TYPR IF NOT NIL
!
          DO ITRAC=1,NTRAC
            S0TA%ADR(ITRAC)%P%TYPR='0'
            S1TA%ADR(ITRAC)%P%TYPR='Q'
          ENDDO
!         IMPLEMENT STAPLETON ET. AL. (2007)
```

```
      EXT = 0.55D0*SS
      TURB = 139.479D0*LOG10(SS) - 244.736D0
      T902 = 10.D0**((0.0047D0*TURB) + 0.677D0)
      T90EXP = LOG(10.D0)/(0.000011D0*260.D0*60.D0)
      SUNRISE = (6.D0*3600.D0)/86400.D0
      MIDDAY = (12.D0*3600.D0)/86400.D0
      SUNSET = (18.D0*3600.D0)/86400.D0
      RNGE = IRRDAY - IRRNIGHT
      IF ((FRACD.GT.SUNRISE).AND.(FRACD.LT.SUNSET)) THEN
          IRR = RNGE*SIN(PI*(FRACD-SUNRISE)/MIDDAY)
     &              + IRRNIGHT
      ELSE
          IRR = IRRNIGHT
      END IF
      IF (IRR.GT.260.D0) THEN
          IRR = 260.D0
      END IF
!     DEPTH AVERAGED DECAY
      DO IPOIN2=1,NPOIN2
          DO IPLAN=1,NPLAN
            IPOIN3=IPOIN2+(IPLAN-1)*NPOIN2
!           DEPTH AVERAGED BEER-LAMBERT LAW
            IRRNEW = ALF*IRR*(1.D0-EXP(-EXT*H%R(IPOIN2))
                )/
     &                                  (EXT*H%R(IPOIN2))
            IF (IRRNEW.LT.15.D0) THEN
              IRRNEW = 15.D0
            END IF
            T901 = LOG(10.D0)/(0.000011D0*IRRNEW*60.D0)
            T90 = T902 + T901 - T90EXP
!           LIMIT DEPTH FOR DECAY RATE
            IF (H%R(IPOIN2)<DKTHRESH) THEN
!             CALCULATE DEPTH AVERAGED IRR AT THRESHOLD
```

```
   AND DEPTH
!                  AVERAGED DECAY BASED ON THIS
!                  DEPTH AVERAGED BEER-LAMBERT LAW:
                   IRRNEW = ALF*IRR*(1.D0-EXP(-EXT*DKTHRESH))
                       /
     &                                    (EXT*DKTHRESH)
                   T901 = LOG(10.D0)/(0.000011D0*IRRNEW*60.D0
                       )
                   T90 = T902 + T901 - T90EXP
                 ELSE
!                  T90 = T90
                              ENDIF
                 S1TA%ADR(1)%P%R(IPOIN3) = 2.3D0/T90/3600.D0
               END DO
             END DO
!
          ENDIF
!
!  END OF USER MODIFICATIONS, REMAINDER OF FILE REMOVED
   FOR BREVITY
!
!***********************************************
```

Listing 7: Example Fortran code for the inclusion of the Stapleton et al. [2007a] decay equation in TELEMAC-3D using a staggered approach

```
!                       **********************
                        SUBROUTINE SOURCE_TRAC
!                       **********************
     &  (LT)
!
!
!*****************************************************
! TELEMAC3D   V7P1
!*****************************************************
!
!brief     PREPARES SOURCE TERMS FOR DIFFUSION OF TRACERS.
!
!previous history removed for brevity
!
!history  J KING (CU)
!+        2018
!+        V7P2
!+   Inclusion of Stapleton (2007b) staggered decay rate (
   T90 decay)
!
!~~~~~~~~~~~~~~~~~~~~~~~~~~~~~~~~~~~~~~~~~~~~~~~~~~~~~~~~~
!| LT                |-->| ITERATION NUMBER
!~~~~~~~~~~~~~~~~~~~~~~~~~~~~~~~~~~~~~~~~~~~~~~~~~~~~~~~~~
!
      USE BIEF
      USE DECLARATIONS_TELEMAC,ONLY : COUPLING
      USE DECLARATIONS_TELEMAC3D
!     HEAT EXCHANGE WITH ATMOSPHERE
      USE EXCHANGE_WITH_ATMOSPHERE
      USE DECLARATIONS_WAQTEL,ONLY : NEBU,ZSD,WAQPROCESS,
          RAYEFF
```

```
      USE INTERFACE_WAQTEL
      USE INTERFACE_TELEMAC3D, EX_SOURCE_TRAC =>SOURCE_TRAC
!
      USE DECLARATIONS_SPECIAL
      IMPLICIT NONE

!-----------------------------------------------------------------------
!
      INTEGER, INTENT(IN)             :: LT
!-----------------------------------------------------------------------
!
!-----------------------------------------------------------------------
!
      INTEGER ITRAC
      DOUBLE PRECISION DUMM(2)
!
!       INTEGER IPLAN, I, J
!       DOUBLE PRECISION TREEL, SAL, RO, LAMB, RAY_SOL, LATITUDE
    , LONGITUDE
!       DOUBLE PRECISION KD
!
!-----------------------------------------------------------------------
!
      INTEGER IPOIN3, IPOIN2, IPLAN, SURF
      DOUBLE PRECISION OSECS, OFRAC, TFRAC, NDAYS, FRACD
      DOUBLE PRECISION SUNRISE, SUNSET, MIDDAY
      DOUBLE PRECISION IRR, EXT, TURB, RNGE, IRRNEW
      DOUBLE PRECISION, PARAMETER :: IRRNIGHT = 15.D0
      DOUBLE PRECISION, PARAMETER :: IRRDAY = 170.D0
      DOUBLE PRECISION T90, T90EXP, T901, T902, LAYDEP
      DOUBLE PRECISION, PARAMETER :: ALF = 1.D0
      DOUBLE PRECISION, PARAMETER :: SS = 84.82D0
      DOUBLE PRECISION, PARAMETER :: PI=4.D0*ATAN(1.D0)
```

```
      DOUBLE PRECISION, PARAMETER :: DKTHRESH = 0.05D0
!
!-----------------------------------------------------------------
!
!       FRACTIONAL TIME OF DAY
!
      OSECS = 7200.D0
      OFRAC = OSECS/86400.D0
      TFRAC = AT/86400.D0
      NDAYS = INT(TFRAC)
      FRACD = TFRAC-NDAYS+OFRAC
      IF (FRACD.GT.1.D0) THEN
          FRACD = FRACD - 1.D0
      END IF
!
!-----------------------------------------------------------------
!
!       SETS SOURCE TERMS TO ZERO
!
      IF(NTRAC.GE.1) THEN
!
!         CALL OS ( 'X=C       ' , X=S0TA , C=0.D0 )
!         CALL OS ( 'X=C       ' , X=S1TA , C=0.D0 )
!
!         SOURCE TERMS SIMPLY MARKED
!
!         BEWARE, PUT Q INSTEAD OF 0 IN TYPR IF NOT NIL
!
          DO ITRAC=1,NTRAC
            S0TA%ADR(ITRAC)%P%TYPR='0'
            S1TA%ADR(ITRAC)%P%TYPR='Q'
          ENDDO
!         IMPLEMENT STAPLETON ET. AL. (2007)
```

```
        EXT = 0.55D0*SS
        TURB = 139.479D0*LOG10(SS) - 244.736D0
        T902 = 10.D0**((0.0047D0*TURB) + 0.677D0)
        T90EXP = LOG(10.D0)/(0.000011D0*260.D0*60.D0)
        SUNRISE = (6.D0*3600.D0)/86400.D0
        MIDDAY = (12.D0*3600.D0)/86400.D0
        SUNSET = (18.D0*3600.D0)/86400.D0
        RNGE = IRRDAY - IRRNIGHT
        IF ((FRACD.GT.SUNRISE).AND.(FRACD.LT.SUNSET)) THEN
            IRR = RNGE*SIN(PI*(FRACD-SUNRISE)/MIDDAY)
     &                + IRRNIGHT
        ELSE
            IRR = IRRNIGHT
        END IF
        IF (IRR.GT.260.D0) THEN
            IRR = 260.D0
        END IF
!       IRR VALUE VARIABLE WITH DEPTH (AND BETWEEN LAYERS)
        DO IPOIN2=1,NPOIN2
            DO IPLAN=1,NPLAN
              IPOIN3=IPOIN2+(IPLAN-1)*NPOIN2
!             DECAY CALCULATED BASED ON LAYER DEPTH
                              SURF = IPOIN2+(NPLAN-1)*NPOIN2
!             ACCOUNT FOR WATER SURFACE BEING ABOVE /
    BELOW 0.0 DATUM
              LAYDEP=(ZPROP%R(IPOIN3)-ZPROP%R(SURF))*(-1.
                  D0)
!             LIGHT INTENSITY AT DEPTH
              IRRNEW = ALF*IRR*EXP(-EXT*LAYDEP)
              IF (IRRNEW.LT.15.D0) THEN
                IRRNEW = 15.D0
              END IF
              T901 = LOG(10.D0)/(0.000011D0*IRRNEW*60.D0)
```

```
                T90 = T902 + T901 - T90EXP
!               LIMIT DEPTH FOR DECAY RATE IN SAND
                IF (H%R(IPOIN2)<DKTHRESH) THEN
!                 CALCULATE DEPTH AVERAGED IRR AT THRESHOLD
   AND DEPTH
!                 AVERAGED DECAY BASED ON THIS
!                 DEPTH AVERAGED BEER-LAMBERT LAW:
                  IRRNEW = ALF*IRR*(1.D0-EXP(-EXT*DKTHRESH))
                      /
     &                                    (EXT*DKTHRESH)
                  T901 = LOG(10.D0)/(0.000011D0*IRRNEW*60.D0
                      )
                  T90 = T902 + T901 - T90EXP
                ELSE
!                 T90 = T90
                                ENDIF
                S1TA%ADR(1)%P%R(IPOIN3) = 2.3D0/T90/3600.D0
              END DO
            END DO
!
        ENDIF
!
!  END OF USER MODIFICATIONS, REMAINDER OF FILE REMOVED
   FOR BREVITY
!
!***************************************************
```

The following is an example of user modifications made to the sub-routine `debsce.f` for improved source representation, using TELEMAC version v7p2r3. The example uses two transects and one stand alone source point from which release is unaffected. Similar modifications were made to `trsce.f` but an example has been omitted for brevity.

Listing 8: Example Fortran code for improved source representation

```
!                       ********************************
                        DOUBLE PRECISION FUNCTION DEBSCE
!                       ********************************
!
     &( TIME , I , DISCE )
!
!*****************************************************
! TELEMAC2D   V6P2
  07/10/2011
!*****************************************************
!
!brief     GIVES THE PRESCRIBED DISCHARGE OF EVERY SOURCE
  POINT.
!+
!+              VARIATIONS WRT TIME AND SPACE MAY BE
  IMPLEMENTED.
!
!note      T2DVEF IS THE SOURCES FILE IN TELEMAC-2D
!
!previous history removed for brevity
!
!history  J KING (CU)
!+        2018
!+        V6P2
!+   Improved source representation for 2 transects and
  stand alone
```

```
!+    source point when run in parallel
!
!~~~~~~~~~~~~~~~~~~~~~~~~~~~~~~~~~~~~~~~~~~~~~~~~~~~~~~~~~~~
!| DISCE          |-->| ARRAY OF DISCHARGES OF SOURCES.
!|                |   | READ IN THE PARAMETER FILE.
!|                |   | NAME OF DISCE IS DSCE IN TELEMAC-2
   D.
!| I              |-->| NUMBER OF THE SOURCE
!| TIME           |-->| TIME
!~~~~~~~~~~~~~~~~~~~~~~~~~~~~~~~~~~~~~~~~~~~~~~~~~~~~~~~~~~~
!
      USE BIEF
      USE DECLARATIONS_SPECIAL
          USE DECLARATIONS_PARALLEL
      USE DECLARATIONS_TELEMAC2D, ONLY: MAXSCE,AT,ENTET,
         NREJET,DT,
     &                                  T2D_FILES,T2DVEF,
        OKDEBSCE,
     &                                  MESH,ISCE,H
!
      IMPLICIT NONE
!
!+-+-+-+-+-+-+-+-+-+-+-+-+-+-+-+-+-+-+-+-+-+-+-+-+-+-+-
!
      DOUBLE PRECISION, INTENT(IN) :: TIME,DISCE(*)
      INTEGER         , INTENT(IN) :: I
!
!+-+-+-+-+-+-+-+-+-+-+-+-+-+-+-+-+-+-+-+-+-+-+-+-+-+-+-
!
!     NREJET = NUMBER OF SINKS / SOURCES
      INTEGER, DIMENSION(NREJET) :: SRCGLOBAL,SRCLOCAL
      DOUBLE PRECISION, DIMENSION(NREJET) :: SRCDEP,
         SRCMINDEP
```

```
      DOUBLE PRECISION, PARAMETER :: TH = 0.D0
      INTEGER J,IR,INDXONE,INDXTWO
!
!-+-+-+-+-+-+-+-+-+-+-+-+-+-+-+-+-+-+-+-+-+-+-+-+-+-+-+-+-+-+-+-+-+-+-
!
      CHARACTER(LEN=9) FCT
      DOUBLE PRECISION DEBSCE1,DEBSCE2
!
!-+-+-+-+-+-+-+-+-+-+-+-+-+-+-+-+-+-+-+-+-+-+-+-+-+-+-+-+-+-+-+-+-+-+-
!
#if defined (HAVE_MPI)
      INTEGER IER
!
!-----------------------------------------------------------------
!
!     IF SOURCES FILE EXISTING, ATTEMPT TO FIND
!     THE VALUE IN IT. IF YES, OKDEBSCE REMAINS TO .TRUE.
   FOR NEXT CALLS
!                              IF NO, OKDEBSCE SET TO .FALSE.
!
      IF(OKDEBSCE(I).AND.T2D_FILES(T2DVEF)%NAME(1:1).NE.'
        ') THEN
!
!       FCT WILL BE Q(1), Q(2), ETC, Q(99), DEPENDING ON I
        FCT='Q(       '
        IF(I.LT.10) THEN
          WRITE(FCT(3:3),FMT='(I1)') I
          FCT(4:4)=')'
        ELSEIF(I.LT.100) THEN
          WRITE(FCT(3:4),FMT='(I2)') I
          FCT(5:5)=')'
        ELSE
          WRITE(LU,*) 'DEBSCE NOT PROGRAMMED FOR MORE THAN
```

```
                99 SOURCES'
            CALL PLANTE(1)
            STOP
          ENDIF
          CALL READ_FIC_SOURCES(DEBSCE1,FCT,AT-DT,T2D_FILES(
              T2DVEF)%LU,
     &                                ENTET,OKDEBSCE(I))
          CALL READ_FIC_SOURCES(DEBSCE2,FCT,AT    ,T2D_FILES(
              T2DVEF)%LU,
     &                                ENTET,OKDEBSCE(I))
!
!         USER PROGRAMMABLE PART
!         USER MODIFICATIONS
!         ISCE = NEAREST POINTS OF SOURCES
          IR = ISCE(I)
!         SRCGLOBAL INDICIES:
!         1-2 : TRANSECT 1
!         3-5 : TRANSECT 2
!         6   : STANDALONE SRC
          SRCGLOBAL = (/4554,2871,4859,3677,7295,1652/)
!         INITIALISE SRCDEP TO ZERO - REMOVE VALUES FROM
    LAST TIMESTEP
          DO J=1,NREJET
                SRCDEP(J) = 0.D0
          ENDDO
!         GET LOCAL NODE NUMBERS (I.E. IN SUBDOMAIN)
          DO J=1,NREJET
            SRCLOCAL(J) = GLOBAL_TO_LOCAL_POINT(SRCGLOBAL(J)
                ,MESH)
            SRCDEP(J) = H%R(SRCLOCAL(J))
          END DO
          CALL MPI_ALLREDUCE(SRCDEP,SRCMINDEP,NREJET,
     &          MPI_DOUBLE_PRECISION,MPI_SUM,MPI_COMM_WORLD,
```

```
          IER)
!
!         IF LOCAL COORDINATE ARRAY(INDEX OF MIN(SRCMINDEP))
!         IS IN THE SUBDOMAIN, ALLOW DISCHARGE, ELSE BLOCK
!
          INDXONE = MINLOC(SRCMINDEP(1:2),1,MASK=(SRCDEP
              (1:2)>TH))
          INDXTWO = MINLOC(SRCMINDEP(3:5),1,MASK=(SRCDEP
              (3:5)>TH))
          INDXTWO = INDXTWO + 2
          IF ((IR.EQ.SRCLOCAL(INDXONE)).OR.(IR.EQ.SRCLOCAL(
              INDXTWO))
     &          .OR.(IR.EQ.SRCLOCAL(6)).OR.(IR.EQ.SRCLOCAL(7)
          ))THEN
                DEBSCE=(DEBSCE1+DEBSCE2)*0.5D0
          ELSE
                DEBSCE = 0.D0
          ENDIF
!
        ENDIF
!
!       BEWARE, AN ERROR IN THE SOURCES FILE MAY REMAIN
    UNNOTICED
!       BECAUSE WE RESORT HERE TO THE PARAMETER FILE
!       DEBSCE SET TOP ZERO TO NOTIFY USER IF ANY ERROR
    READING SRC FILE
!
        IF (.NOT.OKDEBSCE(I).OR.T2D_FILES(T2DVEF)%NAME(1:1).
            EQ.' ') THEN
!
!         PROGRAMMABLE PART
!         DISCE IS TAKEN IN THE PARAMETER FILE
!
```

```
!       GLOBAL NUMBER OF SOURCE I IS ISCE(I) IN TELEMAC-2D
                DEBSCE = 0.D0
!
      ENDIF
!
#else
!
!
      IF(LNG.EQ.1) WRITE(LU,*) 'SERIAL MODE - NO CHANGES
         TO SRC CODE'
      IF(LNG.EQ.2) WRITE(LU,*) 'SERIAL MODE - NO CHANGES
         TO SRC CODE'
!
!     IF SOURCES FILE EXISTING, ATTEMPT TO FIND
!     THE VALUE IN IT. IF YES, OKDEBSCE REMAINS TO .TRUE.
   FOR NEXT CALLS
!                          IF NO, OKDEBSCE SET TO .FALSE.
!
      IF(OKDEBSCE(I).AND.T2D_FILES(T2DVEF)%NAME(1:1).NE.'
         ') THEN
!
!       FCT WILL BE Q(1), Q(2), ETC, Q(99), DEPENDING ON I
        FCT='Q(          '
        IF(I.LT.10) THEN
          WRITE(FCT(3:3),FMT='(I1)') I
          FCT(4:4)=')'
        ELSEIF(I.LT.100) THEN
          WRITE(FCT(3:4),FMT='(I2)') I
          FCT(5:5)=')'
        ELSE
          WRITE(LU,*) 'DEBSCE NOT PROGRAMMED FOR MORE THAN
              99 SOURCES'
          CALL PLANTE(1)
```

```
            STOP
          ENDIF
          CALL READ_FIC_SOURCES(DEBSCE1,FCT,AT-DT,T2D_FILES(
              T2DVEF)%LU,
     &                                  ENTET,OKDEBSCE(I))
          CALL READ_FIC_SOURCES(DEBSCE2,FCT,AT    ,T2D_FILES(
              T2DVEF)%LU,
     &                                  ENTET,OKDEBSCE(I))
          DEBSCE=(DEBSCE1+DEBSCE2)*0.5D0
!
        ENDIF
!
!       BEWARE, AN ERROR IN THE SOURCES FILE MAY REMAIN
    UNNOTICED
!       BECAUSE WE RESORT HERE TO THE PARAMETER FILE
!
        IF(.NOT.OKDEBSCE(I).OR.T2D_FILES(T2DVEF)%NAME(1:1).
            EQ.' ') THEN
!
!         PROGRAMMABLE PART
!         DISCE IS TAKEN IN THE PARAMETER FILE
!
!         GLOBAL NUMBER OF SOURCE I IS ISCE(I) IN TELEMAC-2D
          DEBSCE = DISCE(I)
!
        ENDIF
!
#endif
!
!-----------------------------------------------------------------------
!
        RETURN
        END
```

B.2 Bacterial modelling

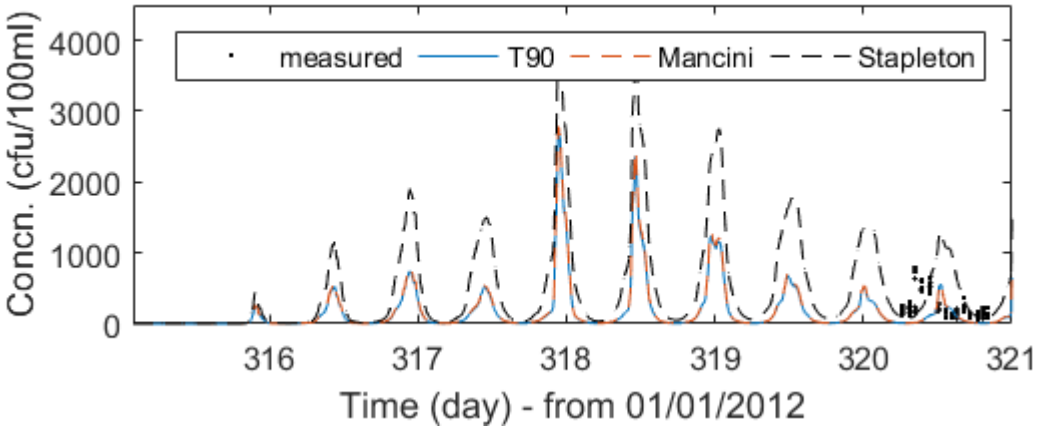

Figure 1: Comparison between the measured and predicted EC concentration at site S2 using three decay functions in the 2D model; T_{90} = 50h constant, Mancini [1978] and Stapleton et al. [2007a]

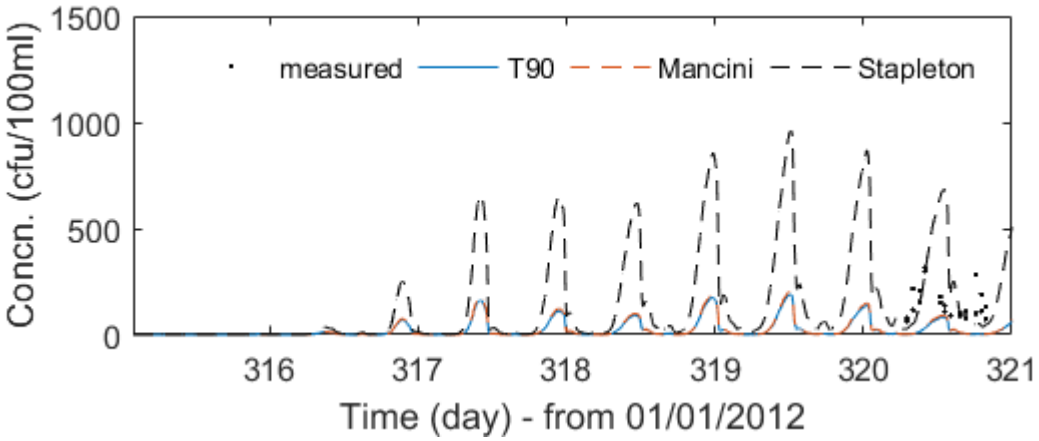

Figure 2: Comparison between the measured and predicted EC concentration at site S3 using three decay functions in the 2D model; T_{90} = 50h constant, Mancini [1978] and Stapleton et al. [2007a]

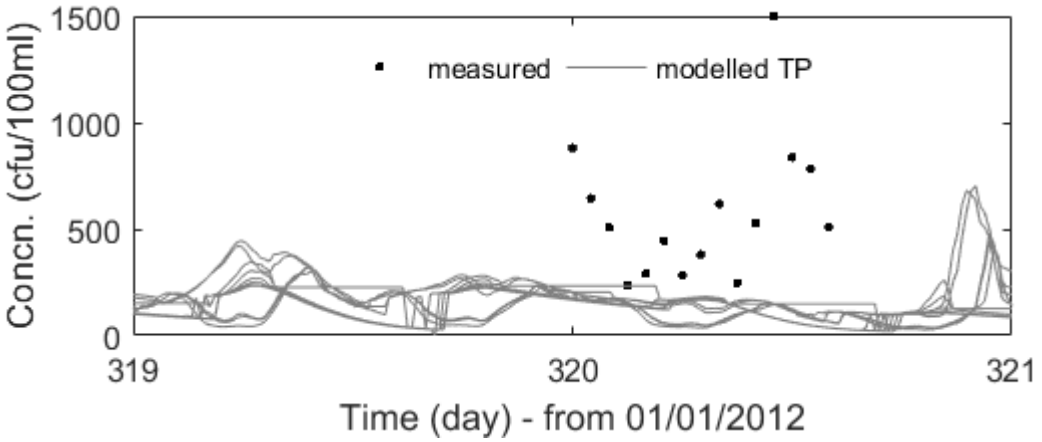

Figure 3: Comparison between the measured and predicted *E.coli* concentrations at each monitoring location along the Swansea Bay DSP transect (TP), using the Mancini [1978] decay function in the 2D model

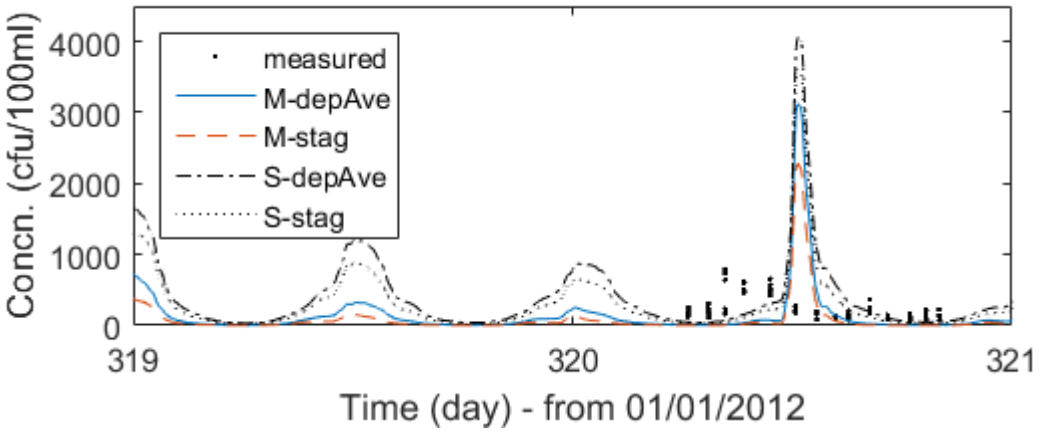

Figure 4: Comparison between the measured and 3D model predictions of *E.coli* concentrations at the site S2 using depth-averaged (depAve) and staggered (stag) functions with the Mancini [1978] (M) and Stapleton et al. [2007a] (S) decay models

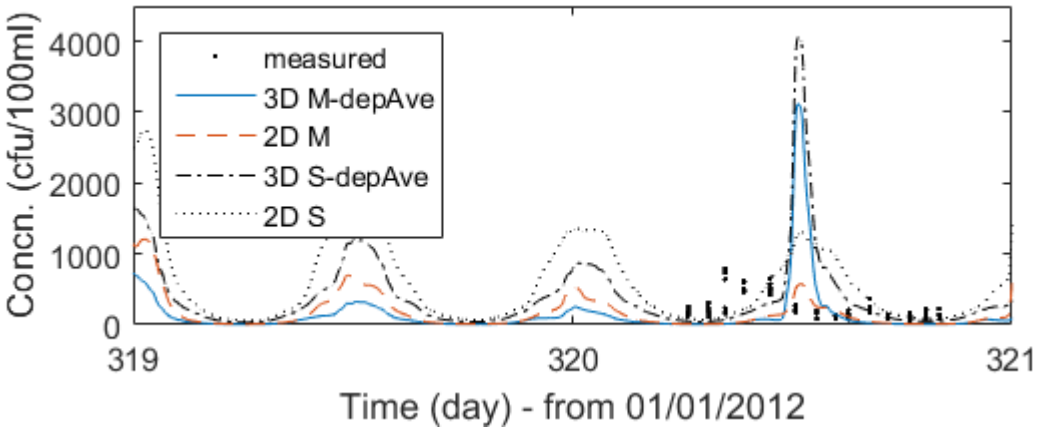

Figure 5: Comparison between the measured, 2D and 3D model predictions of *E.coli* concentrations at site S2, using the Mancini [1978] (M) and Stapleton et al. [2007a] (S) decay functions

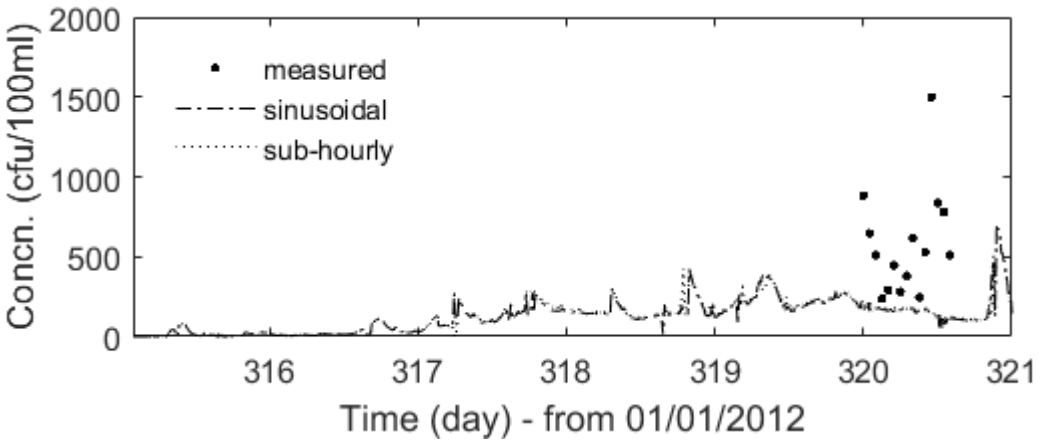

Figure 6: Comparison between the use of a sinusoidal light intensity function and sub-hourly measured data in the 2D model, using the Mancini [1978] decay function

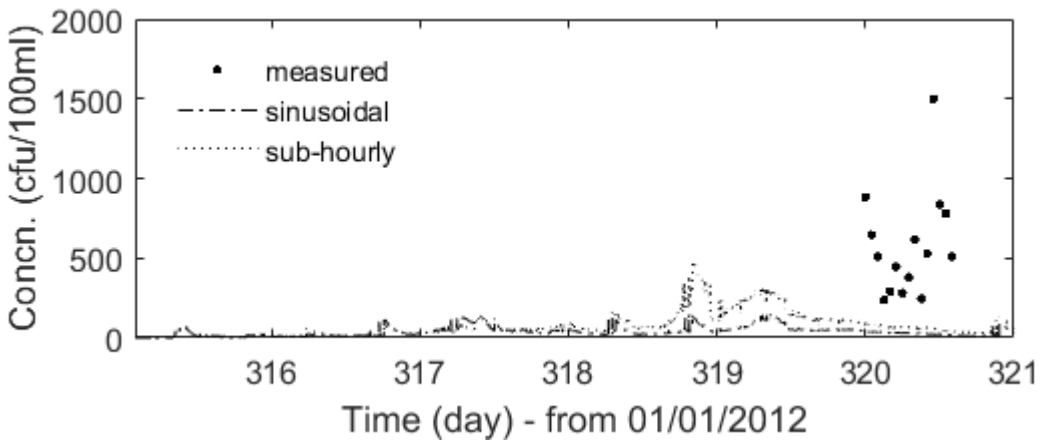

Figure 7: Comparison between the use of a sinusoidal light intensity function and sub-hourly measured data in the 2D model, using the depth staggered Mancini [1978] decay function

Table 7: List of primary bacterial sources in Swansea Bay included within the TELEMAC-2D and 3D models

Source #	**Name**	**Source type**
301	Swansea STW FE	Sewage Effluent
304	Afan STW FE	Sewage Effluent
311	Port Tawe - CSO 989	Sewage Effluent
328	Tata FE	Industrial Effluent
601	Norton Avenue	Surface Water
701	Washinghouse Brook	Surface Water
1701	Brockhole Stream	Surface Water
1801	Clyne River	Surface Water
1901	Sketty Lane Stream	Surface Water
2101	University Stream	Surface Water
2201	Brynmill Stream	Surface Water
2401	Patti Pavillion	Surface Water
2701	Tawe Barrage	Brackish Water
5101	River Afan	Surface Water
5301	Ffrwd Wyllt	Surface Water
5401	Abbey Beach Culvert	Surface Water
4401 total:	River Neath total	Surface Water
4001	Afon Clydach	Surface Water
4101	Roman Way Stream	Surface Water
4301	Betts Nursery Stream	Surface Water
4401	River Neath	Surface Water
4601	Llantwit Stream	Surface Water
4701	Gnoll Brook	Surface Water
4801	Cryddan Brook	Surface Water
5001	Baglan Brook	Surface Water

Table 8: Analytical solution of Equation 2.2 at each layer (L) using Equations 3.34 and 5.3

	Concentration / Time (d)			
L	0	0.5	1	2
5	1000	0.01	7.0E-08	4.9E-18
4	1000	144.5	20.9	0.4
3	1000	499.6	249.6	62.3
2	1000	584.9	342.1	117.0
1	1000	596.7	356.1	126.8
μ	1000	365.1	193.7	61.3

Table 9: Finite difference solution of Equation 5.2 at each layer (L) using Equation 3.34; $\nu_T = 0$

	Concentration / Time (d)			
L	0	0.5	1	2
5	1000	7.6E-03	5.8E-08	3.3E-18
4	1000	144.1	20.8	0.4
3	1000	499.4	249.4	62.2
2	1000	584.8	342.0	116.9
1	1000	596.6	356.0	126.7
μ	1000	365.0	193.6	61.3

Table 10: Analytical solution of Equation 2.2 at each layer (L) using Equations 3.32 and 5.3

	Concentration / Time (d)			
L	0	0.5	1	2
5	1000	456.4	208.3	43.4
4	1000	456.4	208.3	43.4
3	1000	456.4	208.3	43.4
2	1000	456.4	208.3	43.4
1	1000	456.4	208.3	43.4

Table 11: Finite difference solution of Equation 5.2 at each layer (L) using Equation 3.32; $\nu_T = 0$

	Concentration / Time (d)			
L	0	0.5	1	2
5	1000	456.2	208.2	43.3
4	1000	456.2	208.2	43.3
3	1000	456.2	208.2	43.3
2	1000	456.2	208.2	43.3
1	1000	456.2	208.2	43.3

Table 12: Finite difference solution of Equation 5.2 at each layer (L) using Equation 3.34; $\nu_T = 1\text{x}10^{-6}$

	Concentration / Time (d)			
L	0	0.5	1	2
5	1000	0.01	1.1E-06	2.2E-08
4	1000	144.1	20.8	0.4
3	1000	499.4	249.4	62.2
2	1000	584.8	342.0	116.9
1	1000	596.6	356.0	126.7
μ	1000	365.0	193.7	61.3

Table 13: Finite difference solution of Equation 5.2 at each layer (L) using Equation 3.34; $\nu_T = 1$

	Concentration / Time (d)			
L	0	0.5	1	2
5	1000	7.0	2.1	0.4
4	1000	149.0	47.3	10.1
3	1000	431.4	188.0	44.8
2	1000	558.8	294.9	81.3
1	1000	590.2	336.6	101.3
μ	1000	347.3	173.8	47.6

Table 14: Finite difference solution of Equation 5.2 at each layer (L) using Equation 3.32; $\nu_T = 1\text{x}10^{-6}$

	Concentration / Time (d)			
L	0	0.5	1	2
5	1000	456.2	208.2	43.3
4	1000	456.2	208.2	43.3
3	1000	456.2	208.2	43.3
2	1000	456.2	208.2	43.3
1	1000	456.2	208.2	43.3

Table 15: Finite difference solution of Equation 5.2 at each layer (L) using Equation 3.32; $\nu_T = 1$

	Concentration / Time (d)			
L	0	0.5	1	2
5	1000	456.2	208.2	43.3
4	1000	456.2	208.2	43.3
3	1000	456.2	208.2	43.3
2	1000	456.2	208.2	43.3
1	1000	456.2	208.2	43.3

Table 16: Contingency table for predicted *E.coli* concentrations at the Swansea Bay DSP from 12th July to 4th August 2011, using the rBWD 'excellent' limit

		Measured > Threshold		
		Yes	No	
Predicted > Threshold	Yes	1	96	97
	No	20	146	166
		21	242	263

Table 17: Contingency table for predicted *E.coli* concentrations at the Swansea Bay DSP from 5th August to 30th September 2011, using the rBWD 'excellent' limit

		Measured > Threshold		
		Yes	No	
Predicted > Threshold	Yes	65	238	303
	No	42	200	242
		107	438	545

Table 18: Contingency table for predicted *E.coli* concentrations closest in magnitude to the sampled data at the Swansea Bay DSP, from 12th July to 4th August 2011, calculated using the rBWD 'excellent' limit and a threshold depth of 0.05 m

		Measured > Threshold		
		Yes	No	
Predicted > Threshold	Yes	1	100	101
	No	20	142	162
		21	242	263

Table 19: Contingency table for predicted *E.coli* concentrations closest in magnitude to the sampled data at the Swansea Bay DSP, from 5th August to 30th September 2011, calculated using the rBWD 'excellent' limit and a threshold depth of 0.05 m

		Measured > Threshold		
		Yes	No	
Predicted > Threshold	Yes	95	207	302
	No	12	231	243
		107	438	545

References

Aberystwyth University and University College Dublin. Smart Coasts, 2018. URL http://smartcoasts.eu/. Accessed: 2018-08-18. xxv, xxx, 5, 102, 110, 113, 115, 116, 122, 166, 167, 171

R. Ahmadian, S. Bomminayuni, R. Falconer, and T. Stoesser. SSC Numerical modelling of flow and faecal indicator organism transport at Swansea Bay, UK. Technical report, 2013. 101, 113, 167

R. Ahmadian, R. a. Falconer, and J. Wicks. Benchmarking of flood inundation extent using various dynamically linked 1D-2D approaches. *Journal of Flood Risk Management*, pages n/a–n/a, 2015. ISSN 1753318X. doi: 10.1111/jfr3.12208. 14

U. Alkan, D. J. Elliott, and L. M. Evison. Survival of enteric bacteria in relation to simulated solar radiation and other environmental factors in marine waters. *Water Research*, 29(9):2071–2080, 1995. ISSN 00431354. doi: 10.1016/0043-1354(95)00021-C. 30

E. W. Alm, Q. R. Daniels-Witt, D. R. Learman, H. Ryu, D. W. Jordan, T. M. Gehring, and J. Santo Domingo. Potential for gulls to transport bacteria from human waste sites to beaches. *Science of the Total Environment*, 615:123–130, 2018. ISSN 18791026. doi: 10.1016/j.scitotenv.2017.09.232. 4

K. Anastasiou and C. T. Chan. Solution of the 2D Shallow Water Equations Using the Finite Volume Method on Unstructured Triangular Meshes. *International Journal for Numerical Methods in Fluids*, 24(24):1225–1245, 1997. ISSN 02712091. doi: 10.1002/(SICI)1097-0363(19970615)24:11⟨1225::AID-FLD540⟩3.0.CO;2-D. 13, 14

H. Aoyagi, M. Inada, H. Otobe, and R. Takimoto. Experiment of particle dispersion on the sea surface with GPS tracked drifters. pages 139–145, 2003. ISBN 0780386698. 58

L. Aragones, I. Lopez, A. Palazon, R. Lopez-Ubeda, and C. Garcia. Evaluation of the quality of coastal bathing waters in Spain through fecal bacteria Escherichia coli and Enterococcus. *Science of the Total Environment*, 566-567:288–297, 2016. ISSN 18791026. doi: 10.1016/j.scitotenv.2016.05.106. 4, 27, 33

I. Arana and I. Barcina. Ecological Significance and Possible Risks of Nonculturable Intestinal Bacteria in Water Systems. In T. V. Dijk, editor, *Microbial Ecology Research Trends*, chapter V, pages 115–137. Nova Science Publishers, Inc., New York, 2008. ISBN 0100716032. doi: 10.1016/j.bums.2007.10.001. 33

S. Araújo, I. S. Henriques, S. M. Leandro, A. Alves, A. Pereira, and A. Correia. Gulls identified as major source of fecal pollution in coastal waters: A microbial source tracking study. *Science of the Total Environment*, 470-471:84–91, 2014. ISSN 18791026. doi: 10.1016/j.scitotenv.2013.09.075. 4

ARCCA. Advanced Research Computing, 2018. URL https://www.cardiff.ac.uk/advanced-research-computing/about-us/our-supercomputers. Accessed: 2018-12-15. 6

B. F. Arnold, K. C. Schiff, A. Ercumen, J. Benjamin-Chung, J. A. Steele, J. F. Griffith, S. J. Steinberg, P. Smith, C. D. McGee, R. Wilson, C. Nelsen, S. B. Weisberg, and J. M. Colford. Acute Illness among Surfers after Exposure to Seawater in Dry-and Wet-Weather Conditions. *American Journal of Epidemiology*, 186(7):866–875, 2017. ISSN 14766256. doi: 10.1093/aje/kwx019. 34

M. T. Auer and S. L. Niehaus. Modeling fecal coliform bacteriaI. Field and laboratory determination of loss kinetics. *Water Research*, 27(4):693–701, 1993. ISSN 00431354. doi: 10.1016/0043-1354(93)90179-L. 18, 24, 28, 33

A. Avdis, A. S. Candy, J. Hill, S. C. Kramer, and M. D. Piggott. Efficient unstructured mesh generation for marine renewable energy applications. *Renewable Energy*, 116:842–856, 2018. ISSN 18790682. doi: 10.1016/j.renene.2017.09.058. 14

A. Bakar, R. Ahmadian, and R. Falconer. Modelling the transport and decay of microbial tracers in a macro-tidal estuary. *Water Research*, 123:802–824, 2016. doi: 10.1201/b21902-17. 16, 17, 101

A. Bakar, R. Ahmadian, and R. Falconer. Diffuse bacteria loading from intertidal marshland and impacts to adjacent estuarine water quality. *Proceedings of the 37th IAHR World Congress*, pages 3563–3570, 2017. 17, 160

A. A. Bakar, R. Ahmadian, and R. A. Falconer. Microbial tracer transport as particles with biphasic-decay. In *Proc. of the 5th IAHR Europe Congress New Challenges in Hydraulic Research and Engineering*, pages 171–172, 2018. ISBN 9789811127311. doi: 10.3850/978-981-11-2731-1. 19

G. K. Batchelor. Diffusion in a field of homogeneous turbulence. 2 The relative motion of particles. *Proceedings of the Cambridge Philosophical Society*, 48: 345–362, 1952. 57, 58, 89

BBC. Blue Flag beach record for Wales, 2006. URL http://news.bbc.co.uk/1/hi/wales/4772539.stm. Accessed: 2018-12-03. 2

BBC. UK attracting record numbers of tourists, 2017. URL https://www.bbc.co.uk/news/business-41564655. Accessed: 2018-12-03. 2

Z. Bedri, M. Bruen, A. Dowley, and B. Masterson. A Three-Dimensional Hydro-Environmental Model of Dublin Bay. *Environmental Modeling and Assessment*, 16(4):369–384, 2011. ISSN 14202026. doi: 10.1007/s10666-011-9253-7. 15, 114, 185

Z. Bedri, M. Bruen, A. Dowley, and B. Masterson. Environmental consequences of a power plant shut-down: A three-dimensional water quality model of Dublin Bay. *Marine Pollution Bulletin*, 71(1-2):117–128, 2013. ISSN 0025326X. doi: 10.1016/j.marpolbul.2013.03.025. 15, 16, 29, 124

Z. Bedri, A. Corkery, L. Deering, K. Demeter, W. G. Meijer, and B. Masterson. Hydro-environmental Modeling of Sewage and Riverine Discharges into a Coastal Area: Comparison of Depth-averaged and Three-dimensional Models. *3rd IAHR Europe Congress*, pages 1–11, 2014a. 14, 15, 124

Z. Bedri, A. Corkery, J. J. O'Sullivan, M. X. Alvarez, A. C. Erichsen, L. a. Deering, K. Demeter, G. M. P. O'Hare, W. G. Meijer, and B. Masterson. An integrated catchment-coastal modelling system for real-time water quality forecasts. *Environmental Modelling and Software*, 61:458–476, 2014b. ISSN 13648152. doi: 10.1016/j.envsoft.2014.02.006. 4, 13, 14, 18

Z. Bedri, J. J. O. Sullivan, L. A. Deering, K. Demeter, B. Masterson, W. G. Meijer, and G. O. Hare. Assessing the water quality response to an alternative sewage disposal strategy at bathing sites on the east coast of Ireland. *Marine Pollution Bulletin*, 91(1):330–346, 2015. ISSN 0025-326X. doi: 10.1016/j.marpolbul.2014.11.008. 4, 16, 18, 124

Z. Bedri, A. Corkery, J. J. O'Sullivan, L. A. Deering, K. Demeter, W. G. Meijer, G. O'Hare, and B. Masterson. Evaluating a microbial water quality prediction model for beach management under the revised EU Bathing Water Directive. *Journal of Environmental Management*, 167:49–58, 2016. ISSN 10958630. doi: 10.1016/j.jenvman.2015.10.046. xxxiv, 4, 18, 103, 172, 173

J. Bellair, G. Parr-Smith, and I. Wallis. Significance of diurnal variations in faecal coliform die-off rates in the design of ocean outfalls. *Journal WPCF*, 77:2022–2030, 1977. 21, 27

N. D. Bennett, B. F. Croke, G. Guariso, J. H. Guillaume, S. H. Hamilton, A. J. Jakeman, S. Marsili-Libelli, L. T. Newham, J. P. Norton, C. Perrin, S. A. Pierce, B. Robson, R. Seppelt, A. A. Voinov, B. D. Fath, and V. Andreassian. Characterising performance of environmental models. *Environmental Modelling & Software*, 40:1–20, 2013. ISSN 13648152. doi: 10.1016/j.envsoft.2012.09.011. xxxiv, 12, 172, 173

R. A. Blaustein, Y. Pachepsky, R. L. Hill, D. R. Shelton, and G. Whelan. Escherichia coli survival in waters: Temperature dependence. *Water Research*, 47(2):569–578, 2013. ISSN 00431354. doi: 10.1016/j.watres.2012.10.027. 19, 24

Blue Flag. Blue Flag, 2018. URL http://www.blueflag.global/. Accessed: 2018-12-15. 2

S. Bomminayuni. *Modelling tidal flow for assessment of hydro-kinetic energy and bathing water quality in coastal waters*. PhD thesis, 2015. 14, 103

A. G. Borthwick, S. Cruz León, and J. Józsa. Adaptive quadtree model of shallow-flow hydrodynamics. *Journal of Hydraulic Research*, 39(4):413–424, 2001. ISSN 00221686. doi: 10.1080/00221680109499845. 14

M. Bougeard, J. C. Le Saux, N. Pérenne, C. Baffaut, M. Robin, and M. Pommepuy. Modeling of Escherichia coli Fluxes on a Catchment and the Impact on Coastal Water and Shellfish Quality. *Journal of the American Water Resources Association*, 47(2):350–366, 2011. ISSN 1093474X. doi: 10.1111/j.1752-1688.2010.00520.x. 17

S. E. Bourban, S. J. Couch, A. Baldock, and S. Cheeseman. Coastal shelf model of northern european waters to inform tidal power industry decisions: SMARTtide. *Underwater Technology*, 32(1):15–26, 2014. ISSN 17560551. doi: 10.3723/ut.32.015. 15

K. F. Bowden. Horizontal mixing in the sea due to a shearing current. *Journal of Fluid Mechanics*, 21(01):83, 1965. ISSN 0022-1120. doi: 10.1017/S0022112065000058. 48, 49, 50

B. a. Boye, R. a. Falconer, and K. Akande. Integrated water quality modelling: Application to the Ribble Basin, U.K. *Journal of Hydro-environment Research*, pages 1–13, 2014. ISSN 15706443. doi: 10.1016/j.jher.2014.07.002. 16, 26, 27, 28, 31, 114

British Oceanographic Data Centre. UK Tide Gauge Network: Download Data, 2016. URL https://www.bodc.ac.uk/. Accessed: 2016-09-01. 116

J. D. Brookes, J. Antenucci, M. Hipsey, M. D. Burch, N. J. Ashbolt, and C. Ferguson. Fate and transport of pathogens in lakes and reservoirs. *Environment International*, 30(5):741–759, 2004. ISSN 01604120. doi: 10.1016/j.envint.2003.11.006. 32

K. I. Brown and A. B. Boehm. Comparative decay of Catellicoccus marimmalium and enterococci in beach sand and seawater. *Water Research*, 83:377–384, 2015. ISSN 18792448. doi: 10.1016/j.watres.2015.06.055. 32

P. Brufau, M. E. Vzquez-Cendon, and P. Garca-Navarro. A numerical model for the flooding and drying of irregular domains. *International Journal for Numerical Methods in Fluids*, 39(3):247–275, 2002. ISSN 02712091. doi: 10.1002/fld.285. 13, 14

A. L. Buer, G. Gyraite, P. Wegener, X. Lange, M. Katarzyte, G. Hauk, and G. Schernewski. Long term development of Bathing Water Quality at the German Baltic coast: spatial patterns, problems and model simulations. *Marine Pollution Bulletin*, 135:1055–1066, 2018. ISSN 18793363. doi: 10.1016/j.marpolbul.2018.08.048. 5

G. Bussi, P. G. Whitehead, A. R. Thomas, D. Masante, L. Jones, B. Jack Cosby, B. A. Emmett, S. K. Malham, C. Prudhomme, H. Prosser, and J. Cosby. Climate and land-use change impact on faecal indicator bacteria in a temperate maritime catchment (the River Conwy, Wales) Climate and land-use change impact on faecal indicator bacteria in a temperate maritime catchment (the River. *Journal of Hydrology Conwy Journal of Hydrology*, 2017. ISSN 00221694. doi: 10.1016/j.jhydrol.2017.08.011. 2

M. N. Byappanahalli, M. B. Nevers, A. Korajkic, Z. R. Staley, and V. J. Harwood. Enterococci in the Environment. *Microbiology and Molecular Biology Reviews*, 76(4):685–706, 2012. ISSN 1092-2172. doi: 10.1128/MMBR.00023-12. 34

V. J. Cabelli, A. P. Dufour, L. J. McCabe, and M. A. Levin. Swimming-associated Gstroenteritis and Water Quality. *American Journal of Epidemiology*, 115(4):606–616, 1982. 34

C. J. A. Campos, S. R. Kershaw, and R. J. Lee. Environmental Influences on Faecal Indicator Organisms in Coastal Waters and Their Accumulation in Bivalve Shellfish. *Estuaries and Coasts*, 36(4):834–853, 2013. ISSN 15592723. doi: 10.1007/s12237-013-9599-y. 4, 32

J. C. Canteras, J. A. Juanes, L. Pérez, and K. N. Koev. Modelling the coliforms inactivation rates in the Cantabrian Sea (Bay of Biscay) from in situ and laboratory determinations of T90. *Water Science and Technology*, 32(2):37–44, 1995. doi: 10.1016/j.bums.2007.10.001. 26

Cardiff Harbour Authority. Water Quality Forecast, 2018. URL https://cardiffharbour.com/water-quality-forecast/. Accessed: 2018-12-03. 11

K. Cederwall. A float diffusion study. *Water Research*, 5(10):889–907, 1971. ISSN 00431354. doi: 10.1016/0043-1354(71)90025-X. 38, 58, 59, 89

X. Chao, Y. Jia, F. D. Shields, S. S. Y. Wang, and C. M. Cooper. Three-dimensional numerical modeling of cohesive sediment transport and wind wave impact in a shallow oxbow lake. *Advances in Water Resources*, 31(7):1004–1014, 2008. ISSN 03091708. doi: 10.1016/j.advwatres.2008.04.005. 13

S. C. Chapra. *Surface Water-Quality Modeling*. Mc-Graw Hill, Singapore, 1997. 19, 22, 25, 28, 32, 44, 51, 52

C. Chen. An unstructured-grid, finite-volume community ocean model fvcom user manual (3rd edition). C, 2010. 13

W. B. Chen and W. C. Liu. Investigating the fate and transport of fecal coliform contamination in a tidal estuarine system using a three-dimensional model. *Marine Pollution Bulletin*, 116(1-2):365–384, 2017. ISSN 18793363. doi: 10.1016/j.marpolbul.2017.01.031. 4, 14, 32

H. Chick. An Investigation of the Laws of Disinfection. *The Journal of hygiene*, 8(1):92–158, 1908. ISSN 0022-1724. doi: 10.1017/S0022172400006987. 19

K. H. Cho, Y. A. Pachepsky, D. M. Oliver, R. W. Muirhead, Y. Park, R. S. Quilliam, and D. Shelton. Modeling fate and transport of fecally-derived microorganisms at the watershed scale: State of the science and future opportunities. *Water Research*, 100:38–56, 2016. ISSN 00431354. doi: 10.1016/j.watres.2016.04.064. 29

V. T. Chow. *Open-channel hydrualics*. McGraw-Hill Book Company, New York, 1959. 64, 111, 116

Y. Chu, C. Salles, M. G. Tournoud, P. Got, M. Troussellier, C. Rodier, and A. Caro. Faecal bacterial loads during flood events in Northwestern Mediterranean coastal rivers. *Journal of Hydrology*, 405(3-4):501–511, 2011. ISSN 00221694. doi: 10.1016/j.jhydrol.2011.05.047. 11

City and County of Swansea. online air quality & meteorological readings in Swansea, 2018. URL http://swansea.airqualitydata.com/. Accessed: 2018-07-12. 166

K. Clements, R. S. Quilliam, D. L. Jones, J. Wilson, and S. K. Malham. Spatial and temporal heterogeneity of bacteria across an intertidal shellfish bed: Implications for regulatory monitoring of faecal indicator organisms. *Science of the Total Environment*, 506-507:1–9, 2015. ISSN 18791026. doi: 10.1016/j.scitotenv.2014.10.100. 4

J. P. Connolly, A. F. Blumberg, and J. D. Quadrini. Modeling Fate of Pathogenic Organisms in Coastal Waters of Oauhu. *Journal of Environ- mental Engineering*, 125:398–406, 1999. 33

S. Corti and V. Pennati. A 3-D hydrodynamic model of river flow in a delta region. *Hydrological Processes*, 14(2000):2301–2309, 2000. 15

Country Living. These are the 65 cleanest beaches in England, with Blue Flag awards to prove it, 2018. URL https://www.countryliving.com/uk/wildlife/countryside/a20739569/best-cleanest-beaches-england-2018-blue-flag-awards/. Accessed: 2018-12-15. 2

R. Courant, K. Friedrichs, and H. Lewy. On the Partial Difference Equations of Mathematical Physics. *IBM Journal of Research and Development*, 11(2): 215–234, 1967. ISSN 0018-8646. doi: 10.1147/rd.112.0215. 124

N. Coz. *Modelling hydrodynamic, solute and sediment transport processes for marine renewable energy tidal range structures*. Unpublished doctoral thesis, Cardiff University, 2019. 86

S. R. Crane and J. A. Moore. Modeling enteric bacterial die-off: A review. *Water, Air, & Soil Pollution*, 27(3-4):411–439, 1986. ISSN 00496979. doi: 10.1007/BF00649422. 18

J. Crowther, D. Hampson, I. Bateman, D. Kay, P. Posen, C. Stapleton, and M. Wyer. Generic Modelling of Faecal Indicator Organism Concentrations in the UK. *Water*, 3(4):682–701, 2011. ISSN 2073-4441. doi: 10.3390/w3020682. 5, 18

S. P. Cuttle, J. P. Newell-Price, D. Harris, D. R. Chadwick, M. A. Shepherd, S. G. A. Anthony, C. J. A. Macleod, P. M. Haygarth, and B. J. Chambers. A method-centric User Manual' for the mitigation of diffuse water pollution from agriculture. *Soil Use and Management*, 32:162–171, 2016. ISSN 02660032. doi: 10.1111/sum.12242. 17

A. de Brauwere, B. de Brye, P. Servais, J. Passerat, and E. Deleersnijder. Modelling Escherichia coli concentrations in the tidal Scheldt river and estuary. *Water Research*, 45(9):2724–2738, 2011. ISSN 00431354. doi: 10.1016/j.watres.2011.02.003. 4, 17, 23, 25

A. de Brauwere, O. Gourgue, B. de Brye, P. Servais, N. K. Ouattara, and E. Deleersnijder. Integrated modelling of faecal contamination in a densely populated river-sea continuum (Scheldt River and Estuary). *Science of the Total Environment*, 468-469:31–45, 2014a. ISSN 18791026. doi: 10.1016/j.scitotenv.2013.08.019. 13, 17, 32

A. de Brauwere, N. K. Ouattara, and P. Servais. Modeling fecal indicator bacteria concentrations in natural surface waters: a review. *Critical Reviews in Environmental Science and Technology*, 44(21):2380–2453, 2014b. ISSN 1064-3389. doi: 10.1080/10643389.2013.829978. 18, 24, 25, 32, 33

B. de Brye, A. de Brauwere, O. Gourgue, T. Kärnä, J. Lambrechts, R. Comblen, and E. Deleersnijder. A finite-element, multi-scale model of the Scheldt tributaries, river, estuary and ROFI. *Coastal Engineering*, 57(9):850–863, 2010. ISSN 03783839. doi: 10.1016/j.coastaleng.2010.04.001. 13, 14, 17

R. V. de Souza, C. J. Campos, L. H. Garbossa, and W. Q. Seiffert. Developing, cross-validating and applying regression models to predict the concentrations of faecal indicator organisms in coastal waters under different environmental scenarios. *Science of The Total Environment*, 630:20–31, 2018a. ISSN 00489697. doi: 10.1016/j.scitotenv.2018.02.139. 11

R. V. de Souza, C. J. A. de Campos, L. H. P. Garbossa, L. F. d. N. Vianna, and W. Q. Seiffert. Optimising statistical models to predict faecal pollution in coastal areas based on geographic and meteorological parameters. *Marine Pollution Bulletin*, 129(1):284–292, 2018b. ISSN 18793363. doi: 10.1016/j.marpolbul.2018.02.047. 11

S. DeFlorio-Barker, C. Wing, R. M. Jones, and S. Dorevitch. Estimate of incidence and cost of recreational waterborne illness on United States surface waters. *Environmental Health: A Global Access Science Source*, 17(1):1–10, 2018. ISSN 1476069X. doi: 10.1186/s12940-017-0347-9. 2

Deltares. Processes Library Description, Technical Reference Manual. Technical report, Deltares, 2014a. 22, 25, 26, 29

Deltares. Delft3D-FLOW, User Manual. Technical report, Delft, 2014b. 13, 14

Deltares. D-Flow Flexible Mesh, D-Flow FM in Delta Shell, User Manual. Technical report, Delft, 2016. 14

J. Desombre, C.-T. Pham, C. Goeury, and A. Joly. TELEMAC-3D Software Release 7.0 Operating Manual. Technical report, 2016. 42, 43, 52, 124

DHI. MIKE11, a Modelling System for Rivers and Channels. Reference Manual. Technical report, DHI Group, Horshølme, Denmark, 2013a. 13

DHI. MIKE 3 Flow Model FM. Hydrodynamic Module-User Guide. Technical report, DHI Group, Horshølme, Denmark, 2013b. 13

DHI. Bathing Water Quality Forecast at Your Fingertips, 2017a. URL https://www.dhigroup.com/global/news/2017/02/bathing-water-quality-forecast-at-your-fingertips. Accessed: 2017-06-27. 4

DHI. WATER FORECAST, 2017b. URL http://www.waterforecast.com/. Accessed: 2017-02-06. 4

R. L. Droste. *Theory and Practice of Water and Wastewater Treatment*. John Wiley & Sons, Inc, New York, 1 edition, 1997. 23

J. W. Elder. The dispersion of marked fluid in turbulent shear flow. *Journal of Fluid Mechanicsuid Mechanics*, 5(4):544–560, 1959. 37, 47, 49, 56, 57

Electricité de France. open TELEMAC-MASCARET, 2018. URL http://docs.opentelemac.org/. Accessed: 2018-08-18. 125

EMU Limited. Swansea Bay Current Monitoring Operational Report. Technical report, 2012. 116

F. Engelund. Dispersion of floating particles in uniform channel flow. *Journal of the Hydraulics Division*, 95(4):1149–1162, 1969. 37, 57

European Environment Agency. Bathing water quality. Technical report, 2005. URL http://www.eea.europa.eu/data-and-maps/indicators/bathing-water-quality. Accessed: 2016-01-27. 4

European Environment Agency. European water policies and human health Combining reported environmental information. Technical Report 32, 2016. URL https://www.eea.europa.eu/publications/public-health-and-environmental-protection. Accessed: 2016-12-22. 17

C. o. t. E. U. European Parliament. Directive 2000/60/EC of the European Parliament and of the Council of 23 October 2000 establishing a framework for Community action in the field of water policy. Technical Report 22.12.2000, 2000. 17

C. o. t. E. U. European Parliament. Directive 2006/7/EC of the European Parliament and of the Council of 15 February 2006 concerning the management of bathing water quality and repealing Directive 76/160/EEC. *Official Journal of the European Union*, L 064/37, 2006. xvi, xxxiii, 2, 3

P. Evans and E. Langley. Impacts of a Tidal Lagoon on Urban Drainage and Pollutant Dispersion in a Coastal Embayment. In *European Wave & Tidal Energy Conference (EWTEC)*, pages 1–10, 2017. 5, 12

R. Falconer, B. Lin, D. Kay, and C. Stapleton. Predicting coastal health risks using combined water quality and epidemiological models. In *Proceedings of 3rd International Conference on Hydroinformatics, Copenhagen*, pages 1213–1218, Rotterdam, 1998. A.A. Balkema. 35

R. A. Falconer. Water Quality Simulation Study of a Natural Harbor. *Journal of waterway, port, coastal, and ocean engineering*, 112(15):235–259, 1986. ISSN 0733-950X. doi: 10.1061/(ASCE)0733-950X(1986)112. 13

R. A. FALCONER. Some Observations on Nested Modelling of Flow and Solute Transport in Rectangular Harbours. *Proceedings of the Institution of Civil Engineers*, 89(1):15–38, 1990. ISSN 1753-7789. doi: 10.1680/iicep.1990.5249. 14

Z. Feng, A. Reniers, B. K. Haus, H. M. Solo-Gabriele, J. D. Wang, and L. E. Fleming. A predictive model for microbial counts on beaches where intertidal sand is the primary source. *Marine Pollution Bulletin*, 94(1-2):37–47, 2015. ISSN 18793363. doi: 10.1016/j.marpolbul.2015.03.019. 4, 27, 33, 155, 186

H. B. Fischer. Longitudinal dispersion and turbulent mixing in open-channel flow. *Annual Review of Fluid Mechanics*, 5:59–78, 1973. 45

J. C. Galland, N. Goutal, and J. M. Hervouet. TELEMAC: A new numerical model for solving shallow water equations. *Advances in Water Resources*, 14 (3):138–148, 1991. ISSN 0309-1708. doi: 10.1016/0309-1708(91)90006-A. 14

G. Gao. *Numerical Modelling of Hydrodynamic and Sediment-Bacteria Interaction Processes in Estuarine and Coastal Waters*. PhD thesis, Cardiff University, 2008. 43

G. Gao, R. A. Falconer, and B. Lin. Numerical modelling of sediment-bacteria interaction processes in surface waters. *Water Research*, 45(5):1951–1960, 2011a. ISSN 00431354. doi: 10.1016/j.watres.2010.12.030. 32, 33

G. Gao, R. A. Falconer, and B. Lin. Numerical Modelling Sediment-Bacteria Interaction Processes in the Severn Estuary. *Journal of Water Resource and Protection*, 03(01):22–31, 2011b. ISSN 1945-3094. doi: 10.4236/jwarp.2011.31003. 16

G. Gao, R. A. Falconer, and B. Lin. Modelling importance of sediment effects on fate and transport of enterococci in the Severn Estuary, UK. *Marine Pollution Bulletin*, 67(1-2):45–54, 2013. ISSN 0025326X. doi: 10.1016/j.marpolbul.2012.12.002. 16, 32

G. Gao, R. A. Falconer, and B. Lin. Modelling the fate and transport of faecal bacteria in estuarine and coastal waters. *Marine Pollution Bulletin*, 2015. ISSN 0025326X. doi: 10.1016/j.marpolbul.2015.09.011. 16

J. García-Alba, J. F. Bárcena, C. Ugarteburu, and A. García. Artificial neural networks as emulators of process-based models to analyse bathing water quality in estuaries. *Water Research*, 2018. ISSN 00431354. doi: 10.1016/j.watres.2018.11.063. 12, 172

M. W. Gardner and S. R. Dorling. Statistical surface ozone models: An improved methodology to account for non-linear behaviour. *Atmospheric Environment*, 34(1):21–34, 2000. ISSN 13522310. doi: 10.1016/S1352-2310(99)00359-3. 12

L. Gascón and J. M. Corberán. Construction of second-order TVD schemes for non-homogeneous hyperbolic conservation law. *Journal of Computational Physics*, 172:261–297, 2001. ISSN 00219991. doi: 10.1006/jcph.2001.6823. 13, 14

K. Y. H. Gin and S. G. Goh. Modeling the effect of light and salinity on viable but non-culturable (VBNC) Enterococcus. *Water Research*, 47(10):3315–3328, 2013. ISSN 00431354. doi: 10.1016/j.watres.2013.03.021. 28, 33, 34

S. Given, L. H. Pendleton, and A. B. Boehm. Regional public health cost estimates of contaminated coastal waters: A case study of gastroenteritis at southern California beaches. *Environmental Science and Technology*, 40(16):4851–4858, 2006. ISSN 0013936X. doi: 10.1021/es060679s. 2

S. Goldstein. *Modern Development in Fluid Dynamics, Vol. 1.* Oxford University Press, Oxford, 1938. 46

M. Gómez-Doñate, A. Casanovas-Massana, M. Muniesa, and A. R. Blanch. Development of new host-specific Bacteroides qPCRs for the identification of fecal contamination sources in water. *MicrobiologyOpen*, 5(1):83–94, 2016. ISSN 20458827. doi: 10.1002/mbo3.313. 5

O. Gourgue, W. Baeyens, M. S. Chen, A. de Brauwere, B. de Brye, E. Deleersnijder, M. Elskens, and V. Legat. A depth-averaged two-dimensional sediment transport model for environmental studies in the Scheldt Estuary and tidal river network. *Journal of Marine Systems*, 128:27–39, 2013. ISSN 09247963. doi: 10.1016/j.jmarsys.2013.03.014. 17, 124

A. D. Gronewold, S. S. Qian, R. L. Wolpert, and K. H. Reckhow. Calibrating and validating bacterial water quality models: A Bayesian approach. *Water Research*, 43(10):2688–2698, 2009. ISSN 00431354. doi: 10.1016/j.watres.2009.02.034. 11, 18

A. D. Gronewold, L. Myers, J. L. Swall, and R. T. Noble. Addressing uncertainty in fecal indicator bacteria dark inactivation rates. *Water Research*, 45(2):652–664, 2011. ISSN 00431354. doi: 10.1016/j.watres.2010.08.029. 22

J. F. Guillaud, A. Derrien, M. Gourmelon, and M. Pommepuy. T90 as a tool for engineers: Interest and limits. *Water Sciences and Technology*, 35(11-12):277–281, 1997. 19, 21, 31, 53

D. Gutiérrez-Cacciabue, A. G. Cid, and V. B. Rajal. How long can culturable bacteria and total DNA persist in environmental waters? The role of sunlight and solid particles. *Science of the Total Environment*, 539:494–502, 2016. ISSN 18791026. doi: 10.1016/j.scitotenv.2015.07.138. 31

C. Haas, J. Rose, and C. Gerba. *Quantitative microbial risk assessment.* John-Wiley & Sons, New York, 1999. 35

J. M. Hamrick. A three-dimensional environmental fluid dynamics computer code: theoretical and computational aspects. Technical report, Virginia Institute of Marine Science, College of William and Mary, Gloucester Point, VA, 1992. 13

E. J. Han, I. Park, Y. Do Kim, and I. W. Seo. A study of surface mixing in a meandering channel using GPS floaters. *Environmental Earth Sciences*, 75 (10):901, 2016. ISSN 1866-6280. doi: 10.1007/s12665-016-5702-6. 39, 58

M. R. Hashemi, S. P. Neill, P. E. Robins, A. G. Davies, and M. J. Lewis. Effect of waves on the tidal energy resource at a planned tidal stream array. *Renewable Energy*, 75:626–639, 2015. ISSN 18790682. doi: 10.1016/j.renene.2014.10.029. 15

F. Hassard, C. L. Gwyther, K. Farkas, A. Andrews, V. Jones, B. Cox, H. Brett, D. L. Jones, J. E. McDonald, and S. K. Malham. Abundance and distribution of enteric bacteria and viruses in coastal and estuarine sediments-A review. *Frontiers in Microbiology*, 7, 2016. ISSN 1664302X. doi: 10.3389/fmicb.2016.01692. 32, 33

J.-M. Hervouet. *Hydrodynamics of Free Surface Flows: Modelling with the Finite Element Method*. Wiley, Chichester, 2007. 5, 13, 14, 42, 43, 55, 56, 91, 93

M. R. Hipsey, J. P. Antenucci, and J. D. Brookes. A generic, process-based model of microbial pollution in aquatic systems. *Water Resources Research*, 44(7), 2008. ISSN 00431397. doi: 10.1029/2007WR006395. 18

R. E. Horton. Weir Experiments, Coefficients and Formulas. Technical report, Department of the Interior United States Geological Survey, Washington, 1907. 72

HPC Wales. HPCW/SCW Portal, 2018. URL `http://portal.hpcwales.co.uk`. Accessed: 2018-08-18. 153

G. Huang, R. a. Falconer, B. a. Boye, and B. Lin. Cloud to coast: integrated assessment of environmental exposure, health impacts and risk perceptions of faecal organisms in coastal waters. *International Journal of River Basin*

Management, pages 1–14, 2015a. ISSN 1571-5124. doi: 10.1080/15715124.2014.963863. 16, 33, 35

G. Huang, R. A. Falconer, and B. Lin. Integrated river and coastal flow, sediment and Escherichia coli modelling for bathing water quality. *Water*, 2015b. doi: 10.3390/w70x000x. 16, 22, 32

G. Huang, R. A. Falconer, and B. Lin. Integrated hydro-bacterial modelling for predicting bathing water quality. *Estuarine, Coastal and Shelf Science*, 2017. ISSN 02727714. doi: 10.1016/j.ecss.2017.01.018. 16, 17, 33

G. Huang, R. A. Falconer, and B. Lin. Evaluation of E.coli losses in a tidal river network using a refined 1-D numerical model. *Environmental Modelling & Software*, 2018. ISSN 13648152. doi: 10.1016/j.envsoft.2018.07.009. 17

ISO. Water flow measurement in open channels using weirs and venturi flumes - Part 1: Thin plate weirs. Technical report, International Organization of Standards, 1980. 72

J. Jang, H. G. Hur, M. J. Sadowsky, M. N. Byappanahalli, T. Yan, and S. Ishii. Environmental Escherichia coli: ecology and public health implicationsa review. *Journal of Applied Microbiology*, 123(3):570–581, 2017. ISSN 13652672. doi: 10.1111/jam.13468. 34

J. E. Jones and A. M. Davies. *An intercomparison between finite difference and finite element (TELEMAC) approaches to modelling west coast of Britain tides*. PhD thesis, 2005. 15

J. E. Jones and A. M. Davies. Application of a finite element model (TELEMAC) to computing the wind induced response of the Irish Sea. *Continental Shelf Research*, 26(12-13):1519–1541, 2006. ISSN 02784343. doi: 10.1016/j.csr.2006.03.013. 14, 15

C. Karul, S. Soyupak, A. F. Çilesiz, N. Akbay, and E. Germen. Case studies on the use of neural networks in eutrophication modeling. *Ecological Modelling*, 134:145–152, 2000. ISSN 03043800. doi: 10.1016/S0304-3800(00)00360-4. 12

S. M. Kashefipour, B. Lin, and R. A. Falconer. Dynamic Modelling of Bacterial Concentrations in Coastal Waters: Effects of solar Radiation on Decay. In *Proceedings of the 13th IAHR APD Congress, Singapore.*, pages 528–533, 2002a. doi: 10.1142/9789812776969. 19

S. M. Kashefipour, B. Lin, E. Harris, and R. a. Falconer. Hydro-environmental modelling for bathing water compliance of an estuarine basin. *Water Research*, 36(7):1854–1868, 2002b. ISSN 00431354. doi: 10.1016/S0043-1354(01)00396-7. 19, 27, 53

S. M. Kashefipour, B. Lin, and R. A. Falconer. Modelling the fate of faecal indicators in a coastal basin. *Water Research*, 40(7):1413–1425, 2006. ISSN 00431354. doi: 10.1016/j.watres.2005.12.046. 18, 22, 29

D. Kay, F. Jones, M. Wyer, J. Fleisher, R. Salmon, a.F Godfree, a. Zelenauch-Jacquotte, and R. Shore. Predicting likelihood of gastroenteritis from sea bathing: results from randomised exposure. *The Lancet*, 344(8927):905–909, 1994. ISSN 01406736. doi: 10.1016/S0140-6736(94)92267-5. 34

D. Kay, C. Stapleton, M. Wyer, A. McDonald, J. Crowther, N. Paul, K. Jones, C. Francis, J. Watkins, J. Wilkinson, N. Humphrey, B. Lin, L. Yang, R. Falconer, and S. Gardner. Decay of intestinal enterococci concentrations in high-energy estuarine and coastal waters: towards real-time T90 values for modelling faecal indicators in recreational waters. *Water Research*, 39(4):655–667, 2005. ISSN 00431354. doi: 10.1016/j.watres.2004.11.014. 18, 19, 30, 31, 32, 34, 53

D. Kay, J. Crowther, C. Stapleton, M. Wyer, L. Fewtrell, S. Anthony, M. Bradford, A. Edwards, C. Francis, M. Hopkins, C. Kay, A. McDonald, J. Watkins, and J. Wilkinson. Faecal indicator organism concentrations and catchment export coefficients in the UK. *Water Research*, 42(10-11):2649–2661, 2008. ISSN 00431354. doi: 10.1016/j.watres.2008.01.017. 17

R. Kopmann and M. Markofsky. Three-dimensional water quality modelling with TELEMAC-3D. *Hydrological Processes*, 14(13):2279–2292, 2000. ISSN 08856087. doi: 10.1002/1099-1085(200009)14:13⟨2279::AID-HYP28⟩3.0.CO;2-7. 15

P. Lang, J. Desombre, R. ATA, C. Goeury, and J. M. Hervouet. TELEMAC-2D Software Release 7.0 User Manual. Technical report, 2014. 42, 43, 55, 124, 151

W. Lea and E. Section. Bathing water quality. 1996. 4

C. W. Li and J. H. Wang. Large eddy simulation of free surface shallow-water flow. *International Journal for Numerical Methods in Fluids*, 34(1):31–46, 2000. ISSN 02712091. doi: 10.1002/1097-0363(20000915)34:1⟨31::AID-FLD47⟩3.0.CO;2-U. 47

D. Liang, R. a. Falconer, and B. Lin. Comparison between TVD-MacCormack and ADI-type solvers of the shallow water equations. *Advances in Water Resources*, 29(12):1833–1845, 2006. ISSN 03091708. doi: 10.1016/j.advwatres.2006.01.005. 13, 14

D. Liang, B. Lin, and R. a. Falconer. A boundary-fitted numerical model for flood routing with shock-capturing capability. *Journal of Hydrology*, 332(3-4): 477–486, 2007. ISSN 00221694. doi: 10.1016/j.jhydrol.2006.08.002. 13

D. Liang, X. Wang, R. a. Falconer, and B. N. Bockelmann-Evans. Solving the depth-integrated solute transport equation with a TVD-MacCormack scheme. *Environmental Modelling & Software*, 25(12):1619–1629, 2010. ISSN 13648152. doi: 10.1016/j.envsoft.2010.06.008. 13, 14

Q. Liang, G. Du, A. G. Borthwick, and J. W. Hall. Flood Inundation Modeling with an Adaptive Quadtree Grid Shallow Water Equation Solver. *Journal of Hydraulic Engineering*, 134(11):1603–1610, 2008. ISSN 0733-9429. doi: 10.1061/(ASCE)0733-9429(2008)134:11(1603). 14

B. Lin and R. A. Falconer. Numerical modelling of three-dimensional suspended sediment for estuarine and coastal waters. *Journal of Hydraulic Research*, 34 (4):435–456, 1996. ISSN 0022-1686. 13

J. E. List, G. Gartrel, and C. D. Winant. DIFFUSION AND DISPERSION IN COASTAL WATERS. *Journal of Hydraulic Engineering*, 116(10):1158–1179, 1990. 57, 58

A. Malcherek. Application of TELEMAC-2D in a narrow estuarine tributary. *Hydrological Processes*, 14(13):2293–2300, 2000. ISSN 08856087. doi: 10.1002/1099-1085(200009)14:13⟨2293::AID-HYP29⟩3.0.CO;2-4. 14

J. L. Mancini. Numerical Estimates of Coliform Mortality Rates under Various Conditions. *Water Pollution Control Federation*, 50(11):2477–2484, 1978. xxvi, xxvii, xxviii, xxxi, xxxii, 16, 23, 24, 25, 27, 50, 51, 52, 126, 127, 128, 130, 131, 134, 135, 136, 139, 140, 141, 142, 144, 145, 146, 150, 162, 190, 191, 194, 200, 222, 227, 249, 250, 251, 252

Marine Conservation Society. Good Beach Guide, 2018. URL https://www.mcsuk.org/nearyou. Accessed: 2018-12-03. 2

I. Masters, A. Williams, T. N. Croft, M. Togneri, M. Edmunds, E. Zangiabadi, I. Fairley, and H. Karunarathna. A comparison of numerical modelling techniques for tidal stream turbine analysis. *Energies*, 8(8):7833–7853, 2015. ISSN 19961073. doi: 10.3390/en8087833. 14

E. Matta, F. Selge, G. Gunkel, and R. Hinkelmann. Three-dimensional modeling of wind- and temperature-induced flows in the Icó-Mandantes Bay, Itaparica Reservoir, NE Brazil. *Water (Switzerland)*, 9(10), 2017. ISSN 20734441. doi: 10.3390/w9100772. 14, 15

M. C. Mattioli, L. M. Sassoubre, T. L. Russell, and A. B. Boehm. Decay of sewage-sourced microbial source tracking markers and fecal indicator bacteria in marine waters. *Water Research*, 108:106–114, 2017. ISSN 18792448. doi: 10.1016/j.watres.2016.10.066. 29

J. A. McCorquodale, I. Georgiou, S. Carnelos, and A. J. Englande. Modeling coliforms in storm water plumes. *Journal of Environmental Engineering and Science*, 3(5):419–431, 2004. ISSN 1496-2551. doi: 10.1139/S03-055. 23, 26

N. McIntyre. *Analysis of uncertainty in river water quality modelling*. PhD thesis, University of London, 2004. 12

G. C. Miller and R. G. Zepp. Effects of suspended sediments on photolysis rates of dissolved pollutants. *Water Research*, 13(5):453–459, 1979. ISSN 00431354. doi: 10.1016/0043-1354(79)90038-1. 31

G. G. Morianou, N. N. Kourgialas, and G. P. Karatzas. Comparison between Curvilinear and Rectilinear Grid Based Hydraulic Models for River Flow Simulation. *Procedia Engineering*, 162:568–575, 2016. ISSN 18777058. doi: 10.1016/j.proeng.2016.11.102. 14

C. Moulinec, C. Denis, C. T. Pham, D. Rougé, J. M. Hervouet, E. Razafindrakoto, R. W. Barber, D. R. Emerson, and X. J. Gu. TELEMAC: An efficient hydrodynamics suite for massively parallel architectures. *Computers and Fluids*, 51(1):30–34, 2011. ISSN 00457930. doi: 10.1016/j.compfluid.2011.07.003. 14, 16, 114, 185

Natural Resources Wales. Morfa Monitoring Station, 2018a. URL http://rloi.naturalresources.wales/ViewDetails?station=4111. Accessed: 2018-08-18. 110

Natural Resources Wales. Neath Tidal Monitoring Station, 2018b. URL http://rloi.naturalresources.wales/ViewDetails?station=4112. Accessed: 2018-08-18. 122

Natural Resources Wales and Welsh Government. Lle: A Geo-Portal for Wales, 2018. URL http://lle.gov.wales. Accessed: 2018-08-18. 110

V. T. Nguyen and N. Yun. Numerical Investigation of Sediment Transport and Bedmorphology on a Stretch of Nakdong River. *Procedia Engineering*, 154: 550–556, 2016. ISSN 18777058. doi: 10.1016/j.proeng.2016.07.551. 15

J. Norton. An introduction to sensitivity assessment of simulation models. *Environmental Modelling and Software*, 69:166–174, 2015. ISSN 13648152. doi: 10.1016/j.envsoft.2015.03.020. 12

J. K. Okoye. Characteristics of transverse mixing in open-channel flows. 1970. 37, 57, 68, 69, 85, 87, 99, 100

A. Okubo. Some Speculations on Oceanic Diffusion Diagrams. *Symposium on the Physical Processes Responsible for the of Pollutants in the Sea with Special Reference to the Nearshore Zone*, 167:77–85, 1974. 49, 57

A. Okubo. Discussion of Diffusion and Dispersion in Coastal Waters by E. John List, G. Gartrell, and C. D. Winant (October, 1990, Vol. 116, No. 10). 118(4): 655–656, 1992. 57

A. I. Olbert, M. Hartnett, T. Dabrowski, and U. Mikolajewicz. Long-term inter-annual variability of a cyclonic gyre in the western Irish Sea. *Continental Shelf Research*, 31(13):1343–1356, 2011. ISSN 02784343. doi: 10.1016/j.csr.2011.05.010. 13

A. I. Olbert, T. Dabrowski, S. Nash, and M. Hartnett. Regional modelling of the 21st century climate changes in the Irish Sea. *Continental Shelf Research*, 41: 48–60, 2012. ISSN 02784343. doi: 10.1016/j.csr.2012.04.003. 13

G. T. Orlob. Eddy Diffusion in Homegenous Turbulence. *Journal of the Hydraulics Devision*, 85:75–101, 1959. doi: 10.1016/j.bums.2007.10.001. 36, 57, 58, 90

N. K. Ouattara, J. Passerat, and P. Servais. Faecal contamination of water and sediment in the rivers of the Scheldt drainage network. *Environmental Monitoring and Assessment*, 183(1-4):243–257, 2011. ISSN 01676369. doi: 10.1007/s10661-011-1918-9. 17, 32

Y. a. Pachepsky and D. R. Shelton. Escherichia coli and Fecal Coliforms in Freshwater and Estuarine Sediments. *Critical Reviews in Environmental Science and Technology*, 41(12):1067–1110, 2011. ISSN 1064-3389. doi: 10.1080/10643380903392718. 33

A. Palazón, I. López, L. Aragonés, Y. Villacampa, and F. J. Navarro-González. Modelling of Escherichia coli concentrations in bathing water at microtidal coasts. *Science of the Total Environment*, 593-594:173–181, 2017. ISSN 18791026. doi: 10.1016/j.scitotenv.2017.03.161. 25, 27, 32

K. Y. Park and A. G. Borthwick. Quadtree grid numerical model of nearshore wave-current interaction. *Coastal Engineering*, 42(3):219–239, 2001. ISSN 03783839. doi: 10.1016/S0378-3839(00)00060-0. 14

A. Plaza, R. Montenegro, and L. Ferragut. An improved derefinement algorithm of nested meshes. *Advances in Engineering Software*, 27(1-2):51–57, 1996. ISSN 09659978. doi: 10.1016/0965-9978(96)00005-1. 14

M. Pommepuy, J. F. Guillaud, E. Dupray, A. Derrien, F. L. Guyader, and M. Cormier. Enteric Bacteria Survival Factors. *Water Science and Technology*, 25(12):93–103, 1992. doi: 10.1016/j.bums.2007.10.001. 21, 31

M. R. Raith, C. A. Kelty, J. F. Griffith, A. Schriewer, S. Wuertz, S. Mieszkin, M. Gourmelon, G. H. Reischer, A. H. Farnleitner, J. S. Ervin, P. A. Holden, D. L. Ebentier, J. A. Jay, D. Wang, A. B. Boehm, T. G. Aw, J. B. Rose, E. Balleste, W. G. Meijer, M. Sivaganesan, and O. C. Shanks. Comparison of PCR and quantitative real-time PCR methods for the characterization of ruminant and cattle fecal pollution sources. *Water Research*, 47(18):6921–6928, 2013. ISSN 00431354. doi: 10.1016/j.watres.2013.03.061. 5

B. D. Rogers, A. G. Borthwick, and P. H. Taylor. Mathematical balancing of flux gradient and source terms prior to using Roe's approximate Riemann solver. *Journal of Computational Physics*, 192(2):422–451, 2003. ISSN 00219991. doi: 10.1016/j.jcp.2003.07.020. 13, 14

J. C. Salomon and M. Pommepuy. Mathematical model of bacterial contamination of the Morlaix estuary (France). *Water Research*, 24(8):983–994, 1990. 15

A. G. Samaras, M. G. Gaeta, A. Moreno Miquel, and R. Archetti. High resolution wave and hydrodynamics modelling in coastal areas: operational applications for coastal planning, decision support and assessment. *Natural Hazards and Earth System Sciences Discussions*, (2000):1–32, 2016. ISSN 2195-9269. doi: 10.5194/nhess-2016-63. 14

B. F. Sanders. Non-reflecting boundary flux function for finite volume shallow-water models. *Advances in Water Resources*, 25(2):195–202, 2002. ISSN 03091708. doi: 10.1016/S0309-1708(01)00055-0. 14

W. W. Sayre and A. R. Chamberlain. Exploratory Laboratory Study of Lateral Turbulent Diffusion at the Surface of an Alluvial Channel. Technical report, US Geological Survey, Washington DC, 1964. 36, 57, 58, 69, 90

W. W. Sayre and F. M. Chang. A laboratory investigation of open-channel dispersion processes for dissolved, suspended, and floating dispersants. Technical report, U. S. Geological Survey, Washiington DC, 1968. 35, 36, 37, 46, 47, 57, 58

I. Schnauder, B. Lin, and B. Bockelmann-Evans. Modelling faecal bacteria pathways in receiving waters. *Proceedings of the ICE - Maritime Engineering*, 160 (4):143–153, 2007. ISSN 1741-7597. doi: 10.1680/maen.2007.160.4.143. 16, 17

Scottish Government. Value of bathing waters and influence of bathing water quality: final research report. Technical report, 2018. URL https://www.gov.scot/publications/. Accessed: 2018-12-03. 2

P. Servais, T. Garcia-Armisen, I. George, and G. Billen. Fecal bacteria in the rivers of the Seine drainage network (France): Sources, fate and modelling. *Science of the Total Environment*, 375(1-3):152–167, 2007. ISSN 00489697. doi: 10.1016/j.scitotenv.2006.12.010. 4

F. J. Simões. Finite Volume Model for Two-Dimensional Shallow Environmental Flow. *Journal of Hydraulic Engineering*, 137(2):173–182, 2011. 14

J. Smagorinsky. General circulation experiments wiht the primitive equations I. The basic experiment. *Monthly Weather Review*, 91(3):99–164, 1963. ISSN 0036-8075. doi: 10.1126/science.27.693.594. 47, 56, 124

S. Smolders, T. Maximova, and J. Vanlede. Salinity in the 3D TELEMAC model Scaldis (the Scheldt Estuary): tracer diffusion, dispersion and numerical diffusion. In *Proceedings of the 22st TELEMAC-MASCARET User*

Conference,15th-16th October 2015, Daresbury Laboratory UK, page 8, 2015. 14, 15, 17, 125

M. Solic and N. Krstuloviic. Separate and combined effects of solar radiation, temperature, salinity, and pH on the survival of faecal coliforms in seawater. *Marine Pollution Bulletin*, 24(8):411–416, 1992. ISSN 0025326X. doi: 10.1016/0025-326X(92)90503-X. 18, 24, 25, 29, 30

J. A. Soller, M. Schoen, J. A. Steele, J. F. Griffith, and K. C. Schiff. doi: 10.1016/j.watres.2017.05.017. 34

H. M. Solo-Gabriele, V. J. Harwood, D. Kay, R. S. Fujioka, M. J. Sadowsky, R. L. Whitman, A. Wither, M. Caniça, R. Carvalho da Fonseca, A. Duarte, T. a. Edge, M. J. Gargaté, N. Gunde-Cimerman, F. Hagen, S. L. McLellan, A. Nogueira da Silva, M. Novak Babič, S. Prada, R. Rodrigues, D. Romão, R. Sabino, R. a. Samson, E. Segal, C. Staley, H. D. Taylor, C. Veríssimo, C. Viegas, H. Barroso, and J. C. Brandão. Beach sand and the potential for infectious disease transmission: observations and recommendations. *Journal of the Marine Biological Association of the United Kingdom*, 96(1):1–20, 2015. ISSN 0025-3154. doi: 10.1017/S0025315415000843. 33

C. M. Stapleton, M. D. Wyer, D. Kay, M. Bradford, N. Humphrey, J. Wilkinson, B. Lin, L. Yang, R. A. Falconer, J. Watkins, C. a. Francis, J. Crowther, N. D. Paul, K. Jones, and a. T. McDonald. Fate and transport of particles in estuaries - Volume III : Laboratory experiments , enterococci decay rates and association with sediments. Technical report, Environment Agency, Bristol, 2007b. 16, 113, 167

C. M. Stapleton, M. D. Wyer, D. Kay, M. Bradford, N. Humphrey, J. Wilkinson, B. Lin, L. Yang, R. A. Falconer, J. Watkins, C. a. Francis, J. Crowther, N. D. Paul, K. Jones, and a. T. McDonald. Fate and transport of particles in estuaries - Volume IV: Numerical modelling for bathing water enterococci estimation in the Severn estuary. Technical report, Environment Agency, Bristol, 2007a. xxvi, xxvii, xxviii, xxix, xxx, xxxi, xxxii, 16, 19, 21, 50, 53, 54, 104, 114, 129, 130, 132, 134, 135, 136, 137, 138, 139, 140, 141, 144, 145, 146, 147, 148, 149, 150, 157, 162, 165, 168, 169, 179, 187, 190, 191, 209, 232, 237, 249, 250, 251

B. M. Steets and P. A. Holden. A mechanistic model of runoff-associated fecal coliform fate and transport through a coastal lagoon. *Water Research*, 37(3): 589–608, 2003. ISSN 00431354. doi: 10.1016/S0043-1354(02)00312-3. 23

K. Suara, C. Wang, Y. Feng, R. J. Brown, H. Chanson, and M. Borgas. High-resolution GNSS-tracked drifter for studying surface dispersion in shallow water. *Journal of Atmospheric and Oceanic Technology*, 32(3):579–590, 2015. ISSN 15200426. doi: 10.1175/JTECH-D-14-00127.1. 39

K. Suara, H. Chanson, M. Borgas, and R. J. Brown. Relative dispersion of clustered drifters in a small micro-tidal estuary. *Estuarine, Coastal and Shelf Science*, 194:1–15, 2017. ISSN 02727714. doi: 10.1016/j.ecss.2017.05.001. 39, 58

Supercomputing Wales. Supercomputing Wales, 2018. URL https://www.supercomputing.wales/. Accessed: 2018-12-15. 6

Surfers Against Sewage. Surfers Against Sewage, 2018. URL https://www.sas.org.uk/. Accessed: 2018-12-15. 1

G. I. Taylor. Diffusion by Continuous Movements. *Proceedings of the London Mathematical Society*, 20(1):196–212, 1922. 58

The Guardian. Shellfish warning over water pollution, 2001. URL https://www.theguardian.com/uk/2001/oct/22/physicalsciences.foodanddrink. Accessed: 2018-12-15. 1

The National Oceanography Centre. National Tidal and Sea Level Facility: Chart datum & ordnance datum, 2016. URL http://www.ntslf.org/tides/datum. Accessed: 2016-09-01. 109, 116

The National Oceanography Centre. Continental Shelf Model (CS3 and CS3-3D), 2018. URL https://www.noc.ac.uk/. Accessed: 2018-08-18. 108

The University of Edinburgh. EDINA Marine Digimap Service, 2016a. URL https://digimap.edina.ac.uk/. Accessed: 2016-09-01. 104, 107

The University of Edinburgh. 1 Arcsecond Gridded Bathymetry [ASC geospatial data], 2016b. URL http://digimap.edina.ac.uk. Accessed: 2016-09-01. 104, 107

W. Thoe, M. Gold, a. Griesbach, M. Grimmer, M. L. Taggart, and a. B. Boehm. Predicting water quality at Santa Monica Beach: Evaluation of five different models for public notification of unsafe swimming conditions. *Water research*, 67C:105–117, 2014. ISSN 1879-2448. doi: 10.1016/j.watres.2014.09.001. 5, 11, 12

R. V. Thomann and J. A. Mueller. *Principles of Surface Water Quality Modeling and Control*. HarperCollins, New York, 1987. 19, 44

J. Topf and C. Hormann. OpenStreetMapData, 2016. URL http://openstreetmapdata.com/. Accessed: 2016-01-20. 107

UK Beach Guide. 2018 Blue Flag Award Beaches, 2018. URL https://www.thebeachguide.co.uk/best-beaches/blue{_}flag.htm. Accessed: 2018-12-03. 1

T. van Kessel, J. Vanlede, and J. de Kok. Development of a mud transport model for the Scheldt estuary. *Continental Shelf Research*, 31(10 SUPPL.):S165–S181, 2011. ISSN 02784343. doi: 10.1016/j.csr.2010.12.006. 17

C. Villaret, J. M. Hervouet, R. Kopmann, U. Merkel, and A. G. Davies. Morphodynamic modeling using the Telemac finite-element system. *Computers and Geosciences*, 53:105–113, 2013. ISSN 00983004. doi: 10.1016/j.cageo.2011.10.004. 15

Visit Britain. GB Tourism Survey: 2017 overview, 2017. URL https://www.visitbritain.org/gb-tourism-survey-2017-overview. Accessed: 2018-12-03. 2

R. A. Walters. A model for tides and currents in the English Channel and southern North Sea. *Advances in Water Resources*, 10(3):138–148, 1987. ISSN 03091708. doi: 10.1016/0309-1708(87)90020-0. 13

V. Weitbrecht, G. Kühn, and G. H. Jirka. Large Scale PIV Measurements at the Surface of Shallow Water Flows. *Flow Measurement and Instrumentation*, 13 (5-6):237–245, 2002. ISSN 09555986. doi: 10.1016/S0955-5986(02)00059-6. 68, 88

E. White, A. Saunders, J. Gibson, and N. Barcock. Tidal Lagoon Seansea Bay MArine Water Quality Assessmnet. Appendix 7.2 Supporting Technical Information Report. Technical report, 2014. 113, 167, 170

R. Whitman, V. J. Harwood, T. A. Edge, M. Nevers, M. Byappanahalli, K. Vijayavel, J. Brandão, J. Michael, E. Halliday, J. Kinzelman, G. Kleinheinz, and K. Przybyla-kelly. *NIH Public Access*, volume 13. 2015. ISBN 1115701493408. doi: 10.1007/s11157-014-9340-8.Microbes. 29

J. Wilkinson, A. Jenkins, M. Wyer, and D. Kay. Modelling faecal coliform concentrations in streams. Technical Report 127, 1995. 30, 32

World Health Organization. Guidelines for safe recreational water. Volume 1: Coastal and Fresh Waters. 1:219, 2003a. URL `http://www.who.int/water{_}sanitation{_}health/bathing/srwe2full.pdf`. 3

World Health Organization. Faecal pollution and water quality. *Guidelines for Safe Recreational Environments. Volume 1: Coastal and Fresh Waters*, pages 51–101, 2003b. 3

Y. Wu, R. Falconer, and B. Lin. Modelling trace metal concentration distributions in estuarine waters. *Estuarine, Coastal and Shelf Science*, 64(4):699–709, 2005. ISSN 02727714. doi: 10.1016/j.ecss.2005.04.005. 13

M. D. Wyer, R. Ahmadian, D. Kay, and R. Falconer. SSC Hydrodynamic Comparison Vol. 1: Main Report. Technical report, 2015. 11

A. J. Wyness, D. M. Paterson, E. C. Defew, M. I. Stutter, and L. M. Avery. The role of zeta potential in the adhesion of E. coli to suspended intertidal sediments. *Water Research*, 142:159–166, 2018. ISSN 18792448. doi: 10.1016/j.watres.2018.05.054. 32

K. M. Yamahara, S. P. Walters, and A. B. Boehm. Growth of enterococci in unaltered, unseeded beach sands subjected to tidal wetting. *Applied and Environmental Microbiology*, 75(6):1517–1524, 2009. ISSN 00992240. doi: 10.1128/AEM.02278-08. 4, 33

C. Yang and Y. Liu. Simulation of the fate of faecal bacteria in estuarine and coastal waters based on a fractionated sediment transport model. *China Ocean Engineering*, 31(4):389–395, 2017. ISSN 0890-5487. doi: 10.1007/s13344-017-0045-y. 28, 32, 33

L. Yang. *Development of a Hydroinformatics Software Tool - Enteric Bacteria Transport Modelling Associated with Sediment Transport*. PhD thesis, Cardiff University, 2005. 185

L. Yang, B. Lin, and R. a. Falconer. Modelling enteric bacteria level in coastal and estuarine waters. *Proceedings of the ICE - Engineering and Computational Mechanics*, 161(4):179–186, 2008. ISSN 1755-0777. doi: 10.1680/eacm.2008.161.4.179. 23, 32, 33

J. Ye and J. A. McCorquodale. Depth-Averaged Hydrodynamic Model in Curvilinear Collocated Grid. *Journal of Hydraulic Engineering*, 123(5):380–388, 1997. ISSN 0733-9429. doi: 10.1061/(ASCE)0733-9429(1997)123:5(380). 14

L. Yu, Z. Geng, W. N. Roma, A. M. Righetto, and S. Xiong. Two- and three-dimensional nested simulation by using FEM and FVA to analyze flows in an estuary. *Mathematical and Computer Modelling*, 28(11):115–134, 1998. ISSN 08957177. doi: 10.1016/S0895-7177(98)00168-X. 14

M. Zhang and W. M. Wu. A two dimensional hydrodynamic and sediment transport model for dam break based on finite volume method with quadtree grid. *Applied Ocean Research*, 33(4):297–308, 2011. ISSN 01411187. doi: 10.1016/j.apor.2011.07.004. 14

Q. Zhang, X. He, and T. Yan. Differential Decay of Wastewater Bacteria and Change of Microbial Communities in Beach Sand and Seawater Microcosms. *Environmental Science and Technology*, 49(14):8531–8540, 2015. ISSN 15205851. doi: 10.1021/acs.est.5b01879. 32

Z. Zhang, Z. Deng, and K. a. Rusch. Development of predictive models for determining enterococci levels at Gulf Coast beaches. *Water Research*, 46(2): 465–474, 2012. ISSN 00431354. doi: 10.1016/j.watres.2011.11.027. 12